

# Size Exclusion Chromatography (GPC)

**Theodore Provder, EDITOR**  
*Glidden Coatings and Resins*

Based on a symposium  
sponsored by the Division of  
Analytical Chemistry at the  
178th National Meeting of the  
American Chemical Society  
Washington, D.C.,  
September 10–14, 1979.

A C S   S Y M P O S I U M   S E R I E S **138**

**AMERICAN CHEMICAL SOCIETY**  
**WASHINGTON, D. C.      1980**



## Library of Congress Data

Size exclusion chromatography (GPC).  
(ACS symposium series; 138 ISSN 0097-6156)

Includes bibliographies and index.

1. Gel permeation chromatography—Congresses. 2. Polymers and polymerization—Analysis—Congresses. I. Provder, Theodore, 1939- . II. American Chemical Society. Division of Analytical Chemistry. III. American Chemical Society. IV. Series: American Chemical Society. ACS symposium series; 138.

QD272.C444S59 547.7'046 80-22015  
ISBN 0-8412-0586-8 ASCMC 8 138 1-312 1980

Copyright © 1980

American Chemical Society

All Rights Reserved. The appearance of the code at the bottom of the first page of each article in this volume indicates the copyright owner's consent that reprographic copies of the article may be made for personal or internal use or for the personal or internal use of specific clients. This consent is given on the condition, however, that the copier pay the stated per copy fee through the Copyright Clearance Center, Inc. for copying beyond that permitted by Sections 107 or 108 of the U.S. Copyright Law. This consent does not extend to copying or transmission by any means—graphic or electronic—for any other purpose, such as for general distribution, for advertising or promotional purposes, for creating new collective works, for resale, or for information storage and retrieval systems.

The citation of trade names and/or names of manufacturers in this publication is not to be construed as an endorsement or as approval by ACS of the commercial products or services referenced herein; nor should the mere reference herein to any drawing, specification, chemical process, or other data be regarded as a license or as a conveyance of any right or permission, to the holder, reader, or any other person or corporation, to manufacture, reproduce, use, or sell any patented invention or copyrighted work that may in any way be related thereto.

PRINTED IN THE UNITED STATES OF AMERICA

**American Chemical  
Society Library**  
1155 16th St. N. W.  
Washington, D. C. 20036

## ACS Symposium Series

**M. Joan Comstock**, *Series Editor*

### *Advisory Board*

David L. Allara

Kenneth B. Bischoff

Donald G. Crosby

Donald D. Dollberg

Robert E. Feeney

Jack Halpern

Brian M. Harney

Robert A. Hofstader

W. Jeffrey Howe

James D. Idol, Jr.

James P. Lodge

Leon Petrakis

F. Sherwood Rowland

Alan C. Sartorelli

Raymond B. Seymour

Gunter Zweig

## FOREWORD

The ACS SYMPOSIUM SERIES was founded in 1974 to provide a medium for publishing symposia quickly in book form. The format of the Series parallels that of the continuing ADVANCES IN CHEMISTRY SERIES except that in order to save time the papers are not typeset but are reproduced as they are submitted by the authors in camera-ready form. Papers are reviewed under the supervision of the Editors with the assistance of the Series Advisory Board and are selected to maintain the integrity of the symposia; however, verbatim reproductions of previously published papers are not accepted. Both reviews and reports of research are acceptable since symposia may embrace both types of presentation.

# PREFACE

**S**ize exclusion chromatography or gel permeation chromatography (GPC) became a practical technique for obtaining the molecular weight distribution of polymers around 1964 through the pioneering efforts of John C. Moore. Since that time, GPC has become the analytical method of choice for fractionating and analyzing the molecular weight distribution of macromolecules. The field has grown and the output of journal articles has remained at a high level—during the past five years there have been on the order of 400 to 500 papers published annually.

Recent technological advances over the past five years have sparked a new level of activity in the field of size exclusion chromatography (GPC). These include: (1) the development of high-performance, high-speed column technology; (2) the development and increased use of multiple in-line detectors (for example, differential refractometer, ultraviolet and infrared spectrophotometric detectors, visometry, light scattering, gravimetry, densitometry, etc.); and (3) the application of minicomputer and microcomputer technology for instrument control and data analysis.

These developments in turn have led to new and improved applications of size exclusion chromatography (GPC) as well as higher quality information. The topics in this book that reflect some of these new technological advances include particle size analysis of latex by chromatography methods; gel content measurements; determination of polymer chain branching and copolymer composition as a function of molecular weight; high-resolution GPC analysis of oligomers and micellar systems; applications of aqueous GPC; improved data analysis methods; and kinetic modeling of polymerization reactions.

These new technological advances also have impacted the work of the American Society for Testing and Materials (ASTM). The ASTM committee D20.70.04 currently is involved in developing new size exclusion chromatography methods (GPC) that incorporate these advances.

It is hoped that this book will spur further activity in the field of size exclusion chromatography (GPC).

The editor wishes to thank the authors for their effective oral and written communications and the reviewers for their critiques and constructive comments.

Glidden Coatings and Resins  
Strongsville, Ohio 41136

THEODORE PROVDER

May 20, 1980

# Particle Size Analysis by Chromatography

A. J. McHUGH<sup>1</sup>, D. J. NAGY<sup>2</sup>, and C. A. SILEBI

Department of Chemical Engineering and Emulsion Polymers Institute,  
Lehigh University, Bethlehem, PA 18015

The use of column chromatography for fractionating polymer latex suspensions has been growing rapidly. Figure 1 shows a schematic breakdown of the several methods.

One method, developed by Small (1,2), involves pumping the latex suspension through columns packed with nonporous beads. Separation by size results from the interaction between the electrostatically stabilized particles and eluant velocity gradients in the interstices between the packing. Thus the term Hydrodynamic Chromatography or HDC has been used to describe the process. Under conditions where van der Waals attraction between the particles and packing can predominate (such as at high eluant ionic strength), the particles may interact with or deposit onto the packing. The possibility exists for controlling the deposition - reintraintment behavior of the particles in this regime, based on either size or any of the physico-chemical parameters involved in the potential energy of interaction between the particles and packing. The term Potential Barrier Chromatography or PBC has been used to describe this process (3,4).

A second chromatographic method, similar in operation to HDC, involves the use of porous packing (as in GPC) and has been referred to as Liquid Exclusion Chromatography or LEC. Krebs and Wunderlich (5) were the first to report the use of large pore silica gels for the fractionation of polystyrene and polymethylmethacrylate latexes. More recently, Coll (6) and Singh and Hamielec (7) have investigated the separation of polystyrene latexes up to one micron in diameter using controlled-pore, silica glass packing. Their choice of packing size and pore diameters clearly resembled those of traditional GPC systems. As a result of some of the studies to be discussed in this paper, a separate regime is possible when the packing pores are large

Current address: <sup>1</sup>Department of Chemical Engineering  
University of Illinois  
Urbana, Illinois 61801  
<sup>2</sup>\*Air Products and Chemicals  
Trexlerstown, Pennsylvania 18105

compared to the particle size. Such a process we refer to as Porous Hydrodynamic Chromatography. A third method involves flow of the particle suspension through long, small bore, open capillary tubes and has been referred to as Capillary Hydrodynamic Chromatography (8,9). In this process the flow separation mechanism appears to be related to the "tubular pinch effect" discussed in the work of Segre and Silberberg (10) and the name Tubular Pinch Chromatography (TPC) has also been associated with it. Since the phenomenon only occurs above a critical Reynolds number (11), it may be most applicable to particles larger than a micron in diameter.

Another area of rapid growth for particle separation has been that of Field-Flow Fractionation (FFF) originally developed by Giddings (12,13,14,15) (see also papers in this symposium series). Like HDC, the separation in field-flow fractionation (FFF) results from the combination of force field interactions and the convected motion of the particles, rather than a partitioning between phases. In FFF the force field is applied externally while in HDC it results from internal interactions.

This paper will be limited to a discussion of our packed column studies in which we have addressed attention to questions regarding, (a) the role of ionic strength and surfactant effects on both HDC and porous packed column behavior, (b) the effects of pore size and pore size distribution on resolution, and (c) the effects of the light scattering characteristics of polystyrene on signal resolution and particle size distribution determination. The discussions include references to previous publications which contain detailed development of some of the material presented here.

### Nonporous Packing: HDC

i) Background. Details of the experimental aspects of HDC column design and operation are given in several references (1,16,17,18). The basic technique involves pumping a dilute suspension of latex particles through beds packed with styrene-divinylbenzene copolymer beads. Particles are detected by monitoring the turbidity of the eluant stream in a flow-through cell at 254 nm. Over a range of ionic strengths, particles elute from the columns ahead of a dissolved marker species (dichromate ion) with particle residence time decreasing with increasing diameter.

Particle separation can be characterized by the separation factor,  $R_F$ , which is the ratio of eluant to particle elution volumes, or, by the difference in elution volume,  $\Delta V$ , between particle and eluant marker turbidity peaks. For polystyrene monodisperse standards, a linear relationship occurs between the log of the particle diameter and  $\Delta V$ , with a series of parallel lines resulting for different concentration of either salt or surfactant below its critical micelle concentration (17,18,19). The separation factor has also been shown to be independent of eluant

flow rate (18,19).

To quantify  $R_F$  in terms of a fundamental model for the particle residence time the definition in terms of average velocities is used,

$$R_F = \frac{\langle v_p \rangle}{\langle v_E \rangle} \quad (1)$$

where  $v_p$  and  $v_E$  refer to the particle and eluant axial velocity, and the brackets refer to the appropriate averaging taken over the cross section of the assumed equivalent bed interstitial geometry. For the capillary bed model (18)

$$\langle v_p \rangle = \frac{\int_0^{R_0 - R_p} v_p(r) e^{-\phi(r)/kT} r \, dr}{\int_0^{R_0 - R_p} e^{-\phi(r)/kT} r \, dr} \quad (2)$$

In equation (2)  $R_0$  is the equivalent capillary radius calculated from the bed hydraulic radius (17),  $R_p$  is the particle radius, and the exponential function contains, in addition the Boltzman constant and temperature, the total energy of interaction between the particle and capillary wall force fields. The particle streamline velocity  $v_p(r)$  contains a correction for the wall effect (18). A similar expression for  $\langle v_E \rangle$  results with the exception that for the marker the van der Waals attraction and Born repulsion terms as well as the wall effect are considered to be negligible (18).

Calculations for  $R_F$  as a function of the relevant experimental parameters (eluant ionic species concentration-including surfactant, packing diameter, eluant flow rate) and particle physical and electrochemical properties (Hamaker constant and surface potential) show good agreement with published data (18,19). Of particular interest is the calculation which shows that at very low ionic concentration the separation factor becomes independent of the particle Hamaker constant. This result indicates the feasibility of universal calibration based on well characterized latices such as the monodisperse polystyrenes. In the following section we present some recent results obtained with our HDC system using several monodisperse standards and various surfactant conditions.

ii) Effects of Ionic Concentration on Material Recovery and Universal Calibration. Figure 2 illustrates the effect of ionic strength on the  $R_F$  - particle diameter relationship for the



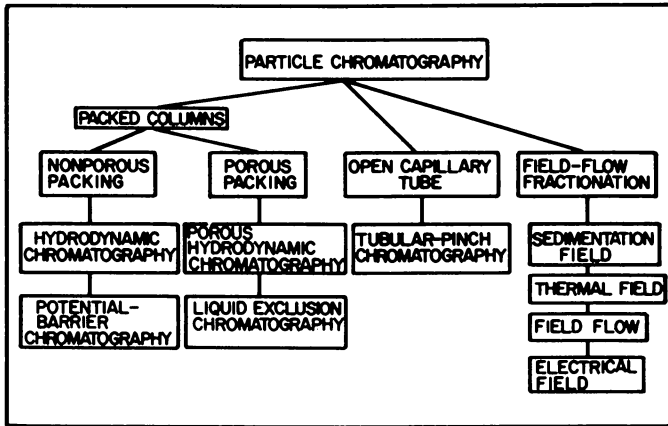


Figure 1. Classification of principal areas of colloidal particle chromatography

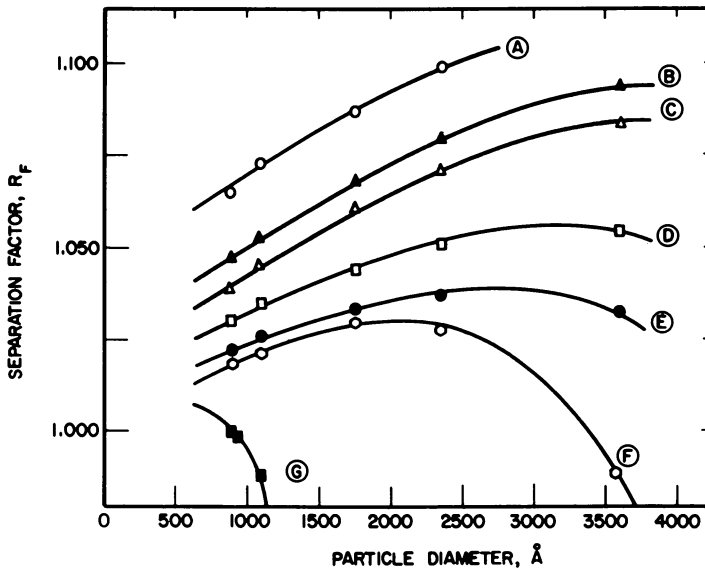


Figure 2. Effect of ionic strength on  $R_F$  for different polystyrene particle sizes using SLS or AMA in eluant.

Molar concentrations in millimoles (quantities in parentheses are total ionic strengths calculated from Equation 4). (○) 0.33mM AMA; (▲) 1.29mM AMA; (△) 2.78mM AMA; (□) 23mM SLS (60mM); (●) 30mM SLS (84mM); (○) 35mM SLS (101mM); (■) 105mM (342mM).

polystyrene standards for a variety of ionic strengths using surfactant either sodium lauryl sulfate, SLS, or aerosol MA, AMA, sodium dihexylsulfosuccinate as noted, only in the eluant phase. Curves A, B, and C are for concentrations of SLS or AMA below the CMC (CMC of AMA = 0.028M, (20), CMC of SLS = .008M, (21)) in which case the ionic strength is given by the standard definition

$$I = 1/2 \sum C_i Z_i^2 \quad (3)$$

where  $C_i$  is the total bulk concentration of species  $i$  and  $Z_i$  is the ionic charge with the summation taken over all ionic species. Curves D, E, F, and G are for concentrations of SLS above the CMC. The close correlation between these curves and those of Figure 6, reference 1, indicate that the contribution of the anionically charged SLS micelles (above the CMC) may be accounted for in terms of the ionic strength.

From electrophoretic data for SLS micelles under various ionic conditions (22), values of 80 for the aggregation number and 23 for the effective charge of the kinetic micelles can be used. This gives the following formula for the eluant total ionic strength.

$$I = 1/2 [[Na^+](+1)^2 + [SL^-](-1)^2 + [SLS]_m(Q)^2] \quad (4)$$

In equation (4)  $[Na^+]$  is the total molar concentration of free sodium ions,  $[SL^-]$  is the molar concentration of ionic  $C_{12}H_{25}SO_4^-$ , and  $[SLS]_m$  is the concentration of the SLS micelles. The corresponding ionic strengths are indicated in the figure heading. The capillary model can also be used to account for the ionic strength effects seen in Figure 2 and is discussed elsewhere (23).

A practical upper limit for the fractionation of particles by HDC exists using 20  $\mu$ m packing (1). In order to further elucidate this effect a series of runs was made using a column by-pass line to allow turbidity peak area comparisons for the same samples run through the column and by-pass. Table I shows percent recoveries based on the turbidity signal for various particle sizes of polystyrene (PS), polyvinylchloride (PVC), and polystyrene butadiene (PSBD) at a low ionic strength of  $4.4 \times 10^{-4}$ M SLS and a wavelength of 254 nm. Particle diameters less than about 250 nm are essentially all recovered, while the practical upper limit is about 350 nm. Reduced recovery may be due to a deposition of particles on the packing beads or a "filtration" effect due to the small degree of polydispersity of the packing (23).

Complete recoveries are essential for the calculation of accurate particle size distributions from HDC data. In Small's work (1) NaCl was used to increase the ionic strength of the eluant phase, however, quantitative results were not reported for any of the recoveries, especially at high ionic strengths, other than the statement that no latexes of 338 nm or 357 nm diameter were eluted at 0.176 M. In our case using SLS only in the mobile

phase leads to significantly improved sample recoveries. Table II shows a comparison using polystyrene latices and either NaCl or SLS as the ionic species.

Table I. Percent Recoveries of Latexes in HDC

<u>Particle Diameter (<math>\text{\AA}</math>)</u>	<u>% Recovery</u>
880 PS	100
910 PS	100
1090 PS	100
1160 PVC	100
1400 PVC	100
1760 PS	100
2140 PVC	47
2340 PS	75
3140 PSBD	31
3570 PS	13

Table II. Percent Recoveries of Polystyrene Using SLS and NaCl

<u>Particle Diameter (<math>\text{\AA}</math>)</u>	<u>I = 0.090 M*</u>	<u>I = 101 M**</u>
880	64	100
1090	49	100
1760	40	100
2340	22	81
3570	3	22

\*I = 0.090 M (0.017 M SLS + 0.050 M NaCl)

\*\*I = 0.101 M (0.035 M SLS)

The increased concentration of NaCl can lead to poor recoveries of latex, probably due to flocculation and adsorption of the particles onto the packing. However, the use of only SLS in the mobile phase can significantly improve recoveries even at these high ionic strengths and no doubt reflects the stabilizing effect of the adsorbed surfactant on the latex. At very high SLS concentrations, such as curve G of Figure 2 where  $I = 0.342M$ , only the 88 nm, 91 nm, and 109 nm particles eluted and at 10 to 15% recovery. Nonetheless, this ionic strength is more than double that reported for the highest concentration of NaCl used by Small (1).

Figure 3 shows calibration plots of  $\log$  (particle diameter) vs. elution volume difference ( $\Delta V$ ) between marker and particle using three different monodisperse latexes at a low eluant ionic strength of 1.29 mM SLS. These results illustrate the feature of universal calibration behavior predicted by the capillary bed model as mentioned earlier. Of note also is the fact that the curve deviates from linearity for the 38 nm particle and begins to approach the origin as also indicated by the model calculations.

As noted before, the whole spectrum of particle sizes between 38 and 357 nm is encompassed with a  $\Delta V$  of 4.0 ml or about 6% of the total column void volume. This low capacity of the HDC system is counterbalanced by its excellent resolution both of itself and in comparison to porous packing systems. The latter point is addressed in the next section.

### LEC and Porous HDC

Porous packed systems represent in addition to the hydrodynamic effect, the possibility for separation due to size-related exclusion of particles from the pores, essentially LEC. In this section a brief overview of some of our more recent results pertaining to the question of pore size distribution effects will be given. More detailed discussions are presented elsewhere (23,24).

### Experimental

The following is a description of the experimental set-up and conditions used for the investigation of porous systems.

#### 1. Equipment:

The experimental set-up used for porous chromatography is virtually identical to that used for HDC as described elsewhere (16,17). The use of stainless steel columns for the LEC work required 316 stainless steel column end-fittings and 1/16" O.D. capillary tubing.

#### 2. Columns and Packing:

The packing material used for the LEC work was Controlled-Pore Glass (CPG) from Electronucleonics, Fairfield, N.J. with various pore diameters similar to those used by others (6,25) (500-10,000 Å). Each 4.6 mm I.D. x 100 cm column was dry packed with the CPG of a specific pore size by tapping and vibration until a terminal bed volume was reached. Stainless steel 20- $\mu$ m frits were used on each end of the column along with the appropriate low-dead volume end-fittings.

For the work with large-pore, porous systems, Fractosil 25,000 silica glass was used (EM Laboratories, #9395-3E) having a particle size ranging from 63 to 125  $\mu$ m and a nominal pore size of 2.5  $\mu$ m. Fractosil has a highly irregular geometry and an extremely high porosity as shown by scanning electron microscopy (23). The pores can be considered to be essentially open and flow through, with little, if any, dead spaces. The porous glass was pre-washed before packing with hot, distilled water several times to remove any residual inorganic contaminants. The glass was then slurry packed into a glass column (9.0 mm I.D. x 110 cm) with slight tapping and vibration, until a terminal bed volume was reached. Typical residence times of a latex sample through the Fractosil column were 30 to 40 minutes at a flow rate of 1.5 ml/min.

The mobile phase consisted of either sodium lauryl sulfate

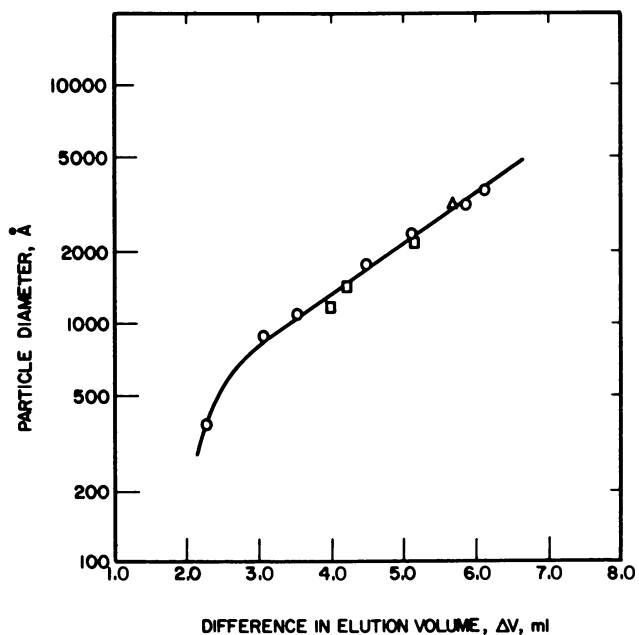


Figure 3. HDC universal calibration curve (eluant ionic strength 1.29mM AMA; monodisperse lattices: (○) polystyrene; (□) polyvinyl chloride; (△) poly(styrene-co-butadiene))

(SLS) or sodium dihexylsulfosuccinate (AMA) with no added salt. Monodisperse latex (the Dow polystyrene standards and PVC standards) samples were used.

### LEC Results

Experimentation with Controlled-Pore Glass involved the use of several column sets packed with the pore diameters in angstrom units shown in Table III.

Table III. Porous Column Setup

	<u>Set I</u>	<u>Set II</u>	<u>Set III</u>
Column A	500	1000	10,000
Column B	1000	2000	----
Column C	2000	3000	----

Each set of columns was run with AMA as the surfactant in the mobile phase at a concentration of  $5.2 \times 10^{-3}$  M, and  $R_F$  vs.  $D_p$  data were obtained using the polystyrene standards. These results are shown in Figure 4 and illustrate the effect of pore size distribution on the values of  $R_F$ . Figure 5, the calibration curve for Set I, shows two distinct linear regions: that for 880, 910, and 1090 Å diameter particles and that for 1760, 2340, and 3570 Å. Figure 5 also includes data obtained with the PVC standards and for both systems the changed slopes indicate the smaller particles are penetrating the porous matrix and that the larger particles are being totally excluded from the pores for this particular pore size distribution. This sharp distinction between penetration and exclusion regions of the calibration curve points to an upper limit on the diameter of the particles which can penetrate the pores. Pore diameters must be two to three times greater than the particles to be fractionated for significant pore penetration to occur. A much less dramatic effect is seen for the  $R_F$  curve of Set II where pores of up 3000 Å were used resulting in a greater availability for pore penetration by all the particles. For Set III, where only pores of 10,000 Å were used, all particles can now pass through all the pores resulting in a nearly linear dependence of  $R_F$  vs.  $D_p$ .

The values of  $R_F$  using the small pore diameters of CPG packing such as for Set I and Set II are considerably larger than those found for HDC. As with Coll's work, this is due to the fact that the marker species ( $\text{Na}_2\text{Cr}_2\text{O}_7$ ) can sample the total column volume and since most of the latex particles sample only a small fraction, if any, of the pore volume, the resulting values for  $R_F$  are large. Note, however, that when pores of 10,000 Å are used,  $R_F$  values are much lower (nearer to those of HDC) since now latex and marker can both sample a significant fraction of the pores. Universal calibration has also been

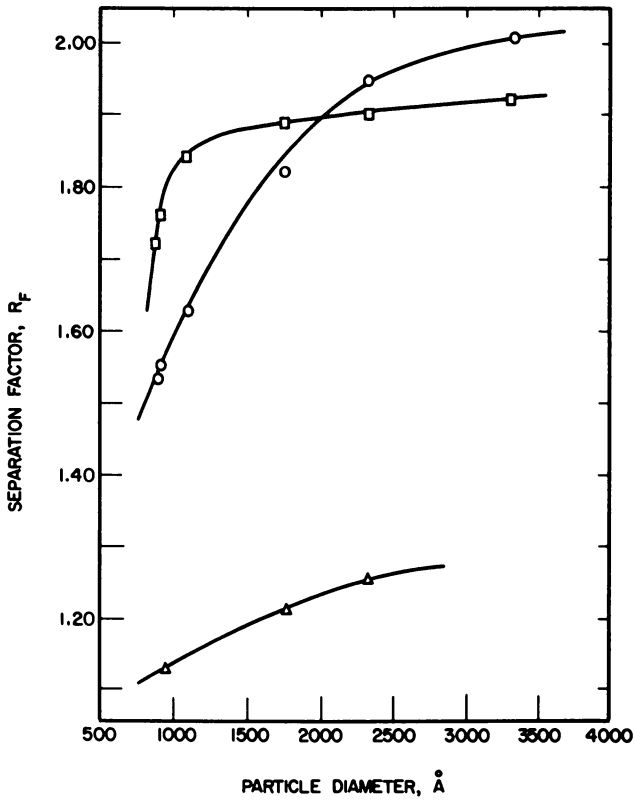


Figure 4. Effect of pore size distribution on  $R_F$  for various LEC systems at 5.2mM AMA (pore diameters: (□) 500, 1000, 2000 Å; (○) 1000, 2000, 3000 Å; (△) 10,000 Å)

observed for a similar system although at high ionic concentration (25).

Calculation of material balances of the polystyrene latexes through these LEC systems showed significant retention of the sample within the column. Percent recoveries of polystyrene latexes calculated at 254 nm for the columns of Set II are given in Table IV. The small particle sizes (<1000 Å) are completely recovered, while significant loss of sample is seen for the larger particle sizes.

Table IV

Percent Recoveries of Polystyrene Latexes Using Column Set II

$D_p$ (Å)	%
880	100
910	91
1090	100
1760	45
2340	24
3570	2

Peak skewing or tailing of the latex chromatographic peaks exhibited a general increase with increasing particle size, as also noted by Coll (6). This was attributed to steric exclusion from the pores as the particle diameters approached the upper limit of the pore size distribution. However, increasing skewness with increasing particle size, as well as the corresponding decrease in percent recoveries of sample is a strong indication of particle entrapment within the porous bed. It points to the necessity of using a more uniform, larger pore size.

#### Porous HDC Results

The rate of particle transport using Fractosil packing with a nominal pore size of 2.5  $\mu\text{m}$  is considerably different from that of the previously described LEC systems. Since the specified pore size of the Fractosil packing is almost an order of magnitude larger than the particle diameters to be fractionated, virtually complete penetration of the pores by all the particle diameters is to be expected. The partition coefficients measured for the polystyrene latexes on the Fractosil system are compared to values obtained using the LEC system of Set II at an ionic strength of  $5.5 \times 10^{-3}$  M, and are shown in Table V. The significant increase in the degree of pore penetration by all particle diameters is clearly evident with the Fractosil system. This system might be more accurately described as an example of permeation chromatography with the enhanced hydrodynamic effects within the pores increasing the rate of particle transport through the bed, thus



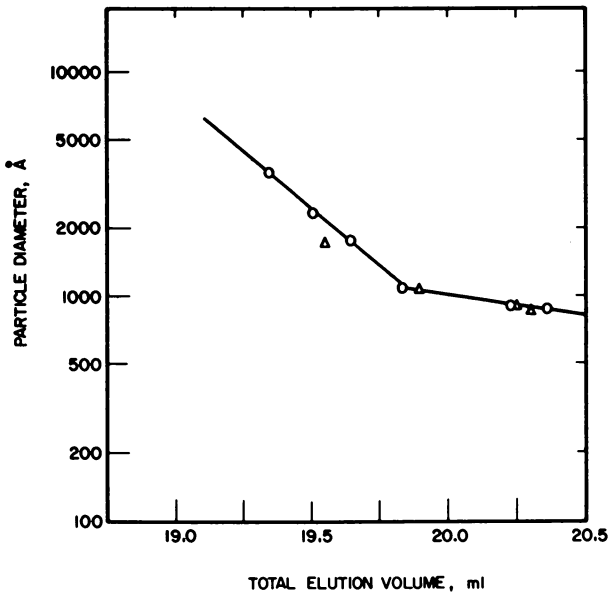
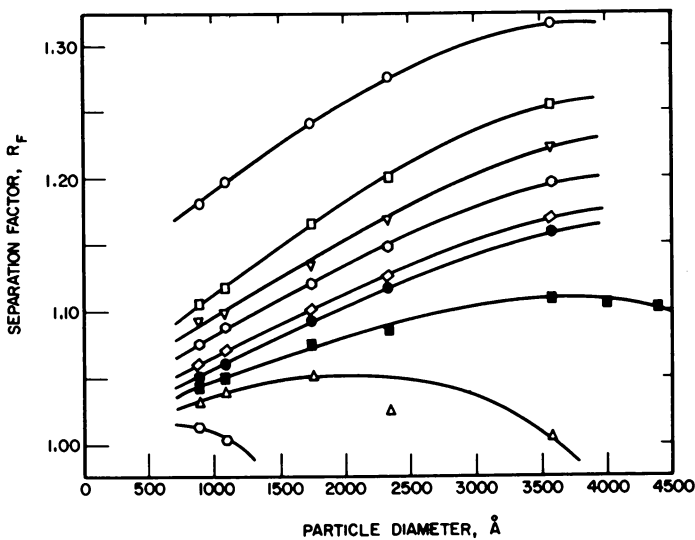


Figure 5. Calibration curve for LEC system of Set I (500, 1000, 2000 Å pore sizes): (○) polystyrene standards; (△) polyvinyl chloride standards



Plenum Publishing Corporation

Figure 6. Effect of ionic strength on  $R_F$  for different polystyrene particle sizes using the porous Fractosil system (24).

Molar concentrations in millimoles (quantities in parentheses are total ionic strengths calculated from Equation 4). (○) 0.22mM; (□) 0.55mM SLS; (▽) 1.03mM SLS; (◇) 1.29mM AMA; (◇) 5.15mM AMA; (●) 10.1mM AMA; (■) 21mM SLS (53mM); (△) 35mM SLS (101mM); (○) 105mM SLS (342mM).

the terminology porous HDC of Figure 1 is indicated for this system. The CPG system is more of an example of exclusion chromatography (exclusion from the porous matrix) in which only the hydrodynamic effects of the interstitial regions predominate, as in nonporous HDC. The relative difference between partition coefficients for the various particle sizes of the CPG system of Table V, although, seem to indicate superior particle separation over the Fractosil. However, the improved peak separation resolution seen with LEC needs to be balanced against the possibility of problematical size distribution results.

Table V. Partition Coefficients for CPG and Fractosil Packings

$D_p$ (Å)	CPG*	Fractosil <sup>†</sup>
Na <sub>2</sub> Cr <sub>2</sub> O <sub>7</sub>	1.00	1.00
800	0.25	0.84
910	0.23	0.83
1090	0.16	0.81
1760	0.02	0.75
2340	0	0.69
3570	0	0.59

\*3 columns: Pore sizes of 1000, 2000, 3000 Å (Set II)

<sup>†</sup>1 column: Pore size of 25,000 Å

Figure 6 shows the results of a series of experiments to determine the dependence of the separation factor,  $R_F$ , as a function of eluant ionic strength for the Fractosil system. Here, the ionic strength ranges from  $2.2 \times 10^{-4}$  M to 0.342 M and includes only surfactant at concentrations above and below the CMC. As in HDC, the particles move with an average velocity greater than that of the fluid stream, and the  $R_F$  values are up to 10% greater than those observed for the corresponding ionic strengths in HDC. This fact indicates the significant role played by the 2.5  $\mu$ m pores in the enhancement of the rate of particle transport through the bed, even though the packing size of the silica glass ranges from 63-120  $\mu$ m. According to Small (1), as the packing size increases,  $R_F$  will decrease; however, we see the opposite effect due to the presence of the porous matrix, indicating the hydrodynamic effects exhibited within the interstitial void regions are significantly less than those within the pores.

Several of the concentrations in Figure 6 were above the CMC of SLS and since the trends were exactly the same as seen in Figure 2, the contribution of the anionically charged micelles was accounted by Equation 4 to calculate the total ionic strengths indicated.

Overall material recoveries were also significantly improved by use of emulsifier above the CMC, as was seen in the previous

section with HDC. It is interesting to note that at moderate to high ionic strengths (>50 mM) the recovery of latex from the column was as good as the HDC system and that the porous matrix and highly irregular packing geometry contribute little to material loss. Also, the symmetrical nature of the Fractosil peaks for polystyrene, although non-Gaussian, tend to further support the concept of complete particle penetration of the pores (23).

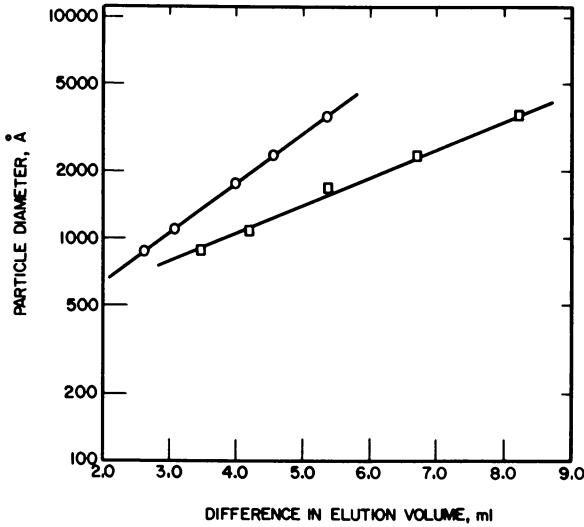
Figure 7 shows a comparison between the calibration curves ( $\log D_p$  vs.  $\Delta V$ ) for the HDC and porous Fractosil systems for the polystyrene standards at an ionic strength of  $1.29 \times 10^{-3}$  M. The range of  $\Delta V$  for the Fractosil system for particle diameters of 880 and 3570 Å is almost 75% greater than that of HDC, even though total column volumes for the Fractosil and HDC systems are 50 cm<sup>3</sup> and 68 cm<sup>3</sup>, respectively. The effective elution range of these particle diameters has been significantly increased using the Fractosil, and this behavior is reflected in the magnitude of the separation factor, as shown in Figure 6. As with HDC, the separation factor was found to be independent of flow rate (23). As discussed elsewhere (23) the capillary bed model can be extended to account for the effect of the pores on the separation factor analysis.

The slopes of the calibration curves for the HDC and Fractosil systems are 0.512 and 0.289, respectively. This indicates that the "resolution of the peak separation" for the Fractosil system is superior to that of HDC, since resolution is considered to be inversely proportional to the slope of the log particle diameter -  $\Delta V$  calibration curve (26). However when peak spreading is taken into account, the actual relative resolution between particle populations is less for the Fractosil system (24) a result which indicates that overall, for size distribution resolution, the HDC system is superior.

### Signal Resolution

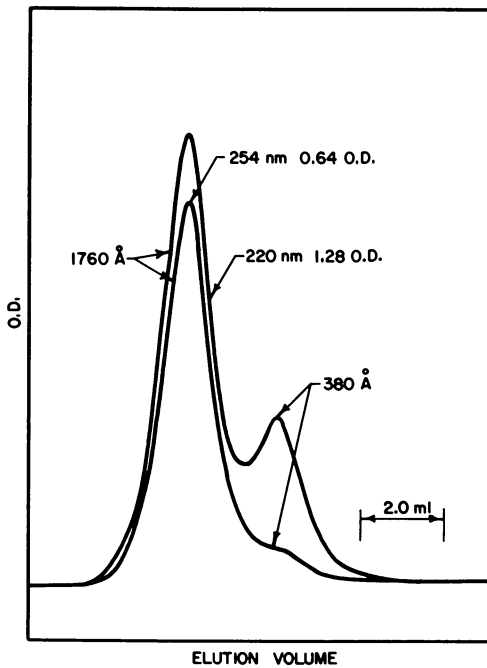
Particle size distribution calculations (19,27) have illustrated that modifications in the more standard methods for evaluating the integral dispersion equation are necessary in order to achieve good comparison between measured and calculated results. A major source of the problem for systems with wide size distributions (and therefore relatively small numbers of small particles) is the strong dependence of the scattering cross section on particle diameter in the nonabsorbing wavelength range. Calculations have indicated that a means for improving relative resolution is to choose a wavelength where the particles can absorb as well as scatter (27).

This feature is illustrated in Figure 8 which shows the turbidity signal characteristics for a 1.0 to 1.2, by weight, mixture of 380 Å and 1760 Å polystyrene standards chromatographed through the HDC columns. The chromatogram shows that when turbidity at 254 nm. wavelength is used (pure scattering) the 380 Å



Plenum Publishing Corporation

Figure 7. Comparison of polystyrene calibration curves for HDC and porous Fractosil systems (eluant ionic strength, 1.29mM AMA; (○) HDC; (□) Fractosil) (24)



Plenum Publishing Corporation

Figure 8. HDC separation of a synthetic bimodal mixture of 380 Å and 1760 Å polystyrene standards at 220-nm and 254-nm wavelength (weight ratio is 1.00/120) (24)

population shows up only as a small shoulder in output despite the fact that the smaller particles are present in a ratio of over 80 to 1 by number. Decreasing the wavelength to 220 nm (in the absorbing region) results in a dramatic change in the relative peak heights as well as the overall signal intensity.

In order to calculate particle size distributions in the adsorption regime and also to determine the relative effects of wavelength on the extinction cross section and imaginary refractive index of the particles, a series of turbidity measurements were made on the polystyrene standards using a variable wavelength UV detector. More detailed discussions are presented elsewhere (23), shown here is a brief summary of some of the major results and conclusions.

Experimentally, the turbidity signal for dilute, non-interacting suspensions, is given by the Beer-Lambert expression.

$$\tau = 2.303 (O.D.) = NR_{ext} X \quad (5)$$

In equation (5),  $\tau$  is the turbidity, O.D. is the optical density measured from the photometer,  $N$  is the number density of particles,  $X$  is the optical path length and  $R_{ext}$  is the extinction cross section. For combined scattering and absorption,  $R_{ext}$  is given by,

$$R_{ext} = R_{scat} + R_{abs} \quad (6)$$

where  $R_{scat}$  and  $R_{abs}$  represent the particle scattering and absorption cross sections respectively. For a given particle size the slope of the optical density versus weight fraction curve can be used in conjunction with equation (5) to determine  $R_{ext}$  and also the specific extinction coefficient (23). As a good approximation one can assume over a limited size range (28) that

$$R_{ext} \propto R_p^k \quad (7)$$

A resulting log-log plot of the  $R_{ext}$  versus  $R_p$  data is shown in Figure 9 for a wavelength of 220 nm. From the slope of plots such as these the value of  $k$  for various wavelengths was determined and these results are shown in Figure 10. These results illustrate, in effect, a means for varying the signal dependence on particle size so as to optimize the desired size averaging characteristics of the instrument output. This illustrates a concept which has been previously addressed computationally in the literature (25). Figure 10 shows that at 254 nm a roughly fourth power dependence of  $R_{ext}$  on particle radius is occurring while at 227 nm the third power dependence indicates the signal will be proportional to the mass of the suspension and therefore be a weight averaged signal independent of particle diameter (25). At 220 nm the size dependence has dropped to 2.7.

Calculations of the extinction cross section at a given wave-

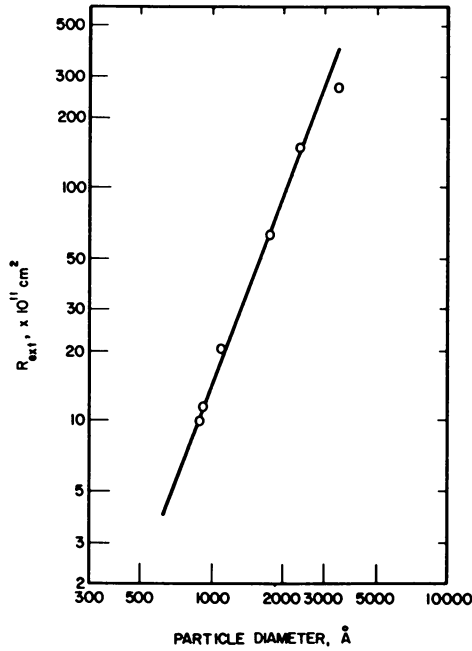


Figure 9. Experimental extinction cross section  $R_{ext}$  for polystyrene as a function of particle diameter at 220 nm

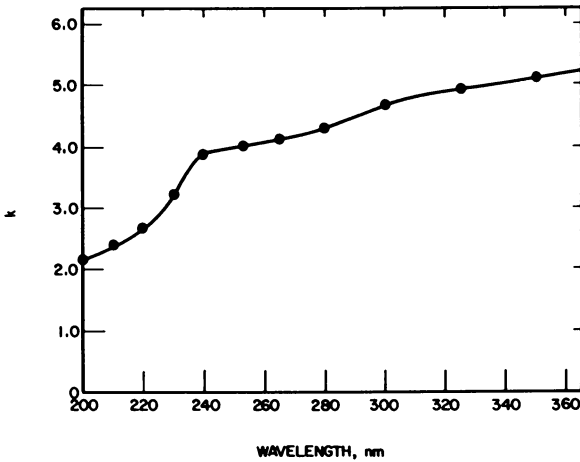


Figure 10. Power dependence of the extinction cross section for polystyrene as a function of wavelength for particle diameters 88 nm to 357 nm

length were also carried out as a function of the imaginary refractive index using the Mie Theory algorithm discussed elsewhere (27). By comparison with the experimentally determined  $R_{ext}$ , best fit values of the imaginary refractive index were obtained. (Since  $R_{ext}$  shows a much stronger dependence on particle size in the small particle region, the best value of imaginary refractive index was obtained from the fit in this region (23)). Figure 11 shows the resulting values for refractive index as a function of wavelength for the polystyrene standards.

### Resolution of Particle Size Distribution

In order to calculate a particle size distribution directly from the output chromatogram for a polydisperse system, the integral dispersion equation for the chromatogram signal,  $F(V)$ , as a function of elution volume,  $V$ , needs to be evaluated (27).

$$F(V) = \int_{V_1}^{V_2} W(y) G(V,y) dy \quad (8)$$

In equation (8),  $G(V,y)$  is the normalized instrumental spreading function for the component with a mean retention volume  $y$  and  $W(y)$  is the area under the chromatogram due to that species. The integral is evaluated over the limits of the chromatogram,  $V_1$  to  $V_2$ . The area  $W(y)$  is related to the number density of the particles by

$$N(y) = \frac{2.303 W(y)}{R_{ext} X} \quad (9)$$

The solution of equation (8) for  $W(y)$  involves approximating the instrumental spreading function and then employing any of several means for inverting the integral (27). It is important to realize that the nonlinear conversion of  $W(y)$  to  $N(y)$  through equation (9) is a major factor in size distribution resolution with respect to small particles. As indicated in the previous section this problem is exacerbated when the turbidity signal is used at wavelength where the particles are pure scatterers. This necessitates accurate fitting of the chromatogram for the distribution especially in the small particle region. The choice of a wavelength in the absorbing region for improved signal detection decreases the nonlinear dependence between  $N(y)$  and  $W(y)$ .

A modification of the method proposed by Ishige, Lee, and Hamielec (29) has been shown to work well for calculating  $W(y)$  to compute a PSD (27). This iterative method starts with a first estimate of  $W(y)$  obtained from the polydisperse chromatogram assuming no axial dispersion. Equation (8) is then evaluated from which the computed chromatogram  $F^*(V)$  is obtained. From

this, the distribution  $W(y)$  is then corrected at each integration point depending upon the error between the computed and measured chromatogram. The correction factor has the following form:

$$w_i^{j+1} = w_i^j \prod_{k=-n}^n \frac{F_{i+k}^*}{F_{i+k}} \quad (10)$$

where  $j$  refers to the level of iteration,  $F^*$  is the computed chromatogram and  $F$  the actual chromatogram. The quantity  $\alpha$  is a weighting coefficient taken from the actual contributions of the neighboring particle sizes within  $+ 2\sigma$  of the elution volume of interest, where  $\sigma$  is the standard deviation or second moment of the chromatogram. The number of symmetric terms about  $F_i$  (i.e.,  $n$ ) was chosen according to the spread in the chromatogram. The interested reader is referred to reference (27) for a complete detailing of the development of the various methods for calculating  $W(y)$  for a PSD.

Since the modified iterative method is completely numerical, data can be used directly from the monodisperse chromatograms to characterize the axial dispersion, eliminating the need for a specific axial dispersion function. The monodisperse standards were used to represent the spreading behavior for particle ranges as given in reference (27).

An illustration of the potential for improved resolution in the determination of size distributions with particles in the small size range is indicated in Figures 12 to 14. These results are for a polydisperse polystyrene (labelled 2D2) which has been doped by the addition (29% by number) of the Dow 380 Å polystyrene standard.

Two mixtures were chromatographed through the HDC columns under standard operating conditions with the turbidity detection signal measured at either 254 nm or 220 nm wavelength. Figure 12 shows the chromatogram fit resulting from the previously mentioned algorithm and Figure 13 shows the resulting particle size distribution calculation and a comparison with the distribution determined by electron microscopy. Despite the close fit of the chromatogram, the calculated size distribution shows a marked mismatch in the small particle region. Figure 14 shows that for the same system when the turbidity signal is instead measured at 220 nm and the same size distribution analysis carried out, the agreement between calculated and measured particle size is greatly improved.

As a final illustration of the poorer resolving power of the porous Fractosil system alluded to earlier, Figures 15 through 18 illustrate results of the size distribution analysis of a bimodal latex mixture chromatographed through the Fractosil column at 220 nm. The bimodal mixture was synthesized from a mixture of the 88 nm, 91 nm, and 109 nm standards mixed in a 60:40 number ratio with the 176, 190, and 234 nm standards. Figure 15 shows a good chrom-



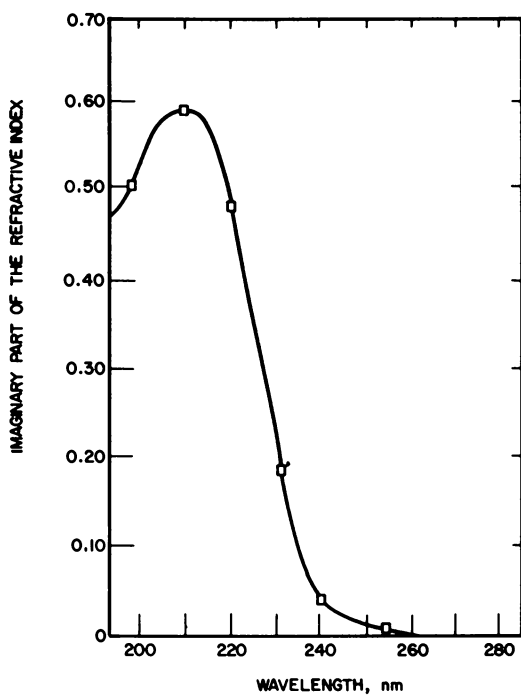


Figure 11. Imaginary part of complex refractive index for polystyrene

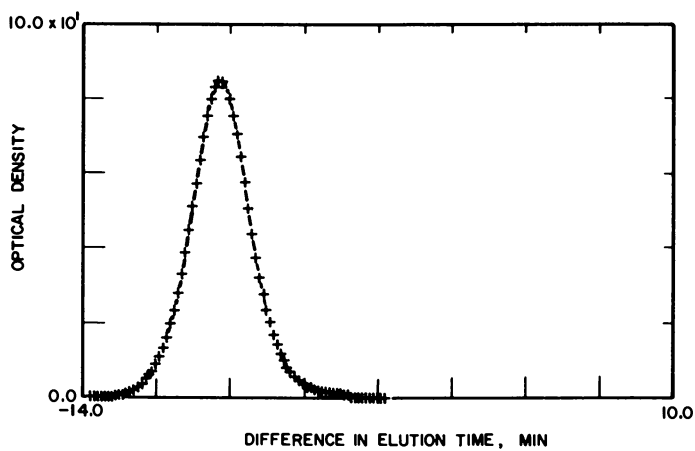


Figure 12. Experimental (—) and calculated (+) chromatogram for the 2D2/380 latex at 254 nm

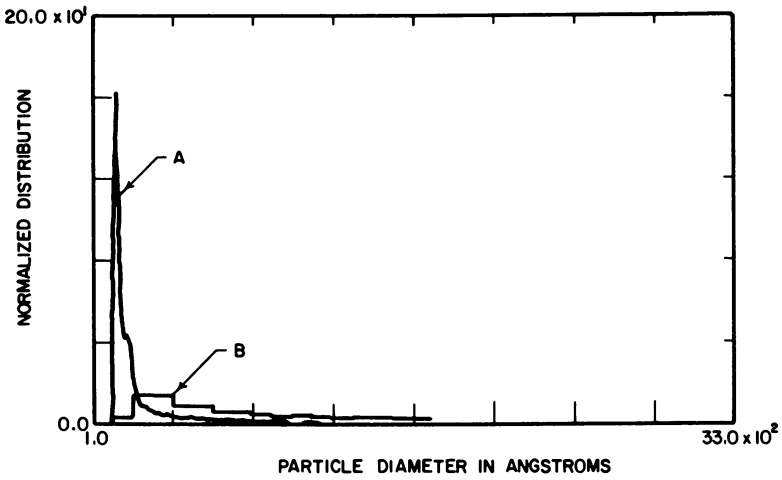


Figure 13. Comparison between measured particle size distribution for 2D2/380 latex (B) and that calculated at 254 nm (A)

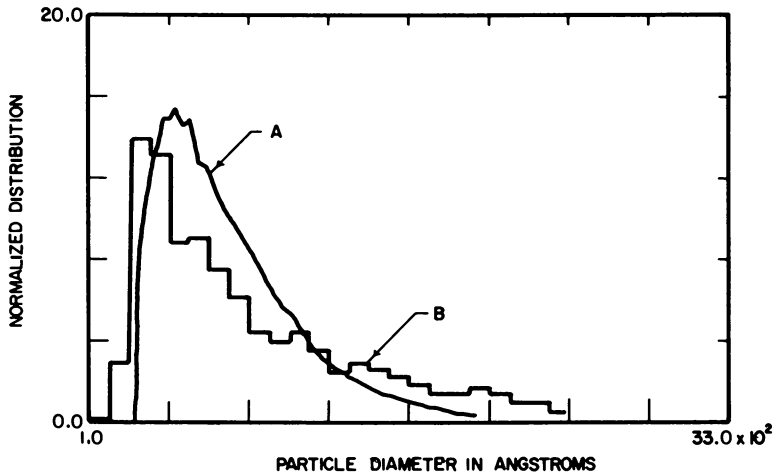


Figure 14. Comparison between measured particle size distribution for 2D2/380 latex (B) and that calculated at 220 nm (A)

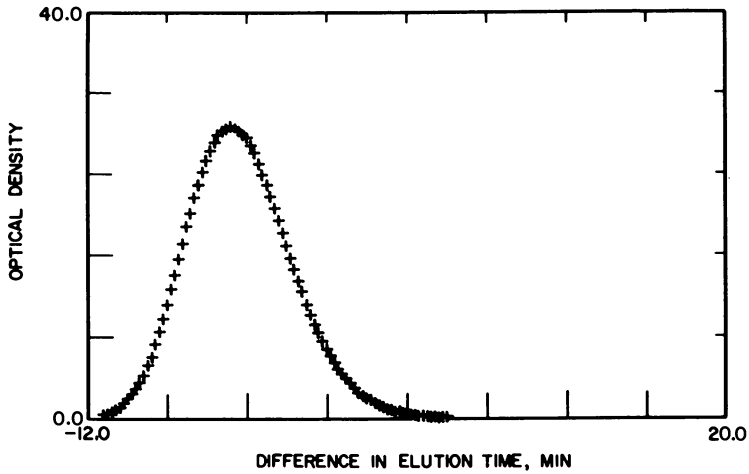


Figure 15. Experimental (—) and calculated (+) chromatogram for the bimodal system at 220-nm wavelength for the Fractosil system

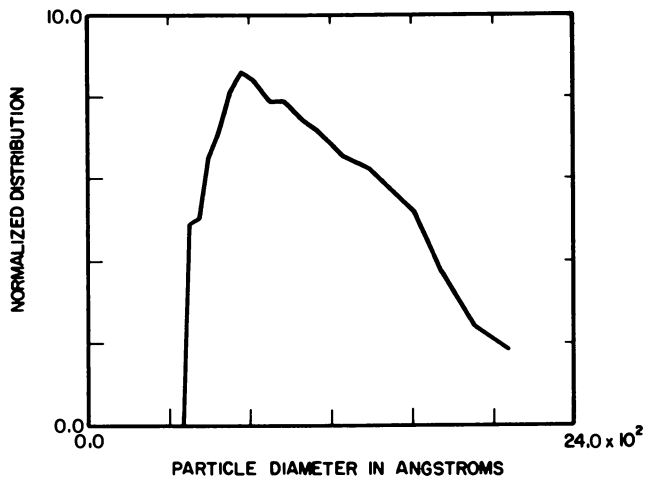


Figure 16. Calculated size distribution for the bimodal mixture of Figure 15

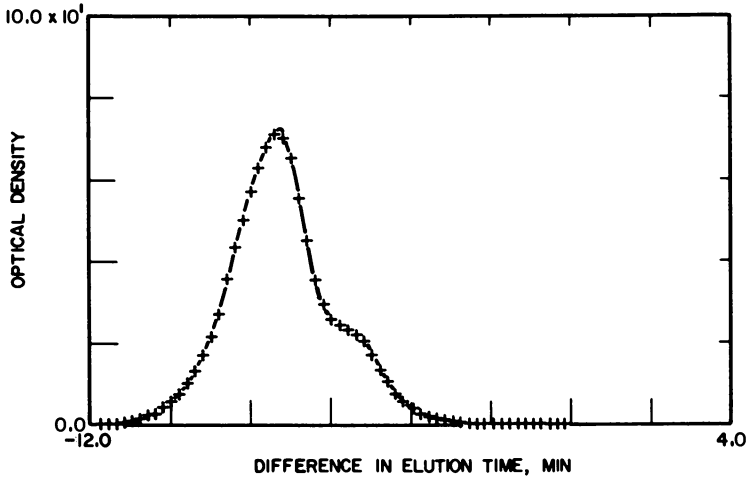


Figure 17. Experimental (—) and calculated (+) chromatogram for the bimodal system at 220-nm wavelength using the HDC columns

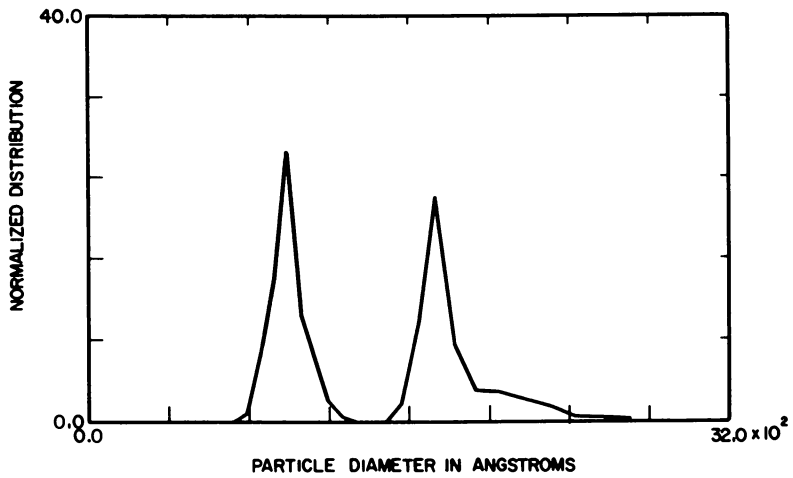


Figure 18. Calculated particle size distribution from the chromatogram of Figure 17

atogram fit, however, for the resulting size distribution calculation, Figure 16 shows that the Fractosil system is unable to resolve the discontinuous mixture into its primary components. Figure 17 shows the chromatogram obtained from the HDC columns for the same system clearly indicating the presence of two populations while Figure 18 shows the calculated bimodal distribution obtained from the chromatogram.

### Summary and Conclusions

In summary, we believe that several important features of particle size analysis by packed column chromatography have been demonstrated. First, the size separation mechanism can be quantified by means of a simple model which accounts for all of the important parameters in the process and enables an accurate understanding of the conditions for universal calibration behavior. Second, though in principle improved resolution should be possible using porous packing and increases in the separation factor,  $R_F$  over HDC are seen, the increased peak spreading which is also characteristic of the systems studied leads to an overall decrease in the specific resolution. Third, complete size distribution determination is possible using calculation algorithms which are variations on methods developed for GPC. Also improvements in the signal detection characteristics are possible by using wavelengths which optimize the particle size dependence of the signal intensity over the particular particle size range of interest. Improvements in the particle size resolving power of a given instrument are thus possible.

### Acknowledgments

This work has been carried out under a grant from the National Science Foundation (ENG 77-0741) along with funds from the Industrial Liaison Program of the EPI. One of us (D.N.) has also received partial support from a Lever Brothers Company Foundation Fellowship.

### Literature Cited

1. Small, H. J. Colloid Interface Sci., 1974, 48, 147.
2. Small, H.; Saunders, F. L.; Solc, J. Adv. Colloid Interface Sci., 1976, 6, 237.
3. Ruckenstein, E.; Prieve, D. C. AIChE J., 1976, 22, 276.
4. Ruckenstein, E.; Marmur, A.; Gill, W. N. J. Colloid Interface Sci., 1977, 61, 183.
5. Krebs, K. F.; Wunderlich, W. Angew. Makromol. Chem., 1971, 20, 203.
6. Coll, H.; Fague, G. R. J. Colloid Interface Sci., in print.
7. Singh, S.; Hamielec, A. E. J. Appl. Polym. Sci., 1978, 22, 577.

8. Mullins, M. E.; Orr, C. Int. J. Multiphase Flow, in press.
9. Noel, R. J.; Gooding, K. M.; Regneir, R. E.; Ball, D. M.; Orr, C.; Mullins, M. E. J. Chromatogr., 1978, 166, 272.
10. Segre, G.; Silberberg, A. J. Fluid Mech., 1962, 14, 115.
11. Goldsmith, H. L.; Mason, S. G. J. Colloid Sci., 1962, 17, 448.
12. Giddings, J. C. J. Chromatogr., 1971, 125, 3.
13. Giddings, J. C.; Meyers, M. N.; Moellmer, J. F. J. Chromatogr., 1978, 149, 501.
14. Giddings, J. C.; Fisher, S. R.; Meyers, M. N. Am. Labor., 1978, 10, 15.
15. Giddings, J. C. J. Colloid Interface Sci., 1977, 60, 575.
16. Stoitsits, R. F.; Poehlein, G. W.; Vanderhoff, J. J. Colloid Interface Sci., 1976, 57, 337.
17. McHugh, A. J.; Silebi, C.; Poehlein, G. W.; Vanderhoff, J. W. "Colloid and Interface Science"; vol. IV, Academic Press, New York, 1976, p. 549.
18. Silebi, C. A.; McHugh, A. J. AIChE J., 1978, 24, 204.
19. Silebi, C. A.; McHugh, A. J. "Emulsions, Latices, and Dispersions", Becher, P.; Yudenfreund, M. N., Ed., Marcel Dekker, New York, 1978, p. 155.
20. Warson, H. "Application of Synthetic Resin Emulsions", Ernst Benn Ltd., London, 1972, p. 74.
21. Vijayendran, B. R. J. Colloid Interface Sci., 1977, 60, 418.
22. Mysels, K.; Stigter, D. J. Phys. Chem., 1955, 59, 45.
23. Nagy, D. J. "Column Chromatography of Polymer Latexes", PhD Dissertation, Lehigh University, 1979.
24. Nagy, D. J.; Silebi, C. A.; McHugh, A. J. "Polymer Colloids II", Fitch, R. M., Ed., Plenum, to be published.
25. Hamielec, A. E.; Singh, S. J. Liq. Chromatogr., 1978, 1(2), 187.
26. Friis, N.; Hamielec, A. E. Adv. Chromatogr., 1975, 13, 41.
27. Silebi, C. A.; McHugh, A. J. J. Appl. Polym. Sci., 1979, 23, 1699.
28. Kerker, M. "The Scattering of Light and Other Electromagnetic Radiation", Academic Press, New York, 1969, p. 331.
29. Ishige, T.; Lee, S. I.; Hamielec, A. E. J. Appl. Polym. Sci., 1971, 15, 1607.

RECEIVED May 27, 1980.

# Size Exclusion Chromatography of Model Latices

## A Feasibility Study

J. E. JOHNSTON, C. L. COWHERD, and T. B. MacRURY

Union Carbide Corporation, South Charleston, WV 25303

The rapid, accurate, and precise measurement of particle size distributions is required in both laboratory synthesis and commercial production. It is essential for the design of new latex products and processes and for the monitoring of existing commercial processes. Two of the chromatographic techniques which offer promise in the area of particle size distribution determinations are hydrodynamic chromatography (HDC) and liquid or size exclusion chromatography (SEC). The former has been investigated by Small (1, 2, 3), McHugh and co-workers (4, 5, 6), and Stoitsits (7) and the latter by Krebs and Wunderlich (8), Gaylor and James (9), Coll, Fague and Robillard (10) and Singh and Hamielec (11).

The two techniques differ in that HDC employs a nonporous stationary phase. Separation is affected as a result of particles of different size sampling different velocities in the interstitial spaces. Size exclusion chromatography is accomplished by superimposing a steric selection mechanism which results from the use of a porous bed. The pore sizes may vary over a wide range and the separation occurs as a result of essentially the same processes present in the gel permeation chromatography of macromolecules.

If a single pore size is employed in the stationary phase, which is larger than the largest particle to be analyzed, the technique has been termed porous HDC. A model for the separation in this type of system has been described by DiMarzio and Guttman (12, 13).

The nature of the stationary phase in SEC precludes the elution of sample prior to a volume equivalent to that contained in the interstitial spaces,  $V_I$ . This is also known as the excluded volume,  $V_E$ . The remainder of the total system void volume,  $V_T$ , is made up of the pore volume,  $V_p$ . For an eluting species the volume increment at which it appears,  $V_S$ , will be related to the interstitial and pore volumes as:

$$V_S = V_I + k_d V_p$$

where  $k_d$ , the partition coefficient, is a measure of the retardation of the particle because of penetration of the pores. If the particle samples all of the pores  $k_d = 1$ , if none,  $k_d = 0$ . Since in the absence of adsorption or diffusion effects,  $0 < k_d < 1$  the resolution is limited by the available pore sizes. The broader the range of sizes and the greater their density, the larger will be the difference in partition coefficient for different particle sizes. This is the basis for the more efficient, high resolution packings currently available in GPC.

Small (1) has defined a separation factor,  $R_f$ , for HDC:

$$R_f = \frac{V_m}{V_s}$$

where  $V_m$  and  $V_s$  are the elution volumes of an ionic marker species and a colloidal particle, respectively. For HDC, if there are no adsorption effects,  $R_f$  must be  $\geq 1$ . An analogous situation exists in SEC. Because of the presence of pores in the stationary phase, particles of a given size will only sample a portion of the available pore volume, i.e.,  $k_d < 1$ . For this reason, SEC will tend to exhibit higher values of the separation factor,  $R_f$ , than HDC.

It has been observed that improvement in the values of  $R_f$  may be obtained in HDC by decreasing the packing size (1). This is done at the cost of particle size range however, since decreasing the packing size decreases the interstitial channel diameter. In the case of SEC,  $R_f$  may be increased by increasing the range and density of pores without changing the packing diameters and hence without significantly affecting the particle size range. These observations are illustrated in Figure 1 where the effect of changing packing size on  $R_f$  in HDC is shown in comparison to the effect of changing pore size on  $R_f$  in SEC.

The other component of the resolution in chromatographic systems is the tendency for particles of the same size to elute at different retention volumes because of axial dispersion or instrument spreading. The result of this spreading phenomenon is that the effective resolution of the chromatograph is decreased to the extent that instrument spreading increases. This effect is particularly pronounced in SEC of particles because of diffusion in the porous matrix. In the case of gel permeation chromatography, the magnitude of the contribution of instrument spreading to the observed chromatogram is considerably less than in SEC of latices because of the larger values for the diffusion constants of molecules as compared with colloidal particles.

In addition to instrument spreading, which is generally treated as being Gaussian in nature (15, 16), skewing can also be observed in SEC of latices because of entrapment of particles within the porous matrix. This effect generally increases with increasing particle size.

The detector most often employed in SEC of particles is the ultraviolet photometer. Detection takes place at essentially 180



degrees relative to the incident beam. Hence, it is the turbidity,  $\tau$ , which is measured by the decrease in transmitted light:

$$\tau = \frac{1}{\lambda} \ln (100/T) \quad (1)$$

$\lambda$  = optical path length

T = % transmittance

In general, the number of particles present in the cell at a retention volume ( $v$ ) is related to the turbidity as:

$$N(v) \propto \tau (v) K(v)^{-1} D(v)^{-2} \quad (2)$$

where  $K(v)$  = the scattering coefficients from Mie theory  
(18, 19)

$D(v)$  = the particle size at retention volume  $v$  based  
on a calibration curve

The assumptions made at this point are that there is no multiple scattering, i.e., concentrations  $< 0.1\%$ , and that the spheres are nonabsorbing.

Equation (2) is true in the case where there is no instrumental spreading, that is, where all particles present in the detector cell are of exactly the same diameter. Because of axial dispersion, and skewing caused by entrapment or adsorption, corrections for instrumental spreading are required. In this case  $\tau(v)$  is described by:

$$\tau(v) = F(v) = \int_0^{\infty} W(y) G(v,y) dy, \quad (3)$$

where  $W(y)$  is the detector response corrected for dispersion  
 $G(v,y)$  is the instrumental spreading correction function

If  $W(y)$  can be evaluated at each point knowing  $G(v,y)$  and  $F(v)$ , or if the integral can be evaluated analytically, then the number of particles can be determined. Evaluation of  $W(y)$  knowing  $G(v,y)$  can be done iteratively using a form of  $G(v,y)$  proposed by Tung (15, 16). In this method the instrument spreading is assumed to be uniform Gaussian. This approach is not successful for monodisperse samples which exhibit skewing. The method can be refined by the use of a polynomial to describe the change in variance as a function of  $y$  (20). This technique has been extended by Ishige, Hamielec, and Lee (21) for cases in which the spreading function was non-uniform and unsymmetrical. In principle, this technique can be used to recover particle size distributions. In the case

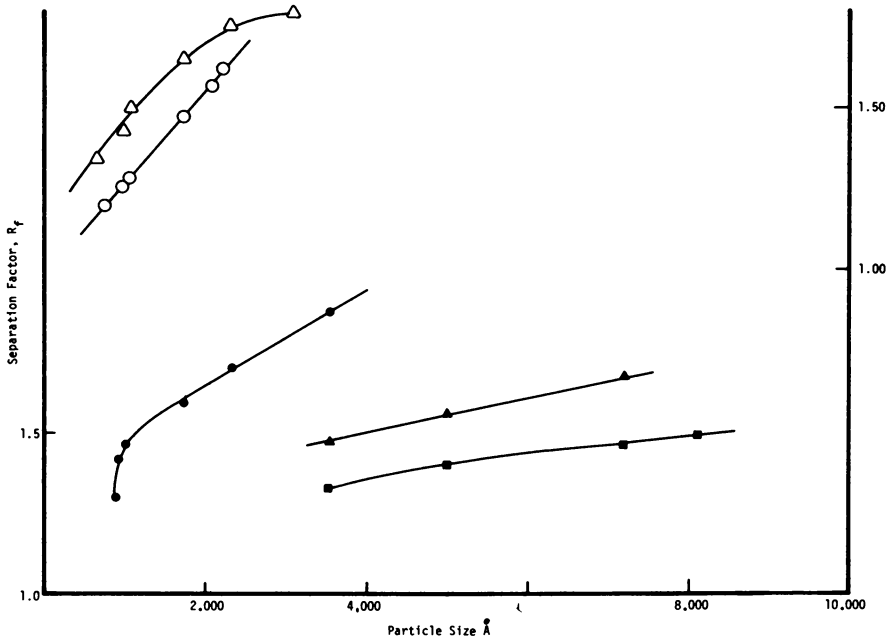


Figure 1. Effect of packing diameter on HDC and pore size on sec (data from Ref. 1: (●) 18  $\mu$ ; (▲) 40  $\mu$ ; (■) 58  $\mu$ ; data from Ref. 10: (○) CPG 3000; (△) CPG 500, 1000, 2000, 3000)

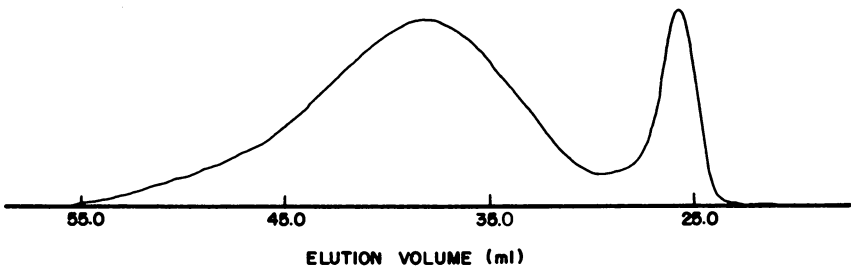


Figure 2. Blend: polystyrene standards (0.103  $\mu$ /0.312  $\mu$  50%/50%)

of HDC, Silebi and McHugh (22) have shown it can provide reasonably good results. However, they noted the deficiency that this approach assumes that the contribution at each elution volume is due to a single particle size. In cases where the instrument spreading is not severe, this assumption may be valid. Our experience has been that this approach breaks down, however, when applied to SEC results in which the spreading corrections are large.

If the integral in Equation (3) can be evaluated analytically without regard to the functional form of  $W(y)$  then the particle size averages may be obtained. Hamielec and Singh (17) have proposed such a method for calculating the various particle diameter averages. Recently, Husain, Vlachopoulos, and Hamielec (23) have extended this treatment to the Mie scattering regime using a series expansion to approximate the scattering coefficients at each elution volume (particle size):

$$K(v)^{-1} = \sum_{i=1}^n (A_i \exp \{-B_i V\}) \quad (4)$$

This technique assumes a Gaussian spreading function and thus does not take into account skewness or kurtosis resulting from instrumental considerations. It can, however, be modified to accommodate these corrections. The particle size averages reported here have been derived using the technique as proposed by Husain, Vlachopoulos, and Hamielec (23).

### Experimental

Three column sets were used in this study. All consisted of 0.95 x 122 cm stainless steel columns slurry packed with Controlled-Pore Glass from Electronucleonics. The configurations were:

- Set I: (1) 3000 Å CPG, 120/200 mesh
- Set II: (1) 3000 Å, (1) 1000 Å, 120/200 mesh
- Set III: (1) 3000 Å, (1) 1000 Å CPG, 200/400 mesh

The mobile phase consisted of degassed distilled water containing 1.0 grams/liter of Aerosol<sup>®</sup>-OT and varying amounts of sodium nitrate,  $\text{NaNO}_3$ . The detector was a DuPont Model 840 UV photometer with a fixed wavelength of 254 nm.

Potassium dichromate was used as a molecular marker to measure total system volume and plate count (1). The three column sets exhibited the equivalent of approximately 250-300 plates per foot. This was adequate, even with Set I, to give near baseline resolution of an equal weight blend of the 103 nm and 312 nm samples as shown in Figure 2. This is approximately an 84:1 number ratio.

## Results and Discussion

The separation factors and partition coefficients for each column set are shown in Tables I, II, and III. As expected, values of  $R_f$  increase with increasing particle size while values of  $k_d$  decrease. The two factors are related as follows:

$$k_d = \left( \frac{1}{R_f} - 1 \right) \frac{V_T}{V_p} + 1 .$$

The sudden decrease in  $k_d$  between 220 and 312 nm samples reflects the almost total exclusion of the larger particle size from the pores.

Table II also shows the effect of electrolyte concentration on  $R_f$  and  $k_d$ . Both effects reflect the fact that at the higher ionic strengths particle/substrate repulsion is decreased, thus effectively increasing the available pore volume at a given particle size. These results are illustrated in Figure 3. Included in this figure are data from work by Nagy (14) with a column set similar in configuration to that employed here.

Separation factor can also be influenced by the size of the packing material. This is shown in Figure 4. The difference in  $R_f$  values is not as large as might be observed in HDC. However, it should be noted that for the smaller packing diameter, i.e., 200/400 mesh, particles larger than about 210 nm do not pass through the column without substantial sample loss. This is the result of the smaller interstitial channel radii obtained with the smaller packing. It should be noted that particle recoveries were not measured for these columns. However, a previous study of particle recoveries using CPG packed columns indicates some loss of sample at particle sizes larger than 1000 Å (14). Interestingly, changing the packing size has little, if any, effect on the partition coefficient, probably because there has been no real change in pore volume.

Values of the calibration curves for the various column sets are given in Table IV. The curves themselves are shown in Figure 5. The slope of the calibration curves decrease with increasing ionic strength. This is the result of reduced electrostatic repulsion between particles and substrate which permits greater penetration of the porous matrix.

The best measure of the resolving capabilities of a given column set takes into account both the slope of the calibration curve and the mean variance exhibited by monodisperse samples over the elution range of the columns. The product of the slope of the calibration curve and the variance,  $D_2 \sigma^2$ , is given in Table V. These values show that despite changes in calibration slope, there is essentially no change in system resolution capability with either greater column length or higher ionic strength.

TABLE I  
SEPARATION FACTOR AND PARTITION COEFFICIENT  
COLUMN SET I

Sample (nm)	$V_{\text{Sample}}$ ml	$R_f$	$k_d$
69	41.8	1.20	0.66
73	41.8	1.20	0.66
98	39.6	1.26	0.57
103	39.2	1.28	0.55
176	34.0	1.47	0.34
209	31.4	1.59	0.23
220	30.8	1.62	0.21
312	26.6	1.88	0.03

---


$$V_{\text{Total}} = 50.00 \text{ ml}$$

$$V_{\text{Interstitial}} = 25.80 \text{ ml}$$

$$V_{\text{Pore}} = V_T - V_I = 24.20 \text{ ml}$$

Column: (1) 3000 Å, 120-230 mesh

Mobile Phase: 0.1% Aerosol <sup>®</sup>-OT, 12.35 mM NaNO<sub>3</sub>

TABLE II  
SEPARATION FACTOR AND PARTITION COEFFICIENT  
COLUMN SET II

<u>Sample (nm)</u>	<u>V<sub>Sample</sub> ml</u>	<u>R<sub>f</sub></u>	<u>k<sub>d</sub></u>
1. 7.0 mM Electrolyte			
69	63.40	1.54	0.32
73	63.40	1.54	0.32
98	61.28	1.60	0.28
103	59.84	1.63	0.25
176	55.32	1.77	0.16
209	53.04	1.84	0.11
220	52.52	1.86	0.10
312	49.52	1.97	0.05
2. 23.0 mM Electrolyte			
69	67.68	1.45	0.40
73	67.60	1.45	0.40
98	64.20	1.52	0.34
103	63.12	1.55	0.31
176	58.72	1.67	0.23
209	55.60	1.76	0.17
220	54.92	1.78	0.05
312	49.52	1.97	0.05

Columns: (1) 3000 Å, (1) 1000 Å CPG, 120/200 mesh

Mobile Phase: 0.1% Aerosol<sup>®</sup>-OT, 2.47 mM/18.5 mM NaNO<sub>3</sub>

V<sub>Total</sub> = 97.84 ml, V<sub>Interstitial</sub> = 47.20 ml

V<sub>Pore</sub> = 50.64 ml

TABLE III  
SEPARATION FACTOR AND PARTITION COEFFICIENT  
COLUMN SET III

Sample (nm)	$V_{\text{Sample}}$ (ml)	$R_f$	$k_d$
69	64.80	1.56	0.32
73	64.00	1.57	0.31
98	61.80	1.63	0.26
103	60.90	1.65	0.25
176	56.00	1.80	0.15
209	53.40	1.89	0.11
220	--	--	--
312	--	--	--

$V_{\text{Total}} = 100.80$

$V_{\text{Interstitial}} = 47.80$

$V_{\text{Pore}} = 53.0$

Column: (1) 1000 Å, (1) 3000 Å, 200/400 mesh

Mobile Phase: 0.1% Aerosol<sup>®</sup>-OT, 2.47 mM NaNO<sub>3</sub>

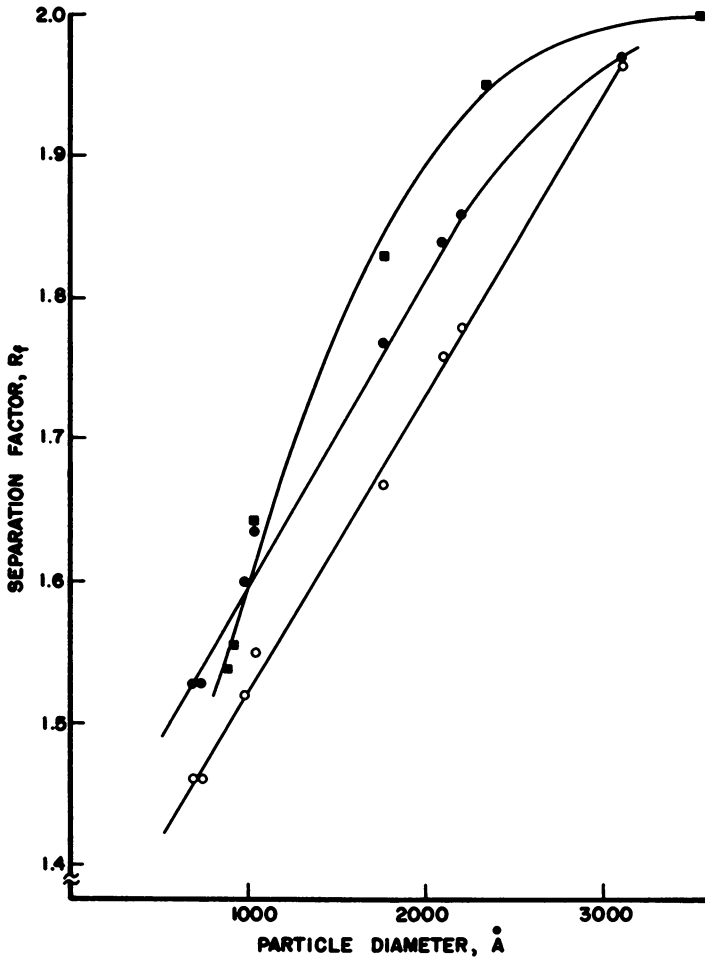


Figure 3. Effect of electrolyte on  $R_f$  ((■) 3000 Å, 2000 Å, 1000 Å CPG, 5.2mM electrolyte (14); (●) 3000Å, 1000Å CPG, 7.0mM electrolyte; (○) 3000Å, 1000 Å CPG, 23.0mM electrolyte)



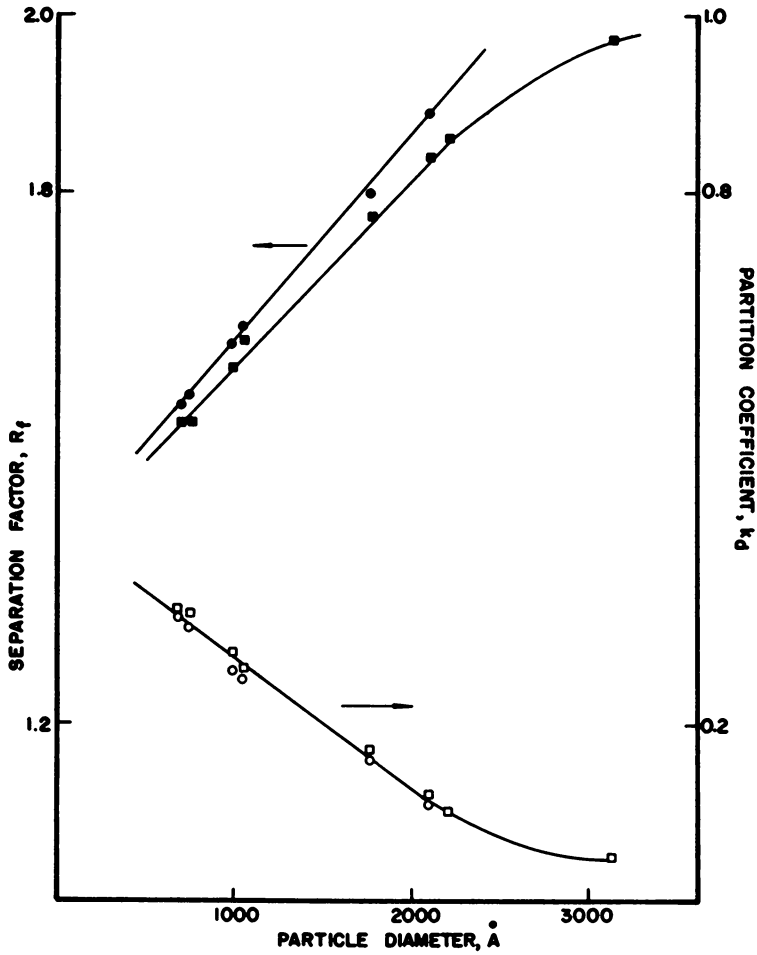


Figure 4. Effect of packing diameter on  $R_f$ ,  $k_d$  ((●, ○) 3000 Å, 1000 Å, 200/400 mesh; (■, □) 3000 Å, 1000 Å, 120/200 mesh)

TABLE IV  
SEC CALIBRATION <sup>1</sup> CURVES AND EFFECT  
OF ELECTROLYTE CONCENTRATION

<u>Column Set</u>	<u>A</u>	<u>B</u> <u>x 10<sup>2</sup></u>	<u>Electrolyte Conc.</u> <u>mM</u>
3000 Å, 1000 Å CPG 200/400 mesh	4.666	-4.359	7.0
3000 Å, 1000 Å CPG	4.725	-4.516	7.0
3000 Å, CPG	3.641	-4.220	16.9
3000 Å, 1000 Å CPG	4.356	-3.687	23.0

---

<sup>1</sup>  $\log D = A + B \cdot V$  with V in ml

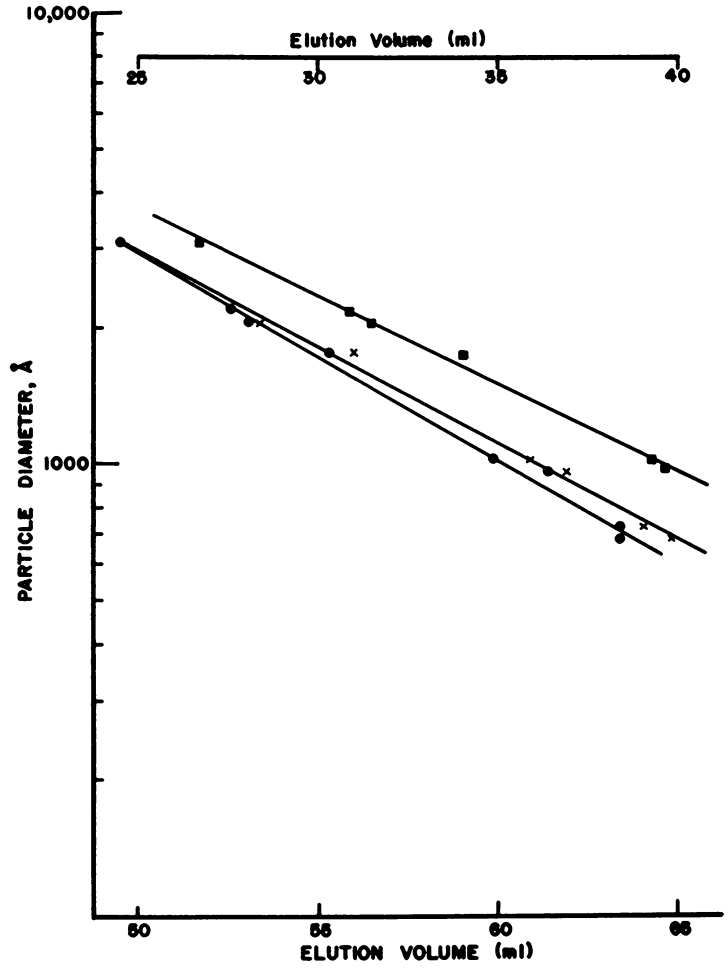


Figure 5. SEC calibration curves ((■) 3000 Å CPG; (●) 3000 Å, 1000 Å CPG; (×) 3000 Å, 1000 Å CPG; 200/400 mesh)

Publication Date: November 26, 1980 | doi: 10.1021/bk-1980-0138.ch002

TABLE V  
 VARIANCE, SKEWNESS AND KURTOSIS  
 OF OBSERVED CHROMATOGRAMS

	Sample (nm)	$V_{\text{Sample}}$ Counts	Variance, $\sigma^2$ , counts <sup>2</sup>	$D_2\sigma^2$	Skewness $A_3$	Kurtosis $A_4$
1.	73	20.9	5.13	0.21	0.38	2.85
	176	17.0	5.21		0.75	3.53
	209	15.7	5.52		1.10	4.38
	220	15.4	3.65		0.71	3.09
	312	13.3	0.66		1.85	7.31
2.	73	31.7	4.77	0.23	0.39	2.89
	176	27.7	4.69		0.86	3.86
	209	26.5	6.25		1.13	4.20
	220	26.3	4.93		0.99	3.80
	312	24.8	1.36		2.03	7.96
3.	73	33.8	8.11	0.22	0.54	3.06
	176	29.4	5.49		0.31	2.63
	209	27.8	4.57		0.64	3.13
	220	27.5	5.56		0.95	3.89

1. Column Set I, 3000 Å CPG, 16.9 mM electrolyte

2. Column Set II, 3000 Å, 1000 Å CPG, 7.0 mM electrolyte

3. Column Set III, 3000 Å, 1000 Å CPG, 23.0 mM electrolyte

However, it should be noted, sample recoveries would be expected to be higher at lower ionic strength.

Both the variance and the skewness of the observed chromatograms influence the calculation of the particle diameters. As mentioned earlier, the large variance observed in SEC systems as a result of axial dispersion causes problems with the numerical techniques used to determine  $W(y)$ . In addition, the variance is a function of the elution volume. The changes in variance, skewness and kurtosis are shown in Table V as functions of particle size and elution volume. For Column Set I the variance increases slightly with increasing particle size. This observation is in contrast to that of Hamielec and Singh (11). For particles larger than about 200 nm, however, the variance decreases with increasing particle size. For the 312 nm sample, the variance is extremely small as would be expected with a sample whose size excluded it from essentially all the pores, i.e.,  $k_d = 0.03$ . The high value of skewness for this sample may be the result of restricted movement thru the interstitial spaces, retention within the few available pores in the matrix, and some irreversible adsorption onto the stationary phase. The latter phenomenon is less likely at the relatively low ionic strengths employed here.

Lowering the electrolyte content tends to cause a decrease in the observed variance as might be expected because of decreased available pore volume. Values for the variance and skewness at the lower electrolyte content, 7.0 mM, also show a rising then falling trend as a function of increasing particle size, peaking at about 200 nm. At the highest electrolyte level, 23.0 mM, the variance tends to decrease with increasing particle size over the whole particle size range consistent with the observations of Singh and Hamielec (11). This reflects the larger available pore volume at high ionic strength. This results in less exclusion and entrapment, as estimated by the lower skewness values.

Use of the method of Husain, Vlachopoulos and Hamielec (23) can yield reasonable values for the particle diameter even when some skewness is apparent in the observed chromatogram. Table VI contains data for four poly(styrene) standards as calculated using this approach. All data were corrected for Mie scattering. The table shows the differences due to the correction for axial dispersion assuming a uniform variance over the sample elution volume. The 312 nm sample whose variance was small because of effective pore exclusion shows the least change in diameter averages on applying the axial dispersion correction. The 98 nm standard conversely shows the largest change on application of the dispersion corrections as would be expected since its partition coefficient was the highest for the four samples.

Table VII contains the weight-average particle diameters as calculated by this technique for all the standards employed using Column Set I. There is some difference between the values of variance used to obtain these averages and those cited in Table V. This is in fact due to the necessity to correct for skewness by

TABLE VI  
NUMBER AND WEIGHT AVERAGE DIAMETERS  
CALCULATED USING MIE SCATTERING

Sample (nm)	$\bar{D}_N(UC)$ (nm)	$\bar{D}_N(C)$ (nm)	$\bar{D}_W(UC)$ (nm)	$\bar{D}_W(C)$ (nm)
98	34	94	51	106
176	42	112	86	173
220	98	203	161	222
312	268	287	297	305

- $D(V) = 3028.38 \exp(-0.1707V)$
- $K(V)^{-1} = 0.8584 \times 10^{-2} \exp(0.3134V) + 0.9445 \times 10^{-8} \exp(0.9742V)$
- UC = Uncorrected for Axial Dispersion  
C = Corrected for Axial Dispersion

TABLE VII  
CALCULATED PARTICLE DIAMETERS <sup>1</sup>

Sample (nm)	Variance $\tau^2$ , Counts	$\bar{D}_W$ (nm)
73	5.1	--
98	5.5	106
103	5.6	113
176	5.4	172
209	7.0	219
220	6.5	222
312	0.67	305

<sup>1</sup> Calculated using the method of Husain, Vlachopoulos and Hamielec (23) Column Set I, 3000 Å CPG

increasing the sample variance since the calculations as used contain no term for skewness corrections. One of the problems encountered with this technique when skewing has occurred is that the calculated diameter averages do not necessarily follow the expected order of increasing magnitude:

$$\bar{D}_N < \bar{D}_S < \bar{D}_V < \bar{D}_{SS} < \bar{D}_W < \bar{D}_t$$

This problem may be corrected by the incorporation of the proper skewness term in the analytical treatment (24).

It would appear that, in principle, SEC offers the potential for high resolution and rapid analysis. The remaining difficulties are two-fold. First, the calculation of either particle size distributions or particle diameter averages must be modified to account for the larger values of variance and the increasing skewing observed in SEC of particles in suspension as compared with the SEC of molecules in solution. Second, there is a need for improved stationary phase technology to optimize resolution while at the same time reducing axial dispersion and skewing. Much the same approach as was successfully employed to produce high resolution, high speed SEC columns for molecules could be used here. The ideal packing should be relatively large in diameter, 80-100 nm, and be available with a pore size range from 500 to 10,000 Å. The pores should be uniform in size distribution and shallow to reduce diffusion times. Improvements of this type will lead to the use of size exclusion chromatography for particle size determinations in the routine manner in which it is now employed for molecular weight determinations.

### Abstract

Some model lattices have been used to test the capabilities of a size exclusion chromatographic system as applied to the measurement of particle size distributions. Poly(styrene) standards have been employed for the initial calibration of the chromatograph and to allow testing of the computational software used to correct for axial dispersion and detector response characteristics. Preliminary results have shown that a linear calibration is obtained for particle sizes in the range of 0.06 to 0.30 microns using any of three different column configurations. The effect of mobile phase electrolyte content and stationary phase pore size and packing sizes have been investigated.

### Acknowledgement

The authors wish to acknowledge the help of W. E. Coiner and J. L. Sills, Jr. who contributed to data acquisition and analysis. Also, we wish to thank Professor A. E. Hamielec and Dr. A. Husain for providing us with computational software and for their helpful discussions throughout the course of this work.

Literature Cited

1. Small, H. J. Coll. and Int. Sci., 1974, 48, 147.
2. Small, H.; Saunders, F. L.; Sok, J. Adv. Coll. and Int. Sci., 1976, 6, 237.
3. Small, H. Chemtech, 1977, 7, 196.
4. McHugh, A. J.; Silebi, C. A.; Poehlein, G. W.; Vanderhoff, J. W. Coll. and Int. Sci., 1976, Vol. IV, 549.
5. Silebi, C. A.; McHugh, A. J., "Emulsions, Latices, and Dispersion", P. Becher and M. N Yudenfreund, Eds., Marcel-Dekker, N. Y., 1978, p. 155.
6. Silebi, C. A.; McHugh, A. J. A.I.Ch.E.J., 1978, 24, 204.
7. Stoitsits, R. F.; Poehlein, G. W.; Vanderhoff, J. W. J. Coll. and Inst. Sci., 1976, 57, 337.
8. Krebs, K. F.; Wunderlich, W. Die Angew, Makromol. Chem., 1971, 20, 203.
9. Gaylor, V. F.; James, H. L., Preprints, Pittsburgh, Conference on Analytical Chemistry, Cleveland, Ohio, March 1975.
10. Coll. H.; Fague, G. R.; Robillard, K. A., "Exclusion Chromatography of Colloidal Dispersion", unpublished, Eastman Kodak Co., Rochester, N. Y., 1975.
11. Singh, S.; Hamielec, A. E. J. Appl. Polym Sci., 1978, 22, 577.
12. DiMarzio, E. A.; Guttman, C. M. Polym. Lett., 1969, 7, 267.
13. DiMarzio, E. A.; Guttman, C. M. Macromolecules, 1970, 3, 131, 681.
14. Nagy, D. J., "Column Chromatography of Polymer Latexes", Ph.D. Dissertation, Lehigh University, May 1979.
15. Tung, L. H. J. Appl. Polym. Sci., 1966, 10, 375.
16. Tung, L. H.; Moore, J. C.; Knight, G. W. J. Appl. Polym. Sci., 1976, 10, 1261.
17. Hamielec, A. E.; Singh, S. J. Liquid Chromatography, 1978, 1, 187.



18. Mie, G. Ann. Physik, 1908, 25, 377.
19. Dave. J. W., "Subroutines for Computing the Parameters of the Electromagnetic Radiation Scattered by a Sphere", IBM Report No. 320-3237, IBM Scientific Center, Palo Alto, California, 1968.
20. Chang, K. S.; Huang, Y. M. J. Appl. Polym. Sci., 1969, 13, 1459.
21. Ishige, T.; Hamielec, A. E.; Lee, S-I. J. Appl. Polym. Sci., 1971, 15, 1607.
22. Silebi, C. A.; McHugh, A. J. J. Appl. Polym. Sci., 1979, 23, 1699.
23. Husain, A.; Vlachopoulos, J.; Hamielec, A. E. J. Liquid Chromatography, 1979, 2, 193.
24. Husain, A., Private Communication, July 1979.

RECEIVED May 7, 1980.

# Particle Size Analysis Using Size Exclusion Chromatography

A. HUSAIN, A. E. HAMIELEC, and J. VLACHOPOULOS

Department of Chemical Engineering, McMaster University,  
Hamilton, Ontario, L8S 4L7, Canada

Herein is reported an experimental investigation of particle size measurement using size exclusion chromatography. The merits of calibrating one column at a time are discussed. The column packing procedure is shown to strongly influence the entrapment of large diameter particles. The monodispersity of standard latex particles used for calibration is examined. Significant deviation from theory is observed for the measured extinction coefficients. A comparison is made of the detector signal in the absorption versus scattering mode. Particle sizes are calculated for the standard latex samples and their mixtures using recently reported analytical methods which account for imperfect resolution.

The publications on a technique of particle size measurement called hydrodynamic chromatography (HDC) by Hamish Small (1,2), whereby a dilute suspension of submicron particles in a carrier solvent undergoes size separation as it flows through a bed of non-porous beads, was followed by a spurt of publications reporting on attempts to predict the effect of various parameters on peak separation (3,4,5,6) and the determination of particle size distributions (3,7). The latter involved the numerical solution of the integral equation describing peak broadening. The complementary technique known as size exclusion chromatography (SEC), which employs porous packing material, has been the subject of far fewer investigations, presumably due to the difficulty in quantitatively describing pore dispersion.

Krebs and Wunderlich (8) were the first to report a separation of polymethylmethacrylate and polystyrene latex particles using silica gel having very large pores (500-50000Å). This was followed by the work of Gaylor and James (9) who fractionated latices using columns packed with porous glass and water compatible polymeric porous gels. Coll et al (10) experimenting with porous glass packing found it necessary to add electrolyte as well as surfactant to the aqueous eluent. In the absence of electrolyte, latex particles

**American Chemical**

0-8412-0 Society Library 047\$07.25/0

© 1980 American Chemical Society

could not sample the pore volume. Hamielec and Singh (11) presented the first comprehensive theoretical and experimental investigation of SEC. Using the carrier solvent suggested by Coll et al. and porous glass and silica packing, they established the universality of the particle diameter-retention volume calibration using latices of different composition. They derived analytical expressions for a general detector which corrected the diameter averages calculated from the chromatogram, for imperfect resolution. One of the detectors considered was a turbidity detector in the Rayleigh scattering regime. They had marginal success in predicting particle diameter averages for injected monodispersed latices. Very recently Husain et al. (12) obtained an analytical solution to the integral equation describing peak broadening for a turbidity detector in the Mie scattering regime.

In the present paper we report on an experimental investigation of SEC. Main emphasis is placed on particle size measurement using analytical methods of correcting for imperfect resolution.

### Experimental

The apparatus employed for chromatographing particle suspensions in this laboratory has been reported in detail elsewhere (11). A sample loop of approximately 0.4 ml was used. The detector was a Pharmacia UV-spectrophotometer with a cell of 1 cm path length and an operating wavelength of either 254, 280 or 350 nm. The volume counter had a capacity of 1 ml.

The carrier fluid was deionized water containing 1 gm/l of Aerosol OT and 1 g/l sodium nitrate. Compared to the use of potassium nitrate as electrolyte, suggested by Coll et al. (10), the carrier solvent used in this investigation has much better clarity and at room temperature has no tendency to precipitate the surfactant.

The columns used were dry packed using a packing apparatus (purchased from Mandle Scientific). The packing employed was CPG of pore sizes 1000, 2000 and 3000 Å and 200-400 mesh size. The columns were calibrated using Dow and Polysciences monodispersed polystyrene latices.

Sample preparations were made by dispersing a few drops of standard polystyrene latices (Dow and Polysciences) in 100 ml of carrier fluid. Solute charges were typically less than 0.01 wt. %.

### Calibration of Columns

Three columns of 3000 Å pore size and one each of 2000 Å and 1000 Å were packed. They were individually calibrated. All three 3000 Å columns showed similar peak separation characteristics for particle sizes between 312 nm and 57 nm. However, peak broadening was much larger for one of the 3000 Å columns. This column was discarded. Of the remaining two 3000 Å columns, one was subjected to the following:

The column was disconnected from the chromatograph and mounted on the packing apparatus which was then activated. This caused the packing in the column to further settle. Additional packing material was then added. The column was once again calibrated. The improvement in the calibration curve was not significant. A significant retention of the higher particle sizes occurred in the column following this additional treatment. This is clearly shown in Fig.1 for a 312 nm sample which was injected before and after the treatment. Also note the shift in peak position probably caused by loss of pore volume due to attrition between particles of the glass packing. This additional treatment was subsequently abandoned.

The 1000 Å column did not show any resolution between 312 nm and 57 nm particle sizes. Shown in Fig.2 are the calibration curves for the 2000 Å and 3000 Å columns and for their combination. The 57 nm particle standard appears to have been erroneously characterized by the supplier. This was subsequently confirmed by electron microscopy. The 2000 Å column exhibited a sharp upturn in its calibration curve close to the exclusion limit. It is to be noted that while data points corresponding to 312 and 275 nm diameter particles appear on individual column calibration curves, they are not indicated for the calibration curve of the combination. This is because these larger diameter particles were completely retained in the packed columns, generating no detector response. The percentage recovery for these particles from individual columns was considerably less than 100% resulting in their complete retention when the columns were combined in series.

At this stage it is useful to make a comparison of our calibration procedure with that of previous workers. Coll et al.(10) employed a set of 5 columns with a total length of 6 m packed with CPG 3000, 2000, 2000, 1000 and 500 Å porous glass. They obtained a linear calibration curve in the range 200 to 25 nm. They did not calibrate each column individually and it is very likely that the 1000 and 500 Å columns contributed insignificantly to peak separation. Hamielec and Singh (11) investigated peak separation using several column combinations. Like their predecessors, columns were not calibrated one at a time. Their best calibration curve obtained using two 4 ft columns packed with CPG 2500 and 1500 Å porous glass, respectively, had a slope of  $.0928 \text{ ml}^{-1}$ . In the present work we have been able to obtain a slope of  $.05968 \text{ ml}^{-1}$  with a total of 6 ft of packed column. To discriminate between columns the correct quantity for comparison is the product  $(D_2\sigma)^2$ . While identical conditions were not used, the variances measured in the present work were considerably smaller than those reported earlier (11), leading to a smaller  $(D_2\sigma)^2$  value. The merit in individual column calibration is the elimination of columns with either poor resolution (high  $D_2$ ) or with large peak broadening (high  $\sigma^2$ ) or both. Finally, Hamielec et al could detect particles up to 500 nm while the upper limit in the present work is less than 275 nm. The latter appears to be related to the packing density of the

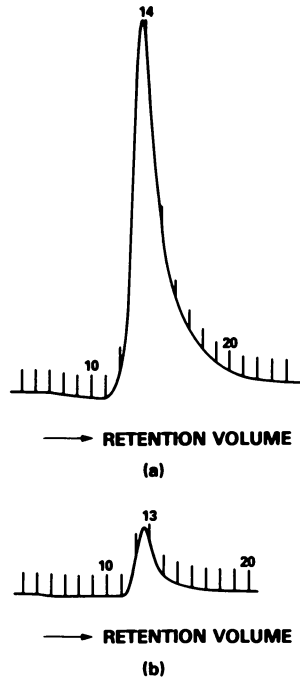


*Figure 1. Chromatogram of 312-nm sample (a) before treatment and (b) after treatment*

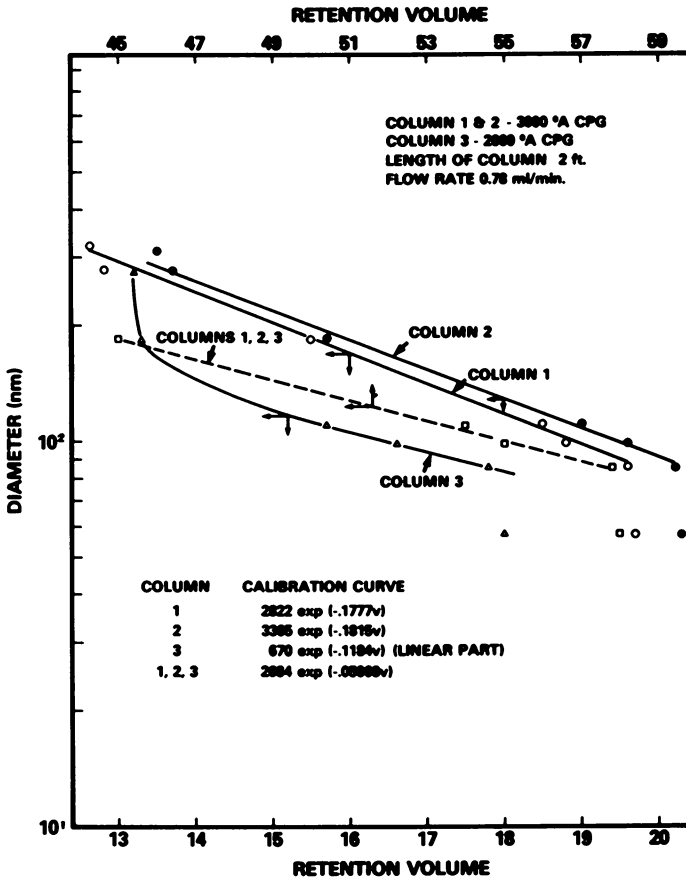


Figure 2. Particle diameter-retention volume calibration curves

columns; the denser the packed bed, the lower the maximum particle size that can elute.

### Calibration of Detector

The detector was calibrated by pumping solutions of sodium dichromate of known absorbance through the sample port of the detector. The solutions were prepared in the carrier fluid which served as reference. The recorder response was measured as the ultimate height reached on the chart paper above the baseline when the sample fluid was switched to a sodium dichromate solution of known absorbance. The calibration was insensitive to flow-rate variations.

The data shown in Fig. 3 indicate a linear response at wavelengths of 254 and 350 nm. However, at 280 nm a distinct departure from linearity occurred at low sample absorbance. This non-linearity has implications in particle size measurement.

### Particle Standards - How Monodispersed are They (?)

For the purpose of calibration and particle size calculations, it was decided to confirm the reported particle sizes of the various latices supplied by Dow and Polysciences, using scanning electron microscopy. Unfortunately, after subtracting the thickness of the gold layer with which the particles were coated from the size shown on the micrographs, some inconsistencies were noted with respect to the measured sizes of the particles and their elution behaviour. It was therefore decided to assume the reported sizes as true values with the exception of the 57 nm particle.

The micrographs however, revealed that the latex particle standards were not monodispersed as claimed by the suppliers. This can clearly be noted from the micrographs in Fig. 4,a-e. They indicate a distinct polydispersity; the micrographs of the 275 and 312 nm samples in fact reveal two distinct particle populations.

### Measurement of Extinction Coefficients

Heller and Tabibian (13) noted that errors, due to laterally scattered light and the corona effect, as large as to cause a 30% reduction in measured turbidity, may result 'if instruments which are perfectly suitable for ordinary absorption measurements are used for turbidity measurements without proper modifications'. To evaluate the performance of our turbidity detector, particle suspensions of various concentrations of several polystyrene latex standards were prepared. Their extinction coefficients were measured using both a bench-top UV spectrophotometer (Beckman, Model 25) and the online detector (Pharmacia).

In the absence of multiple scattering, the turbidity of a colloidal suspension is given as

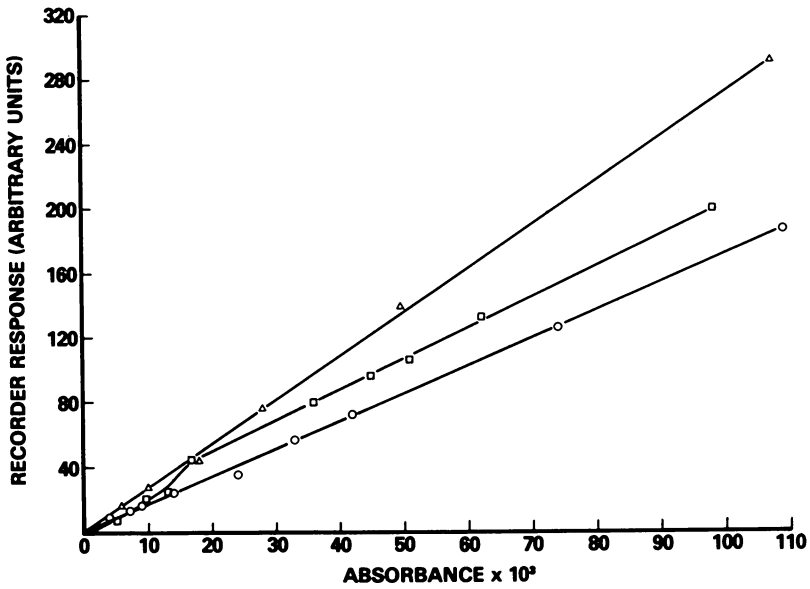
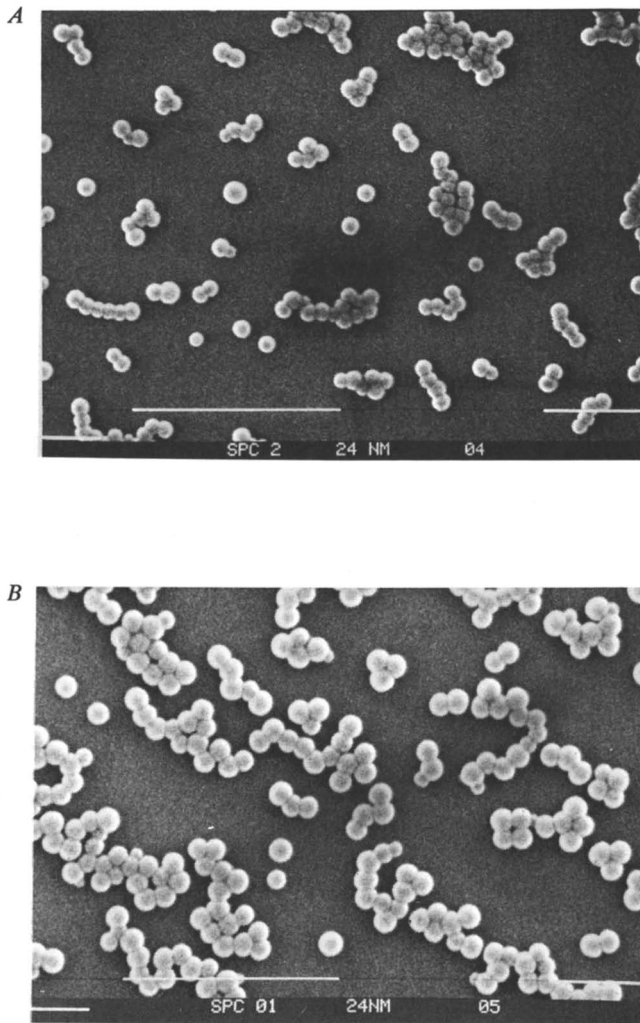
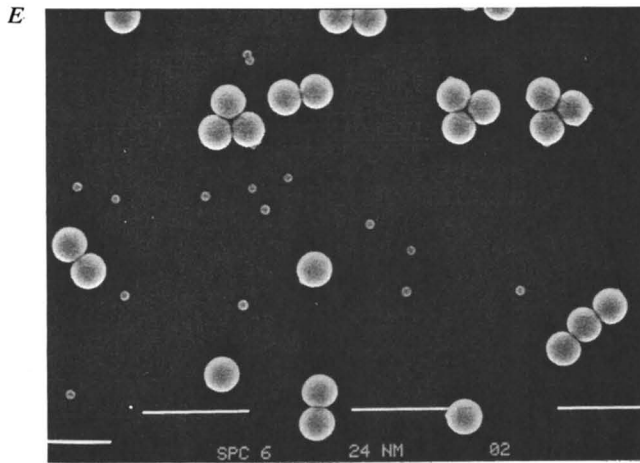
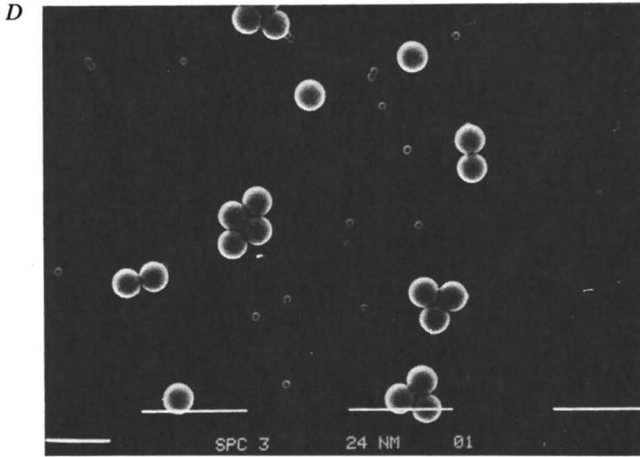
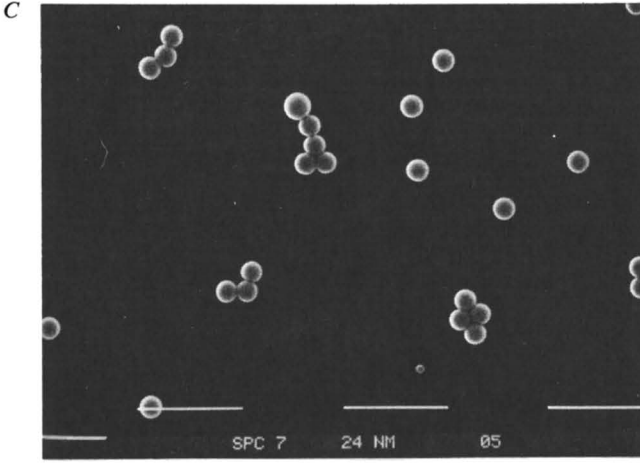


Figure 3. Calibration curves of detector at wavelengths (○) 254 nm, .32X; (□) 280 nm, .16X; and (△) 350 nm, .16X (test solute: sodium dichromate)





**Figure 4.** Scanning electron micrographs of standard lattices: (A) Polysciences 57-nm polystyrene latex at magnification 20 K; (B) Polysciences 98-nm polystyrene latex at magnification 20 K; (C—facing page) Polysciences 183-nm polystyrene latex at magnification 10 K; (D—facing page) Polysciences 275-nm polystyrene latex at magnification 10 K; (E—facing page) Dow 312-nm polystyrene latex at magnification 20 K



$$\tau = \frac{1}{\ell} \ln \frac{I_0}{I} = N \frac{\pi}{4} D^2 k \quad (1)$$

where  $\ell$  is the optical path length, cm

$I_0$  is the intensity of the incident beam

$I$  is the intensity of the emerging beam

$N$  is the particle concentration, number/cm<sup>3</sup>

$D$  is the particle diameter, cm

$k$  is the extinction coefficient, dimensionless. It is a function of the parameters,  $\alpha = \pi D/\lambda$  and  $m$ , where  $\lambda$  is the wavelength in the medium and  $m$  is the ratio of the refractive indices of particle and medium.

Turbidity is related to the absorbance,  $A$ , by

$$\tau = \frac{2.303}{\ell} A \quad (2)$$

When the particle concentration is expressed as a weight percent  $c$ , the above relations take the form

$$\tau = \frac{2.303}{\ell} A = 0.015 \frac{\rho_p k c}{\rho_s D} \quad (3)$$

where  $\rho_p$  and  $\rho_s$  are the densities of the particle and system respectively.  $A$  versus  $c$  data collected from a Beckman spectrophotometer then yields the value of  $k$  for a known  $D$  at any specific wavelength.

To measure  $k$  using the online detector, the packed columns were replaced by a length of 1/16 in OD ss tubing and peak areas corresponding to injections of various particle suspensions and sodium dichromate solutions were recorded on chart paper. The following analysis was then applied.

The recorder response  $F(v)$  is related to the absorbance of the detector cell contents  $A'(v)$  by

$$F(v) = \beta A'(v) \quad (\text{when response is linear}) \quad (4)$$

$$\text{Therefore} \quad \int_0^{\infty} F(v) dv = \beta \int_0^{\infty} A'(v) dv = \beta A V_s \quad (5)$$

where  $A$  is the absorbance of the injected sample and  $V_s$  is the sample volume. The product  $\beta V_s$  may be estimated from the slope of a peak area versus  $A$  plot for sodium dichromate. For known weight concentrations of particle suspensions injected,  $A$  is considered the unknown;  $A$  versus  $c$  data are then obtained from a measurement of their peak areas and hence  $k$  calculated from equation (3). It should be noted from equation (5) that in the absence of stray light effects mentioned earlier, peak area versus absorbance data for the different sized particles and sodium dichromate solute

must fall on the same straight line.

The extinction coefficient for non-absorbing particles may be theoretically evaluated from the light scattering theory developed by Mie (14, 15). It is calculated from the relationship

$$k = \frac{2}{\alpha^2} \sum_{n=1}^{\infty} (2n + 1) (|a_n|^2 + |b_n|^2) \quad (6)$$

where  $a_n$  and  $b_n$  are functions of  $\alpha$  and  $m$ .

The data from the Beckman spectrophotometer measured at three different wavelengths, 254, 280 and 350 nm are shown in Figures 5 A-C. Figures 6 A-D indicate the data measured using the online detector. The measured and calculated extinction coefficients are given in Table I.

Table I. Comparison of Measured and Calculated Extinction Coefficient

Wave-length (nm)		Diameter (nm)					
		85	98	109	176	183	220
254	Mie theory <sup>+</sup>	0.1755	0.2530	0.3330	1.0686	1.1636	1.6600
	Beckman	0.2372	0.3801	0.5260	1.5850	1.8330	2.4030
	On-line detector	0.2264	0.3898	0.5054 (0.72)*	1.3280 (1.89)*	1.6640	2.1460
280	Mie theory <sup>+</sup>	0.1188	0.1755	0.2299	0.7831	0.8468	1.2518
	Beckman	0.1121	0.2008	0.2796	0.9606	1.1710	1.5590
	Mie theory <sup>+</sup>	0.0472	0.0749	0.1030	0.3639	0.4056	0.6378
350	Beckman	0.0327	0.0654	0.1000	0.3467	0.4830	0.6547
	On-line detector	-	-	-	0.312	-	0.6295

+ Refractive Index of Polystyrene (16) =  $1.5683 + 10.087 \cdot 10^{-11} / \lambda_0^2$

Refractive Index of water (16) =  $1.3240 + 3.046 \cdot 10^{-11} / \lambda_0^2$

where  $\lambda_0$  is the wavelength in vacuum (cm)

\* Measured from data of ref. (7).

The data shown in Figures 6 A-D indicate that while the smaller particles: 85, 98 and 109 nm are indistinguishable from the dissolved solute, sodium dichromate, in as far as detector behaviour is concerned, the detector response differs significantly for the larger diameter particles. The reduced peak area and hence turbidity indicated for the larger particles is a direct result of the optical effects noted earlier. The observations are consistent with the findings of Heller and Tabibian that the corona effect

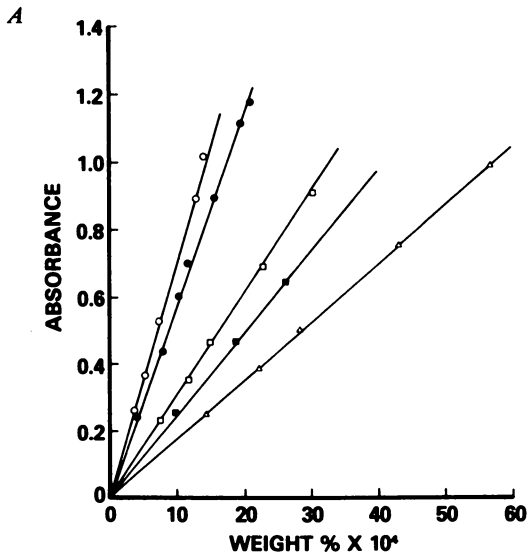
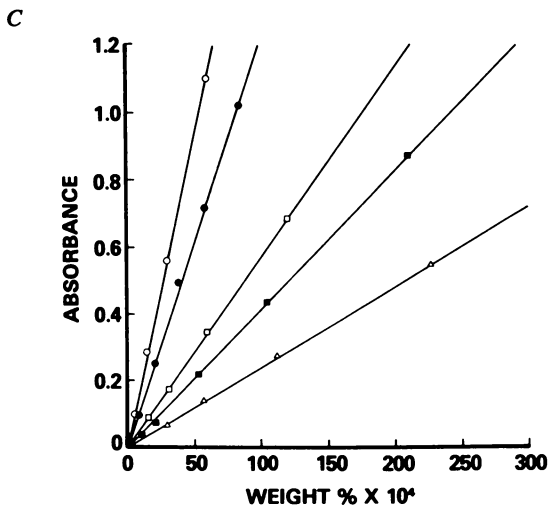
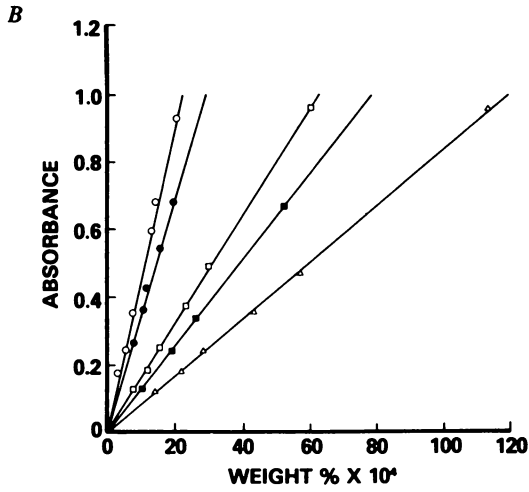


Figure 5. Absorbance vs. weight percent of standard lattices at (A) 254 nm; (B—facing page) 280 nm; (C—facing page) 350 nm (particles: (○) 220 nm; (●) 176 nm; (□) 109 nm; (■) 98 nm; (△) 85 nm)



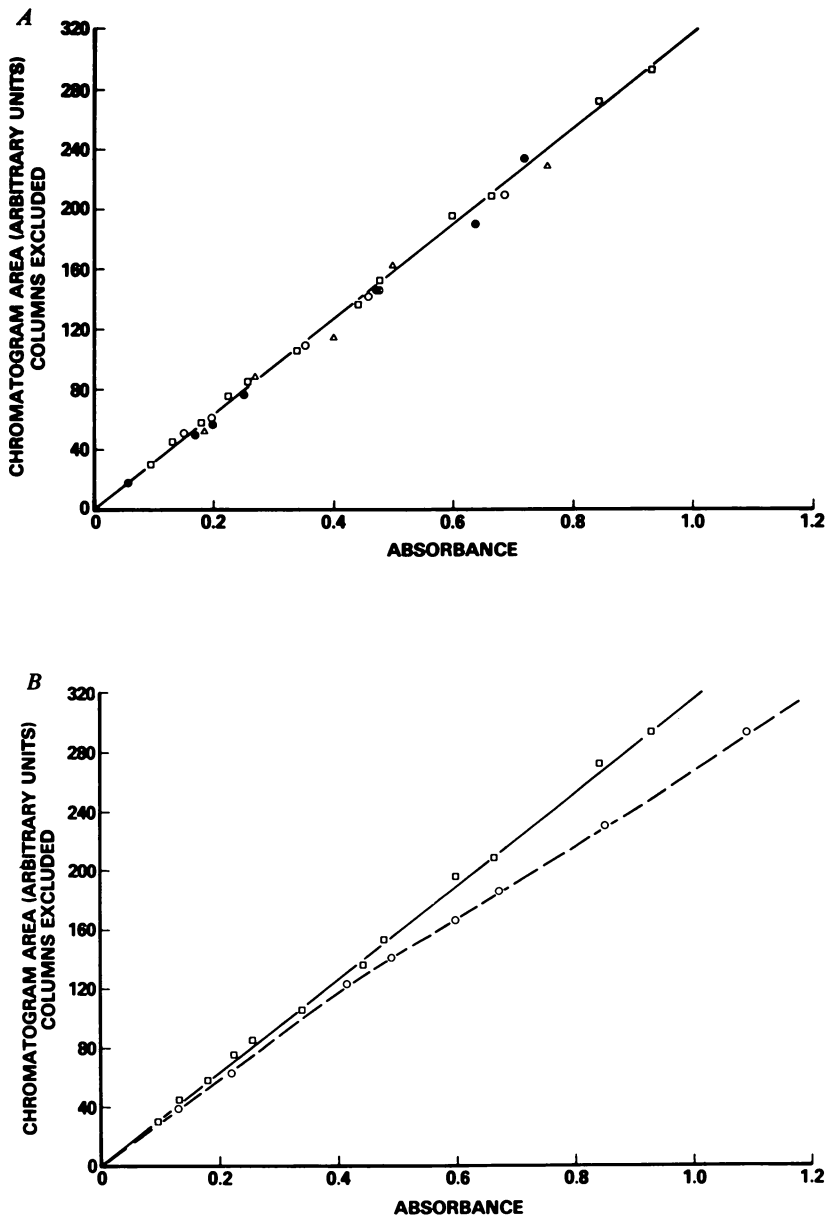
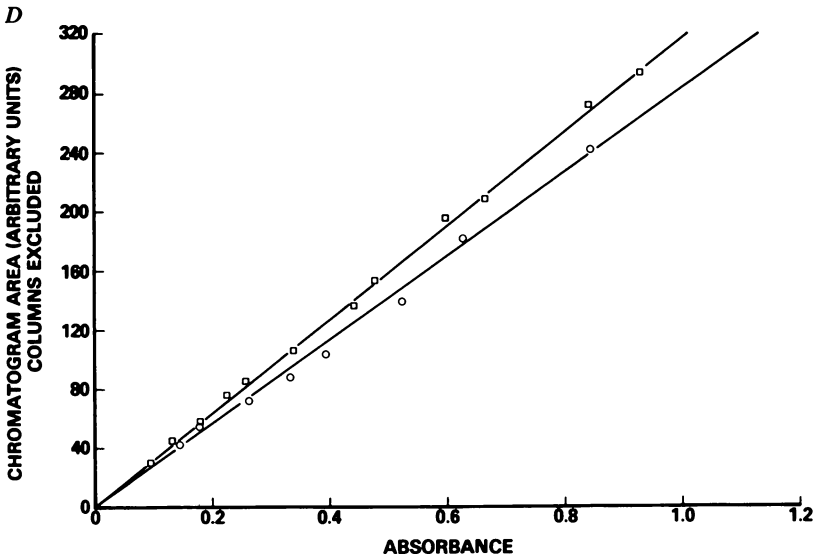
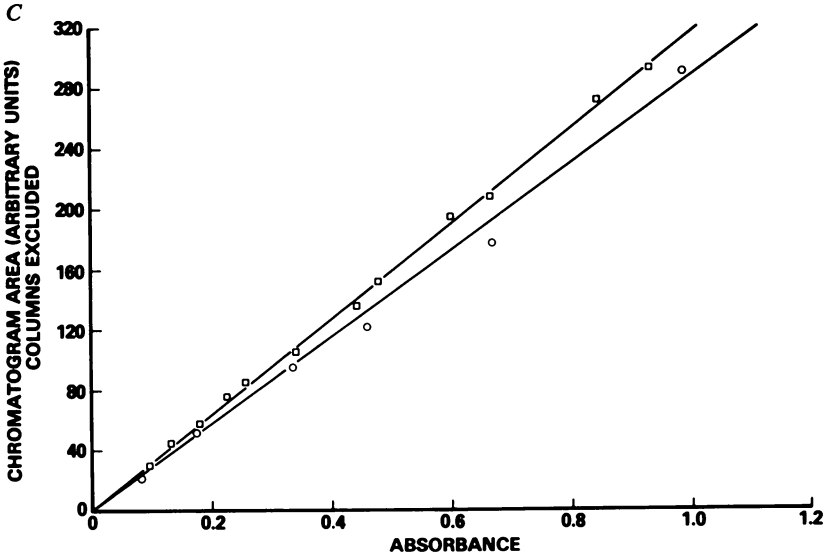


Figure 6. Comparison of detector response of sodium dichromate (SD) (□) and (A) 85- (Δ); 98- (●); and 109-nm (○) latex particles; (—) regressed through SD data; (B) 176-nm (○) latex particles; (—) regressed through SD data; (---) curve drawn through data; (C—facing page) 183-nm (○) latex particles; (—) regressed through data points; (D—facing page) 220-nm (○) latex particles; (—) regressed through data points. Operating wavelength 254 nm.





and the interference effect of laterally scattered light cause a reduction in measured turbidity, the effects being more pronounced for larger particles and causing a departure from the linear dependence of turbidity on concentration at concentrations lower than those at which it would occur in the absence of such effects.

Table I compares the measured values of extinction coefficients with the values calculated from theory at wavelengths of 254, 280 and 350 nm. The lower values of extinction coefficients for the larger particles measured, using the online detector compared to the Beckman instrument, are due to the optical effects discussed above. The disagreement between the extinction coefficients calculated from Mie theory for non-absorbing spheres and the measured values from the Beckman instrument is very significant, particularly at 254 and 280 nm.

Silebi and McHugh (7) concluded from the investigation of their detector response that instrument errors were not present, and that Mie theory for non-absorbing particles was applicable in evaluating the turbidity signal. However, it appears that their measured values of extinction cross-section are consistently larger than calculated values, despite a deceptively close agreement indicated on a log (extinction cross-section) versus log (diameter) plot. Values of extinction coefficient calculated from their data are also shown in Table I.

In an attempt to resolve the discrepancy between calculated and measured extinction coefficients, one can consider the possible contributing factors which follow:

1. Polystyrene particles absorb light at 254 nm.
2. The particles contain residual styrene monomer which strongly absorbs light at 254 and 280 nm wavelength.
3. Additives in the latex formulations such as emulsifier etc. absorb in the UV range.
4. The latex particles are not monodispersed. This has already been demonstrated.

Accordingly GPC analysis of dried latex samples were carried out. The carrier solvent was tetrahydrofuran and peaks were monitored by a Waters' dual absorbance detector at wavelengths of 254 and 340 nm. The latter detection was the closest to 350 nm available.

Fig. 7 A shows the GPC traces obtained at wavelength 254 and 340 nm for a 312 nm Dow latex sample. Note the response at 340 nm is at twenty-five times the sensitivity of the response at 254 nm and hence considerably exaggerated in comparison. At 254 nm two peaks are clearly noted, a polymer peak and a secondary peak whose retention volume corresponds to that of styrene monomer. At 340 nm, since neither monomer nor polymer absorb, the observed peak is attributable to the presence of additives such as emulsifier.

For the other Dow samples: 85, 109, 176 and 220 nm, the response shown in Fig. 7 B for the 220 nm sample was typical. Note the hump in the trailing end of the GPC trace. At 340 nm wavelength there was a distinct response though much smaller than observed for the 312 nm sample.

The GPC traces for the 98 and 183 nm Polysciences samples are shown in Figures 7 C and D. These are similar to the response of the 312 nm particle at 254 nm, though at 340 nm wavelength the effect was considerably smaller and comparable to the other Dow samples.

On the basis of the above observations it is concluded that at 350 nm the discrepancy between calculated and measured extinction coefficients may be attributed to the additives in the latices and the size disparity of the particles in them. The presence of residual styrene monomer in the particles is strongly suspected. The data are inconclusive in this regard. Whether or not polystyrene latices absorb at 254 nm can only be established once the contributions to the extinction coefficients from the additives and residual monomer if any, are established. A combination of the aforementioned are probably responsible for departure from theory at 254 and 280 nm.

### Particle Recovery

From equation (5) it follows that the number of particles  $N_{out}$  which elute from the column for an injection, are given by

$$N_{out} = \frac{2.303 \int_0^{\infty} F(v) dv}{\beta \ell \frac{\pi}{4} D^2} \quad (7)$$

For a known injection of concentration  $c_o$  (particles/cc), the number of particles injected is given by  $c_o V_s$ . Therefore the number percent recovery,  $R$ , is calculated as

$$R = \frac{2.303 \int_0^{\infty} F(v) dv}{\beta \ell c_o v_s \frac{\pi}{4} D^2} \times 100 \quad (8)$$

Alternatively it follows from equation (7) that  $R$  may be evaluated as

$$R = \frac{(\int_0^{\infty} F(v) dv)_c}{(\int_0^{\infty} F(v) dv)_{wc}} \times 100 \quad (9)$$

where the integrals in the numerator and denominator represent peak areas for the same sample obtained with and without the columns respectively. A correction factor must be incorporated in equation (8) to account for instrumental errors. Equation (9) is valid in such an event, however.

Particle recoveries calculated according to equation (9) for our samples indicated essentially 100% recoveries for the 85, 98 and 109 nm samples. However, the recovery for the 183 nm sample was only 41%.

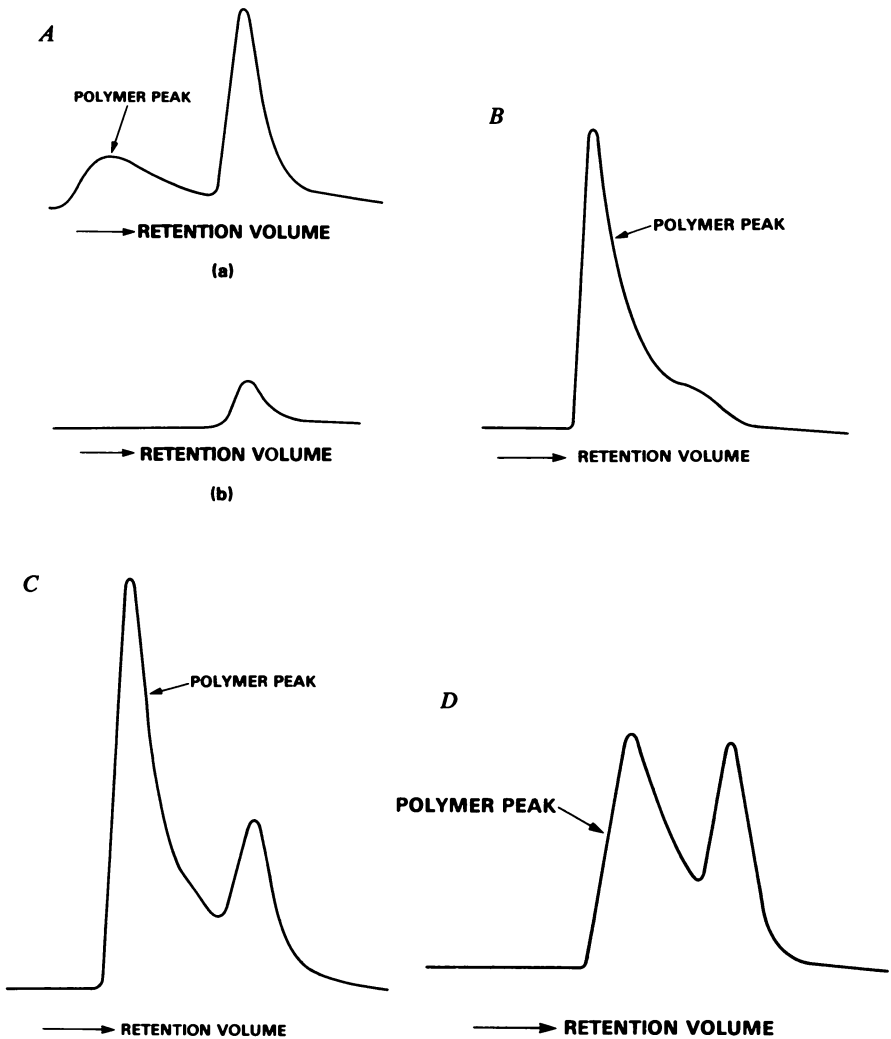


**Figure 7.** GPC analysis of (A) 312-nm Dow latex sample: SE Dupont silica columns—(a) response at 254-nm wavelength (full scale 0.5 Å); (b) response at 340-nm wavelength (full scale 0.02 Å); (B) 220-nm Dow latex sample: E-Linear Water's silica columns—response at 254-nm wavelength (full scale 0.5 Å); (C) 98-nm Polysciences latex sample: E-Linear Water's silica columns—response at 254-nm wavelength (full scale 0.5 Å); (D) 183-nm Polysciences latex sample: E-Linear Water's silica columns—response at 254-nm wavelength (full scale 0.5 Å)

Particle Size Measurement

Theory. We will outline theory developed earlier (11,12) for converting the detector response  $F(v)$  from a turbidity detector into particle size information.  $F(v)$  is related to the dispersion-corrected chromatogram  $W(y)$  by the integral equation

$$F(v) = \int_0^{\infty} W(y) G(v,y) dy \quad (10)$$

where  $G(v,y)$  is the instrumental spreading function which may be approximated by a Gaussian distribution with variance  $\sigma^2$ .

$$G(v,y) = \frac{1}{\sqrt{2\pi} \sigma^2} \exp\left(\frac{-(v-y)^2}{2\sigma^2}\right) \quad (11)$$

$\sigma^2$  is the variance of the chromatogram of a monodispersed sample. In this analysis it is considered to be a constant independent of particle diameter or retention volume,  $y$ . The particle diameter-retention volume calibration curve is assumed linear and given by

$$D(v) = D_1 \exp(-D_2 v) \quad (12)$$

The frequency distribution uncorrected for imperfect resolution is given by

$$f(D) dD = \frac{-F(v) k^{-1}(v) D^{-2}(v) dv}{\int_0^{\infty} F(v) k^{-1}(v) D^{-2}(v) dv} \quad (13)$$

For non-absorbing spherical particles which behave as Rayleigh scatterers, the above equation reduces to

$$f(D) dD = \frac{-F(v) D^{-6}(v) dv}{\int_0^{\infty} F(v) D^{-6}(v) dv} \quad (14)$$

Equation (14) can be used to calculate uncorrected diameter averages. For the number, surface, volume, specific surface, weight and turbidity diameter averages (their definitions have been stated elsewhere (11,12)), the following relations can be derived:

$$\left. \begin{aligned} D_N(c) &= D_N(uc) \exp\left(\frac{11}{2} D_2^2 \sigma^2\right) \\ D_S(c) &= D_S(uc) \exp(5 D_2^2 \sigma^2) \\ D_V(c) &= D_V(uc) \exp\left(\frac{9}{2} D_2^2 \sigma^2\right) \end{aligned} \right\} \quad (15)$$

$$\left. \begin{aligned} D_{SS}(c) &= D_{SS}(uc) \exp\left(\frac{7}{2} D_2^2 \sigma^2\right) \\ D_W(c) &= D_W(uc) \exp\left(\frac{5}{2} D_2^2 \sigma^2\right) \\ D_T(c) &= D_T(uc) \exp\left(\frac{3}{2} D_2^2 \sigma^2\right) \end{aligned} \right\}$$

where  $c$  and  $uc$  designate corrected and uncorrected diameter averages.

When the more general Mie scattering theory is applied the approach adopted in deriving the previous formulae cannot be used. One is, however, able to derive an analytical expression for the moments of the size distribution within the detector cell. They are given as:

$$I(\gamma, v) = \sum_1^n C_i \exp\{-E_i v + (E_i \sigma)^2 / 2\} F(v - E_i \sigma^2) \quad (16)$$

where  $I(\gamma, v)$  is the  $\gamma$ th moment of the frequency distribution at retention volume  $v$  and

$$C_i = A_i D_1^{\gamma-2} \quad (17)$$

$$E_i = -\{B_i + (2-\gamma)D_2\} \quad (18)$$

$A_i$  and  $B_i$  are the coefficients in the fit of the inverse of the extinction coefficient against retention volume.

$$k^{-1}(y) = \sum_1^n \{A_i \exp(B_i y)\} \quad (19)$$

$[k(y)]$  can typically vary over six decades across the chromatogram.  $n=2$  generally gives an adequate fit. Initial parameter estimates can be obtained by assuming that at the high and low ends of the  $k(y)$  data, one exponential term suffices to represent it. A non-linear estimation routine is used to estimate the parameters. Occasionally improved fit in the low end results from the use of a multivariable search routine which minimises the objective function

$$\sum_{\text{over all } y} \left( \frac{\hat{k}(y) - k(y)}{k(y)} \right)^2 \quad \text{where } \hat{k}(y) \text{ is an estimate of } k(y)$$

Equation (16) can be used to generate the desired moments and hence the diameter averages as a function of retention volume. This information together with  $I(0, v)$  which represents the number of particles in the detector cell at retention volume  $v$ , leads to the evaluation of overall sample diameter averages.

In contrast to the method based on Rayleigh scattering, the procedure based on Mie scattering theory: (a) is not restricted to small particles, (b) chemical absorption may be considered, (c) and lastly, it can be extended to permit the use of a nonlinear

particle diameter-retention volume calibration curve.

#### Measurement of Particle Diameter Averages

In spite of the disagreement between measured and calculated extinction coefficients, it is of interest to examine the diameter averages obtained using Mie and Rayleigh theories. We will first illustrate the calculations for the individual particle chromatograms and then examine bimodal mixtures. The success of the analytical techniques outlined earlier depends on the instrumental spreading function being Gaussian. We assume that the variance of the spreading function is given by the measured variance of the chromatograms of the particle standards. This approximation in spite of the heterogeneity of the particle standards, is valid if the contribution of the spreading function to the measured variance is dominant. Extinction coefficients calculated from Mie theory (17) were fitted against the retention volume by a sum of two exponentials. Excellent fit was obtained.

Individual Latex Samples. Figure 8 shows the chromatograms for the 85, 98, 109 and 183 nm particles measured at a wavelength of 254 nm. While skewing exists in all the chromatograms, it is most pronounced for the largest particle size. The calibration data and measured variances are shown in Table II. It must be noted that while the calibration curve spans a retention volume range of 13 ml, the chromatograms span about twice this volume. The extension of the calibration curve beyond a retention volume of 58 ml poses less of a risk, in view of the acknowledged capacity of LEC in resolving small diameter particles, than in its extension to retention volumes of less than 45 ml. The latter has the implication of counting particles as large as 278 nm (corresponds to a retention volume of 38 ml; see Fig. 8) which have earlier been shown to be totally trapped in the columns.

Table II. Calibration Data and Measured Variances

Sample (nm)	Peak Retention Volume (ml)	Measured Variance (ml <sup>2</sup> )		
		Wavelength (nm)		
		254	280	350
85	58	12.42	12.97	12.66
98	55	12.56	13.58	13.58
109	54	13.26	13.42	13.05
183	45	14.15	-	13.96

Tables III, IV & V contain the results of the particle size analysis for data measured at the three different wavelengths. The diameter averages,  $D_N$  to  $D_T$  are arranged in increasing order of magnitude which is also the order of decreasing imperfect resolution correction factors. In view of the low value of  $(D_2\sigma)^2$ , the magnitude of the correction factors is fairly small. The measured diameter averages for all but the 183 nm sample are in

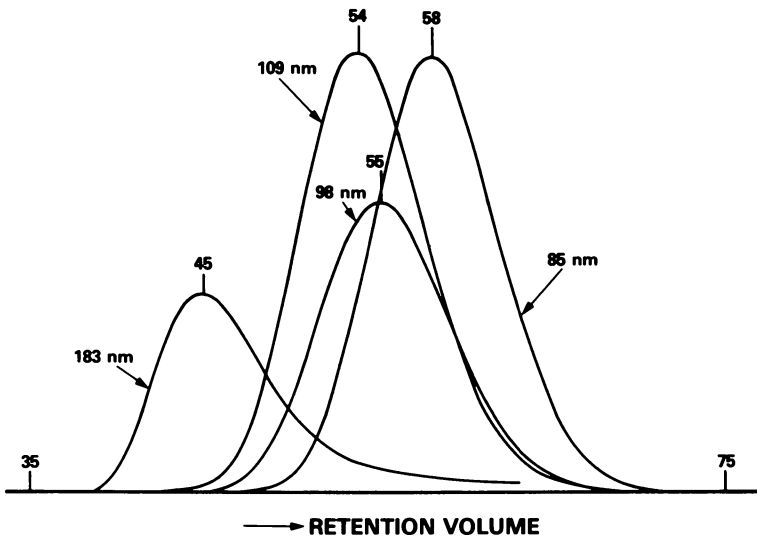


Figure 8. Chromatograms of standard lattices measured at 254-nm wavelength

Table III. Diameter Averages for Latex Particles Measured at 254 nm

For each sample,

Row 1. Uncorrected diameter averages from Rayleigh theory (equation 14).

Row 2. Uncorrected diameter averages from Mie theory (Equation 13).

Row 3. Diameter averages in row 1 corrected using Rayleigh correction factors (Equation 15).

Row 4. Diameter averages in row 2 corrected using Rayleigh correction factors (Equation 15).

Row 5. Corrected diameter averages from Mie theory (Equation 16).

Sample	Variance $\sigma^2(\text{ml}^2)$	$D_N$	$D_S$	$D_V$	$D_{SS}$	$D_W$	$D_T$ (nm)
85	12.423	63.1	64.7	66.3	69.7	73.2	76.7
		65.6	67.3	69.1	72.7	76.4	80.2
		80.5	80.7	80.9	81.3	81.7	82.0
		83.7	84.0	84.3	84.9	85.4	85.7
		80.7	80.8	81.1	81.7	81.9	82.1
98	12.560	74.8	76.6	78.5	82.5	86.8	91.0
		78.4	80.5	82.6	87.0	91.6	96.1
		95.6	95.8	96.1	96.5	97.0	97.4
		100.3	100.6	101.0	101.8	102.4	102.7
		95.8	96.0	96.3	96.9	97.4	97.7
109	13.258	76.2	78.7	81.2	86.4	91.6	96.6
		81.1	83.8	86.5	92.1	97.6	102.8
		98.9	99.6	100.4	101.9	103.1	103.7
		105.2	106.2	107.0	108.7	109.8	110.3
		100.2	101.0	101.7	103.2	103.7	104.1
183	14.152	105.6	111.0	116.7	129.1	141.6	152.3
		121.9	128.3	134.6	148.0	159.3	168.2
		139.3	142.8	146.5	154.0	160.6	164.3
		160.8	165.1	168.8	176.5	180.7	181.4
		150.9	154.4	157.3	163.6	167.8	169.9



excellent agreement with their reported values. They increase from  $D_N$  to  $D_T$  in the order expected. For the 183 nm sample, though  $D_{SS}$ ,  $D_W$  and  $D_T$  are fairly close,  $D_N$ ,  $D_S$  and  $D_V$ , are rather low. This appears to be related to the pronounced skewing of the chromatogram; the approximation of a Gaussian spreading function in such an event being inaccurate insofar as the smaller diameter averages are concerned.

Table IV. Diameter Averages for Latex Particles Measured at 280 nm  
For each sample,

Row 1. Uncorrected diameter averaged from Mie theory (Equation 13).

Row 2. Diameter averages in row 1 corrected using Rayleigh correction factors (Equation 15).

Row 3. Corrected diameter averages from Mie theory (Equation 16).

Sample	Variance $\sigma^2(\text{ml}^2)$	$D_N$	$D_S$	$D_V$	$D_{SS}$	$D_W$	$D_T$ (nm)
85	12.966	63.8	65.7	67.6	71.6	75.6	79.6
		82.3	82.7	83.2	84.1	84.9	85.3
		79.8	80.2	80.6	81.3	81.8	82.2
98	13.575	74.3	76.6	79.0	84.0	89.1	94.0
		96.9	97.6	98.2	99.5	100.5	101.1
		94.2	94.2	94.4	95.1	96.0	96.5
109	13.421	81.1	83.7	86.4	91.9	97.3	102.6
		105.5	106.4	107.1	108.6	109.7	110.2
		101.1	101.8	102.3	103.3	104.1	104.4

In terms of the accuracy of measurement, it appears from Tables III - V that detection of a narrow distribution particle mixture at 350 or 280 nm is just as advantageous as detection at 254 nm. However for a broad particle size distribution sample, detection at 254 nm or lower where particles absorb, provides a distinct improvement in small particle detection (7).

The diameter averages calculated using Mie scattering theory are consistently lower than those calculated using Rayleigh scattering theory. This appears to be a numerical problem associated with the rather high values of  $\sigma^2$  encountered in particle chromatography. Consider curve ABCD in Figure 9; it represents the path along which any one diameter average varies for a chromatogram synthesized from a Gaussian  $W(y)$  and Gaussian spreading function with the diameter averages based on the portion of the chromatogram between retention volumes X and Y, chromatogram heights beyond X and Y being considered non zero, however. In an experimental chromatogram these heights would be indistinguishable from the baseline. Along ABCD,  $D_N < D_S < D_V < D_{SS} < D_W < D_T$ . When chromatogram heights beyond X and Y were set equal to zero, the path became A'BCD'. Along A'B and CD' the order of the diameter averages were generally completely reversed. This anomaly

occurs because of the nature of the moment equation where each term under the summation is multiplied by the ordinate  $F(v-E_i\sigma^2)$ . At retention volumes in the neighbourhood of Y, evaluation of smaller moments requires ordinates at retention volumes beyond this neighbourhood (higher  $v$ ) while in the vicinity of X, evaluation of higher moments requires ordinates at retention volumes beyond the neighbourhood of X (lower  $v$ ). Departure from ABCD with opposite trends at the respective ends are thus exhibited. The effects cancel each other to a certain extent leaving the overall diameter averages slightly lower than expected. The points B and C approach A and D respectively as  $\sigma^2$  is decreased.

Table V. Diameter Averages for Latex Particles Measured at 350 nm  
For each sample,

Row 1. Uncorrected diameter averages from Mie theory (Equation 13).

Row 2. Diameter averages in row 1 corrected using Rayleigh correction factors (Equation 15).

Row 3. Corrected diameter averages from Mie theory (Equation 16).

Sample	Variance $\sigma^2(\text{ml}^2)$	$D_N$	$D_S$	$D_V$	$D_{SS}$	$D_W$	$D_T$ (nm)
85	12.66	64.3	66.0	67.8	71.4	75.2	79.1
		82.5	82.7	83.0	83.6	84.2	84.6
		81.4	81.2	81.2	81.6	82.3	82.5
98	13.580	73.1	75.4	77.9	82.9	88.0	93.0
		95.4	96.1	96.8	98.2	99.3	100.0
		92.8	93.4	93.8	94.9	96.0	96.3
109	13.050	81.0	83.3	85.7	90.6	95.7	100.8
		104.6	105.1	105.6	106.6	107.5	108.1
		101.1	101.6	101.9	102.6	103.5	103.8
183	13.964	123.9	129.3	134.7	146.2	156.8	165.8
		162.8	165.8	168.5	174.0	177.6	178.6
		154.1	156.5	158.7	164.0	168.1	169.5

Mixtures of Latex Particles. To further assess the success of the theory in calculating particle diameter averages, two binary mixtures were considered. Mixture 1 was a mixture of 183 and 85 nm particles in the weight ratio 38.73/61.27, while mixture 2 was a mixture of 183 and 109 nm particles in the weight ratio 51.05/48.95. Their chromatograms are shown in Figure 10.

The diameter averages calculated from the mixture rule are given in Table VI. While the first row entries for each mixture are the true values, the values that would be obtained from the analysis of the bimodal chromatograms should be compared with the third row entries since these account not only for the less than satisfactory calculations for the 183 nm sample chromatogram, but also for the incomplete recovery of the 183 nm particles.

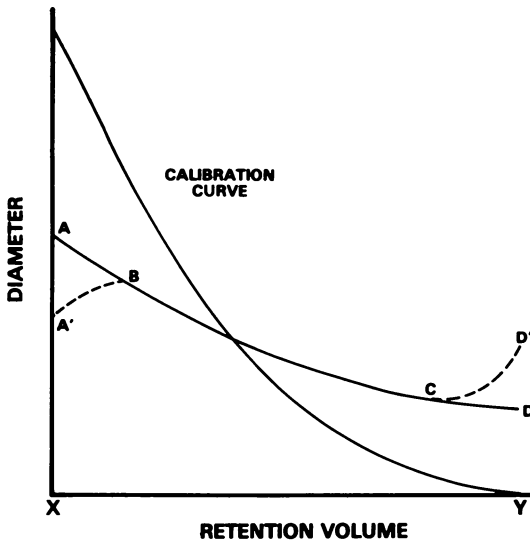
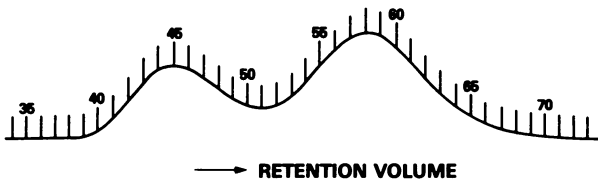
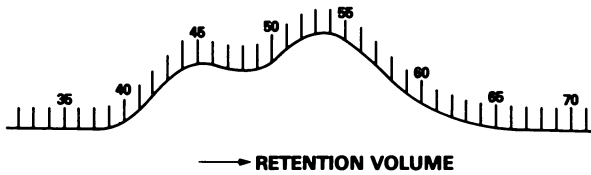


Figure 9. Variation of diameter averages with retention volume



MIXTURE 1: MIXTURE OF 183 AND 85 nm LATICES



MIXTURE 2: MIXTURE OF 183 AND 109 nm LATICES

Figure 10. Chromatograms of Mixtures 1 and 2

Table VI. Diameter Averages Based on Mixture Rule

For each mixture,  
 Row 1. Calculated assuming all diameter averages for each component are equal to their diameter as reported by supplier. For e.g.  $D_N = D_S = D_V = D_{SS} = D_W = D_T = 85$  for 85 nm sample.  
 Row 2. Calculated from diameter averages for each component as given by Mie Theory. For e.g.  $D_N = 80.7$ ,  $D_S = 80.8$ , etc. (Table III) for 85 nm sample.  
 Row 3. Calculated as in row 2 but accounting for incomplete recovery of 183 nm particles.

Mixture	$D_N$	$D_S$	$D_V$	$D_{SS}$	$D_W$	$D_T$ (nm)
1	90.8	93.8	98.0	107.2	123.0	140.1
	84.9	86.9	90.2	98.3	112.2	128.4
	82.6	83.6	85.4	89.7	98.1	111.8
2	122.4	125.6	129.4	137.4	146.8	155.5
	109.4	112.5	116.1	124.7	134.7	143.8
	104.6	106.7	109.1	114.8	122.0	130.6

The diameter averages of the mixtures evaluated using Mie Theory are presented in Table VII. For each mixture they are computed for  $\sigma^2$  values equal to those of individual components and their mean. The averages fortunately are not very sensitive to the  $\sigma^2$  values between those of individual components. Computed values with mean  $\sigma^2$  for each mixture compare very favourably with their row entries for each mixture in Table VI. Similar results were obtained when Rayleigh scattering was considered.

Table VII. Diameter Averages for Mixtures 1 and 2 Calculated Using Mie Theory

Mixture	Variance $\sigma^2$ (ml <sup>2</sup> )	$D_N$	$D_S$	$D_V$	$D_{SS}$	$D_W$	$D_T$ (nm)
1	12.423	81.2	82.2	84.0	88.3	96.8	110.5
	14.152	83.6	84.6	86.0	89.8	98.7	113.4
	13.288	82.2	83.2	85.0	89.3	97.7	111.8
2	13.258	107.4	109.1	110.8	114.9	121.6	129.5
	14.152	108.8	110.4	111.8	115.7	122.3	130.3
	13.705	107.9	109.6	111.1	115.2	121.9	130.0

Considering the inapplicability of either Rayleigh or Mie theory to our data, it is indeed surprising that the calculated diameter averages are in such good agreement with expected values. Equations (16)-(19) derived using Mie theory throw some light on this anomaly. Consider that  $k^{-1}(y)$  in equation (19) is multiplied by  $\epsilon$  where  $\epsilon$  is a constant independent of  $y$ . This in a very

approximate sense described the variation of measured extinction coefficient with  $y$ ; its consequence is to introduce a constant multiplying factor  $\epsilon$  in equation (16). The latter, however, has no effect on the evaluation of the diameter averages.

### Summary and Conclusions

A summary of the preceding discussions and conclusions derived from them now follows:

1. Calibration of each column one at a time results in the weeding out of those columns which have inadequate peak separation, excessive peak broadening and significant particle loss by entrapment in the packing.
2. The column packing procedure strongly influences the retention of large sized particles. The percentage of unretained particles of any size can be estimated from the ratio of its chromatogram areas obtained with and without the columns connected to the chromatograph.
3. The monodispersity of standard latices used for calibration must be considered suspect.
4. Measured extinction coefficients do not agree with calculations from Mie theory for non-absorbing spheres.
5. The chromatograms of standard latices indicate skewing at their trailing ends which becomes more pronounced as the particle size increases, possibly due to particle entrapment.
6. The particle size analysis techniques outlined earlier show promise in the measurement of polydispersed particle suspensions. The assumption of Gaussian instrumental spreading function is valid except when the chromatograms of standard latices are appreciably skewed. Calculation of diameter averages indicate a fair degree of insensitivity to the value of the extinction coefficient.
7. In terms of accuracy of measurement, for a narrow distribution sample, there appears to be no preferred wavelength for signal detection in the UV range.

### Literature Cited

1. Small, H. J. Colloid & Interface Sci., 1974, 48(1), 147.
2. Small, H.; Saunders, F.L; Solc, J. Advances in Colloid & Interface Sci., 1976, 6, 237.
3. Stoitsits, R.F.; Poehlein, G.W.; Vanderhoff, J.W. J. Colloid & Interface Sci., 1976 57(2), 337.
4. McHugh, A.J.; Silebi, C.A.; Poehlein, G.W.; Vanderhoff, J.W. Colloid & Interface Sci., 1976, 4, 549.
5. Silebi, C.A.; McHugh, A.J. AIChE J. 1978(March), 204.
6. Buffham, B.A. J. Colloid & Interface Sci. 1978, 67(1), 154.
7. Silebi, C.A.; McHugh, A.J. J. Applied Polymer Sci., 1979, 23, 1699.

8. Krebs, K.F.; Wunderlich, W. Angew Makromol. Chem., 1971, 20, 203.
9. Gaylor, V.F.; James, H.L. Reprints - Pittsburg Conference on Analytical Chemistry, Cleveland, Ohio, 1975.
10. Coll, H.; Fague, G.R.; Robillard, K.A. Unpublished work, Eastman Kodak Co., Rochester, N.Y, 1975.
11. Hamielec, A.E.; Singh, S. J. Liquid Chromatography, 1978, 1(2), 187.
12. Husain, A.; Vlachopoulos, J.; Hamielec, A.E. J. Liquid Chromatography, 1979, 2(2), 193.
13. Heller, W.; Tabibian, R.M. J. Colloid Sci., 1957, 12, 25.
14. Mie, G. Ann. Phys., 1908, 25, 377.
15. Heller, W.; Pargonis, W.J. J. Chemical Physics, 1957, 26, 498.
16. Kerker, M. "The Scattering of Light and Other Electromagnetic Radiation", P324, Academic Press, New York, 1969.
17. J.V. Dave, "Subroutines for Computing the Parameters of the Electromagnetic Radiation Scattered by a Sphere", IBM Report No. 320-3237, IBM Scientific Center, Palo Alto, Ca. (1968).

RECEIVED May 7, 1980.

# Exclusion Chromatography Analysis of Latex Solutions for Monitoring Nitrile Resin Polymerizations

T. J. WILLIAMSON and V. F. GAYLOR

The Standard Oil Company (Ohio), 4440 Warrensville Center Road, Cleveland, OH 44128

I. PIIRMA

Institute of Polymer Science, University of Akron, Akron, OH 44325

Reports of chromatographic methods for measuring gel contents of elastomers introduced several novel techniques and observations (1, 2). These gel measurement methods were based on solubilizing emulsion polymerized elastomers by mixing aqueous latex with elastomer solvent. The resulting solutions, which also contained solvent swollen gel particles, were then separated and analyzed by exclusion chromatography. The chromatographic separations resulted in separate, well defined peaks for insoluble gel particles, as well as for soluble elastomer and low molecular weight species. These workers found that the chromatographic detector, a differential refractometer, gave equal responses to both insoluble and soluble polymer. They therefore pointed out that total polymer peak area was proportional to total solids content, and that the technic was rapid enough for monitoring polymerization reactions.

The present paper reports preliminary work aimed at extending this chromatographic technology to other types of resins. Two different emulsion polymerization reactions were investigated. One was the polymerization of acrylonitrile and methylacrylate (75/25 AN/MA) in the presence of an acrylonitrile elastomer (70/30 BD/AN) to produce a graft resin. The second was the copolymerization of acrylonitrile and styrene (70/30 AN/S). Chromatographic analyses of latex solutions were conducted periodically during both types of polymerization reactions, using acetonitrile as latex solvent and chromatographic mobile phase. An ultraviolet absorption detector was used in tandem with a differential refractometer detector to obtain chemical composition data (3, 4, 5, 6).

## Experimental

Latex solutions for chromatographic analysis were prepared by adding weighed amounts of latex to known amounts of acetonitrile. Latex solution concentrations were 0.2 g/100 ml for AN/S copolymers and 1.0 g/100 ml for the AN/MA graft resins.

Latex and solvent were mixed in bottles and the capped bottles were shaken for 10 minutes on a Burrell Wrist-Action Shaker. The latex solutions were filtered through a 0.9  $\mu\text{m}$  filter prior to chromatographic analysis. Known volumes of the filtered solutions were injected into the chromatograph by loop injection. Injection volumes were 250  $\mu\text{l}$  of AN/MA solutions and 500  $\mu\text{l}$  of AN/S solutions.

Chromatographic separations were made on a Waters Associates Inc. liquid chromatograph, Model 501, which was equipped with both variable wavelength UV and differential refractometer detectors. The UV detector was operated at 230 nm when analyzing AN/MA solutions and at 254 nm for AN/S solutions. The mobile phase was acetonitrile and flow rate was 1.0 ml/min. Stainless steel columns were prepared from 1/8-in I. D. tubing and were packed with 170-200 mesh controlled porosity glass particles (Electro-Nucleonics). A bank of seven 2-ft. columns was used, and they contained glass particles ranging in pore size (as measured by mercury intrusion) from 75-1250 $\text{\AA}$ . Except for the inlet to the first column, all column end fittings were equipped with 5- $\mu\text{m}$  snubbers.

Chromatographic peak areas were measured by both manual and mechanical integration methods. Total analysis time was less than one hour per sample.

### Chromatographic Interpretation Techniques

Overall goal of this work was to maximize the amount of information obtained from chromatographic analysis of latex solutions. More specific aims were: (1) measure amounts of unreacted monomers, as one measure of conversion, (2) determine amount of polymer, as a second measure of conversion, (3) estimate chemical composition of the polymer formed, and (4) look for evidence of grafting (in the AN/MA polymerization) as evidenced by detection of insoluble polymer formation.

The porous glass packed columns did not yield high resolution separations, but the major species present in a latex were adequately separated, Figure 1. Insoluble polymer, when present, was excluded from the pores and eluted at interstitial volume. Elution order of remaining species was soluble polymer, unreacted monomers, and water. In both types of resins studied, no separation of the two unreacted monomers was achieved. A single chromatographic peak, that included both monomers, was obtained.

Ability to analyze unreacted monomers was dependent on detector selectivity. The UV detector was operated at 254 nm for analysis of AN/S latex solutions. Styrene is a strong UV absorber at this wavelength while acrylonitrile has no measurable absorbance at 254 nm. Thus, the UV detector was entirely selective to monomeric styrene. The refractometer detector was sensitive to both acrylonitrile and styrene when each was present in the desired copolymer proportions (70/30). However,



to achieve that copolymer composition it was necessary to maintain a large excess concentration of acrylonitrile during polymerization. The much smaller amounts of unreacted styrene present were no interference to measuring monomeric acrylonitrile from the refractometer chromatogram.

Unreacted monomers in AN/MA latex solutions were measured similarly. Methylacrylate is a relatively strong UV absorber in the 225-250 nm range while acrylonitrile does not significantly absorb UV radiation at wavelengths above about 220 nm. At 230 nm, the wavelength used, the UV detector responded only to methylacrylate. And the refractive indices of the two monomers are such that, in the 75/25 AN/MA proportions used, the refractometer was insensitive to methylacrylate. The refractometer therefore functioned as a selective detector for acrylonitrile in the presence of methylacrylate.

Similarly, estimation of chemical composition of soluble polymer was also dependent on selectivity of the UV detector. Polymerized acrylonitrile has no significant UV absorbance at 230 and 254 nm. Thus, UV chromatograms were used to estimate amounts of polymerized methylacrylate and styrene in each resin system. The refractometer detector was sensitive to polymerized methylacrylate and styrene, as well as to polymerized acrylonitrile. It was therefore necessary to calculate comonomer contribution to refractometer peak areas in order to estimate concentration of polymerized acrylonitrile. This was done by obtaining a refractometer calibration for all three homopolymers. Quantity of polymerized comonomers measured by UV were then converted to equivalent refractometer peak areas. Peak areas due to polymerized acrylonitrile were then calculated by difference, and used to calculate amount of polymerized acrylonitrile.

Total soluble polymer (solids) in each latex sample was calculated by simply summing the amounts of polymerized acrylonitrile and polymerized comonomer.

#### Calibration Methods

All three monomers were soluble in the chromatographic mobile phase and standard analytical techniques were used for calibration. Solutions containing known quantities of monomer were chromatographed to establish a peak area concentration relationship for the appropriate detector. The homopolymer of methylacrylate was also soluble in the mobile phase. Thus, both UV and refractometer detectors were calibrated for polymerized methylmethacrylate by chromatographing solutions of PMA.

The homopolymers of styrene and acrylonitrile were not soluble in the acetonitrile mobile phase. Calibration factors thus had to be derived from a combination of literature data and experimental measurements. To calibrate the UV detector for polystyrene, 254 nm absorbance of both monomer and polymer was measured with a conventional spectrophotometer, using chloroform

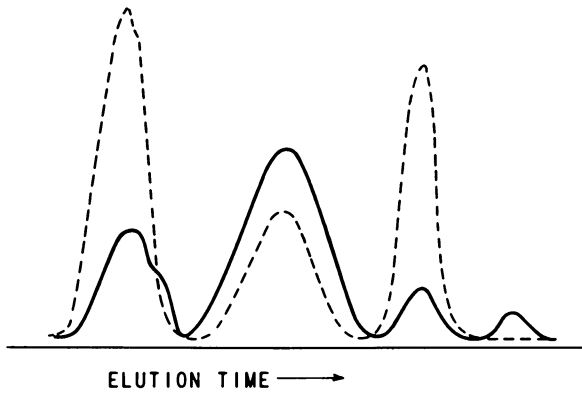


Figure 1. Chromatogram of AN/MA graft polymer ((—) differential refractometer detector; (---) UV absorbance detector)

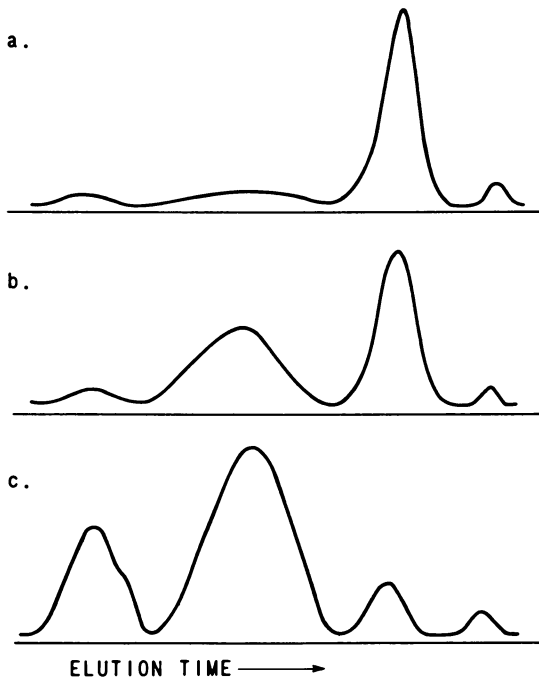


Figure 2. Chromatograms of AN/MA graft polymer (differential refractometer detector: (a) 7% total solids; (b) 11% total solids; (c) 27% total solids)

solvent. These measurements yielded the needed relationship between monomer and polymer absorbance. A chromatographic UV calibration for the polymer was then calculated from the experimentally measured monomer calibration data.

Published refractive index data for the mobile phase, polystyrene, polyacrylonitrile, and the two monomers were used to calculate refractive index detector calibrations for the two homopolymers. The published data were used to determine relationship between refractive index increments of monomer and corresponding homopolymer. Chromatographic refractometer calibrations for the two homopolymers were then calculated from experimentally measured calibration data for the two monomers.

#### Results on AN/MA Graft Resin

The AN/MA graft resin was made by polymerizing the two monomers, in the presence of BD/AN elastomer, in a batch reaction. Chromatographic data at 12 different conversion levels were obtained for this polymerization. Illustrative chromatograms (refractometer detector) for three different conversion levels are shown in Figure 2. These chromatograms graphically demonstrate expected growth in size of the soluble polymer peak with increasing conversion, as well as concomitant decrease in monomer concentration. Further, Figure 2 shows presence of insoluble polymer, even at low conversion. Insoluble polymer at low conversions is probably largely, if not totally, elastomer. The elastomer particles were insoluble in the mobile phase but were eluted from the columns and detected by both detectors. The much larger insoluble polymer peak at high conversions may include insoluble graft polymer. The insoluble polymer peak tended to exhibit bimodal character at high conversion levels.

Chromatographically measured monomer concentrations decreased linearly with increasing conversion, Figure 3, as expected. The fitted line extrapolates to about 28% total monomers at zero solids, in good agreement with the 29% monomers charged. This agreement suggests that the chromatographic method can measure unreacted monomers with good precision. Consumption rates of the two individual monomers were also measured, Figure 4. These two monomers copolymerize randomly and individual consumption rates may vary. In this case, slopes of the fitted lines were 0.37 and 0.09 for acrylonitrile and methylacrylate, respectively. These slopes indicate that acrylonitrile was incorporated into the polymer at a rate about four times greater than was methylacrylate.

The method of calculating chemical composition of solubilized polymer was tested in two different ways. The sum of polymerized monomers calculated from chromatographic data should approximate total solids in the latex samples. Figure 5 compares calculated solids contents with total solids measured by the conventional gravimetric method. A good correlation was

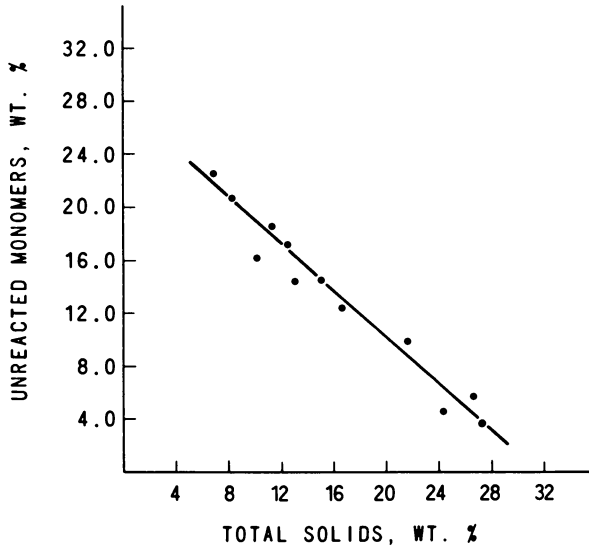


Figure 3. Consumption of monomers during polymerization

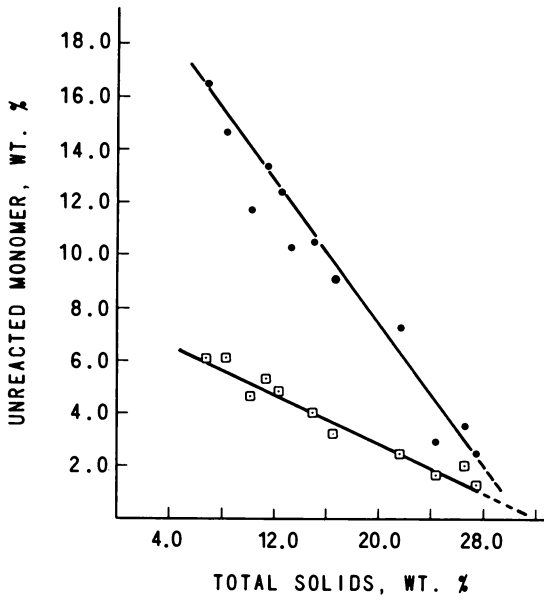


Figure 4. Relative consumption rates of acrylonitrile (●) and methacrylate (□) during polymerization

obtained, but calculated solids values were lower than measured total solids in every case. This was not unexpected. The chromatographic method detected presence of insoluble polymer but peak areas could not be directly related to concentration. The reactor was charged with 3% elastomer which was insoluble in the chromatographic mobile phase. Thus, the relationship between calculated and measured solids contents should have, and did, differ by at least 3% at low conversions. Expected formation of insoluble graft polymer would also have influenced relationship between calculated and measured total solids.

Calculated monomer proportions in solubilized copolymer at each conversion level are compared to unreacted monomer proportions in Table I. At low conversion levels, T<sub>3</sub>-T<sub>5</sub>, the copolymer appeared to be rich in methylacrylate. This anomaly was not detected in unreacted monomer measurements, possibly because the amount of copolymer was small relative to the large excess of unreacted monomers. As conversion increased (T<sub>6</sub>-T<sub>14</sub>) calculated copolymer composition approached the 75/25 AN/MA target and averaged exactly 75/25.

Unreacted monomer proportions (Table I) were essentially constant at 72/28 AN/MA until the T<sub>12</sub> sampling. The last three high conversion samples contained a significantly smaller proportion of acrylonitrile. This decrease in unreacted acrylonitrile was not accompanied by a detectable change in composition of soluble copolymer. However, there was an accompanying change in size of the insoluble polymer peak. Figure 6 compares refractometer peak areas for each of the three species at each conversion level. The insoluble polymer peak was essentially constant in size up to about 12% total solids. The amount of insoluble polymer then appeared to slowly increase with increasing conversion, followed by an apparent sharp rise in amount at very high conversions. Increased amounts of insoluble polymer could be due to presence of either or both graft polymer or high molecular weight, nitrile rich polymer. The chromatographic detectors yield no insight into chemical composition of the insoluble polymer peak. However, theoretical considerations indicate initiation of the polymer graft reaction at about 12% total solids. Increases in amount of insoluble polymer at moderate conversions may reflect that reaction, while additional increases at high conversions may indicate formation of nitrile rich polymer.

In summary, these exploratory data suggest that the chromatographic method used could be a valuable tool for study of this polymerization reaction. Reasonable data were obtained for amount and composition of the copolymer. Formation of graft polymer and/or nitrile rich polymer was detected. More detailed chromatographic study of this batch polymerization could lead to a practical on-line monitoring method.

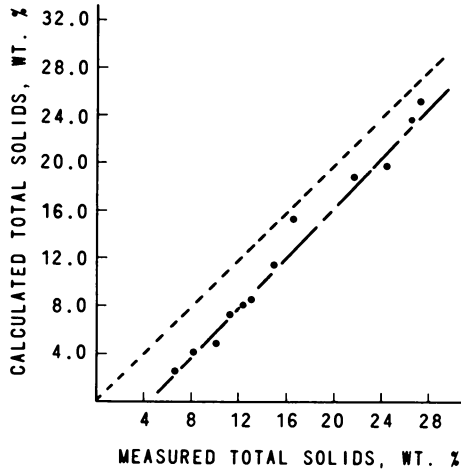


Figure 5. Comparison of calculated and measured total solids ((—) fitted line; (---) 45° line)

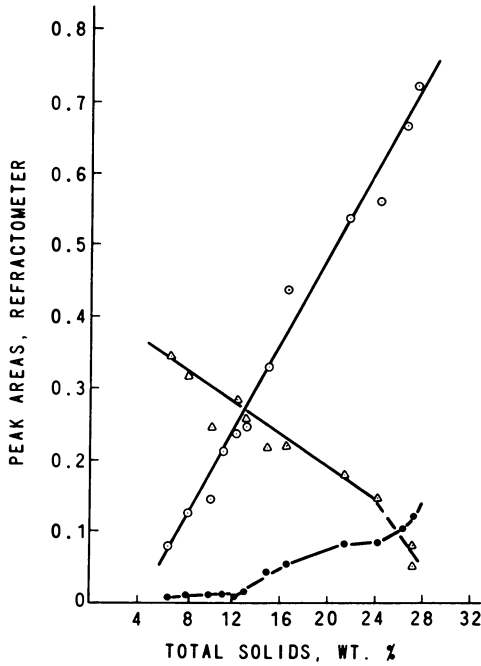


Figure 6. Comparison of peak areas for polymers and monomer ((○) soluble polymer; (●) insoluble polymer; (△) monomer (acrylonitrile))

Table I  
Composition Analyses for AN/MA Graft Terpolymer

<u>Sample</u>	<u>Total Solids*</u>	Unreacted Monomer	Polymerized Monomer
		Proportions	Proportions
		<u>AN/MA</u>	<u>AN/MA</u>
T <sub>3</sub>	6.7	73/27	55/45
T <sub>4</sub>	8.2	71/29	64/36
T <sub>5</sub>	10.1	72/28	65/35
T <sub>6</sub>	11.3	72/28	72/28
T <sub>7</sub>	12.4	72/28	73/27
T <sub>8</sub>	13.1	71/29	73/27
T <sub>9</sub>	15.0	72/28	78/22
T <sub>10</sub>	16.6	74/26	78/22
T <sub>11</sub>	21.6	74/26	79/21
T <sub>12</sub>	24.4	64/36	75/25
T <sub>13</sub>	26.5	63/37	76/24
T <sub>14</sub>	27.3	64/36	75/25

\* Measured gravimetrically

### Results on AN/S Copolymers

Samples taken during three different AN/S polymerizations were analyzed chromatographically. Target composition was 70/30 AN/S for all three polymerizations. It is difficult to prepare high nitrile copolymers of styrene because reactivity ratios of the two monomers are very different. This study used continuous addition of monomers to achieve the desired polymer composition. Addition rates were those needed to maintain an excess of acrylonitrile.

Attempts to accurately measure the monomers chromatographically were of questionable success. Monomer concentrations were less than 5% acrylonitrile and 0.1% styrene. Chromatographic repeatability on both monomers was good. However, the two monomers were also measured by gas chromatographic and titrimetric methods. Agreement between all three methods was poor for both monomers. There was therefore no basis for evaluating quality of liquid chromatography results.

A carefully prepared copolymer of the desired 70/30 proportions dissolved readily in the acetonitrile mobile phase. However, insoluble polymer was detected in all three large scale polymerizations studied. As illustrated in Figure 7, two hour samples contained a significant fraction of insoluble polymer. After a four hour reaction amount of insoluble polymer was not significantly changed, while amount of soluble polymer approximately doubled. After polymerizing six hours there was only a modest increase in amount of soluble polymer, but amount of insoluble polymer doubled. Thus, insoluble polymer was formed very early and very late in the reactions, and this was the case in each of the polymerizations studied.

The homopolymers of both styrene and acrylonitrile were insoluble in the acetonitrile mobile phase. The insoluble polymer found was therefore probably rich in either nitrile or styrene. No definitive compositional analysis of the insoluble polymer was made. However chromatographic composition analyses suggested the insoluble polymer was high acrylonitrile polymer. Composition analyses calculated from chromatographic data on the soluble polymer fraction were compared to values calculated from total nitrogen analyses of coagulated polymers, Table II. Acrylonitrile contents of the soluble polymer fraction were significantly lower than total acrylonitrile contents in every case. These differences could be due to error in the chromatographic calibration method. However, the differences between chemically and chromatographically measured nitrile contents were roughly proportional to the relative amount of insoluble polymer, Figure 8. The insoluble polymer may therefore have been nitrile rich polymer.

The kind of chromatographic information generated on these polymers as a function of reaction time is illustrated in Figure 9. Polymerization to soluble polymer, calculated as % solids,



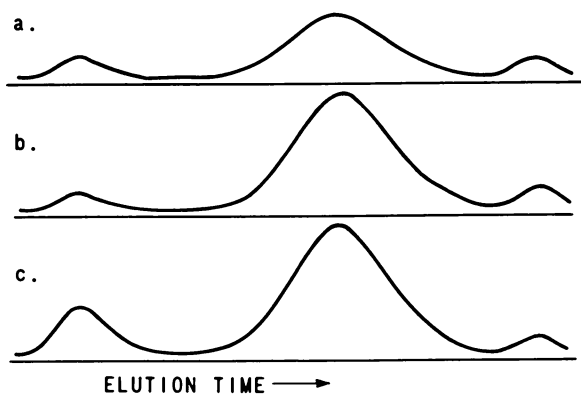


Figure 7. Chromatograms of AN/S copolymers ((a) 2-hr polymerization, 13% total solids; (b) 4-hr polymerization, 24% total solids; (c) 6-hr polymerization, 29% total solids)

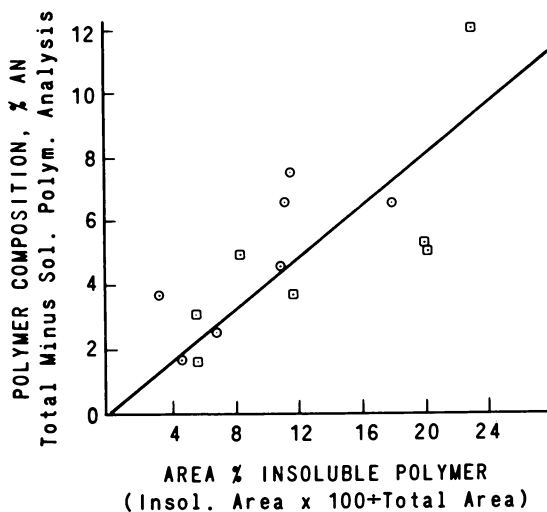


Figure 8. Effect of insoluble polymer on polymer composition analyses ((○) polymerization #1; (□) polymerization #2)

**Table II**  
**Polymer Composition Analyses for AN/S Copolymers**

<u>Polymerization</u>	<u>Total Solids*</u>	Polymerized Acrylonitrile		<u>Difference</u>
		<u>Chromatographic, Soluble Polymer</u>	<u>Chemical Analysis, Total Polymer</u>	
1	10.0%	62%	68%	6%
	18.6	67	70	3
	22.7	69	71	2
	24.9	68	71	3
	27.0	68	73	5
	28.5	67	74	7
2	7.0%	57%	69%	12%
	12.5	66	71	5
	18.5	68	71	3
	23.5	70	72	2
	27.0	69	73	4
	28.9	69	74	5
	29.5	69	74	5

\*Measured gravimetrically

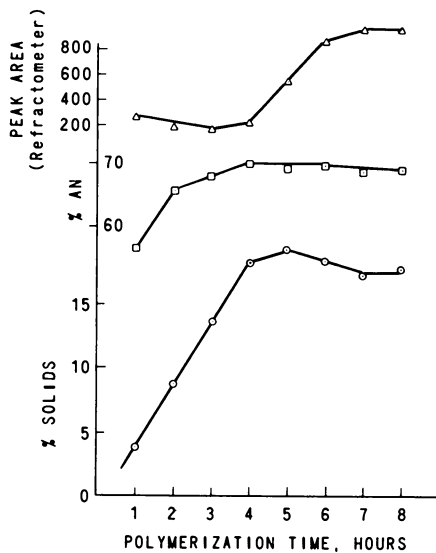


Figure 9. Chromatographic data on AN/S latex ((○) amount of soluble polymer; (◻) composition of soluble polymer, % acrylonitrile; (△) amount of insoluble polymer)

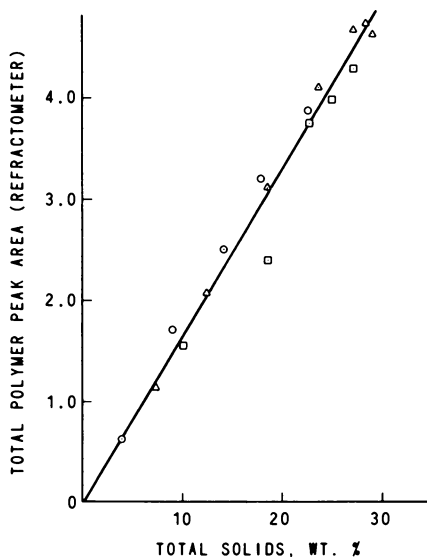


Figure 10. Polymer peak area correlation with total solids ((◻) polymerization #1; (△) polymerization #2; (○) polymerization #3)

ceased at about four hours, and additional reaction time generated only insoluble polymer. Acrylonitrile content of the soluble polymer was low at one and two hours polymerization time but approached the target 70% after three to four hours reaction.

Amount of soluble polymer generated in this reaction (Figure 9) was only 18-19% solids, which was well below the 29% total solids found after reaction completion. Differences between calculated soluble solids and gravimetrically measured total solids were large, but variable, for all three polymerizations studied. Thus, amount of soluble polymer was not proportional to total solids. However, a good correlation between total solids and the sum of refractometer peak areas for both polymer peaks was obtained, Figure 10. This correlation included all three polymerizations and there was little or no batch bias.

In summary, it was not possible to achieve all analytical goals in this study of AN/S polymerizations. We were unable to approximate total solids contents directly because of presence of insoluble polymer. Circumstantial evidence suggested the insoluble polymer contained more than 70% acrylonitrile and that this high nitrile resin was generated in rather large amounts. These studies did, however, suggest that the chromatographic method might be helpful in achieving better control of this polymerization.

#### Literature Cited

1. Gaylor, V. F., James, H. L., Herdering, J. P., J. Polym. Sci., Poly. Chem. Ed., 13, 1575 (1975).
2. James, H. L., Gaylor, V. F., Anthony, N. R., "The Use of Liquid Exclusion Chromatography for Rapid Measurement of Gel in Styrene-Butadiene Elastomers," presented at the 1975 Gel Permeation Chromatography Seminar, Pittsburgh, Pennsylvania (October, 1975).
3. Harmon, D. J., Folt, V. L., Rubber Chem. Technol., 46, 449 (1973).
4. Runyon, J. R., Barnes, D. E. Rudd, J. F., Tung, L. H., J. Appl. Polym. Sci., 13, 2359 (1969).
5. Owens, E. G., Cobler, J. G., 4th International Seminar on Gel Permeation Chromatography, Preprints, pp. 160-166 (1967).
6. Anderson, J. N., J. Appl. Polym. Sci., 18, 2819 (1974).

RECEIVED May 7, 1980.

# Polymer Viscosity Characterization by Size Exclusion Chromatography

W. W. YAU, M. E. JONES, C. R. GINNARD, and D. D. BLY

Central Research and Development Department, E. I. Du Pont de Nemours & Company, Wilmington, DE 19898

Size exclusion chromatography (SEC), historically known as gel permeation chromatography (GPC), is commonly used to determine polymer molecular weights and molecular weight distributions (1). In general practice solute retention in SEC is calibrated against polymer molecular weight (MW) using standard reference materials, and the resulting MW calibration curve is then used to deduce the needed quantitative molecular weight information from the elution curve for unknown polymers. The sample molecular weight distribution curve (MWD) and the weight-average and the number-average molecular weights,  $\bar{M}_w$  and  $\bar{M}_n$ , are usually reported as the most significant experimental results. The present use of SEC is limited mainly to molecular weight and molecular weight distribution analyses, without sample viscosity calculations.

For polymer-solvent systems with known Mark-Houwink coefficients,  $K$  and  $\alpha$ , the polymer intrinsic viscosity value  $[\eta]$  can be estimated from the SEC-MW data using the following equation:

$$[\eta] = K \sum_i W_i M_i^\alpha / \sum_i W_i = K \bar{M}_v^\alpha \quad (1)$$

$$\bar{M}_v = \left( \frac{\sum_i W_i M_i^\alpha}{\sum_i W_i} \right)^{1/\alpha} \quad (2)$$

where  $\bar{M}_v$  is the viscosity average molecular weight;  $W_i$  and  $\bar{M}_i$  are the weight fraction and molecular weight,

respectively, of the  $i^{\text{th}}$  polymer fraction eluting from the SEC system. The  $W_i$  and  $M_i$  values are obtained

experimentally from the SEC elution curve and the SEC-MW calibration curves. This SEC- $[\eta]$  approach was successfully tested by Hellman<sup>(2)</sup> on several polymers including polystyrene, polyethylene and polycarbonate. The results showed that good accuracy can be obtained from SEC calculated  $[\eta]$  values when reliable Mark-Houwink coefficients are available.

General use of the above routine is prevented by the lack of accurate literature K and  $\alpha$  values for different polymer-solvent systems. The usual variance in literature K and  $\alpha$  values is sufficiently large to cause unacceptably large errors in SEC calculated  $[\eta]$  values. It is the purpose of this paper to provide an alternative approach to obtaining  $[\eta]$  by SEC which does not involve polymer K and  $\alpha$  values. In this new approach, SEC solute retention is calibrated directly against  $[\eta]$  by using even broad molecular weight distribution samples of known or measured viscosity as calibration standards. Only two standards are generally required in the proposed method and these can usually be obtained in practice. It is hoped that the improved precision and the practical convenience of the direct viscosity calibration approach will further encourage users of SEC to perform sample intrinsic viscosity  $[\eta]$  calculations in routine SEC analyses.

An added benefit of the direct SEC- $[\eta]$  calibration approach is that a new independent way of determining K and  $\alpha$  values, using only broad MW standards, has also resulted. As few as three standards (or four, if all are narrow MWD) are needed to obtain both MW and  $[\eta]$  calibration curves for a particular polymer-solvent system by using the broad-standard, linear calibration approach. From the experimental calibration constants of the two calibration curves, one can calculate K and  $\alpha$  directly as described later.

Since  $[\eta]$  is a physically measurable quantity and is more directly relatable than the usual SEC calculated  $\bar{M}_n$  and  $\bar{M}_w$  values to the macroscopic viscosity parameters of the polymer solution, a routine SEC- $[\eta]$  method brings SEC a step closer to practical evaluation of the strength and processibility of different polymer samples.

### Experimental

Polystyrene standards of known MW used in this study (Pressure Chemical Company and National Bureau of Standards) were narrow MWD, with MW values ranging from 4000 to 1.8 million, except for one broad standard, NBS 706 (Table 3). A polymethyl methacrylate (PMMA)

sample, Lucite® 40, (E. I. du Pont de Nemours and Company), was characterized in-house and further used to test the accuracy of the  $[\eta]$  calculations. The solvent used for both the SEC and  $[\eta]$  measurements was tetrahydrofuran (THF), distilled-in-glass (Burdick & Jackson). Solutions of 0.25% (w/v) polymers were used with a flowrate of 1 ml/min in the SEC experiment. The effluent was detected with a Micromeritics Model 770 differential refractometer.

SEC data were obtained on a Hupe-Busche Model 1010B liquid chromatograph obtained from Hewlett-Packard. A series of two sets of silanized bimodal PSM columns, 2 x 60A + 2 x 1000A (E. I. du Pont de Nemours & Company), were used to achieve the desired linear SEC calibration curves in this study. Molecular weight calibration curves for this column combination are shown in Figure 1. The peak position calibration curve obtained from narrow standards is plotted as the solid line and a broad-standard calibration is plotted as the dotted line. The latter was obtained using standard NBS 706 and the broad-standard calibration method of reference 3 with a band broadening correction factor equivalent to a peak sigma value of 0.3ml.

The SEC data were collected and handled by the du Pont Experimental Station PDP-10 real-time computer system (4)

The  $[\eta]$  values of all polymers were measured with a Cannon Fenske type capillary viscometer.

## Results and Discussion

A. The Existing or Classical SEC- $[\eta]$  Method. The precision of the existing method which uses literature  $K$  and  $\alpha$  values and experimental SEC-MW data to calculate polymer  $[\eta]$  values according to Eqs. (1) and (2) is tested here to show that the method works well when reliable  $K$  and  $\alpha$  values are used (e.g., with polystyrene) and that the method works poorly when there are appreciable variances in the  $K$  and  $\alpha$  values (e.g., with literature values for PMMA).

In the polystyrene case, carefully handled conventional viscometric techniques were used to obtain  $[\eta]$  values and subsequently the needed  $K$  and  $\alpha$  values. The data are illustrated in Figure 2. The log-log plot of the reported molecular weights of the standards and the measured  $[\eta]$  values (plotted as  $[\eta]$  meas.) gives the expected straight line relationship in the molecular weight range of interest. A  $K$  value of  $1.25 \times 10^{-4}$  dl/g and an  $\alpha$  value of 0.72, which define the solid line shown in the figure, were then used with the SEC

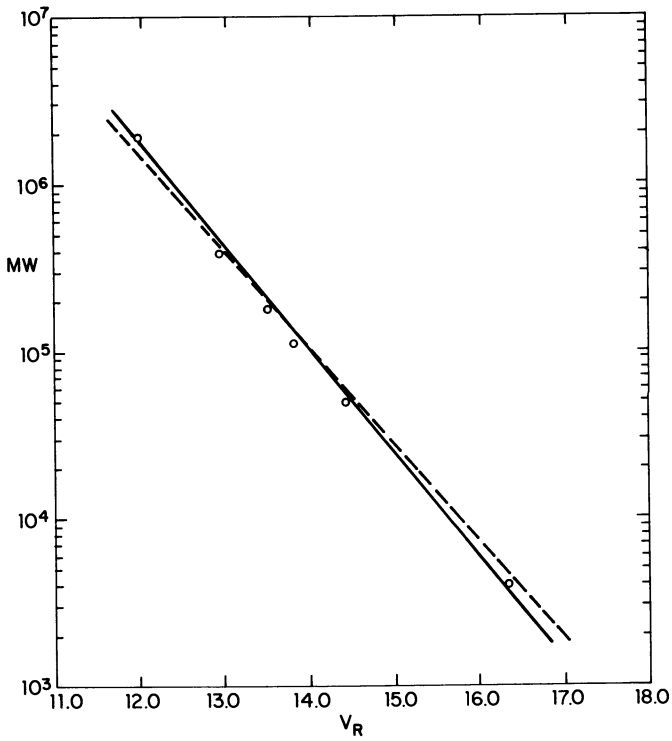


*Figure 1. SEC-MW calibration curves for polystyrene ((—) peak position calibration curve; (---) broad standard calibration; columns: 4 silanized Du Pont bimodal PSM columns; solvent:THF*



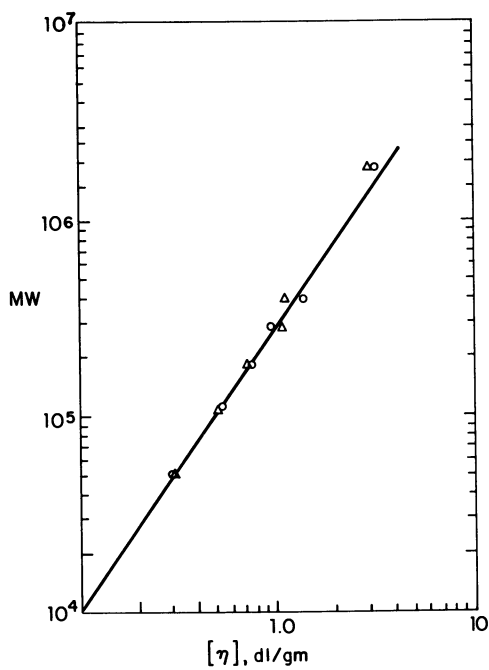


Figure 2. Measured vs .SEC-calculated  $[\eta]$  of polystyrene ( $\circ$ )  $[\eta]_{meas}$ ; ( $\Delta$ )  $[\eta]_{sec}$ :  
 $[\eta] = KM_v^\alpha$ ,  $K = 1.25 \times 10^{-4}$ ,  $\alpha = 0.72$ ;  $\log_e [\eta] = \log K + \alpha \log_e M_v$

elution curves of the narrow standards to calculate the second set of  $[\eta]$  values, plotted also in the figure as  $[\eta]_{\text{SEC}}$ . The figure shows the good agreement between the  $[\eta]_{\text{meas.}}$  and the  $[\eta]_{\text{SEC}}$ . The fact that the data points are rather randomly scattered indicates that precision in the SEC determined  $[\eta]$  values is comparable to the actual  $[\eta]$  measurements obtained by the more involved conventional viscometric techniques.

Since narrow standards are usually not available for most polymers, the experimental determination of  $K$  and  $\alpha$ , as illustrated in Figure 2, is not a generally applicable approach and literature values of  $K$  and  $\alpha$  must normally be used for this SEC- $[\eta]$  calculation. However, the literature values are often not very consistent, as illustrated for PMMA here. (See also Table 10-2, in Reference 1.) As shown in Table 1, the variation for the reported  $K$  value is about 10% and for  $\alpha$ , about 4%. These variations cause a 20% range of uncertainty in the calculated  $[\eta]_{\text{SEC}}$  values as calculated from equations 1 and 2.

B. Direct SEC- $[\eta]$  Calibration. Because the SEC separation process is directly related to the size of the solvated molecules, and for a homopolymer series the molecular size is directly related to MW as well as  $[\eta]$ , it is not necessary to proceed through MW calculations to study polymer intrinsic viscosity. Since SEC retention,  $V_R$ , is monotonically dependent on  $[\eta]$ ,

a unique calibration relationship exists between SEC solute retention and sample  $[\eta]$  as it does with SEC-MW calibration. This can be seen in Figure 3, which is a plot of the above  $[\eta]$  data now plotted against  $V_R$  for the narrow polystyrene standards. The  $[\eta]$ - $V_R$  relationship in Figure 3 is the same as that obtained with the peak position SEC- $[\eta]$  calibration.

With SEC retention volume calibrated against sample viscosity, the viscosity of any sample can be calculated according to equation 3, without involving MW calculations and  $K$  and  $\alpha$  values.

$$[\eta]_{\text{Whole sample}} = \frac{\sum_i W_i [\eta]_i}{\sum_i W_i} \quad (3)$$

where  $W_i$  and  $[\eta]_i$  are the weight fraction and intrinsic viscosity values of the polymer species respectively eluted in the  $i^{\text{th}}$  volume element of the SEC elution chromatogram. The accuracy of this approach is expected to be better than  $[\eta]$  calculations which depend on the classical SEC-MW calibration and  $K$  and  $\alpha$

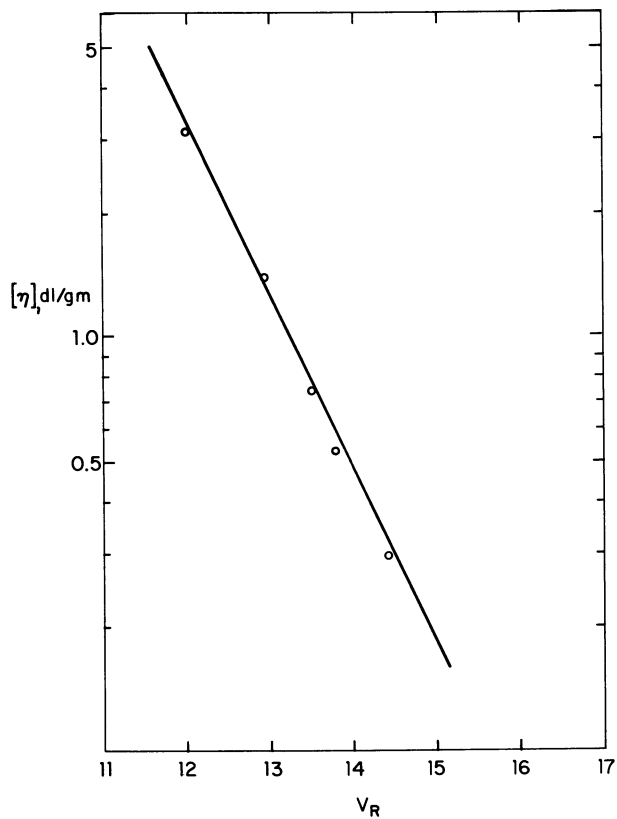


Figure 3. Calibration relationship between  $[\eta]_{\text{meas}}$  and SEC retention ( $\circ$ ) measured  $[\eta]$  of narrow polystyrene standards in THF)

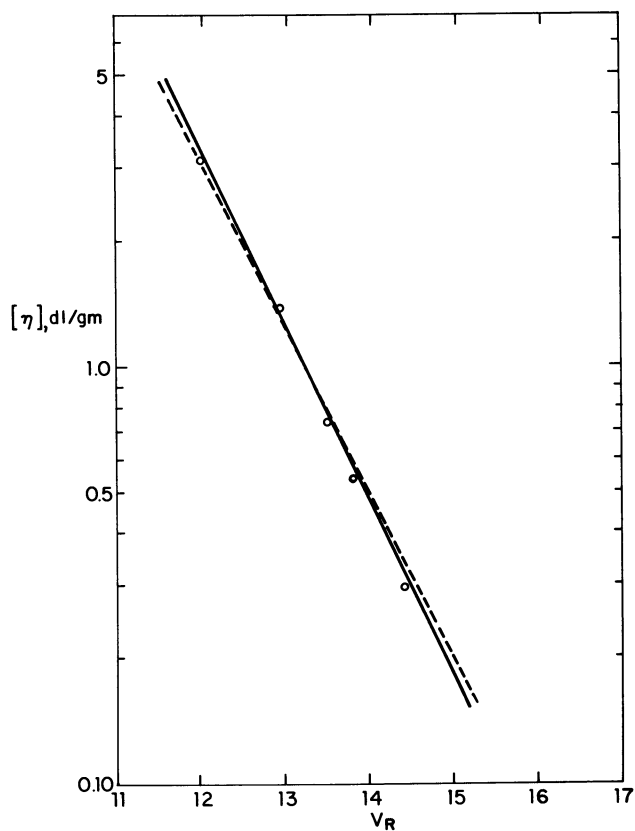


Figure 4. Comparison of broad standard with peak position SEC- $[\eta]$  calibration curves ( $[\eta] = E_1 e^{-E_2 V}$ ;  $\log_e [\eta] = \log_e E_1 - E_2 V$ ; (-○-) peak position calibration curve; (---) broad standard calibration curve; two standards: PS706 and PS60917 in THF)

values. This is especially true for studying branched samples where the actual  $[\eta]$  dependence on MW varies as the  $K$  and  $\alpha$  values change with the extent of polymer branching. However, a more practical method of SEC- $[\eta]$  calibration is needed since the peak position method shown in Figure 3 is (again) not generally applicable to other polymers due to the lack of narrow MWD standards. A solution to this practical problem is offered by the broad-standard, linear SEC- $[\eta]$  calibration method described below.

C. Linear SEC- $[\eta]$  Calibration Using Broad Standards. It is to be noted that the viscosity calibration curve in Figure 3 is essentially linear. This linearity is derived from bimodal SEC column sets. The linear MW calibration curve of the bimodal columns, as shown in Figure 1, is the result of proper matching of the column packing pore sizes (4,5), and such a matching of pore size is relatively easy to accomplish in practice (1). The linear MW calibration can be expressed by equation 4:

$$M = D_1 e^{-D_2 V_R} \quad (4)$$

where  $M$  is the solute molecular weight,  $D_1$  and  $D_2$  are calibration constants, and  $V_R$  is the SEC retention volume. Since polymer viscosity,  $[\eta]$ , is related to MW by the Mark-Houwink equation:

$$[\eta] = KM^\alpha \quad (5)$$

Substitution yields:

$$[\eta] = K(D_1 e^{-D_2 V_R})^\alpha = (KD_1^\alpha) e^{-(\alpha D_2) V_R} \quad (6)$$

or

$$[\eta] = E_1 e^{-E_2 V_R} \quad (7)$$

$$\text{where } E_1 = KD_1^\alpha \quad (8)$$

$$\text{and } E_2 = \alpha D_2 \quad (9)$$

This analogy of functional forms between Equations 7 and 4 indicates that the SEC- $[\eta]$  calibration curve must also be linear. This is experimentally verified by the data in Figure 4. One assumption made here is that the  $K$  and  $\alpha$  in the  $E_1$  and  $E_2$  expressions are not significantly dependent on MW, which is usually the case. The method will be less accurate in the molecular weight ranges where this assumption becomes a poor approximation.

TABLE 1

EFFECT OF LITERATURE K AND  $\alpha$  VALUE\*  
VARIATIONS ON CALCULATED  $[\eta]_{\text{sec}}$

$[\eta]$  OF PMMA, LUCITE® 40

$$\bar{M}_w = 100,000$$

$$[\eta]_{\text{meas.}} = 0.344 \text{ dl/gm.}$$

<u>K</u>	<u><math>\alpha</math></u>	<u><math>[\eta]_{\text{sec}}</math> dl/gm</u>
$0.93 \times 10^{-4}$	0.72	0.377
$1.28 \times 10^{-4}$	0.69	0.330
$1.04 \times 10^{-4}$	0.697	0.291

\*From Table 10.2 in Reference 1.

TABLE 2

BROAD STANDARD SEC- $[\eta]$  CALIBRATION CONCEPT

The  $[\eta]$  Analogy to Two-Standard  $\bar{M}_w$  Calibrations

	<u><math>\bar{M}_w</math> - Calibration</u>	<u><math>[\eta]</math> - Calibration</u>
Averaging Equation	$\bar{M}_w = \frac{\sum_i W_i M_i}{\sum_i W_i}$	$[\eta] = \frac{\sum_i W_i [\eta]_i}{\sum_i W_i}$
Calibration Equation	$M_w = D_1 e^{-D_2 V}$	$[\eta] = E_1 e^{-E_2 V}$
Calibration Constant	$D_1, D_2$	$E_1, E_2$

Equation 7 shows that linear calibration using bimodal columns can be applied to simplify the SEC- $[\eta]$  calibration procedure as has been done for the SEC-MW calibration. The objective of this  $[\eta]$  calibration then is to determine  $E_1$  and  $E_2$  values of the SEC column set for the particular polymer-solvent system of interest. The approach is the same as that for SEC-MW calibration. The similarities between the  $\bar{M}_w$  and the  $[\eta]$  formulations are summarized in Table 2.

Due to the analogous behavior of the  $\bar{M}_w$  and  $[\eta]$  equations,  $E_1$  and  $E_2$  values can be obtained experimentally by using directly the Hamielec, GPCV2 or GPCV3 computer algorithms.<sup>(1)</sup> (In our case these approaches were available on computer and no new programming was required.) The applicable equations are the following:

$$\text{Hamielec} \quad [\eta] = \sum_i W_i (E_i e^{-E_2 V_i}) \quad (10)$$

$$\text{GPCV2} \quad [\eta] = e^{-(\sigma E_2)^2/2} [\sum_i W_i (E_i e^{-E_2 V_i})] \quad (11)$$

$$\text{GPCV3} \quad [\eta] = (1 + \tau E_2) e^{-[(\sigma E_2)^2/2 + \tau E_2]} \sum_i W_i (E_i e^{-E_2 V_i}) \quad (12)$$

where  $\sigma$  and  $\tau$  describe the Gaussian and exponential instrument peak broadening parameters often used in describing SEC column performance.<sup>(1)</sup> For any of the algorithms, in practice two polymer standards (of the same polymer type) having different known  $[\eta]$  values are used to obtain  $E_1$  and  $E_2$  using either equation 10, 11, or 12. The standards used can be broad or narrow MWD. The larger the difference between the two  $[\eta]$  values, the more accurate the determined  $E_1$  and  $E_2$  values will be. The two required standards can be obtained from samples chosen from a series of unknowns, or they can be obtained by collecting two portions of a sample from another SEC elution experiment. The samples chosen as standards should then be measured carefully by classic viscometric techniques to determine their  $[\eta]$  values using the same solvent as used in the SEC experiment. The samples are then chromatographed as the calibration standards to establish the retention volume/intrinsic viscosity relationship.

Two polystyrene standards were used to demonstrate the proposed calibration method. One narrow and one broad-MWD sample were purposely selected to show that the method works for both narrow and broad

TABLE 3VISCOSITY RESULTS OF UNKNOWN SAMPLES

<u>Polystyrene Samples</u>	<u>MW</u>	<u>[<math>\eta</math>] Measured</u>	<u>Two Std. Calib. Curve</u>	<u>% Diff.</u>
11B	4,000	0.06	0.06	0
60917	50,000	0.30	0.30	0
4B	110,000	0.53	0.53	0
3B	390,000	1.40	1.20	0
61124	$1.8 \times 10^6$	3.11	2.82	-14
NBS705	$1.793 \times 10^5$	0.72	0.74	+3
NBS706	$2.578 \times 10^5$	0.94	1.08	+15



standards. The calibration curve obtained is plotted in Figure 4 along with the peak position calibration curve. The agreement between the methods by inspection is very good. Good agreement is also observed between measured and calculated  $[\eta]$  values as shown in Table 3 for the polystyrene samples. The differences seen between the corresponding  $[\eta]$  values are small considering possible experimental uncertainties in either of the two techniques. It is interesting to note that since  $[\eta]_{\text{SEC}}$  is calculated directly from the SEC elution curve and is applicable equally well for either high or low viscosity samples, the SEC- $[\eta]$  approach may, in fact, be able to study samples with viscosity values which are too low to be measured accurately by conventional viscometry once a SEC- $[\eta]$  calibration has been established in this region.

In summary, the unique features of this practical SEC- $[\eta]$  approach are as follows:

- knowledge of polymer  $K$  and  $\alpha$  values is not required;
- the method is not limited by the availability of narrow MWD standards, (broad MWD standards are usually more readily available for all polymer types);
- knowledge of the molecular weight of the standards is not required.

D. SEC Measurement of Mark-Houwink Constants Using Only Polydispersed Standards. If the SEC-MW calibration curve of the polymer-solvent system is known in addition to the  $[\eta]$  calibration, the Mark-Houwink constants of the polymer-solvent system are easily calculated from the calibration constants  $D_1$ ,  $D_2$ ,  $E_1$ , and  $E_2$  as:

$$\alpha = E_2/D_2 \quad (13)$$

$$K = E_1 \cdot D_1^{-\alpha} E_2/D_2 \quad (14)$$

Note that equations 13 and 14 are simple rearrangements of equations 8 and 9.

Depending on the availability of calibration standards, the standards for the MW calibration ( $D_1$  and  $D_2$ ) can be the same or different from those used to calibrate the  $[\eta]$  ( $E_1$  and  $E_2$ ) curve. The requirements

for the MW calibration standards are that  $\bar{M}_w$  and  $\bar{M}_n$  values for a single broad standard be known or two different  $\bar{M}_w$  and/or  $\bar{M}_n$  values for two standards be known. (12)

The broad-standard linear calibration curves for polystyrene in THF in Figure 1 and 4 are used to illustrate the K and  $\alpha$  calculations as follows. The particular calibration curves are found to correspond to the following calibration equations:

$$V_R = 22.75 - 1.76 \text{ Log}_{10} M \quad (15)$$

and

$$V_R = 13.0 - 2.5 \text{ Log}_{10} [\eta] \quad (16)$$

Then,  $D_1 = 8.44 \times 10^{12}$ ,  $D_2 = 1.309$ ,  $E_1 = 1.56 \times 10^5$   
and  $E_2 = 0.92$

By substituting these values into equations (13) and (14), a K value of  $1.28 \times 10^{-4}$  and an  $\alpha$  value of 0.703 are obtained which are in reasonably good agreement with the expected values of  $1.25 \times 10^{-4}$  dl/g and 0.72 mentioned earlier.

The unique features of this method of measuring polymer K and  $\alpha$  are:

- Only polydispersed standards are used;
- Only two to four standards are required;
- Concentration extrapolation is not necessary since SEC samples are already handled as very dilute solutions.

E. Universal Calibration Studies. The use of SEC- $[\eta]$  and MW calibration using broad MWD standards will make it easier to study the accuracy of the universal calibration concept. By combining the  $D_1/D_2$  and  $E_1/E_2$  calibration curves, the universal calibration ( $M[\eta]$ ) can be generated directly as in equation 17.

$$M[\eta] = (D_1 e^{-D_2 V}) (E_1 e^{-E_2 V}) = (D_1 E_1) e^{-(D_2 + E_2) V} \quad (17)$$

where  $(D_1 E_1)$  and  $(D_2 + E_2)$  are now the calibration constants for  $M[\eta]$ .

### Conclusions

The validity of a practical method of direct viscosity calculation from size exclusion chromatographic analysis is demonstrated. The method is convenient to use and is not limited by the availability of narrow MWD standards. It is possible to accurately measure polymer Mark-Houwink constants using the suggested broad standard SEC- $[\eta]$  and SEC-MW calibration procedure.

### Acknowledgement

We thank J. C. Rowell for the intrinsic viscosity data for the polymer samples used in this study.

### ABSTRACT

A new direct method for using size exclusion chromatography (SEC) to evaluate polymer intrinsic viscosity  $[\eta]$  is discussed. Sample viscosity information is obtained by combining SEC elution curve data and calibration data using direct SEC- $[\eta]$  calibration procedures without involving polymer molecular weight calculations. The practical utility, convenience and the expected precision of the proposed method are illustrated.

### Literature Cited

1. Yau, W. W., Kirkland, J. J., and Bly, D. D., "Modern Size Exclusion Liquid Chromatography", John Wiley & Sons, N.Y., 1979, Chapters 9 and 10.
2. Hellman, M. Y., in Chromatographic Science Series, Vol. 8, Liquid Chromatography of Polymers and Related Materials, J. Cazes, ed., Dekker, New York, 1977, p. 29.
3. Yau, W. W., Stoklosa, H. J. and Bly, D. D., J. Appl. Polym. Sci., 21, 1911 (1977).
4. Fok, J. S. and Abrahamson, E. A., *Chromatographia*, 7, 423 (1974).
5. Yau, W. W., Ginnard, C. R. and Kirkland, J. J., J. Chromatography, 149, 465 (1978).

RECEIVED May 20, 1980.

# Characterization of Branched Polymers by Size Exclusion Chromatography with Light Scattering Detection

R. C. JORDAN and M. L. McCONNELL

Chromatix, 560 Oakmead Parkway, Sunnyvale, CA 94086

Size exclusion chromatography (SEC) separates molecules of a polymer sample on the basis of hydrodynamic volume. When the chromatograph is equipped only with a concentration-sensitive detector, i.e. conventional SEC, a molecular weight distribution (MWD) can be obtained from the chromatogram only through use of a calibration function relating molecular weight and elution volume  $V$  (1).

The calibration technique used in conventional SEC does not always give the correct MWD, however. The molecular size of a dissolved polymer depends on its molecular weight, chemical composition, molecular structure, and experimental parameters such as solvent, temperature, and pressure (2). If the polymer sample and calibration standards differ in chemical composition, the two materials probably will feature unequal molecular size/weight relationships. Such differences also will persist between branched and linear polymers of identical chemical composition. Consequently, assumption of the same molecular weight/ $V$  relation for dissimilar calibrant and sample leads to transformation of the sample chromatogram to an apparent MWD.

In some cases the relationship between polymer intrinsic viscosity ( $[\eta]$ ) and molecular weight ( $M$ ) has been established for the SEC solvent and temperature conditions; i.e., the empirical Mark-Houwink coefficients (2)( $K, a$ ) in the equation

$$[\eta] = KM^a \quad (1)$$

have been determined. Under these circumstances the "universal" calibration approach can be utilized to calculate the correct MWD from the sample chromatogram. However,  $K, a$  values are not available for many samples, particularly those with polymer chain branching.

A number of the limitations of conventional SEC can be overcome through use of a low angle laser light scattering (LALLS) detector attached in series with a concentration

detector (SEC/LALLS). The principles and methodology of the technique are described in detail elsewhere (4-7). Data from both detectors are used to obtain the absolute molecular weight at each point in a sample chromatogram. The SEC/LALLS technique is capable of quickly yielding the correct MWD of linear and branched samples without recourse to the approximate column calibration methods used in conventional SEC.

The hydrodynamic volume separation mechanism of SEC, along with the different molecular size/weight relationships of branched and linear polymers of identical chemical composition, can be exploited with the SEC/LALLS method to gain information about polymer branching. In the studies described in this paper both conventional SEC and SEC/LALLS are used to obtain data about branching in samples of poly(vinyl acetate) (PVA) and polychloroprene (PCP).

### Theoretical

The discussion and experimental approach presented here rely on the principles and use of universal calibration for SEC analysis. For a review of this method the reader is referred to several useful articles (1,3,8,9).

For illustration consider SEC chromatograms obtained for two polymers on the same chromatographic system. One sample is a linear homopolymer while the other is a branched polymer with the same chemical composition. In the latter sample assume that the polymer components of different molecular weight have uniform branching characteristics so that all have similar molecular size/weight relationships.

Compare molecular size/weight characteristics of branched and linear species eluting at  $V$  in each chromatogram. Under the universal calibration formalism branched and linear components have the same hydrodynamic volume at  $V$ :

$$([\eta]_b M_b)_V = ([\eta]_l M_l)_V \quad (2)$$

where subscripts  $b$  and  $l$  denote branched and linear polymer components, respectively. If the fraction at  $V$  is homogeneous with respect to hydrodynamic volume, the polymer molecules at  $V$  will be monodisperse with respect to molecular weight. The ratio of the intrinsic viscosities of branched and linear species at  $V$  is obtained by rearranging eq 2

$$g_V = \left( \frac{[\eta]_b}{[\eta]_l} \right)_V = \left( \frac{M_l}{M_b} \right)_V \quad (3)$$

However, the quantity which is frequently discussed and related to specific branching models is the ratio of intrinsic viscosities at constant molecular weight (2)

$$g_M = \left( \frac{[\eta]_b}{[\eta]_l} \right)_M \quad (4)$$

For polymer samples of the type considered here this parameter reflects the reduction in molecular size of branched, relative to linear, material of identical molecular weight.

The relationship between  $g_v$  and  $g_M$  can be found through use of the Mark-Houwink relationship. The intrinsic viscosity of a linear polymer of the same molecular weight ( $M_b$ ) as the branched polymer is

$$([\eta]_l)_{M_b} = KM_b^a \quad (5)$$

where  $K$  and  $a$  are the Mark-Houwink constants for the linear polymer. Equation 3 gives the relation of  $M_b$  to  $M_l$  at  $V$ , so that we can relate the intrinsic viscosity of the linear polymer at  $V$  to the intrinsic viscosity of linear polymer having the same molecular weight as the branched polymer at  $V$ :

$$([\eta]_l)_{M_b} = K \left( \frac{M_l}{g_v} \right)^a \quad (6)$$

Substitution of eq 1 into eq 6 gives

$$([\eta]_l)_{M_b} = K \left( \frac{[\eta]_l}{g_v^a} \right)_v \quad (7)$$

Use of eq 7 in eq 4 gives

$$g_M = \frac{([\eta]_b)_{M_b}}{([\eta]_l/g_v^a)_v} \quad (8)$$

Since we have explicitly specified that branched species of molecular weight  $M_b$  are contained at volume  $V$ , eq 8 can be written:

$$g_M = \frac{([\eta]_b)_V}{([\eta]_l/g_V^a)_V} \quad (9)$$

From eq 3

$$g_M = g_V^{a+1} = \left( \frac{M_l}{M_b} \right)_V^{a+1} \quad (10)$$

For the two illustrative samples cited here, the ratio of the absolute molecular weights of the branched and linear species at the same  $V$ , raised to the  $(a+1)$  power, can be used to calculate  $g_M$ .

The derivation of eq 10 was undertaken with the assumption that the sample effluent was monodisperse in molecular weight at any  $V$ . In reality this is never the case. First, if the frequency of branching varies with molecular weight, species of different molecular weight (but equivalent hydrodynamic volume) may elute at the same  $V$  (10). Second, molecular weight polydispersity at  $V$  results from assorted hardware mixing volumes and band-spreading of the SEC columns (1,11).

The first complication results from the size separation mechanism and cannot be corrected. Effects of the second can be minimized by judicious choice of columns and careful hardware design. In addition, one can invoke a band-spreading correction scheme to approximately account for the effects of this phenomenon. We therefore must define parameters which can be obtained from SEC and used in an equation with the form of eq 10. The SEC/LALLS technique gives the absolute weight average molecular weight  $(M_w)_V$  of the polydisperse mixture at  $V$  (5,6). Also we define at  $V$  an apparent weight-average molecular weight  $(M_w^*)_V$  of linear polymer with identical chemical composition as the sample; this is obtained from use of a universal calibration curve and an approximate band-spreading correction (Appendix). In consideration of the sample molecular weight polydispersity at  $V$ , we define  $g'$  as an approximation to  $g_M$ :

$$g' = \left( \frac{M_w^*_V}{M_w}_V \right)^{a+1} \quad (11)$$

The following work demonstrates the use of SEC/LALLS to study the variation of  $g'$  with molecular weight for broad MWD materials. This approach gives a qualitative indication of polymer branching.

### Experimental

**Materials.** Commercially available poly(vinylacetate) (PVA) and polychloroprene (PCP) were used in this work. The PVA samples (Polysciences) had nominal molecular weights  $5.0 \times 10^5$  (lot no. 0106) and  $1.5 \times 10^6$  (lot no. 0107-066). The PCP (Aldrich, catalogue no. 18,168-4, lot no. 03) had no listed molecular weight data. A broad MWD polystyrene (PS) standard (National Bureau of Standards) had a light scattering  $\bar{M}_w = 257,800$  (SRM 706,  $\bar{M}_w/\bar{M}_n = 2.1$ ). Six of the narrow MWD PS standards (Pressure Chemical Co.) had nominal molecular weights  $6.0 \times 10^5$  (lot no. 60914,  $\bar{M}_w/\bar{M}_n = 1.10$ ),  $3.90 \times 10^5$  (lot no. 3b,  $\bar{M}_w/\bar{M}_n = 1.10$ ),  $2.33 \times 10^5$  (lot no. 50124,  $\bar{M}_w/\bar{M}_n = 1.06$ ),  $1.0 \times 10^5$  (lot no. 70111,  $\bar{M}_w/\bar{M}_n < 1.06$ ),  $5.0 \times 10^4$  (lot no. 60917,  $\bar{M}_w/\bar{M}_n < 1.06$ ), and  $3.7 \times 10^4$  (lot no. 7b,  $\bar{M}_w/\bar{M}_n < 1.06$ ). One narrow MWD PS standard (National Bureau of Standards) had a light scattering  $\bar{M}_w = 179,300$  (SRM 705,  $\bar{M}_w/\bar{M}_n = 1.05$ ).

**Sample Preparation.** All solutions were prepared in THF (Burdick and Jackson "Distilled in Glass"). Stock solutions of PVA and PCP were prepared gravimetrically (w/w). For injection, solutions of PVA with a known concentration (w/v) were prepared by volumetric dilution of the stock. The PCP stock had significant amounts of undissolved material (microgel). After filtration through a 0.5 micron Fluoropore filter (Millipore Corp.) the concentration of the solution was determined by dry-weight analysis. Solutions (w/v) of PS for injection were prepared by dissolving weighed quantities of material and diluting to volume. All solutions for injection were filtered through a 0.2 micron Fluoropore filter (Millipore Corp.).

**SEC/LALLS System and Conditions.** The SEC/LALLS system consisted of a 6000A solvent delivery pump, U6K sample injector, R401 differential refractive index (DRI) detector, and micro-Styragel columns ( $10^6$ ,  $10^5$ ,  $10^4$ ,  $10^3$ , 500 Å pore), all from Waters Associates. A KMX-6 LALLS Photometer (Chromatix) with a flow-through sample cell was serially connected with the DRI detector, as described elsewhere (4-6). The KMX-6 light source is a 2 milliwatt HeNe laser which produces polarized radiation with a wavelength of 6328 Å. Scattering intensity data were collected at a forward scattering angle of  $6^\circ$ - $7^\circ$  (in air) by selection of the appropriate KMX-6 annulus.



Analyses were carried out at ambient (23°C) in THF, using a flow rate of 2.0 ml/min. Data from the detectors were collected and processed with a LDS-2 Data System (Chromatix).

Differential Refractometry (dn/dc); the LALLS Optical Constant (K). Solutions of PVA and PCP with known concentrations (w/v) were prepared in THF as described in "Sample Preparation". For three solutions of each sample the specific refractive index increment (dn/dc) (12) was determined at 25°C with a KMX-16 Laser Differential Refractometer (Chromatix). An average of the three values was taken. Values of dn/dc and the resultant LALLS optical constant K were PVA: dn/dc = 0.0517 ml/gm,  $K = 2.152 \times 10^{-8} \text{ mol-cm}^2/\text{gm}^2$ ; PCP, dn/dc = 0.1274 ml/gm,  $K = 1.152 \times 10^{-5} \text{ mol-cm}^2/\text{gm}^2$ . A value of dn/dc = 0.1845 ml/gm was used for PS (13), giving  $K = 2.741 \times 10^{-7} \text{ mol-cm}^2/\text{gm}^2$ .

Sample Chromatography; Data Handling. During a sample run on the SEC/LALLS system the analog data from the DRI and LALLS detectors were collected and digitized through the two-channel A/D converter of the LDS-2, using the SEC/LALLS software package MOLWT (Chromatix). After a pre-set period following sample injection, 150 data points were taken through a data acquisition period which encompassed the sample chromatogram. Time-based data files were produced for each detector. Use of the flow rate and these data files allowed calculation of the elution volume (V) corresponding to each of the 150 data points. The MOLWT program was used to simultaneously process both data files and give the absolute weight-average molecular weight  $(M_w)_v$  at each V together with the sample Z-average  $(M_z)$ , weight average  $(M_w)$ , and number average  $(M_n)$  molecular weights. A separate program was developed on the LDS-2 to correct the SEC/LALLS  $M_n$  for band-spreading (Appendix).

Conventional SEC calculations were performed with the SEC software package GPC1 (Chromatix). As described below a universal calibration was carried out to obtain the peak position molecular weight at each V; a modified version of GPC1 then was used to calculate weight- and number-average molecular weights for the sample fraction at V (Appendix).

At least two runs were carried out on each of the seven narrow MWD PS standards and data were processed with MOLWT using the second virial coefficient ( $A_2$ ) relationship (14).

$$A_2 = 0.37 M^{-0.187}$$

Injected masses ranged from  $8.88 \times 10^{-4}$  gm to  $2.12 \times 10^{-4}$  gm. The peak maxima of the DRI data files were used to calculate the retention volumes ( $V_R$ ) of the narrow MWD standards. Using

the light-scattering  $\bar{M}_w$  and  $\bar{M}_n$  (corrected for band-spreading) values along with published Mark-Houwink data for PS in THF (25°C) (15), an intrinsic viscosity was calculated for each standard from

$$[\eta] = 1.14 \times 10^{-4} (\bar{M}_w \cdot \bar{M}_n)^{1/2(0.72)} \quad (12)$$

A quantity J which is proportional to the polymer hydrodynamic volume (3) then was calculated:

$$J = [\eta](\bar{M}_w \cdot \bar{M}_n)^{1/2} = 1.14 \times 10^{-4} (\bar{M}_w \cdot \bar{M}_n)^{1.72/2} \quad (13)$$

A universal calibration relation for the SEC/LALLS system was derived by fitting the seven J,  $V_R$  data pairs with a linear equation

$$\ln J = D_1 - D_2 V_R \quad (14)$$

where  $D_1$  and  $D_2$  are constants giving the best fit to the data. The curve fitting was carried out with use of the GPC1 program.

Sample masses of  $8.90 \times 10^{-4}$  gm and  $1.05 \times 10^{-3}$  gm were chromatographed for PVA 0107-066 and PVA 0106, respectively, while  $1.47 \times 10^{-3}$  gm of PCP was injected. An estimated  $A_2$  value of  $5 \times 10^{-4}$  mol-cm<sup>3</sup>/gm<sup>2</sup> was used to process the PVA and PCP data with MOLWT. In view of the relatively small magnitude of the term containing  $A_2$  in the SEC/LALLS equations (5), uncertainty in  $\bar{M}_w$  from this approximation is insignificant.

In order to obtain the variation of  $g'$  (eq 11) with molecular weight for the broad MWD PVA, PCP, and PS samples, data files from the sample runs were used to calculate  $(\bar{M}_w^*)_V$  and  $(\bar{M}_w)_V$  for each of the 150 data points. The MOLWT software directly yielded  $(\bar{M}_w)_V$  values. Using sample file data and published Mark-Houwink coefficients, the GPC1 program was used with the universal calibration relation (eq 14) to calculate the molecular weight for a linear species at  $V$ . The method outlined in the Appendix then was used to transform this quantity to an apparent weight average molecular weight for the linear polymer,  $(\bar{M}_w^*)_V$ . The following Mark-Houwink relations were used for PVA and PCP in THF at 25°C:

$$\text{PVA(16): } [\eta] = 5.1 \times 10^{-5} M^{0.791}$$

$$\text{PCP(17): } [\eta] = 4.18 \times 10^{-5} M^{0.83}$$

The  $K$ , a parameters indicated in eq 12 were used for PS.

## Results

Table I shows molecular weight data obtained from SEC/LALLS measurements on the narrow MWD polystyrene standards. Band-spreading correction of the  $M_n$  values generally resulted in a decrease in  $M_n$  of 1% to 4% below the value directly obtained from treatment of SEC/LALLS data with the MOLWT program. Figure 1 shows data from Table I plotted as  $\log[M_w M_n(\text{corr})]^{1/2}$  vs.  $V_r$  and a line is shown which corresponds to an equation of the form:

$$\log_{10} [M_w M_n(\text{corr})]^{1/2} = 10.82 - 0.1675V_r \quad (15)$$

Equation 15 represents the best linear fit to the data and it was calculated using program GPC1.

The fit of the linear equation to the calibration data in Figure 1 also reflects, of course, the quality of the fit of  $J, V_r$  calibrant data with eq 14. After calculating  $J$  values via eq 13, a best fit to the calibrant data was found with

$$\ln J = 10.54 - 0.3630V_r$$

A value of 0.693 was calculated for the dispersion constant  $\sigma$  by using eq A7 and supplier's  $M_w M_n$  data.

In the high molecular weight region of a chromatogram the LALLS detector has a greater response to a given concentration than in the low molecular weight portion of the chromatogram; this reflects the dual dependence of the LALLS detector on concentration and molecular weight (5,6,10). Values shown in Tables II-IV cover data collected between acceptable signal/noise limits of the LALLS and DRI detectors at the low and high molecular weight ends, respectively, of the chromatograms. Consequently in the high molecular weight portion of chromatograms data were processed when the concentration exceeded 1% of the peak concentration, whereas in the low molecular weight region the lowest concentration used represented 10% of the maximum.

For the NBS standard polystyrene SRM 706 Table II presents SEC/LALLS values of  $(M_w)_v$  as well as band-spreading corrected  $(M_w^*)_v$  values obtained from processing data in the conventional sense. The dependences on  $V$  of  $\log(M_w)_v$  and  $\log(M_w^*)_v$  are plotted in Figure 1. In addition to the  $g'$  values calculated from  $(M_w)_v$  and  $(M_w^*)_v$ , values of  $(M^*/M_w)_v^{1+a}$  are reported in Table II. The parameter  $(M^*)_v$  represents the apparent molecular weight of linear polymer at  $V$ , given by the GPC1 program, but without application of the band-spreading correction (Appendix). Therefore, the difference between  $g'$  and  $(M^*/M_w)_v^{1+a}$  at  $V$  shows the effect of applying the band-spreading correction to data processed in the conventional sense. In addition, Table II

Table I

Data from the SEC/LALLS Analysis of Narrow MWD Polystyrene Standards

SAMPLE <sup>a</sup>	$\bar{M}_w$	$[\bar{M}_w \bar{M}_n (\text{corr})]^{1/2}$ <sup>b</sup>
PC600K	$6.65 \times 10^5$	$6.54 \times 10^5$
PC390K	$3.76 \times 10^5$	$3.72 \times 10^5$
PC233K	$2.50 \times 10^5$	$2.45 \times 10^5$
NBS705	$1.73 \times 10^5$	$1.72 \times 10^5$
PC100K	$9.08 \times 10^4$	$8.99 \times 10^4$
PC50K	$4.87 \times 10^4$	$4.79 \times 10^4$
PC37K	$3.73 \times 10^4$	$3.66 \times 10^4$

a Prefixes PC and NBS refer to the suppliers, Pressure Chemical Co. and National Bureau of Standards, respectively.

b The quantity  $\bar{M}_n(\text{corr})$  is the SEC/LALLS sample number average molecular weight, corrected for band-spreading, while  $\bar{M}_w$  is the sample weight-average molecular weight.

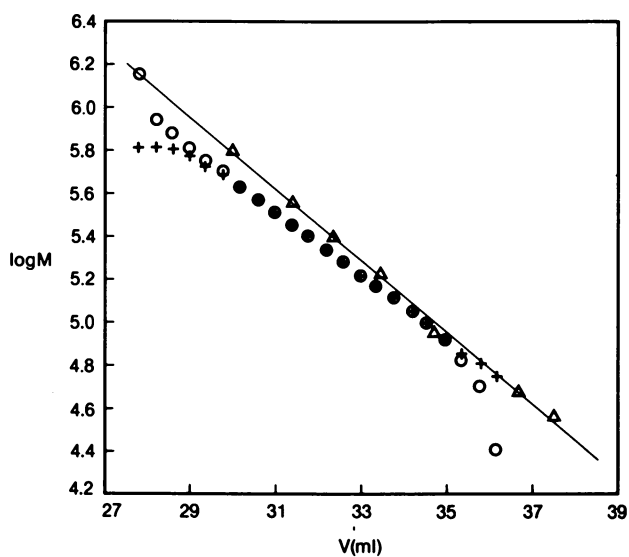


Figure 1. Dependence on  $V$  of  $[M_w M_n(\text{corr})]^{1/2}$  for polystyrene calibrants (Table I), and dependence on  $V$  of  $(M_w)_v$  and  $(M_w^*)_v$  for polystyrene SRM706 (Table II): ( $\Delta$ )  $M = [M_w M_n(\text{corr})]^{1/2}$ ; (+)  $M = (M_w^*)_v$ ; ( $\circ$ )  $M = (M_w)_v$ . The straight line corresponds to Equation 15.

Table II

Data from SEC/LALLS and conventional SEC analysis of NBS SRM706 polystyrene

$V(\text{ml})$	$(M_w)_v \times 10^{-5}$	$(M_w^*)_v \times 10^{-5}$	$g'$	$\left(\frac{M^*}{M_w}\right)_v^{1+a}$
27.79	14.7	6.41	0.24	0.74
28.19	8.95	6.65	0.60	1.30
28.58	7.86	6.60	0.74	1.25
28.98	6.64	6.00	0.84	1.27
29.38	5.78	5.51	0.92	1.25
29.78	5.05	4.90	0.95	1.20
30.17	4.41	4.41	1.00	1.15
30.57	3.82	3.91	1.04	1.11
30.97	3.35	3.45	1.05	1.07
31.36	2.91	3.03	1.07	1.05
31.76	2.55	2.62	1.05	1.00
32.15	2.23	2.28	1.04	0.97
32.55	1.96	2.00	1.04	0.92
32.95	1.72	1.72	1.00	0.88
33.35	1.52	1.50	0.98	0.84
33.75	1.33	1.31	0.97	0.80
34.14	1.15	1.14	0.98	0.79
34.54	0.991	0.979	0.98	0.77
34.94	0.828	0.861	1.07	0.81
35.33	0.676	0.744	1.18	0.88
35.73	0.507	0.659	1.57	1.09
36.13	0.256	0.569	3.95	2.71
<u>SAMPLE AVERAGES<sup>a</sup></u>		<u>SEC/LALLS</u>	<u>SEC</u>	
$M_w(\text{uncorr}) \times 10^{-5}$		2.622	2.751	
$M_w(\text{corr}) \times 10^{-5}$			2.654	
$M_n(\text{uncorr}) \times 10^{-5}$		1.722	1.739	
$M_n(\text{corr}) \times 10^{-5}$		1.635	1.634	

a uncorrected and band-spreading corrected sample averages

Table III

Data from SEC/LALLS and conventional SEC  
analysis of two PVA Samples

PVA 0106				PVA 0107-066				
V(ml)	$(M_w)_v$ $\times 10^{-5}$	$(M_w^*)_v$ $\times 10^{-5}$	$g'$	V(ml)	$(M_w)_v$ $\times 10^{-6}$	$(M_w^*)_v$ $\times 10^{-6}$	$g'(i)^a$	$g'(ii)^b$
27.86	60.5	6.013	0.016	26.16	5.15	1.38	0.094	0.260
28.51	21.3	6.460	0.118	26.81	3.94	1.45	0.167	0.274
29.17	11.1	5.366	0.272	27.47	3.20	1.31	0.202	0.248
29.82	8.04	5.362	0.484	28.12	2.59	1.12	0.223	0.234
30.48	5.94	4.466	0.600	28.78	2.11	0.922	0.227	0.221
31.13	4.51	3.696	0.700	29.43	1.71	0.747	0.227	0.208
31.78	3.47	2.992	0.767	30.08	1.36	0.607	0.236	0.205
32.44	2.67	2.383	0.816	30.73	1.05	0.491	0.256	0.208
33.09	2.02	1.888	0.886	31.39	0.817	0.391	0.267	0.215
33.75	1.60	1.509	0.901	32.05	0.620	0.301	0.274	0.230
34.40	1.27	1.209	0.916	32.70	0.457	0.237	0.308	0.254
35.05	0.976	0.966	0.982	33.35	0.327	0.182	0.349	0.305
35.71	0.740	0.780	1.10	34.01	0.225	0.142	0.441	0.391
36.36	0.495	0.611	1.46	34.66	0.114	0.112	0.965	0.916
37.02	0.365	0.479	1.63					
37.67	0.167	0.371	4.18					

SEC/LALLS Sample Averages<sup>c</sup>

$$\bar{M}_w = 2.77 \times 10^5; \bar{M}_n(\text{corr}) = 0.62 \times 10^5$$

SEC/LALLS Sample Averages<sup>c,d</sup>

$$\bar{M}_w = 1.61 \times 10^6; \bar{M}_n(\text{corr}) = 0.72 \times 10^6$$

a Values of  $g'$  from the  $(M_w)_v$  and  $(M_w^*)_v$  data in columns 6 and 7

b Values of  $g'$  from a duplicate run

c Number-average corrected for band-spreading

d Mean of runs i and ii

Table IV

Data from SEC/LALLS and conventional SEC analysis of PCP

<u>V(ml)</u>	<u><math>(M_w)_v \times 10^{-5}</math></u>	<u><math>(M_w^*)_v \times 10^{-5}</math></u>	<u>g'</u>
26.93	20.4	9.03	0.225
27.60	15.3	8.69	0.355
28.27	12.1	7.71	0.438
28.93	9.57	6.38	0.476
29.60	7.40	5.32	0.547
30.27	5.63	4.33	0.619
30.93	4.20	3.50	0.716
31.60	3.13	2.82	0.826
32.27	2.36	2.25	0.915
32.93	1.80	1.78	0.982
33.60	1.42	1.42	1.00
34.27	1.12	1.14	1.04
34.93	0.860	0.924	1.14
35.60	0.646	0.742	1.29
36.27	0.420	0.591	1.87

SEC/LALLS Sample Averages<sup>a</sup>

$$\bar{M}_w = 3.60 \times 10^5$$

$$\bar{M}_n(\text{corr}) = 1.40 \times 10^5$$

a Number-average corrected for band-spreading



shows the effect of applying the band-spreading correction to the overall sample weight- and number- averages obtained from conventional processing of the data; also reported is the effect on the SEC/LALLS  $\bar{M}_n$  of applying the band-spreading correction.

Table III gives SEC/LALLS  $(M_w)_v$ ,  $(M_w^*)_v$ , and  $g'$  data for the PVA samples in addition to the sample  $\bar{M}_w$  and band-spreading corrected  $\bar{M}_n$  values. Data from Table III are plotted in Figures 2a and 2b as  $\log(M_w)_v$  and  $\log(M_w^*)_v$  vs  $V$ ; plots of  $g'$  vs  $V$  are shown in Figure 3. Table IV presents SEC/LALLS  $(M_w)_v$ ,  $(M_w^*)_v$ , and  $g'$  data for PCP, in addition to the sample  $\bar{M}_w$  and band-spreading corrected  $\bar{M}_n$  values. Data from Table IV are plotted in Figure 4 as  $\log(M_w)_v$  and  $\log(M_w^*)_v$  vs.  $V$ ; a plot of  $g'$  vs.  $\log(M_w)_v$  for PCP is shown in Figure 5.

### Discussion

Data in Figures 3 and 5 show an increase in  $g'$  with decreasing molecular weight for each of the polydisperse PVA and PCP samples. However, the data for PCP and one of the PVA samples (0106) also exhibit  $g'$  values greater than unity at the low molecular weight ends of the molecular weight distributions. Since by its definition  $g'$  is expected to equal or be less than unity, such values are anomalous. Also, some  $g'$  values are suspiciously low in the high molecular weight regions of the PVA samples.

Examination of data for the NBS standard polystyrene SRM 706 gives insight into the behavior of  $g'$  data in the molecular weight extremes of the PVA and PCP samples. The SEC/LALLS data in the  $\log(M_w)_v$  vs  $V$  plot (Figure 1) exhibit linear behavior, along with curvature in the high and low molecular weight regions. This is in contrast to the linear dependence on  $V$  of  $\log(\bar{M}_w/\bar{M}_n)^{1/2}$  which is shown by the narrow MWD polystyrene calibrants. Diminished molecular size resolution in the molecular weight extremes of SRM 706 is a probable cause for this discrepancy. High molecular weight, unresolved species serve to increase SEC/LALLS  $(M_w)_v$  values at low  $V$ , whereas unresolved low molecular weight components decrease  $(M_w)_v$  at high  $V$ .

The other noticeable feature in Figure 1 is the dependence of  $\log(M_w^*)_v$  on  $V$ , obtained by conventional processing of the data;  $\log(M_w^*)_v$  shows the expected linear variation with  $V$  throughout the chromatogram, except for downward curvature in the high molecular weight region. These latter data correspond to points in the extreme high molecular weight end of the chromatogram, i.e., where the concentration is only a few percent of the peak (Results). It is doubtful that material at points in the extreme tails of the chromatogram has a Gaussian distribution of molecular weights, thus invalidating use of the band-spreading calculation (Appendix).

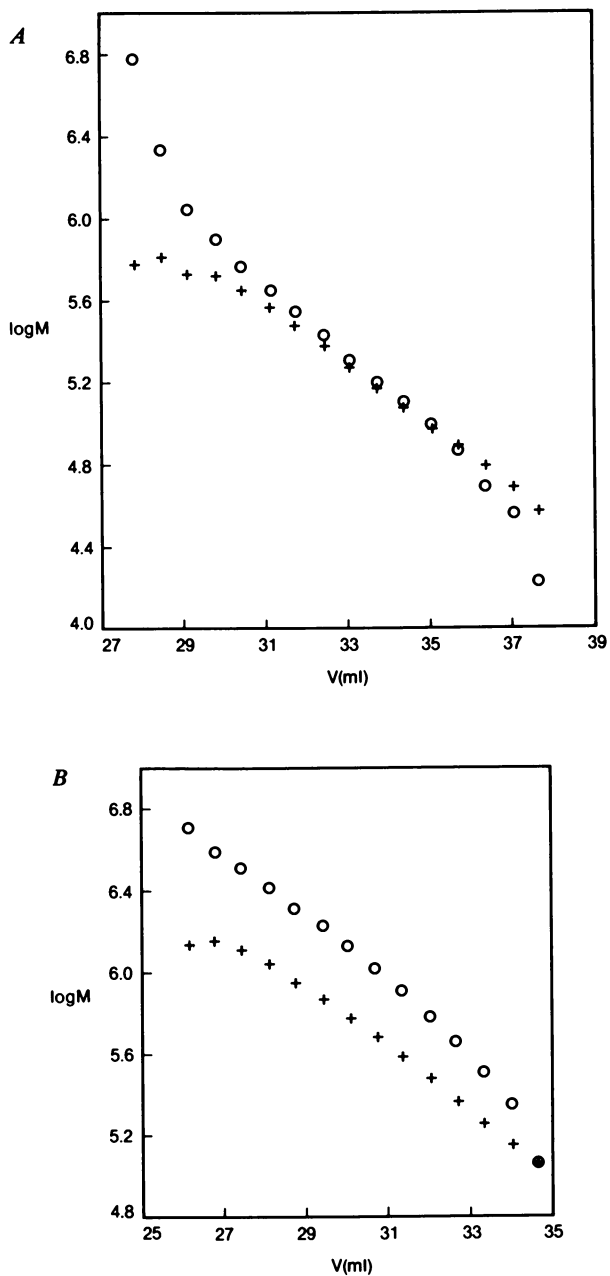


Figure 2. Dependence on V of  $(M_w)_v$  and  $(M_w^*)_v$  for (A) PVA 0106 and (B) PVA 0107-066 (data from Table III: (+)  $M = (M_w^*)_v$ ; (○)  $M = (M_w)_v$ )

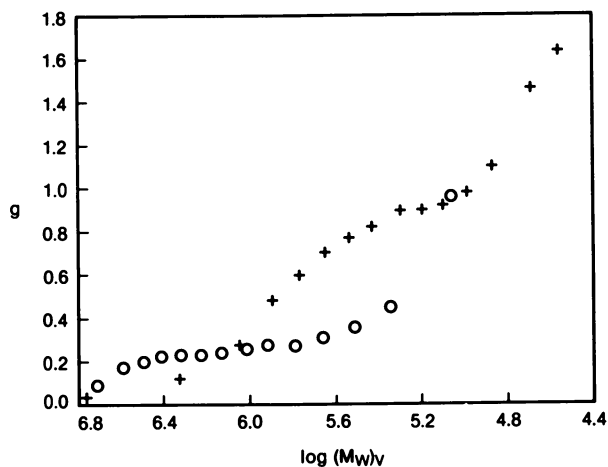


Figure 3. Dependence of  $g'$  on  $(M_w)_v$  for PVA samples (data from Table III: (+) =  $g'$  for PVA 0106; (O) =  $g'$  [=  $g'(i)$ ] for PVA 0107-066; note that for PVA 0106,  $g' = 4.18$  has been deleted from the plot)

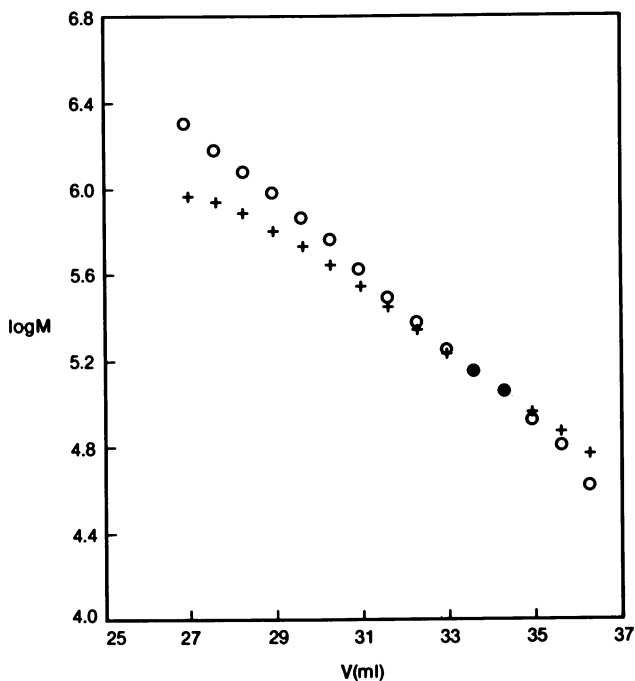


Figure 4. Dependence on  $V$  of  $(M_w)_v$  and  $(M_w^*)_v$  for PCP (data from Table IV: (+)  $M = (M_w^*)_v$ ; (O)  $M = (M_w)_v$ )

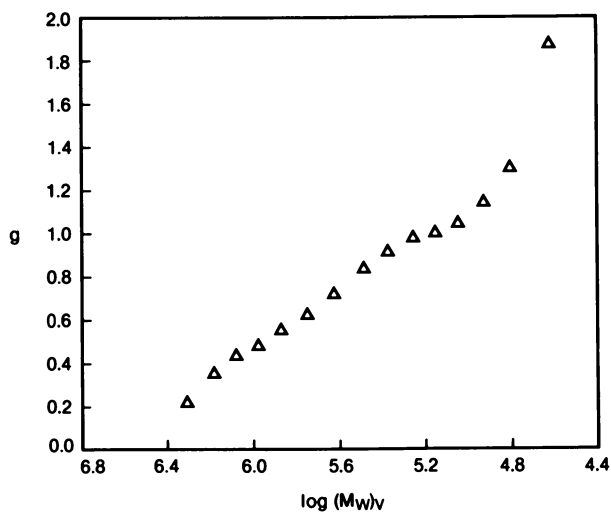


Figure 5. Dependence of  $g'$  on  $(M_w)_v$  for PCP (data from Table IV)

On the other hand concentration detector (DRI) data represent at least 10% of the maximum on the low molecular weight side of the chromatogram (Results), and the Gaussian approximation is probably applicable.

Since polystyrene SRM 706 is supposedly a linear polymer sample,  $g'$  is not expected to deviate strongly from unity. Inspection of Table II shows that  $g'$  values cluster about unity throughout most of the SRM 706 molecular weight distribution. In the tails of the distribution, however, decreased resolution and inapplicability of the band-spreading correction serve to make  $g'$  behave anomalously.

For PVA and PCP the dependences on  $V$  of  $\log(M_w^*)_V$  and  $\log(M_w)_V$  (Figures 2a, 2b and 4) show similar trends as for SRM 706. Noticeable downward curvature of  $\log(M_w)_V$  at low molecular weight occurs in each case, in contrast to relatively linear behavior of  $\log(M_w^*)_V$ . Anomalously large values of  $g'$  result (Figures 3 and 5). In the highest molecular weight region, a sharp downturn in the  $\log(M_w^*)_V$  dependence on  $V$  is apparent which is accompanied by very low  $g'$  values.

The results found in this work indicate that SEC/LALLS can be used to obtain qualitative data about polymer branching. As suggested earlier in the derivation of the expression for  $g'$ , the assumptions inherent in using this parameter as an approximation to  $g_m$  should not be overlooked. Caution should be exercised for polymers with unknown branching characteristics, e.g., where branching frequency is suspected to vary with molecular weight. In this case the molecular weight heterogeneity at  $V$  can be significantly more than allowed for by the linear polymer band-spreading correction used here (18).

The  $g'$  data for the PVA samples (Table III, Figure 3) indicate that branching affects the molecular volume of PVA 0107-066 to a greater extent than the lower molecular weight PVA 0106. Except for the suspect points in the extremes of the MWD the  $g'$  values for PVA 0106 are larger than for PVA 0107-066, and for each sample the data show a decrease in  $g'$  with increasing molecular weight. (The reproducibility of the technique is shown by the agreement of  $g'$  values obtained for successive runs of PVA 0107-066.) Studies (19) have shown that, for PVA samples wherein certain branching characteristics (e.g. branching frequency) increase with the extent of reaction a general decrease in  $g_m$  (eq 4) with increasing molecular weight was found. A similar dependence of  $g'$  on molecular weight is found for the PCP sample (Table IV, Figure 5). The data suggest the presence of branching throughout the MWD, which is consistent with the known propensity of this polymer to exhibit branching under most reaction conditions (17). Anomalous  $g'$  values in the molecular weight extremes again reflect the dependence on  $V$  of  $\log(M_w^*)_V$  and  $\log(M_w)_V$  (Figure 4).

Since the SEC/LALLS technique always yields a weight-average molecular weight  $(M_w)_v$  for the slightly polydisperse fraction at  $V$ , a small overestimation of the sample  $\bar{M}_n$  is expected (5,10). As noted previously (Results) a 1% to 4% decrease in the narrow MWD polystyrene  $\bar{M}_n$  values (Table I) accompanied application of the band-spreading correction; Table II shows that for SRM 706 good agreement is obtained between SEC/LALLS and conventional SEC sample  $\bar{M}_w$  and  $\bar{M}_n$  values when the band-spreading correction was used. However, the NBS 706 polydispersity index  $(\bar{M}_w/\bar{M}_n)$  given by the supplier (ca. 2.1) does not agree with that (1.6) found here using the SEC/LALLS and conventional SEC techniques. Insensitivity of the LALLS detector to a small amount of low molecular weight material may account for a larger sample  $\bar{M}_n$ ; however, this is not supported by the conventional SEC data. The reason for the discrepancy remains unclear.

### Appendix

Yau, et. al., (11) described a computation method, named GPCV2, which corrects for chromatographic dispersion (band-spreading) in the determination of the MWD using SEC. Although developed for use with a single broad standard calibration scheme, the fundamental equations are also valid for a multiple narrow standard calibration. In this study we have composed a minor variation in GPCV2 to facilitate its use with a universal calibration scheme. Also, we have derived a computational method analogous to GPCV2 which can be used to correct for chromatographic dispersion in the determination of the MWD by SEC/LALLS.

To employ GPCV2 in SEC, the column calibration is expressed as

$$M^* = D_1 e^{-D_2 V} \quad (A1)$$

where  $M^*$  is the apparent linear (peak position) molecular weight at retention volume  $V$ .

Because of chromatographic dispersion, the sample fraction in the detector cell is polydisperse. The weight-average and number-average molecular weights of the polydisperse fraction are calculated as

$$(M_w^*)_v = \frac{F(V - D_2 \sigma^2)}{F(V)} \cdot \exp[(D_2 \sigma^2)/2] \cdot M^* \quad (A2)$$

$$(M_n^*)_v = \frac{F(V)}{F(V + D_2 \sigma^2)} \cdot \exp[-(D_2 \sigma^2)/2] \cdot M^* \quad (A3)$$

where  $F(V)$  is the normalized ( $\sum V F(V)=1$ ) chromatogram under the conditions of chromatographic dispersion ( . .  $F(V)$  is the detector response at retention volume  $V$ ). The term  $\sigma$  is the dispersion constant.

The  $\bar{M}_w^*$  and  $\bar{M}_n^*$  of the total sample are calculated as

$$\bar{M}_w^* = \exp[-(D_2\sigma)^2/2] \cdot \Sigma[(F(v)D_1 \exp(-D_2V))] \quad (A4)$$

$$\bar{M}_n^* = \exp[(D_2\sigma)^2/2] / \Sigma \frac{F(V)}{D_1 \exp(-D_2V)} \quad (A5)$$

Combination of eqs (A4) and (A5) yields

$$\frac{\bar{M}_w^*}{\bar{M}_n^*} = e^{-(D_2\sigma)^2} \Sigma[F(V)D_1 e^{-D_2V}] \cdot \Sigma[F(V)/D_1 e^{-D_2V}] \quad (A6)$$

Therefore, if  $\bar{M}_w^*/\bar{M}_n^*$  is known,  $\sigma$  can be calculated as

$$\sigma = D_2^{-1} \sqrt{\ln \left\{ \left( \frac{\bar{M}_w^*}{\bar{M}_n^*} \right) \cdot \Sigma[F(V)D_1 e^{-D_2V}] \cdot \Sigma[F(V)/D_1 e^{-D_2V}] \right\}} \quad (A7)$$

In this study we have used an  $\bar{M}_w^*/\bar{M}_n^*$  calculated from supplier's specifications.

The GPCV2 equations were developed for conventional  $\log(MW)$  vs. retention volume calibrations. When used in conjunction with a universal calibration, the slope term ( $D_2$ ) must be corrected for the different molecular size/weight relationships of the calibrants and the samples as derived in the following equations. To understand this correction, consider the conventional calibration curve that could be created from the universal calibration data.

The slope term,  $D_2$ , for a calibration with polymer 1 is defined at points a and b on the calibration curve as

$$D_2 = \frac{\ln M_{1,b} - \ln M_{1,a}}{V_b - V_a} = \frac{\ln \left( \frac{M_{1,b}}{M_{1,a}} \right)}{V_b - V_a} \quad (A8)$$

the slope term that must be used to correct for dispersion of sample polymer 2 can be similarly defined

$$D_2' = \frac{\ln M_{2,b} - \ln M_{2,a}}{V_b - V_a} = \frac{\ln \left( \frac{M_{2,b}}{M_{2,a}} \right)}{V_b - V_a} \quad (\text{A9})$$

According to the universal calibration concept

$$J_a = K_2 M_{2,a}^{(a_2+1)} = K_1 M_{1,a}^{(a_1+1)} \quad (\text{A10})$$

where  $K_2$ ,  $a_2$  and  $K_1, a_1$  are the Mark-Houwink coefficients of polymer 2 and polymer 1, respectively, and  $J_a$  is the hydrodynamic volume at retention volume  $a$ . Similarly,

$$J_b = K_2 M_{2,b}^{(a_2+1)} = K_1 M_{1,b}^{(a_1+1)} \quad (\text{A11})$$

Reconfiguring A10 and A11 we obtain

$$M_{2,b} = [K_1 M_{1,b}^{(a_1+1)} / K_2]^{1/(a_2+1)} \quad (\text{A12})$$

and

$$M_{2,a} = [K_1 M_{1,a}^{(a_1+1)} / K_2]^{1/(a_2+1)} \quad (\text{A13})$$

therefore

$$\begin{aligned} M_{2,b}/M_{2,a} &= [M_{1,b}^{(a_1+1)} / M_{1,a}^{(a_1+1)}]^{1/(a_2+1)} \\ &= [M_{1,b}/M_{1,a}]^{(a_1+1)/(a_2+1)} \end{aligned} \quad (\text{A14})$$

and

$$\ln (M_{2,b}/M_{2,a}) = [(a_1+1)/(a_2+1)] \ln (M_{1,b}/M_{1,a}) \quad (\text{A15})$$

Combination of eqs A8 and A9 yields

$$D_2' = D_2 \ln (M_{2,b}/M_{2,a}) / \ln (M_{1,b}/M_{1,a}) \quad (\text{A16})$$

Substitution of A15 into A16 yields

$$D_2' = D_2 (a_1+1)/(a_2+1) \quad (\text{A17})$$



Therefore to obtain  $(M_w^*)_v$  and  $(M_n^*)_v$  from  $M^*$  data obtained by universal calibration, eqs A2 and A3 are employed, but  $D_2'$  calculated by A17 is substituted for the  $D_2$  terms in A2 and A3.

Note also that the value of  $\sigma$  obtained for a given linear polymer calibrant is an approximation to the true value for a branched polymer or a polymer of differing monomeric composition, since the dispersion function is likely to vary for the various sample types. Under these conditions, the dispersion correction is a somewhat poorer approximation than the standard GPCV2 corrections.

In SEC/LALLS, the molecular weight measured at any instant is  $(M_w)_v$ . Thus the sample  $\bar{M}_w$  can be calculated by the standard definition

$$\bar{M}_w = \Sigma[F(V) (M_w)_v] \quad (A18)$$

Using eq A2 to eliminate  $M^*$  in eq A3, and substituting  $(M_w)_v$  for  $(M_w^*)_v$ , a dispersion-corrected  $(M_n)_v$  can be determined in the SEC/LALLS experiment:

$$(M_n)_v = \frac{F(V)^2}{F(V+D_2\sigma^2) \cdot F(V-D_2\sigma^2)} \cdot \exp[-(D_2\sigma)^2] \cdot (M_w)_v \quad (A19)$$

then for the total sample

$$\bar{M}_n(\text{corr}) = 1/\Sigma[F(V)/(M_n)_v] \quad (A20)$$

where  $\bar{M}_n(\text{corr})$  denotes the overall sample number-average molecular weight from SEC/LALLS, corrected for band-spreading. The limitations on the application of eq A19 to branched polymers and the use of a constant  $\sigma$  for various polymers in SEC/LALLS are identical to the limitations cited above for GPCV2.

#### Acknowledgements:

The authors wish to acknowledge the valuable technical assistance of Philip J. Christ and Frank Chambers.

LITERATURE CITED

1. Yau, W. W., Kirkland, J. J., and Bly, D. D., "Modern Size Exclusion Chromatography", John Wiley & Sons, New York - N. Y., 1979.
2. Flory, P. J., "Principles of Polymer Chemistry", Cornell University Press, Ithaca, N. Y., 1953.
3. Grubisic, Z., Rempp, P., and Benoit, H., J. Polym. Sci. B, (1967), 5, 753.
4. Application Notes LS-2, LS-3, LS-5, LS-10, Chromatix, 1977-1979.
5. McConnell, M. L., Am. Lab., (1978), 10 (5), 63.
6. Ouano, A. C., and Kaye, W., J. Polym. Sci. Polym. Chem. Ed., (1974), 12, 1151.
7. MacRury, T. B., and McConnell, M. L., J. Appl. Polym. Sci., (1979), 16, 2829.
8. Dubin, P., and Kronstadt, M., in "Plastic Materials Science and Technology", Baijal, M. J., ed., Wiley-Interscience, New York, In press.
9. Weiss, A. R., and Cohn-Ginsburg, E., J. Polym. Sci. B, (1969), 7, 379.
10. Hamielec, A. E., Ouano, A. C., and Nebenzahl, L. L., J. Liq. Chromat., (1978), 1 (4), 527.
11. Yau, W. W., Stoklosa, H. J., and Bly, D. D., J. Appl. Polym. Sci., (1977), 21, 1911.
12. Huglin, M. B., in "Light Scattering from Polymer Solutions", Huglin, M. B., ed., Academic Press, New York, N. Y., 1972 p. 165 ff.
13. Application Note LS-7, Chromatix, 1979.
14. Ouano, A. C., J. Chromatogr., (1976), 118, 303.
15. Hellman, M. Y., in "Liquid Chromatography of Polymers and Related Materials", Cazes, J., ed., Marcel Dekker, New York, N. Y., 1977, p. 31.
16. Park, W. S., and Graessley, W. W., J. Polym. Sci. Polym. Phys. Ed., (1977), 15, 71.
17. Coleman, M. M., and Fuller, R. E., J. Macromol. Sci.-Phys., (1975), B11 (3), 419.
18. Ambler, M. R., Mate, R. D., and Purdon, J. R., Jr., J. Polym. Sci. Polym. Chem. Ed., (1974), 12, 1759.
19. Park, W. S., and Graessley, W. W., J. Polym. Sci. Polym. Phys. Ed., (1977), 15, 85.

RECEIVED May 7, 1980.

## The Molecular Weight and Branching Distribution Method

G. N. FOSTER—Union Carbide Corporation, Bound Brook, NJ 08805

A. E. HAMIELEC—Department of Chemical Engineering, McMaster University, Hamilton, Ontario, Canada L8S 4M1

T. B. MacRURY—Union Carbide Corporation, South Charleston, WV 25303

Free radical polymerization leads to long chain branching (LCB) in commercial polymers such as polyvinyl acetate (PVAc) and low density polyethylene (LDPE) via a transfer to polymer mechanism (1). The branch lengths and spacings between branch points are most probably random for such polymers. Long chain branching content in commercial PVAc and high pressure LDPE ranges from one to twenty branch points per molecule.

It is well known that LCB has a pronounced effect on the flow behavior of polymers under shear and extensional flow. Increasing LCB will increase elasticity and the shear rate sensitivity of the melt viscosity (2). Environmental stress cracking and low-temperature brittleness can be strongly influenced by the LCB. Thus, the ability to measure long chain branching and its molecular weight distribution is critical in order to tailor product performance.

The use of  $^{13}\text{C}$  NMR to measure LCB (3, 4), although absolute, is both time intensive and limited in that it provides information only on the whole polymer. Existing size exclusion chromatographic (SEC) methods (5, 6) have attempted to correct the whole polymer molecular weights for long chain branching. However, both interpretations ignored the fact that the contents of the detector cell are polydispersed and that the LCB is a function of molecular weight.

SEC separates molecules according to hydrodynamic size, which is directly related to the product of the intrinsic viscosity  $[\eta]$  and the molecular weight as demonstrated by Benoit et. al. (7). Recently, Hamielec and Ouano (8) proved that for branched polymers, the instantaneous molecular weight in the detector cell is the instantaneous number average molecular weight  $M_N(V)$ . Therefore, the hydrodynamic size at a given elution volume is equal to the product  $[\eta](V)M_N(V)$ . Hence the detector cell will contain a complex mixture of molecules having the same hydrodynamic size but different molecular weights due to long chain branching.

Ideally one needs on-line detectors for measuring the instantaneous number average molecular weight and weight average molecular weight. Due to the solubility characteristics of resins like polyethylene, these detectors must be able to operate at temperatures up to 150°C. Low angle laser light scattering photometry can be used to determine  $M_W(V)$  directly at elevated temperatures (9). However, high temperature on-line viscometers, needed for the indirect measurement of  $M_N(V)$  from the universal calibration, are not commercially available. Furthermore, the batch type instruments available can not be used with the small elution volumes characteristic of high speed SEC equipment.

Therefore, herein is presented a new method for interpreting SEC data which accounts for the instantaneous polydispersity due to LCB within the detector cell and which allows for the calculation of LCB content and frequency as a function of the instantaneous number average molecular weight. Hereafter, this method will be referred to as the molecular weight and branching distribution (MWBD) method. Applications of the MWBD method will be highlighted using selected PVAc and high pressure LDPE resins.

#### Development of the MWBD Method

As pointed out by Hamielec and Quano (8), the separation of a branched polymer by size in the SEC process results in molecular species of different molecular weights eluting at the same volume. Thus, the molecular weight of these species is not monodispersed and  $M(V)$  must be replaced by the instantaneous number average molecular weight when using the universal calibration procedure for branched polymers,

$$\ln\{[\eta](V)M_N(V)\} = A + BV + \dots \quad (1)$$

The coefficients A, B, ... can be determined from fitting  $\ln\{[\eta](V)M_N(V)\}$  as a function of V for linear narrow distribution standards for which  $M_N(V) = M(V)$ .

It is now clear that the molecular weight obtained for branched polymers, when using the universal calibration procedure, is a number average molecular weight and not a weight average molecular weight as has been suggested in the past (5, 7, 10, 11). The choice of  $M_W$  as the proper molecular weight average to couple with the intrinsic viscosity perhaps evolved from the intuitive feeling that for most polymers the weight average molecular weight is the closest average to the viscosity average molecular weight. Note that for linear polymers  $M_N(V) = M_W(V) = M(V)$  since the contents of the detector cell are monodispersed.

The most direct method for calculating  $M_N(V)$  across the chromatogram would be to use an on-line viscometer to measure  $[\eta](V)$  and then to calculate  $M_N(V)$  from

$$M_N(V) = \exp(A + BV + \dots)/[\eta](V). \quad (2)$$

Unfortunately, an on-line viscometer which can provide instantaneous  $[\eta]$  values at low and high temperatures is not available. Although batch viscometers have been used in the past (12, 13) the use of high speed SEC makes them useless due to the small elution volumes.

We, therefore, propose an indirect method for obtaining the variation of the intrinsic viscosity and number average molecular weight across the chromatogram. First the intrinsic viscosity-molecular weight relationship for a polymer with long chain branching (LCB) is assumed to be expressible in a form similar to that used by Ram and Milts (6),

$$\ln([\eta](V)) = \ln K + a \ln M_N(V) + b(\ln M_N(V))^2 + c(\ln M_N(V))^3. \quad (3)$$

$K$  and  $a$  are the Mark-Houwink constants for the linear homologue in the same solvent and at the same temperature as the SEC measurements. The constants  $b$  and  $c$  are to be determined. If there is no LCB below a certain molecular weight  $M_L$ , the  $c$  in equation (3) can be replaced with

$$c = -b/\ln M_L. \quad (4)$$

The value normally found for  $M_L$  is between 5,000 and 10,000 (6, 13).

Once a value for  $M_L$  is assumed, this leaves one unknown  $b$  which can be determined from the SEC chromatogram and the measured whole polymer intrinsic viscosity in the following manner. First, one estimates a value for  $b$ , and calculates  $M_N(V)$  and  $[\eta](V)$  across the chromatogram using the universal calibration curve and equation (3). Then the whole polymer intrinsic viscosity is obtained from

$$[\bar{\eta}] = \int F(V)[\eta](V)dV, \quad (5)$$

where  $F(V)$  is the normalized concentration detector response. The calculated  $[\bar{\eta}]$  value is compared with the measured value. Further  $b$  values are then tried until the difference between the measured and calculated intrinsic viscosities is minimized. It is also possible to determine both  $M_L$  and  $b$  if  $[\bar{\eta}]$  and  $\bar{M}_N$  are known for the whole polymer.

Having determined  $b$  by the above method, the true number average molecular weight and higher moments for the whole polymer can be calculated as follows:

$$\bar{M}_N = \left\{ \int \frac{F(V)}{M_N(V)} dV \right\}^{-1}, \quad (6)$$

$$\bar{M}_W = \int F(V)M_N(V)dV, \quad (7)$$

$$\bar{M}_Z = \int F(V)(M_N(V))^2dV / \int F(V)M_N(V)dV. \quad (8)$$

Note that the weight and Z average molecular weights so obtained are only approximate and less than the true values. This is a consequence of the universal calibration method giving the instantaneous number average molecular weight across the chromatogram.

The instantaneous weight average molecular weight  $M_W(V)$  can also be measured by using an on-line, low angle laser light scattering device. Such measurements have been performed successfully both at low temperatures (14, 15) and at high temperatures (9). When combined with the method presented here for determining  $M_N(V)$ , the polydispersity in the detector cell ( $M_W(V)/M_N(V)$ ) could be calculated across the chromatogram. Work on the combination of these two methods will be reported at a later date.

Since our indirect method produces both the linear ( $b=0$ ) and branched intrinsic viscosities across the chromatogram, it is possible to estimate several LCB parameters as a function of elution volume or number average molecular weight. The branching factor  $G(V)$  can be written as

$$G(V) = \{[\eta]_b(V)/[\eta]_l(V)\}^{1/\epsilon}, \quad (9)$$

where  $[\eta]_b(V)$  is the instantaneous branched intrinsic viscosity,  $[\eta]_l(V)$  is the instantaneous linear intrinsic viscosity, and the branching structure factor  $\epsilon$  is a constant to be determined. For star polymers a value of  $\epsilon = 0.5$  has been obtained (16, 17) and studies (18) of model comb polymers indicate a value of 1.5. Other work (19) has suggested that  $\epsilon$  is near 0.5 at low LCB frequencies. For a random LCB conformation of higher branching frequency an  $\epsilon$  value between 0.7 and 1.3 might be expected, i.e. somewhere between a star and a comb configuration.

Zimm and Stockmayer (20) derived a theoretical relationship between  $G(V)$  and the number average number of LCB points per molecule  $B_N(V)$ , namely

$$G(V) = \left[ \left( 1 + \frac{B_N(V)}{7} \right)^{1/2} + \frac{4B_N(V)}{9} \right]^{-1/2} \quad (10)$$

Therefore by combining equations (9) and (10) and assuming some appropriate value for  $\epsilon$ , the number average number of LCB points per molecule can be calculated as a function of elution volume. The corresponding whole polymer number average number of LCB points per molecule is given by

$$\bar{B}_N = \bar{M}_N \int \frac{F(V)B_N(V)dV}{M_N(V)}. \quad (11)$$

Another parameter commonly used for characterizing long chain branching is the number of branch points (or frequency) per 1000 repeat units. The number average number of branch points can be calculated across the chromatogram from

$$\lambda_N(V) = 1000 M_R(B_N(V)/M_N(V)), \quad (12)$$

where  $M_R$  is the repeat unit molecular weight. The corresponding whole polymer quantity is

$$\bar{\lambda}_N = 1000 M_R \frac{\bar{B}_N}{\bar{M}_N}. \quad (13)$$

In an analogous fashion, the weight average long chain branching parameters per molecule ( $B_W$ ) and per 1000 repeat units ( $\lambda_W$ ) can be calculated. First  $B_W(V)$  can be determined from the Zimm-Stockmayer equation (20),

$$G(V) = \frac{6}{B_W(V)} \left[ \frac{1}{2} \frac{(2 + B_W(V))^{1/2}}{(B_W(V))^{1/2}} \times \ln \left\{ \frac{(2 + B_W(V))^{1/2} + (B_W(V))^{1/2}}{(2 + B_W(V))^{1/2} - (B_W(V))^{1/2}} \right\} - 1 \right]. \quad (14)$$

Then  $\bar{B}_W$ ,  $\lambda_W(V)$ , and  $\bar{\lambda}_W$  can be obtained from the following expressions:

$$\bar{B}_W = \bar{M}_N \int \frac{F(V)B_W(V)}{M_N(V)} dV, \quad (15)$$

$$\lambda_W(V) = 1000 M_R(B_W(V)/M_N(V)), \quad (16)$$

and

$$\bar{\lambda}_W = 1000 M_R \frac{\bar{B}_W}{\bar{M}_N}. \quad (17)$$

It should be noted that in order to calculate the weight average number of LCB points per 1000 repeat units, one must divide  $\bar{B}_w$  by  $\bar{M}_N$ . The use of  $\bar{M}_w$  here is incorrect.

The method outlined above for characterizing branched polymers will hereafter be referred to as the molecular weight and branching distribution (MWBD) method. In the following sections, its application to the long chain branching in polyvinyl acetate and high pressure low density polyethylene will be demonstrated.

### Long Chain Branching in Polyvinyl Acetate

Under conditions of low radical initiation, Graessely (21) has shown that the following set of equations describes the molecular weight and branching development in the bulk polymerization of vinyl acetate:

$$\frac{dQ_0}{dx} = C_M - \frac{kQ_0}{1-x}, \quad (18)$$

$$\frac{dQ_1}{dx} = 1, \quad (19)$$

$$\frac{dQ_2}{dx} = 2 \left[ 1 + \frac{kx}{1-x} \right] \left[ \frac{1 + \frac{C_p Q_2}{1-x} + \frac{kx}{1-x}}{C_M + \frac{C_p x}{1-x}} \right], \quad (20)$$

$$\frac{d(Q_0 \bar{B}_N)}{dx} = \frac{C_p x + kQ_0}{1-x}, \quad (21)$$

where

$$C_M = k_{fm}/k_p; \quad C_p = k_{fp}/k_p; \quad k = k_p^*/k_p. \quad (22)$$

In the above equations  $k_{fm}$  is the transfer to monomer constant,  $k_p$  is the propagation constant,  $k_{fp}$  is the transfer to polymer constant, and  $k_p^*$  is the constant for terminal double bond reactions. The quantities  $Q_0$ ,  $Q_1$ , and  $Q_2$  are the zeroeth, first, and second moments of the molecular weight distribution, respectively. The number average and weight average molecular weights are given simply by

$$\bar{M}_N = M_m Q_1 / Q_0, \quad (23)$$

$$\bar{M}_w = M_m Q_2 / Q_1, \quad (24)$$



where  $M_m$  is the monomer molecular weight.

The  $\bar{M}_N$ ,  $\bar{M}_w$ , and  $\bar{B}_N$  values predicted by this kinetic model are plotted as a function of conversion in Figure 1. The kinetic parameters used for these calculations are  $C_M = 2.0 \times 10^{-4}$ ,  $C_p = 3.0 \times 10^{-4}$ , and  $k = 1.0$ . Note that whereas  $\bar{M}_N$  is almost independent of conversion,  $\bar{M}_w$  and  $\bar{B}_N$  increase rapidly with increasing conversion. For conversions of 50% and 60%, the  $\bar{M}_N$ ,  $\bar{M}_w$ , and  $\bar{B}_N$ 's obtained for realistic values of  $C_M$ ,  $C_p$ , and  $k$  are listed in Table I.

TABLE I

SOLUTION OF KINETIC EQUATIONS FOR LONG CHAIN BRANCHING IN  
BULK VINYL ACETATE POLYMERIZATION\*

$C_M (\times 10^4)$	$C_p (\times 10^4)$	$k$	$\bar{M}_N (\times 10^{-6})$	$\bar{M}_w (\times 10^{-6})$	$\bar{B}_N$
2	1.5	0.6	0.54-0.58	1.7-2.2	0.6-0.9
2	2.5	0.6	0.54-0.58	2.1-2.7	0.9-1.2
2	3.0	1.0	0.63-0.71	3.0-4.6	1.3-1.9
2	4.0	1.0	0.63-0.71	3.5-5.4	1.5-2.3
2	5.0	1.0	0.63-0.71	3.9-6.2	1.8-2.8

\*Values shown are for conversions of 50-60%, respectively.

In order to estimate the branching factor  $\epsilon$  for polyvinyl acetate we have analyzed the SEC data obtained on sample PVAc-E4 using the MWBD method with various  $\epsilon$  values. This sample was synthesized under kinetically controlled conditions (isothermal,  $T = 60^\circ\text{C}$ ,  $[\text{AIBN}] = 10^{-5}$  g-mole/l, conversion level of 48.5 percent). The SEC measurements were made at  $25^\circ\text{C}$  in tetrahydrofuran. The Mark-Houwink coefficients used for linear polyvinyl acetate are those suggested by Graessley (21), namely  $K = 5.1 \times 10^{-5}$  dl/gm and  $a = 0.791$ . The whole polymer  $\bar{M}_N$ ,  $\bar{M}_w$ , and  $\bar{B}_N$  values obtained are listed in Table II.

The number average number of branch points per molecule decreases with increasing  $\epsilon$  and the molecular weights are independent of  $\epsilon$ . The weight average molecular weight calculated by the MWBD method is slightly less than the value of  $1.6 \times 10^6$  obtained by light scattering. This is consistent with the fact that this method uses a number average molecular weight in the averaging process. The number average molecular weight obtained is close to that predicted by the kinetic model with  $C_M = 2.0 \times 10^{-4}$ ,  $k = 0.6$  and a conversion of 50%. The  $\bar{B}_N$  value of 1.1 for  $\epsilon = 1.0$  is in the range indicated by the second set of kinetic parameters listed in Table I. Thus it is felt that

the MWBD method with  $\epsilon = 1.0$  gives good agreement with kinetic predictions and with the weight average molecular weight obtained by light scattering.

TABLE II

EFFECT OF EPSILON ON  $\bar{B}_N$  OF WHOLE POLYMER SAMPLE PVAc-E4

Epsilon	$\bar{B}_N$	$\bar{M}_N (\times 10^{-6})$	$\bar{M}_W (\times 10^{-6})$
0.5	2.5	0.51	1.37
0.8	1.4	0.51	1.37
1.0	1.1	0.51	1.37
1.2	0.34	0.51	1.37

We have used the MWBD method with  $\epsilon = 1.0$  to analyze the branching in two commercial PVAc standards supplied by the Aldrich Chemical Company, PVAc - Lot 1 and PVAc - Lot 3. A cut-off molecular weight of 5,000 was used in the analysis. The whole polymer  $\bar{M}_N$ ,  $\bar{M}_W$ ,  $\bar{B}_N$ , and  $\bar{\lambda}_N$  values obtained are given in Table III. The calculated molecular weight averages are in reasonable agreement with those quoted by the manufacturer. The number average number of LCB points per molecule and per 1000 repeat units are greater for Lot 1 than Lot 3. However, for both these samples, the branching parameters are less than 1.0.

TABLE III

MWBD RESULTS FOR COMMERCIAL PVAc STANDARDS DISTRIBUTED BY ALDRICH CHEMICAL COMPANY\*

PVAc - Lot 1	PVAc - Lot 2
$\bar{M}_N = 0.092 \times 10^6$ (0.083 $\times 10^6$ ) <sup>+</sup>	$\bar{M}_N = 0.146 \times 10^6$ (0.103 $\times 10^6$ )
$\bar{M}_W = 0.300 \times 10^6$ (0.331 $\times 10^6$ )	$\bar{M}_W = 0.626 \times 10^6$ (0.840 $\times 10^6$ )
$\bar{B}_N = 0.783$	$\bar{B}_N = 0.601$
$\bar{\lambda}_N = 0.748$	$\bar{\lambda}_N = 0.354$

\*Values obtained using  $M_L = 5,000$  and  $\epsilon = 1.0$ .

+Values in parenthesis are those quoted by the manufacturer.

For one of the samples, PVAc - Lot 1, the number average molecular weight distribution is plotted in Figure 2. Also shown is the instantaneous number average number of LCB points per molecule, plotted as a function of number average molecular weight. Note that  $B_N(V)$  increased rapidly with increasing number average molecular weight. The molecular weight and branching distribution of PVAc - Lot 3 is similar to Lot 1 and thus not shown.

### Application of the MWBD Method to LDPE

In order to determine the branching structure factor  $\epsilon$ , Foster (22) studied a large group of high pressure low density polyethylene resins (HP-LDPE). Using the MWBD method, he calculated the whole polymer number average number of branch points per 1000 carbon atoms from SEC data as a function of  $\epsilon$ . Then the  $\bar{\lambda}_N$  values were compared with those obtained by  $^{13}\text{C}$  NMR. Best agreement was found for  $\epsilon = 0.75$ .

An example of this method of determining  $\epsilon$  is shown in Figure 3 where the  $\bar{\lambda}_N$  has been calculated as a function of  $\epsilon$  for three HP-LDPE resins, designated LDPE A, B, and C. LDPE A was produced at the highest conversion and LDPE C at the lowest conversion. The SEC data used were obtained at 140°C in 1,2,4-trichlorobenzene. The Mark-Houwink coefficients used for linear polyethylene were  $K = 5.1 \times 10^{-4}$  dl/gm and  $a = 0.706$ . The  $^{13}\text{C}$  NMR  $\bar{\lambda}_N$  values are indicated by open triangles.

The whole polymer  $\bar{M}_N$ ,  $\bar{M}_w$ ,  $\bar{B}_N$ , and  $\bar{\lambda}_N$  values obtained using the MWBD method and  $\epsilon = 0.75$  for these three LDPE resins are shown in Table IV. The molecular weights and branching parameters are in agreement with expectations based on the levels of conversion. With increasing conversion  $\bar{M}_N$  remains constant whereas  $\bar{M}_w$ ,  $\bar{B}_N$ , and  $\bar{\lambda}_N$  increase.

TABLE IV

MWBD RESULTS FOR COMMERCIAL HIGH PRESSURE LDPE

SUPPLIED BY UNION CARBIDE CORPORATION\*

LDPE	$\bar{M}_N (\times 10^{-3})$	$\bar{M}_w (\times 10^{-3})$	$\bar{B}_N$	$\bar{\lambda}_N$
A	15.6	243	5.05	4.52
B	15.6	116	2.89	2.60
C	19.6	83.9	2.44	1.75

\*Values obtained using  $M_L = 2,000$ ;  $\epsilon = 0.75$

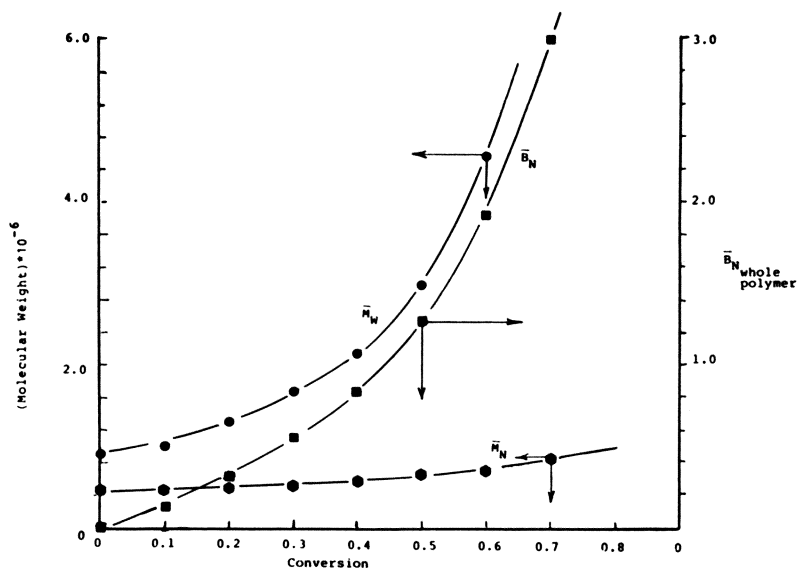


Figure 1. Solution of kinetic equations for molecular weight and LCB development in bulk VAc polymerization.  $\bar{M}_N$ ,  $\bar{M}_W$ , and  $\bar{B}_N$  are plotted as a function of conversion. Model predictions:  $C_M = 2.0 \times 10^{-4}$ ;  $C_P = 3.0 \times 10^{-4}$ ;  $K = 1.0$ .

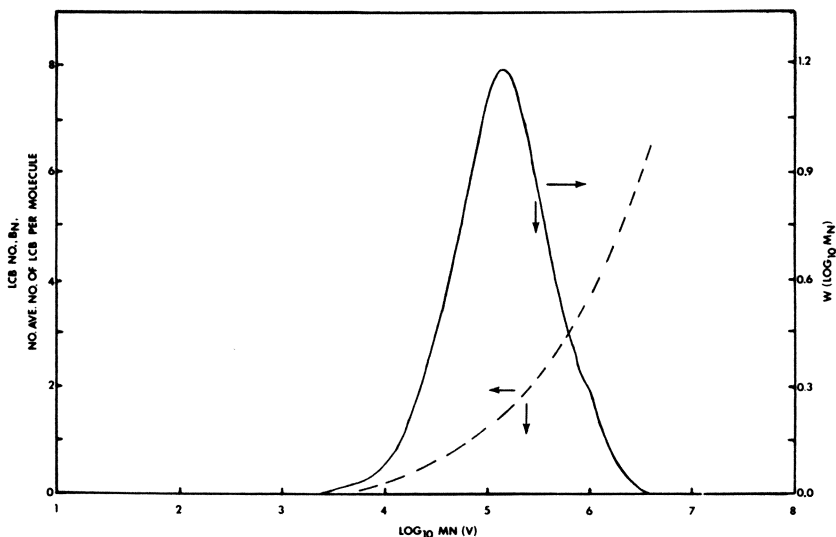


Figure 2. Molecular weight distribution and number average number of LCB points per molecule ( $B_N$ ) as a function of  $M_N(V)$  for PVAc Sample A, Lot 1 ( $\bar{M}_N = 90200$ ;  $\bar{M}_W = 300200$ ;  $\bar{M}_W/\bar{M}_N = 3.33$ ;  $\bar{B}_N = 0.78$ ;  $\bar{\lambda}_N = 0.75$ )

The number average molecular weight distribution and LCB frequency  $\lambda_N(V)$  are plotted in Figures 4 and 5 for the highest and lowest conversion resins. Not only are the molecular weight distributions quite different, but also the LCB distribution are radically different. For LDPE A the molecular weight distribution is very broad ( $\bar{M}_w/\bar{M}_n = 15.5$ ) and  $\lambda_N(V)$  increases to about 5.0, remains constant up to about a number average molecular weight of  $1 \times 10^6$ , and then rapidly increases. In contrast for LDPE C  $\bar{M}_w/\bar{M}_n = 4.3$  and the LCB frequency quickly increases to a maximum of about 2.3 at  $M_N(V) = 9,000$  and then slowly decreases.

Some of the properties of these three resins are listed in Table V. The agreement between  $\bar{\lambda}_N$  calculated from the MWBD method with  $\epsilon = 0.75$  and from  $^{13}\text{C}$  NMR is excellent. Long chain branching frequency is found to correlate well with blown film properties. Increasing LCB, for resins with similar densities, leads to increased haze, decreased gloss, and decreased tear strength. As indicated by the die swell, melt elasticity increases with increasing LCB. A more detailed discussion of the correlation of LDPE physical properties with the long chain branching frequency can be found elsewhere (22).

The MWBD method was also used to determine the long chain branching in the National Bureau of Standards LDPE SRM #1476. The  $\bar{M}_n$ ,  $\bar{M}_w$ , and  $\bar{\lambda}_N$  values calculated using  $\epsilon = 0.75$  are given in Table VI. Included for comparison are the results obtained by Wagner and McCrackin (23) from summing well characterized fractions of 1476 and by MacRury and McConnell (9) from coupling a low angle laser light scattering photometer to a GPC (LALLSP/GPC). The  $\bar{M}_n$  and  $\bar{\lambda}_N$  calculated from MWBD are in good agreement with those determined by the summing of fractions. The  $\bar{M}_w$  value is too low as expected. The  $\bar{M}_n$  value calculated using LALLSP/GPC is too high because an instantaneous weight average molecular weight is used in the averaging. Excellent agreement is found between the  $\bar{M}_w$  determined by LALLSP/GPC and that calculated by the summing of fractions. Thus, as was mentioned earlier in this paper, the MWBD method combined with the LALLSP/GPC yields the correct number average and weight average molecular weights across the chromatogram and for the whole polymer.

The LCB frequency obtained by MWBD is plotted in Figure 6 as a function of number average molecular weight. The open triangles are the  $\bar{\lambda}_N$  values calculated by Wagner and McCrackin for various fractions. Again, good agreement is found between the two methods.

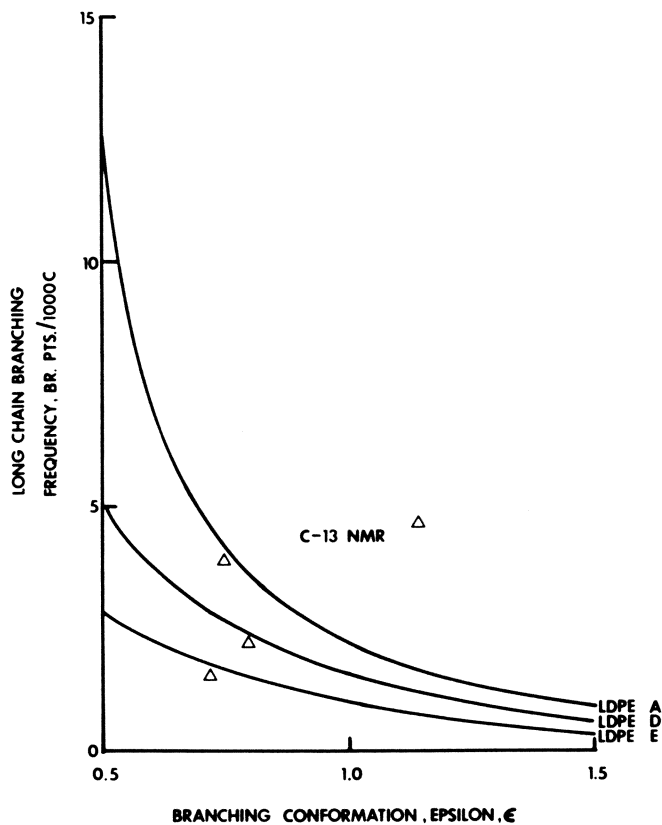


Figure 3. Effect of the branching structure factor ( $\epsilon$ ) on the LCB frequency ( $\bar{\lambda}_N$ ) calculated for three LDPE resins using the MWBD method (( $\Delta$ )  $\bar{\lambda}_N$  values obtained by  $^{13}\text{C}$  NMR)

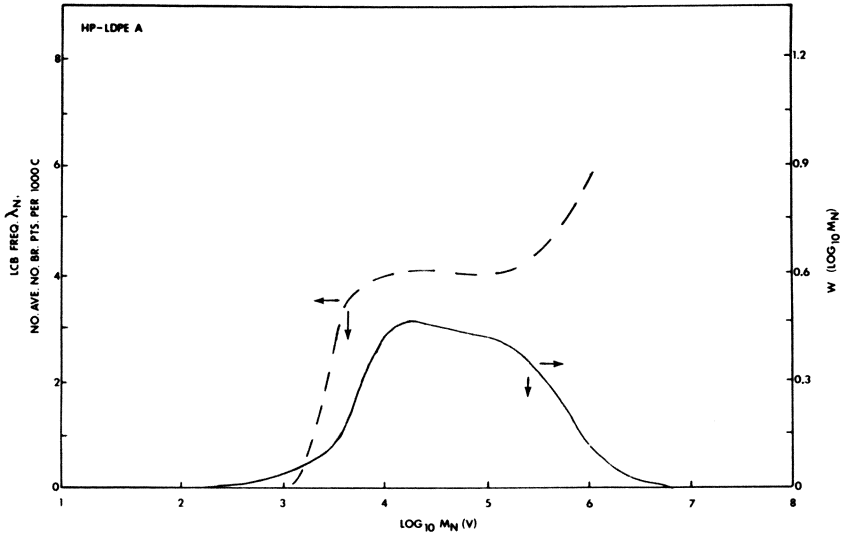


Figure 4. Molecular weight distribution and LCB frequency as a function of  $M_N(V)$  for LDPE A ( $\bar{M}_N = 15600$ ;  $\bar{M}_W = 243100$ ;  $\bar{M}_W/\bar{M}_N = 15.5$ ;  $\bar{B}_N = 5.05$ ;  $\bar{\lambda}_N = 4.52$ )

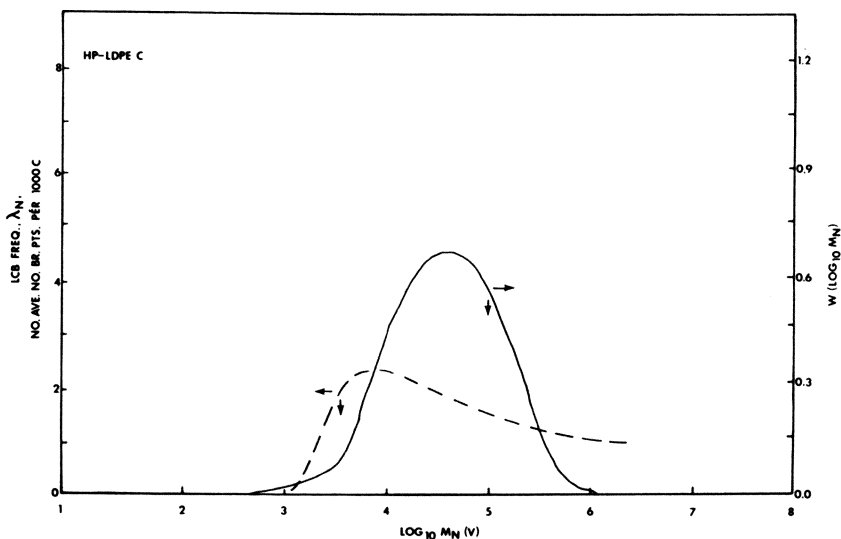


Figure 5. Molecular weight distribution and LCB frequency as a function of  $M_N(V)$  for LDPE C ( $\bar{M}_N = 19600$ ;  $\bar{M}_W = 83900$ ;  $\bar{M}_W/\bar{M}_N = 4.29$ ;  $\bar{B}_N = 2.44$ ;  $\lambda_N = 1.75$ )

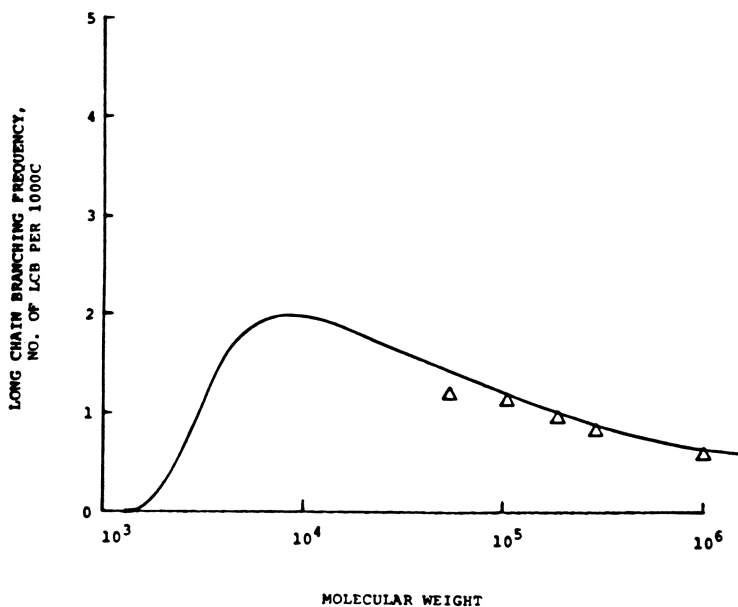


Figure 6. Comparison of the LCB frequency obtained for NBS SRM #1476 using the MWBD method ((—)  $\lambda_N = 1.47$ ) with that obtained by fractionation (( $\Delta$ )  $\lambda_N = 1.05$  (Wagner and McCrackin))



TABLE V  
PROPERTY SUMMARY FOR HIGH PRESSURE, LOW DENSITY POLYETHYLENES

<u>Materials</u>	<u>Melt Index</u>	<u>Die Swell, %</u>	<u>Density, gm/cc</u>	<u>Intrinsic Viscosity</u>	<u>Haze, %</u>	<u>Gloss</u>	<u>Tear Strength, gms</u>	$\bar{\lambda}_N$	$\bar{\lambda}_{NMR}$	$\bar{B}_N$
LDPE A	1.8	72	0.919	0.796	19	53	85	4.52	4.5	5.05
B	2.6	48	0.921	0.825	6.6	122	125	2.60	2.2	2.89
C	2.1	39	0.923	0.925	4.8	156	200	1.75	1.8	2.44

TABLE VI  
MWBD RESULTS FOR NBS SRM #1476

Method	$\bar{M}_N (\times 10^{-3})$	$\bar{M}_W (\times 10^{-3})$	$\bar{\lambda}_N$
MWBD	23.0	88.2	1.47
Sum of Fractions (Wagner & McCrackin (23))	25.0	105	1.05
LALLSP/GPC (MacRury & McConnell (9))	28.0	100	-

### Conclusions

The molecular weight and branching distribution (MWBD) method provides for the rapid determination of the instantaneous number average molecular weight  $M_N(V)$ , number average number of long chain branch points per molecule  $B_N(V)$ , and number average number of long chain branch points per 1000 repeat units  $\lambda_N(V)$ , as well as the corresponding whole polymer quantities. Weight average branching parameters can also be calculated. The weight average molecular weight and higher moments obtained from this method are too low, due to the fact that the instantaneous number average molecular weight is employed in the averaging. The use of an on-line laser light scattering photometer will allow for the determination of the correct instantaneous and whole polymer weight average molecular weight.

There are several assumptions used in the MWBD method. Firstly, it is necessary to establish some relationship between  $[\eta](V)$  and  $M_N(V)$ . For polymers produced by free radical polymerization, we feel that equation (3) provides an adequate relationship. Secondly, we have assumed a value of  $M_l$  instead of determining both  $b$  and  $M_L$  (or  $c$ ) by fitting the SEC data to whole polymer  $[\eta]$  and  $\bar{M}_N$  values.

The MWBD method also requires an independent measure of the branching structure factor  $\epsilon$ . For our analysis of polyvinyl acetate, it was obtained by comparing  $\bar{M}_N$  and  $\bar{B}_N$  values calculated from SEC data, analyzed using the MWBD method and various epsilons, and the  $\bar{M}_N$  and  $\bar{B}_N$  values predicted by Graessley's (21) kinetic model. An epsilon value of 1.0 was found to fit best.

For high pressure low density polyethylene, the branching structure factor was obtained by comparing whole polymer  $\bar{\lambda}_N$  values, calculated from SEC data on a series of resins, with those determined by  $^{13}\text{C}$  NMR. An epsilon value of 0.75 was found to give the best agreement. The long chain branching distributions obtained with the MWBD method for typical commercial high pressure process LDPE's were as would be expected based on free

radical kinetic considerations and showed a good correlation with the melt elastic and blown film properties. Furthermore, the long chain branching distribution calculated for the National Bureau of Standards SRM #1476 was in good agreement with fractionation data obtained by Wagner and McCrackin (23).

The MWBD method, when coupled with high speed SEC techniques, is more rapid for long chain branching measurements than  $^{13}\text{C}$  NMR. In addition, the branching distribution information that it provides, once epsilon has been determined, can not be obtained by other branching characterization methods unless the polymer is fractionated.

### Abstract

A molecular weight and branching distribution (MWBD) method is presented for determining the long chain branching as a function of molecular weight. This method requires a measurement of the intrinsic viscosity of the polymer, size exclusion chromatographic data, and a universal calibration curve, obtained from narrow distribution standards such as polystyrene. The hydrodynamic size is expressed as a function of elution volume, namely  $\ln([\eta]_i M_{N,i}) = f(V_i)$ , and the instantaneous intrinsic viscosity is written in polynomial form as  $\ln[\eta]_i = \ln K + a \ln M_{N,i} + b (\ln M_{N,i})^2 + c (\ln M_{N,i})^3$ . Then the number average molecular weight and the number of long chain branch points are obtained as a function of elution volume. Integration across the chromatogram yields the whole polymer quantities  $\bar{M}_N$ ,  $\bar{B}_N$ , and  $\bar{\lambda}_N$ .

To illustrate the utility of the MWBD method, a series of commercial polyvinyl acetates and low density polyethylenes are analyzed. Either kinetic models or  $^{13}\text{C}$  nuclear magnetic resonance results are used to estimate the branching structural parameter.

### Acknowledgements

Dr. E. S. Hsi (Union Carbide Corporation, Bound Brook, New Jersey) provided the  $^{13}\text{C}$  NMR of the three HP-LDPE's studied.

### Literature Cited

1. Roedel, M. J. J. Amer. Chem. Soc., 1953, 75, 6110.
2. Wild L.; Ranganath, R.; Knobloch, D. C. Polym. Eng. and Sci., 1976, 16, 811.
3. Bovey, F. A.; Schilling, F. C., McCrackin, F. L.; Wagner, H. L. Macromolecules, 1976, 9, 76.
4. Axelson, D. E.; Levy, G. C.; Mandelkern, L. Macromolecules, 1979, 12, 41.
5. Drott, E. E.; Mendelson, R. A. J. Polym. Sci. A-2, 1970, 8, 1373.
6. Ram, A.; Miltz, J. J. Appl. Polym. Sci., 1971, 15, 2639.

**American Chemical  
Society Library**

1155 16th St. N. W.  
Washington, D. C. 20036

7. Grubisic, Z.; Remp, P.; Benoit, H. J. Polym. Sci. B, 1967, 5, 753.
8. Hamielec, A. E.; Ouano, A. C. J. Liq. Chromat. 1978, 1, 111.
9. MacRury, T. B.; McConnell, M. L. J. Appl. Polym. Sci., 1979, 24, 651.
10. Wild, L.; Guliana, R. J. Polym. Sci. A-2, 1967, 5, 1087.
11. Williams, G. R.; Cervenka, A. Eur. Polym. J., 1972, 8, 1009.
12. Meyerhoff, G. Separation Sci., 1971, 6, 239; Goedhard, D.; Opschoor, A. J. Polym. Sci. A-2, 1970, 8, 1227.
13. Barlow, H.; Wild, L.; Ranganath, R. J. Appl. Polym. Sci., 1977, 21, 3319; *ibid*, 1977, 21, 3331.
14. Ouano, A. C.; Kaye, W. J. Polym. Sci. A-1, 1974, 12, 1151.
15. Ouano, A. C. J. Chromat., 1976, 118, 303.
16. Zimm, B. H.; Kilb, R. W. J. Polym. Sci., 1959, 37, 19.
17. Morton, M.; Helmiak, T. E.; Gadrury, S. D.; Buiche, F. J. Polym. Sci., 1962, 57, 471.
18. Noda, I.; Horikawa, T.; Kato, T.; Fryimoto, T.; Nagasawa, N. Macromolecules, 1970, 3, 795.
19. Graessley, W. W., "Detection and Measurement of Branching in Polymers", *Characterization of Macromolecular Structure*, D. McIntyre, Ed., Natl. Acad. of Sci. Publication No. 1573, Washington, D. C., 1969, p. 371-388.
20. Zimm, B. H.; Stockmayer, W. H. J. Chem. Phys. 1949, 17, 1301.
21. Graessley, W. W.; Uy, W. C.; Gandhi, A. I & EC Fundamentals, 1969, 8, 696.
22. Foster, G. N., "Characterization of Long Chain Branching in Polyethylene", presented at the 13th ACS Middle Atlantic Regional Meeting, Monmouth College, West Long Branch, New Jersey, March 1979.
23. Wagner, H. L.; McCrackin, F. L. J. Appl. Polym. Sci., 1977, 21, 2833.

RECEIVED May 7, 1980.

# High-Conversion Polymerization Kinetic Modeling Utilizing Gel Permeation Chromatography

S. T. BALKE and R. D. PATEL

Xerox Research Centre of Canada, Mississauga, Ontario, Canada

## I Introduction

Gel Permeation Chromatography (GPC) is often the source of molecular weight averages used in polymerization kinetic modelling (1,2). Kinetic models also require measurement of molecular weight distribution, conversion to polymer, composition of monomers in a copolymerization reaction mixture, copolymer composition distribution, and sequence length distribution. The GPC chromatogram often reflects these properties (3,4).

However, even homopolymer molecular weight averages calculated from GPC frequently do not agree with those from osmometry and light scattering or for that matter with those from another set of GPC operating conditions (5,6). Copolymers readily provide multimodal chromatograms in contrast to kinetic modelling expectations and are extremely difficult to interpret even with dual GPC detectors (7).

In analysis of homopolymers the critical interpretation problems are calibration of retention time for molecular weight and allowance for the "imperfect resolution" of the GPC. In copolymer analysis these interpretation problems remain but are given added dimensions by the simultaneous presence of molecular weight distribution, copolymer composition distribution and monomer sequence length distribution. Since, the GPC usually separates on the basis of "molecular size" in solution and not on the basis of any one of these particular properties, this means that at any retention time there can be distributions of all three. The usual GPC chromatogram then represents a response to the concentration of some average of each of these properties at each retention time.

The purpose of this paper is to propose solutions to the GPC interpretation problems fitting the needs of high conversion polymerization kinetic modelling.

In particular, for copolymers this required an orthogonal coupling of one GPC to another to achieve the desired cross fractionation before application of dual detectors. This method is really a new polymer analysis member of a family of approaches developed in the literature which we are now terming "Orthogonal Chromatography". It not only provides both a cross fractionation approach for copolymers and a new way of determining the GPC's "imperfect resolution"; it also enables separation mechanisms previously reserved for the liquid chromatography of small molecules to be used for polymer analysis.

Two free radical-initiated polymerizations are used in turn as examples: the homopolymerization of methyl methacrylate and the copolymerization of styrene n-butyl methacrylate.

The kinetic model obtained for the former polymerization was previously published (8). The results have now been utilized in a variety of investigations. In particular, the

0-8412-0586-8/80/47-138-149\$08.50/0

© 1980 American Chemical Society

rate parameter values from the bulk polymerization were successfully employed in predicting emulsion polymerization (9). This paper details and updates the underlying GPC approach involved in determining those rate parameters.

With regards to the copolymerization, a recent kinetic study by Gruber and Knell (10) has indicated that styrene n-butyl methacrylate obeys the classical kinetic theory with regards to composition and sequence length to complete conversion. This theory is applied to high conversion to characterize copolymer samples for GPC analysis.

## II Experimental

Data for the polymerization of MMA was obtained from (11). Kinetics were previously described (8). GPC operating conditions are shown in Table I under GPC 0.

For the copolymerization work, GPC #1 and GPC #2 (Table I) were used. Mark Houwink constants are shown in Table II.

Data processing was accomplished with the aid of a Data General ECLIPSE Minicomputer interfaced to a Data General NOVA 2 Minicomputer which, in turn, was interfaced to the GPCs.

Copolymerizations were performed at 70°C using an ampoule technique similar to that used for MMA. Monomers were purified by distillation. Most of the runs had an initial weight fraction styrene of 0.767 and 1.45 mole % AIBN initiator. Also utilized is one run using 0.235 wt. fraction styrene (0.350 mole % AIBN) and one at 0.557 (1.45 mole % AIBN). Gruber and Knell (10) used both the former compositions. The latter one is the calculated azeotropic composition using their values of the reactivity ratios.

Polystyrene standards used were narrow molecular weight distribution samples produced by anionic polymerization and available from Pressure Chemical Co. Also sample NBS706 from the National Bureau of Standards was used. The sample of poly n-butyl methacrylate was obtained from Aldrich Chemical. It was produced by free radical polymerization with an Mw of 320,000 and an Mn of 73,500 (Cat. No. 18,153-6).

## III Results & Discussion

1. General. The development progressed from homopolymer analysis to copolymer analysis. In each case the results of applying previously published "state-of-the-art" GPC interpretation approaches and comparison with kinetic modelling predictions were examined. For some problems, notably homopolymer molecular weight calibration, these approaches were satisfactory. However, usually this was not the case. The imperfect resolution problem in GPC appeared intractable even for the broad homopolymer chromatograms let alone those of copolymers. Attempts to resolve monomer peaks utilizing GPC was unsuccessful. Application of dual detectors was insufficient to deal with the complexity of copolymer property distributions. Thus, in several cases, new approaches had to be developed.

In homopolymer analysis this meant a closer study of the accuracy and reproducibility of data from GPC to see how resolution correction techniques could be either circumvented or practically applied. In copolymer analysis the limitation of conventional molecular size fractionation emerged as the fundamental difficulty. An orthogonal coupling of GPCs operated so as to achieve the desired cross fractionation before detection is presented as a novel approach with considerable potential.

2. High Conversion Homopolymerization of Methyl Methacrylate. Figure 1 shows a typical chromatogram of high conversion polymethyl methacrylate (PMMA). Also shown is the reproducibility of the chromatogram heights and the low precision of the chromatogram tails.

In analysis of the homopolymer to model this polymerization molecular weight information is the primary requirement.

The two interpretation problems involved are (A) calibration and (B) correction of imperfect resolution caused by axial dispersion.

Calibration refers to characterizing the residence time in the GPC as a function of molecular weight. Axial dispersion refers to the chromatogram being a spread curve even for a monodisperse sample. A polydisperse sample then is the result of a series of overlapping, unseen, spread curves.

**A. Calibration.** No monodisperse calibration standards were available for PMMA. Figures 2 and 3 show calibrations accomplished by two methods:

- (i) Universal Calibration using polystyrene standards (6) and
- (ii) Calibration using a broad standard of known molecular weight distribution (12).

Both methods are in good agreement for the high resolution column set. For the lower resolution one, discrepancies appear at the beginning and end of the curve. These are the areas where the tail heights of the broad standard are utilized.

**B. Axial Dispersion.** Figure 4 shows, for monodisperse polystyrene standards, the ratio of number average molecular weight from osmometry ( $M_n(t)$ ) to that calculated from the GPC Chromatograms assuming perfect resolution ( $M_n(\infty)$ ). Figure 5 shows a similar plot for weight average molecular weights  $M_w(t)$  and  $M_w(\infty)$ . These plots show large disagreement with absolute values at both high and low molecular weights;  $M_w(\infty)$  agreement over the central range is good. However,  $M_n(\infty)$  is too low. Such results can be partly due to inaccurate osmometry  $M_n$ 's and to imprecisely known very high and low ends of the calibration curve. However, they are very typical of axial dispersion effects on GPC molecular weight averages. Axial dispersion correction methods have recently been comprehensively reviewed by Friis and Hamielec (5).

This is a very difficult case for axial dispersion correction:

- (i) The calibration curve is non-linear.
- (ii) Axial dispersion effects are unsymmetrical ( $M_n$  requires more correction than  $M_w$ ).
- (iii) The chromatograms are sometimes bimodal and can include very high molecular weights.

One possibility is that although averages for polystyrene standards require correction, those for PMMA would not. According to symmetrical axial dispersion theory (5) the correction depends upon both the slope of the calibration curve (different for each polymer type) and the variance of the chromatogram of a truly monodisperse sample. Furthermore, the calibration curve to be utilized can be obtained from a broad standard as well as from monodisperse samples. The broad standard method may itself incorporate some axial dispersion correction depending upon how the standard was characterized.

To attempt clarification of this situation the effect of axial dispersion on the chromatogram was examined in two ways:

- (i) Assuming a Gaussian shape function and different resolution factors (proportional to the inverse variance of this function) the method of Ishige, Lee and Hamielec (13) was applied to a PMMA chromatogram. Figure 6 shows the results.
- (ii) Using calibration curves from each of three columns of widely different resolution, uncorrected chromatograms were superimposed on the one axis. Results are shown in Figure 7.

The effect on central chromatogram heights (and more particularly those on each side of the peak) is very small for these broad chromatograms even for conditions of extreme peak broadening ( $h = 0.3$ ). Several similar examples can now be found in the literature on axial dispersion correction (e.g. (14), (6)). This effect is attributed simply to the idea that for a broad chromatogram as many molecules are misplaced from a given retention time as are gained from neighbouring times. This is readily demonstrated theoretically but only if shape functions are assumed for all the distributions involved.

Although the effect of axial dispersion on the chromatogram heights can be small (even when they are transformed to weight fractions using a calibration curve) the

TABLE I: GPC

GPC 0 - Waters Model 100, R-4 Refractometer

COLUMN COMBINATION CODE NO.	MOBILE PHASE		
	COMPOSITION (VOL. %)	FLOW RATE (ml/min)	TEMPERATURE (°C)
25	100 % THF	2.40	24.0 ± 0.5
26	"	"	"
27	"	"	"
28	"	"	"

GPC 1 - Waters GPC/ALC 401, Model 77 UV (254 nm), R401 Refractometer

A1	100 % THF	1.00	25.0 ± 2
A2	"	1.00	"
A3	"	0.53	"
A4	"	0.53	"

GPC 2 - Spectra Physics SP8000, SP8310 U.V. (254 nm), Schoeffel SF770 UV  
(200 nm for B1, 235 nm for others)

B1	46 % Acetonitrile in Water	2.00	40.0 ± 0.1
B2	100 % THF	1.75	"
B3	"	} 2.00	"
B4	57% n-Heptane in THF		
B5	62% n-Heptane in THF		
B6	60% n-Heptane in THF	0.5	25.0 ± 0.1



OPERATING CONDITIONS

NO. OF COLUMNS IN SERIES	COLUMN PACKING DESIGNATIONS (1)
5	S5 x 10 <sup>6</sup> , S5 x 10 <sup>6</sup> , S(0.7-5) x 10 <sup>6</sup> , S10 <sup>4</sup> , S800
7	B2500/1500, C2000/1250, C2000/1250, C2000, C700, S10 <sup>4</sup> , S800
7	S800, S10 <sup>4</sup> , C700, C2000, C2000/1250, C2000/1250, B2500/1500
9	S350/100, S350/100, S800, S10 <sup>4</sup> , C700, C2000, C2000/1250, C2000/1250, B2500/1500
7	SI:100, SI:300, SI:500, μS10 <sup>5</sup> , μS10 <sup>2</sup> , μS10 <sup>2</sup> μS10 <sup>2</sup>
2	μS10 <sup>2</sup> , μS10 <sup>2</sup>
9	SI:1000, SI: 500, SI:100, SI:100, SI:500, SI:300, SI:300, SI:100, PXS10/25
12	μS10 <sup>6</sup> , μS10 <sup>5</sup> , μS10 <sup>3</sup> + columns in code A4
	RP8
9	SI:1000, SI: 500, SI:100, SI:100, SI:500, SI:300, SI:300, SI:100, PXS10/25
2	μS10 <sup>3</sup> , μS10 <sup>4</sup>
3	E300, E500, E (linear)

(1) Columns for each code are listed in the direction of mobile phase flow:

S = Styragel	SI = LiChrospher Silica
C = Corning Porous Glass	RP = LiChrospher Reverse Phase
B = Bioglas	E = μBondagel
μS = Micro Styragel	
PXS = Whatman Silica	

TABLE II  
MARK HOUWINK CONSTANTS

POLYMER	K	$ \eta  = KM^a$		SOURCE
		a		
Polystyrene	$1.6 \times 10^{-4}$	.706		Provdor, T., Rosen, E.M., Sep. Sci., <u>5</u> , 437 (1970)
PMMA				
M $\leq$ 31000	$21.1 \times 10^{-4}$	.406		Provdor, T., Woodbrey, J.C., Clark, J.H., ACS Symposium on GPC, ACS, Houston, Texas February, 1970
M $>$ 31000	$1.04 \times 10^{-4}$	.697		

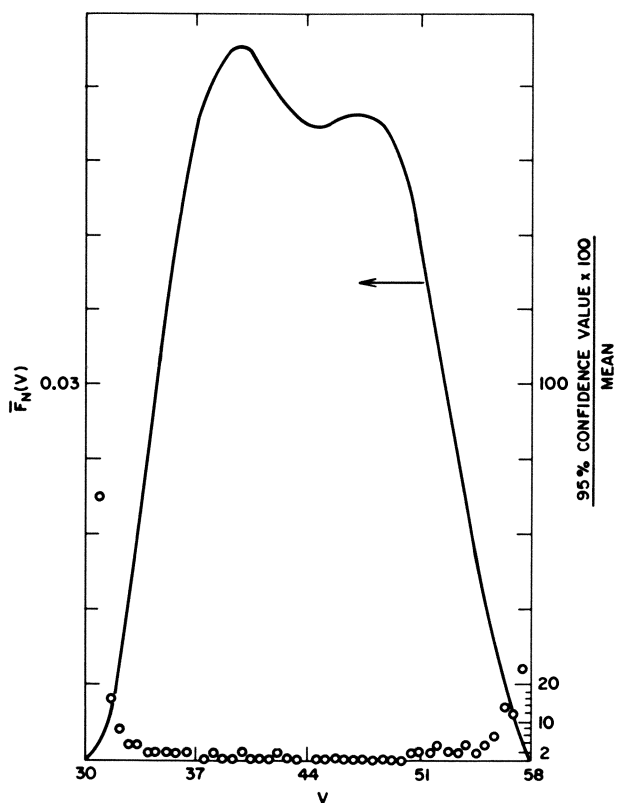


Figure 1. Mean height values of chromatograms of PMMA and 95% confidence value as a percent of mean vs. retention volume

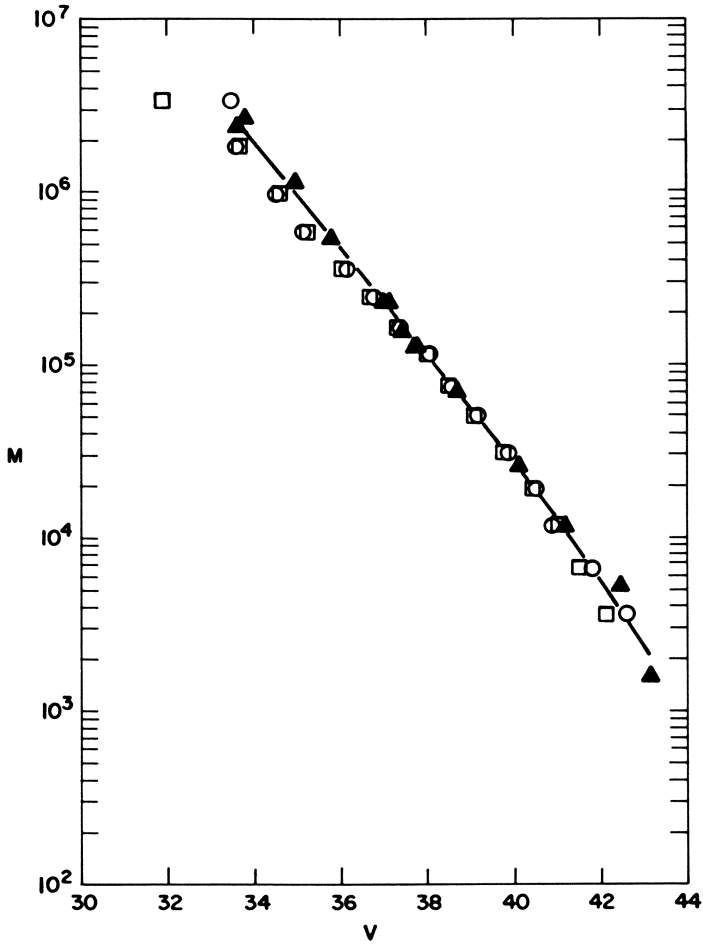


Figure 2. Calibration curve for PMMA, Column Code 25 ((—) polynomial used; (▲) from universal calibration curve; (□, ○) from Weiss method (1.88 mg of RH PMMA standard))

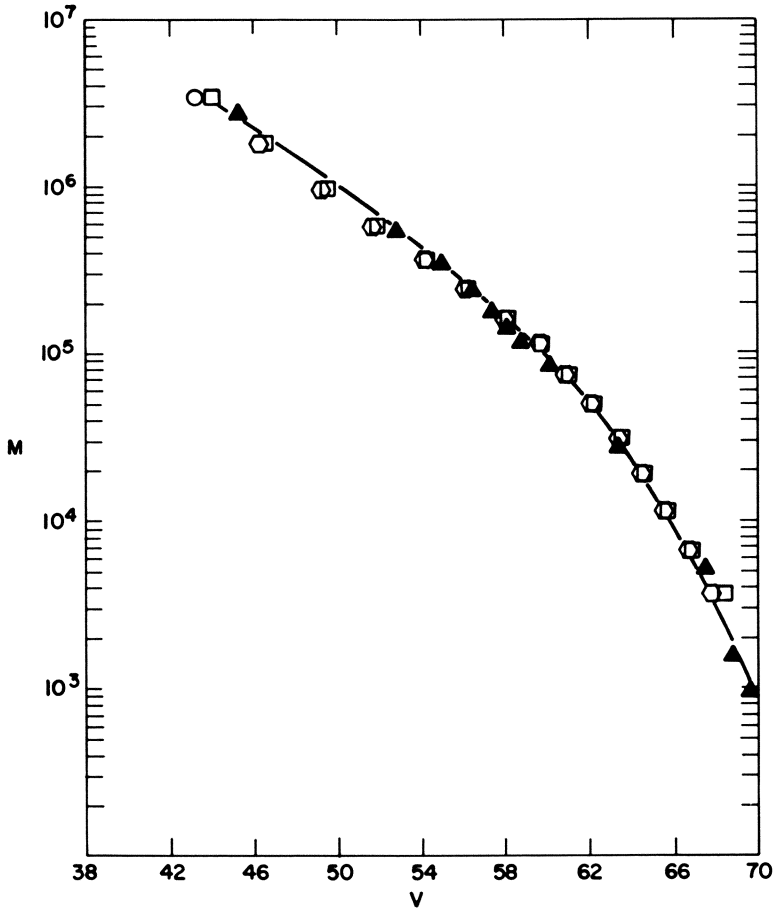


Figure 3. Calibration curve for PMMA, Column Code 28 ((—) polynomial used; (▲) from universal calibration curve; (□) from Weiss Method (3.55 mg of RH PMMA standard); (◐) from Weiss Method (5.33 mg of RH PMMA standard))

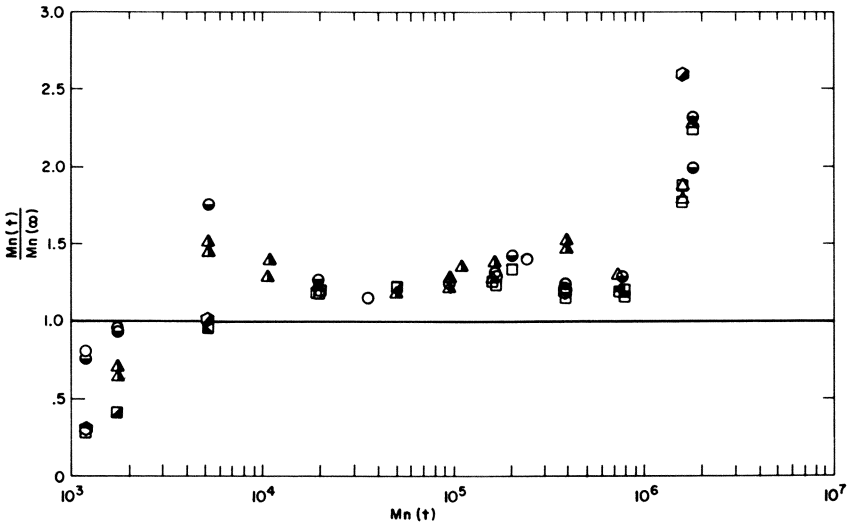


Figure 4. GPC and absolute  $M_n$  comparison (polystyrene standards) (Column Code 25: ( $\blacktriangle$ ,  $\triangle$ ) 1.8 mg; ( $\triangle$ ) .8 mg; Column Code 26: ( $\odot$ ) 1.8 mg; Column Code 27: ( $\blacksquare$ ) 1.77 mg; ( $\blacklozenge$ ) 1.81 mg; ( $\blacktriangleleft$ ) 3.55 mg; ( $\square$ ) 3.99 mg; Column Code 28: ( $\circ$ ) 3.55 mg; ( $\ominus$ ) 5.33 mg)

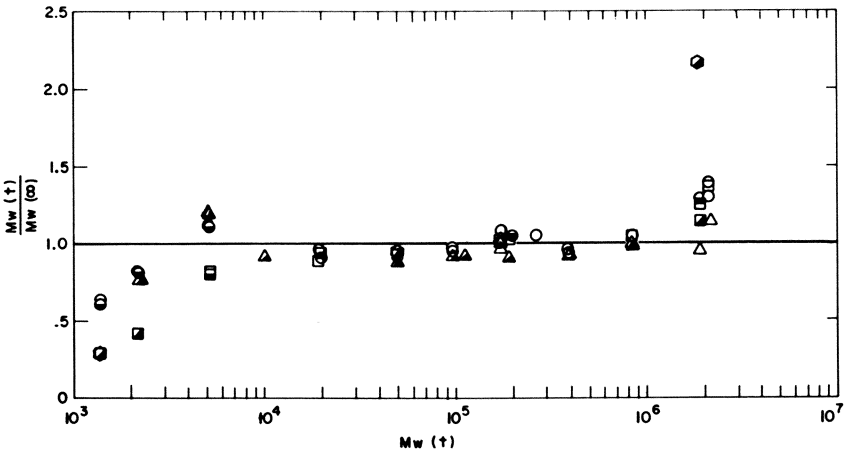


Figure 5. GPC and absolute  $M_w$  comparison (polystyrene standards) (see Figure 4 for symbols)

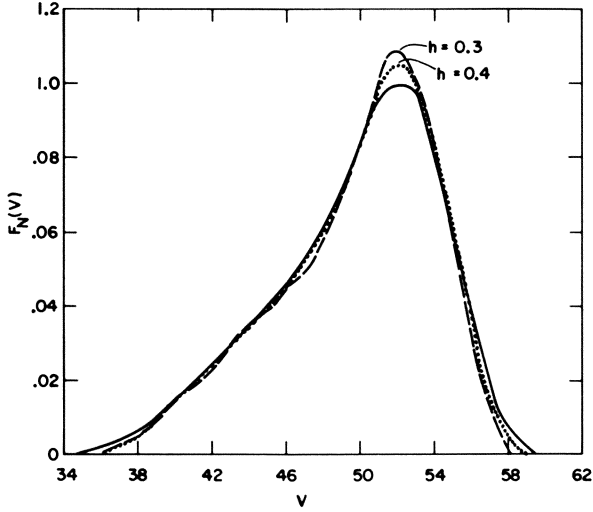


Figure 6. Effect of symmetrical axial dispersion correction on chromatogram heights: experimental chromatogram (—); chromatograms ( $W_N(y)$ ) obtained using Method 2 with smoothing: (---)  $h = 0.3$ ; ( $\cdot \cdot \cdot$ )  $h = 0.4$ . Values of  $h = 0.2$  and  $h = 0.1$  showed oscillations due to numerical instabilities.

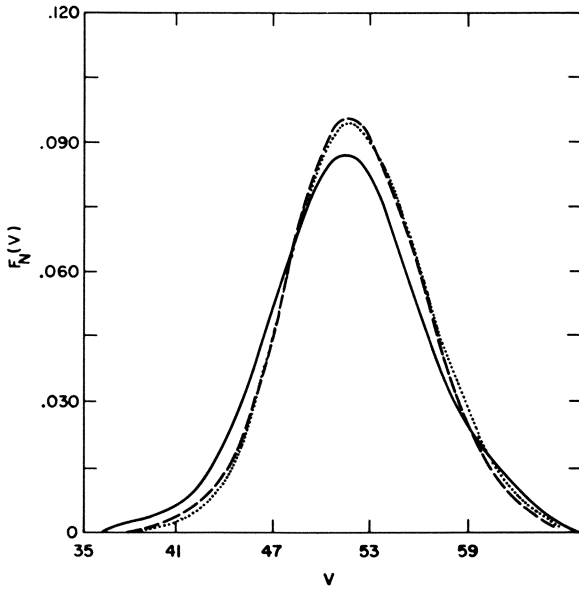


Figure 7. Experimental chromatograms using different column codes ((—) Code 25; (---) Code 27; ( $\cdot \cdot \cdot$ ) Code 28)

molecular weight averages being weighted integrals over the whole curve, are strongly affected. This situation leads to conclusions in the GPC literature that axial dispersion should be corrected for if molecular weight averages disagree with absolute values. However, in polymerization kinetic modeling a very viable option is to model using chromatogram heights. Molecular weight averages, if needed for other purposes, can be obtained from the kinetic model later.

**C. Chromatogram Interpretation.** Tables III and IV show the distinction between using averages and heights of GPC in kinetic modeling.

The advantages of utilizing the individual heights are:

1. The need for axial dispersion correction is minimized for broad distributions.
2. Heights from specific areas of the chromatogram can be chosen to maximize reproducibility or to emphasize one range of molecular weights.
3. The change in concentration with time of a given molecular weight can be estimated and used to provide a guide as to choice of model or an approximate estimate of parameters.

As previously mentioned, the results of this approach in the polymerization of PMMA have already been published (8) and tested (e.g. (9)). Also, a few workers have recently begun to recognize some of the value of utilizing chromatogram heights (15, 16).

From the axial dispersion viewpoint alone there is no doubt that the experimental reduction of dispersion or its correction would be preferable to assuming it negligible. Either of these options require a simple method for the assessment of axial dispersion which does not depend upon absolute molecular weight averages or assumption of distribution functions (5, 6). Such a method will be shown in Section 3 of this report. However, first the problem of copolymer analysis which led to this method as a by-product will be examined.

**3. High Conversion Copolymerization of Styrene n-Butyl Methacrylate.** The copolymer analysis problem becomes increasingly more difficult as we progress from conversion and average property determination to property distribution determination. Also, copolymer composition information appears easiest to obtain as opposed to sequence length and molecular weight information which are much more elusive. However, as will be seen in the following sections, conventional GPC analysis of copolymers is fundamentally unsatisfactory because the GPC fractionation accomplishes a molecular size separation and not a fractionation uniquely related to any one of the property distributions. In fact, there is considerable ambiguity in what is considered a copolymer composition distribution. In GPC analysis the nature of the fractionation leads to calculation of average copolymer composition at each retention time ( $\bar{W}_1(V)$ ) as a function of retention time. However, in polymerization kinetics we require the weight fraction of copolymer as a function of the instantaneous copolymer composition ( $W_1$ ) produced at any reaction time.

The first section below deals with the problem of obtaining the concentrations of the individual monomers (styrene and n-butyl methacrylate) and of the copolymer at any reaction time. This is the information required for conversion (X) and overall average composition ( $\bar{W}_1$ ). Kinetic modelling focusses on the prediction of conversion versus concentration of unreacted styrene ( $w_1$ ). In the second section, the usual dual detector analysis is shown to provide a relationship for the area ratios of the dual detector chromatograms versus  $\bar{W}_1$ . Through ratios of area segments on each chromatogram the average composition at each retention time can be calculated ( $\bar{W}_1(V)$ ). The limitations of this approach are discussed and lead to the orthogonal coupling of GPCs.

**A. Conversion and Average Property Determination for Copolymers.** Figure 8 shows chromatogram obtained on the GPC #1 with Column Code A1 (Table I). Using new

TABLE III  
GPC AND KINETIC MODEL  
MOLECULAR WEIGHT AVERAGES

$$M_K (\infty) = \frac{Q_K}{Q_{K-1}}$$

where  $K = 1$  for  $M_n$   
 $= 2$  for  $M_w$   
 $= 3$  for  $M_z$

GPC

$$Q_K = \int_{-\infty}^{\infty} F(v)M(v)^{K-1} dv$$

MODEL

$$Q_K = M_0^{K-1} \sum_{r=1}^{\infty} r^{K-1} W_r$$



TABLE IV: GPC AND KINETIC MODEL PREDICTED CHROMATOGRAM HEIGHTS

GPC	PREDICTED BY MODEL	AREA UNDER CURVE
<p>(1) CHROMATOGRAM (<math>F(v)</math>)</p> <p><math>F(v)</math> = conventional raw chromatogram heights as a function of retention volume</p>	<p><math>(F(v))_{\text{MODEL}}</math></p> <p><math>F(v)_{\text{MODEL}} = W_r \text{ CUM} \left( \frac{-dI}{dv} \right)_{-\infty}^{\infty} F(v) dv</math></p> <p>where <math>W_r \text{ CUM} = \left( \int_0^x W_r dx \right) / X</math></p>	<p>PROPORTIONAL TO WEIGHT OF POLYMER INJECTED INTO THE GPC</p>
<p>(2) NORMALIZED CHROMATOGRAM (<math>F_N(v)</math>)</p> <p><math>F_N(v) = \frac{F(v)}{\int_{-\infty}^{\infty} F(v) dv}</math></p>	<p><math>(F_N(v))_{\text{MODEL}}</math></p> <p><math>F_N(v)_{\text{MODEL}} = W_r \text{ CUM} \left( \frac{dI}{dv} \right)</math></p>	<p>UNITY</p>
<p>(3) CUMULATIVE CHROMATOGRAM (<math>F_c(v)</math>)</p> <p><math>F_c(v) = F_N(v) \cdot X</math></p>	<p><math>(F_c(v))_{\text{MODEL}}</math></p> <p><math>F_c(v)_{\text{MODEL}} = F_N(v)_{\text{MODEL}} \cdot X</math></p>	<p>X</p>
<p>(4) DIFFERENTIAL CHROMATOGRAM (<math>\Delta F(v)</math>)</p> <p><math>\Delta F(v) = F_c(v)_{X=X_{II}} - F_c(v)_{X=X_I}</math></p>	<p><math>(\Delta F(v))_{\text{MODEL}}</math></p> <p><math>\Delta F(v)_{\text{MODEL}} = F_c(v)_{\text{MODEL}, X=X_{II}} - F_c(v)_{\text{MODEL}, X=X_I}</math></p>	<p><math>X_{II} - X_I</math></p>
<p>(5) NORMALIZED DIFFERENTIAL CHROMATOGRAM (<math>\Delta F_N(v)</math>)</p> <p><math>\Delta F_N(v) = \frac{\Delta F(v)}{X_{II} - X_I}</math></p>	<p><math>(\Delta F_N(v))_{\text{MODEL}}</math></p> <p><math>\Delta F_N(v)_{\text{MODEL}} = \frac{\Delta F(v)_{\text{MODEL}}}{X_{II} - X_I}</math></p>	<p>UNITY</p>

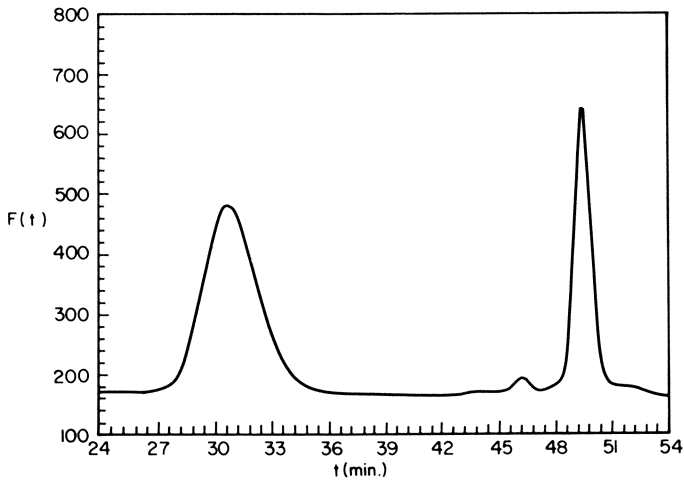


Figure 8. Typical polystyrene n-butyl methacrylate chromatogram (low to intermediate conversions) showing monomer peaks at times 46.2 and 49.2 min resolved by GPC

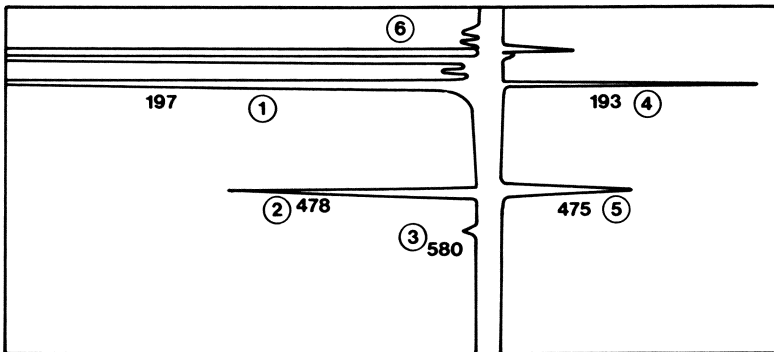


Figure 9. HPLC analysis of a monomer fraction showing retention times and identification: (1, 2, and 3) represent MMA, styrene, and n-BMA at 200 nm; (4 and 5) represent MMA and styrene at 254 nm; (6) are THF impurity peaks

high resolution columns the monomer peaks could be clearly separated from the polymer.

There are several examples in the literature of GPC now being utilized for small molecule analysis (17). However, in this case, attempts to obtain monomer concentrations for kinetic modelling were frustrated by irreproducible impurity peak interference with monomer peaks, time varying refractometer responses and insufficient resolution for utilization of a reference peak. This last point meant that injected concentration would have to be extremely reproducible.

Alternate ways of obtaining the data were considered. GC appears most promising (18). However, entrapment of monomer, polymer degradation and column degradation for high conversion were evident problem areas.

Instead, the idea of Coupled-Column Chromatography was employed (19). Here, this means the manual collection of fractions from one chromatograph and their re-injection into another. Collection of GPC fractions and their analysis by other instruments or re-injection has often been utilized qualitatively in GPC. However, precise quantitative analysis is much less often reported (6).

Figure 9 shows the result of injecting 10  $\mu$ l of the total low molecular weight fraction from GPC #1 (Column Code A2) into GPC #2 (Column Code B1). With this column code, GPC #2 is performing as a High Performance Liquid Chromatograph (HPLC). Separation is based upon solubility (i.e. composition differences) rather than upon molecular size. Methyl methacrylate monomer was used as a reference and added to the solution injected into GPC #1. Concentrations of n-butyl methacrylate, styrene and conversion are readily calculated from the peak areas and initial concentrations.

Results are shown in Figures 10 and 11. HPLC is well known as a reproducible and accurate technique for composition measurement. From the point of view of kinetic model development however, the following points deserve emphasis.

1. Data points fall in Figure 11 between predictions using the two reactivity ratio values quoted by Gruber and Knell (10) in classical kinetics.
2. Very similar variations in average copolymer composition with conversion have recently been observed in the styrene methyl methacrylate system by both Johnson et al (20) and by Dionisio and O'Driscoll (21). The reason for the variation may be due to a viscosity effect on propagation rate constants (20).
3. Fractionation by GPC was assessed by changing injected concentrations and by GPC analysis of polymer before and after fractionation. Efficiency of fractionation of polymer from monomer did not appear to be a source of error. In fact, an advantage of this method over others is that the separation of monomer from the polymer can be clearly monitored and controlled.
4. Total error variance may not be constant with conversion:

At 30% conversion a replicate analysis showed that composition could be determined with  $\pm 1.4\%$  reproducibility (standard deviation as a % of mean) and conversion with  $\pm 2.1\%$ . A duplicate at 52% conversion showed a relative error (difference/mean) of 1.7% and 2.7% respectively. Between 30 and 80% conversion, although no gel effect is evident in the data the polymer/monomer mixture becomes sticky and difficult to handle. Somewhat beyond 80% conversion the n-butyl methacrylate content for these compositions becomes too small to be detected with the procedure developed. Additional optimization of concentration injected and detector utilized is required for very high conversions.

**B. Measurement of Property Distributions for Copolymers.** Figure 12 shows chromatograms of typical products in the copolymerization study (Column Code B2). Since the detector is responding to concentration, composition, and perhaps sequence length, the direct single detector interpretation as described for PMMA is not immediately applicable here. Tacticity variation is yet another consideration but is assumed of second order importance for these samples (22).

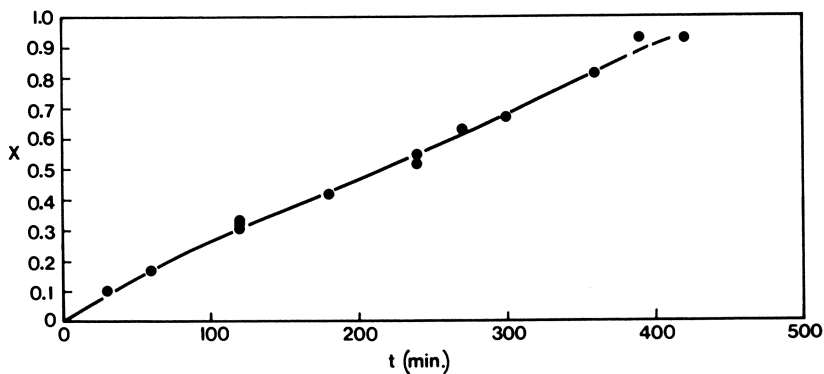


Figure 10. Conversion vs. time, styrene n-butyl methacrylate ( $w_{10} = 0.767$ , 1.45 mol % AIBN, 70°C)

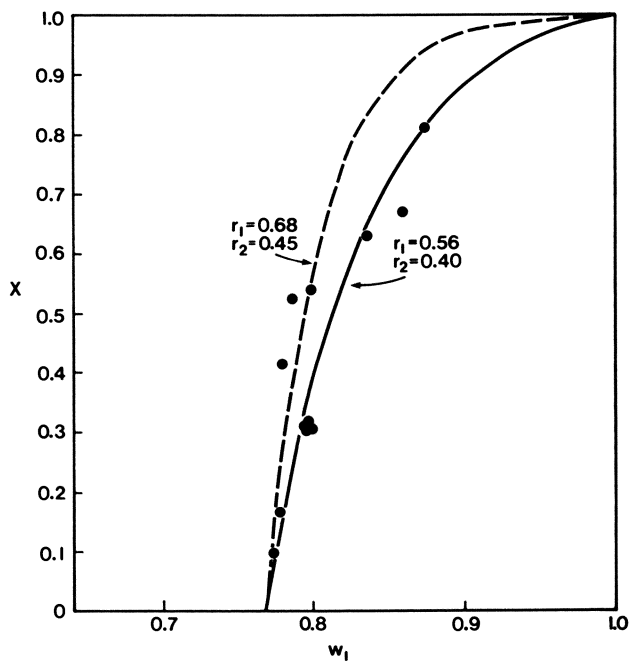


Figure 11. Conversion vs. weight fraction styrene in monomer, styrene n-butyl methacrylate (samples as for Figure 10) (---)  $r_1 = 0.68$ ,  $r_2 = 0.45$ ; (—)  $r_1 = 0.56$ ,  $r_2 = 0.40$ )

Interpretation of copolymer chromatograms in the literature does not include axial dispersion correction (3, 6) and little is known regarding it (5). The usual approach (6) is to utilize dual detectors and to assume that both detectors respond to, at most, both composition and concentration. The two chromatograms then provide two equations in these two unknowns at each retention time.

In our case, detector one ( $\lambda = 254$  nm) responds only to component one. Therefore, considering a chromatogram slice  $dt$  as representing hydrodynamic volumes  $dV$ :

$$K_{1,254} \bar{W}_1(V) g(V) dV = F_1(t) dt \quad (1)$$

where  $K_{1,254}$  is the response constant for component 1 on detector 1

$F_1(t)$  = chromatogram from detector 1

$\bar{W}_1(V)$  = average weight fraction of monomer 1 (styrene) in copolymer contained in chromatogram slice

$t$  = time

$g(V)dV$  = weight of copolymer at  $V$  to  $V+dV$

For detector 2 ( $\lambda = 235$  nm) the response is assumed to be a linear combination of the weight fraction of each component in the copolymer. That is:

$$(K_{1,235} \bar{W}_1(V) + K_{2,235} \bar{W}_2(V)) g(V) dV = F_2(t) dt \quad (2)$$

Integrating each equation over all volumes and times:

$$K_{1,254} \bar{W}_1 = \frac{A_{254}}{g} \quad (3)$$

$$K_{1,235} \bar{W}_1 + K_{2,235} \bar{W}_2 = \frac{A_{235}}{g} \quad (4)$$

$$\text{where } \bar{W}_1 = \frac{w_{10} \cdot (1-X) w_1}{X}$$

$$\begin{aligned} \bar{W}_2 &= 1 - \bar{W}_1 \\ g &= \text{total weight of copolymer} \end{aligned}$$

Usually (e.g. 4, 23) the ratio equivalent to  $A_{254}/A_{235}$  is plotted versus  $\bar{W}_1$  as shown in Figure 13. However, a plot of  $A_{235}/A_{254}$  versus  $(1/\bar{W}_1)$  is also useful. From Equation (3) and (4) the deviation from the straight line derived from the pure homopolymers can then be used to reveal their adequacy of homopolymers for composition calibration and the presence of other variables. Figure 14 shows such a plot.

The detector response ratio is elevated with respect to the homopolymer line but very near parallel to it less than  $\bar{W}_1 = 0.74$ , or number average styrene sequence lengths less than 4. In this case these particular homopolymer standards could not be used alone for the copolymer calibration. Judging from the literature, styrene sequence length is likely responsible for the deviation (10, 24). If so, then this area ratio as an indicator of sequence length is most sensitive above  $\bar{W}_1 = 0.74$ . Below this value the change of

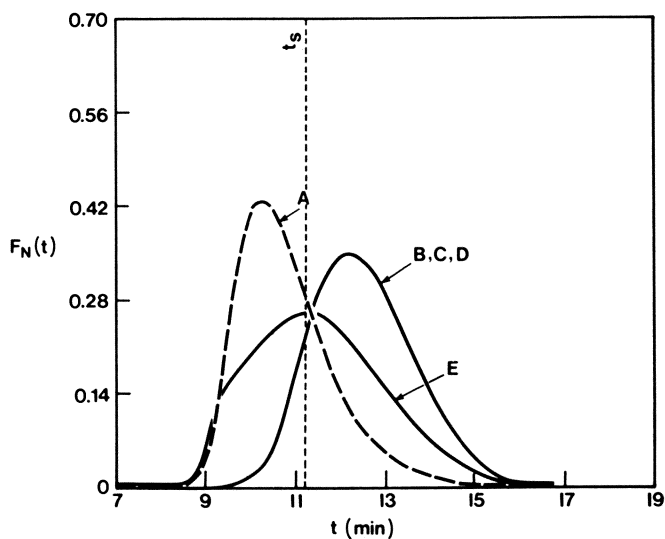


Figure 12. Normalized GPC chromatograms from Column Code B2. Letters correspond to samples in Table V. UV detectors at 254 and 235 nm provide the same curves. Sampling time ( $t_s$ ) shown references Column Code A3.

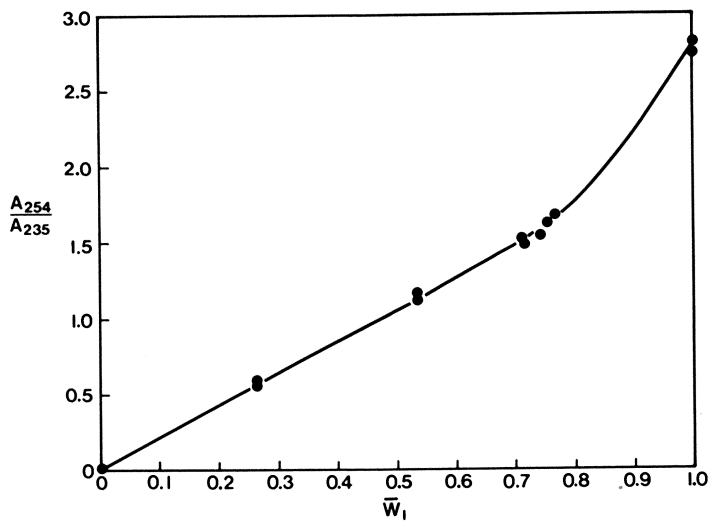


Figure 13. Area ratio from detectors vs. average styrene composition in polymer (weight fraction)

$A_{235}$  with respect to  $A_{254}$  nearly conforms to that expected from homopolymer mixtures.

Using equations (1-4) and Figure (13) the ratio of compositions across the chromatogram can now be obtained from the ratio of the chromatogram heights (i.e. ratios of area segments  $F_1(t)dt/F_2(t)dt$ ).

It was observed that the normalized chromatograms ( $F_N(t)$ ) for detector 1 shown in Figure 12 were superimposable on those for detector 2. Therefore, when the plot shown in Figure 14 is linear over the range of compositions involved in the sample, then (according to equations (1-4) ) the composition of the sample is the same at each retention volume. If the variation with retention volume is negligible the copolymer can then possibly be treated as is a homopolymer in GPC interpretation. In particular, intrinsic viscosity measurements could then lead to estimates of molecular weight via the universal calibration curve.

However, the high conversion chromatogram was superimposable despite that a definite shift of molecular weights to the higher values was observed during the polymerization (Figure 12). Also, the area ratio obtained by experimentally examining only a high molecular weight fraction of the high conversion sample indicated that it was significantly richer in styrene than lower molecular weight fractions. It is evident that the deviation from the linear plot observed in Figure 14 can conceal a composition variation if not somehow taken into account.

Furthermore, in the more general case we are concerned with a variation of composition and sequence length distribution not only as a function of retention volume but within each chromatogram area segment (or "slice") at each retention volume. A significant polydispersity of one of these properties within a chromatogram slice can easily invalidate the polymer analysis described above.

New and multiple detectors are part of the solution to this problem. However, according to the most recent published developments in this area (25,26), alone they have not been able to provide an answer. As will be seen in the following sections, obtaining the desired fractionation by GPC, before multiple detection, offers hope of a general solution.

**4. Cross Fractionation by Orthogonal Chromatography.** The fundamental limitation of conventional GPC analysis of copolymers is that GPC does not fractionate with respect to any one of the property distributions but rather with respect to molecular size--a characteristic potentially common to all of them simultaneously. In the first of the following sections several previously published major advances related to the problem are associated to synthesize a new approach involving the orthogonal coupling of one GPC to another. This approach is then developed in the second section by first presenting the raw output of the second GPC for different copolymers and then comparing this output to:

- a. composition and sequence distribution expected on the basis of polymerization kinetics and
- b. sources of error.

In the final section a practical procedure for applying the method is presented along with some initial results(27).

**A. Synthesis of the Method.** A vast amount of literature is pertinent. The following major developments were of particular relevance:

- i. **Cross Fractionation.** In the literature this refers to a solvent fractionation first with respect to molecular weight and then with respect to composition (6, 28, 29). Here it refers to fractionating first with respect to hydrodynamic volume and then with respect to "non-homopolymer character".

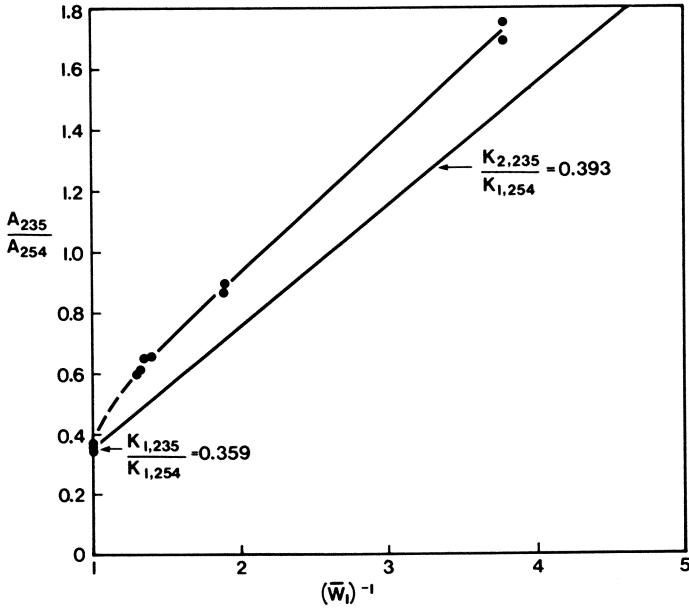


Figure 14. Area ratios plotted to compare with homopolymer calibration

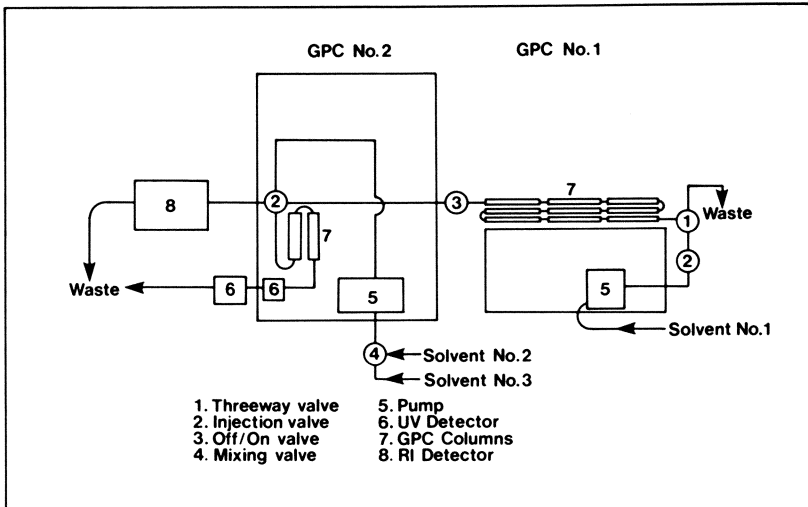


Figure 15. Cross fractionation by orthogonal chromatography: arrangement of GPCs



ii. Coupled-Column Chromatography. In the previous section, this referred to the manual collection and analysis of fractions. Here it refers to the actual physical coupling of one GPC to another. It, thus provides a means for obtaining nearly monodisperse slices of chromatogram for analysis by the second chromatograph. The method has been used in a GPC/HPLC mode and not yet successfully with polymers (19). Here we propose to use it in a GPC/GPC mode and suggest that a general term more descriptive of it is "Orthogonal Chromatography". The use of "steric exclusion" columns in the second instrument provide columns with a stationary phase accessible to polymers.

iii. The Universal Calibration Concept. With THF as solvent and silica columns (GPC #1) the GPC is expected to separate the polymer molecules according to hydrodynamic volume (6).

With use of a THF/n-Heptane mixture for example, in GPC #2 the hydrodynamic volume of polymer molecules rich in one monomer component can be much more affected than those rich in the other. Steric exclusion separation can then distinguish compositional differences.

iv. Partition and Adsorption Mechanisms in GPC #2. Steric exclusion columns are now known to behave as reverse phase partition columns with suitable solvents in small molecule analysis (30). In analysis of polymers by GPC such non-steric exclusion mechanisms as partition and adsorption have been considered undesirable because they cause exceptions to universal calibration. Investigations of such exceptions provide clues as to what solvents can be chosen to enhance a composition or sequence length separation in GPC #2 (31, 32) utilizing these mechanisms.

v. Copolymerization Kinetics. Classical copolymerization kinetics commonly provides equations for instantaneous property distributions (e.g. sequence length) and sometimes for accumulated instantaneous (i.e. for high conversion samples) as well (e.g. copolymer composition). These can serve as the basis upon which to derive equations which would reflect detector response for a GPC separation based upon properties other than molecular weight. These distributions can then serve as calibration standards analogous to the use of molecular weight standards.

Thus, the strategy underlying this approach is as follows:

- (a) The solvent in GPC #2 is chosen so as to favour one monomer component (e.g. n-butyl methacrylate) over the other (e.g. styrene).
- (b) Polymer molecules in the slice taken from GPC #1 will, therefore, be all of the same hydrodynamic volume in pure THF but in the solvent of GPC #2 they will have different hydrodynamic volume and perhaps different partition/adsorption characteristics as well.
- (c) The chromatogram of GPC #2 should, therefore, reflect heterogeneity in the slice examined and we can attempt to find the separation mechanism and calibrate for the heterogeneity.

Figure 15 shows a schematic of the arrangement of the GPCs. Flow from GPC #1 bypassed all columns while awaiting analysis by GPC #2.

B. Development of the Method. Figure 16 shows normalized chromatograms for various copolymers from GPC #2 with 57% n-heptane in THF as its mobile phase. In beginning the development of this technique, two major aspects are important: (i) Variation in Molecular Properties Expected Within a Chromatogram Slice and (ii) Sources of Error in Analyzing for These Properties. These are discussed in turn below.

#### (i) Variation of Molecular Properties According to Polymerization Kinetics

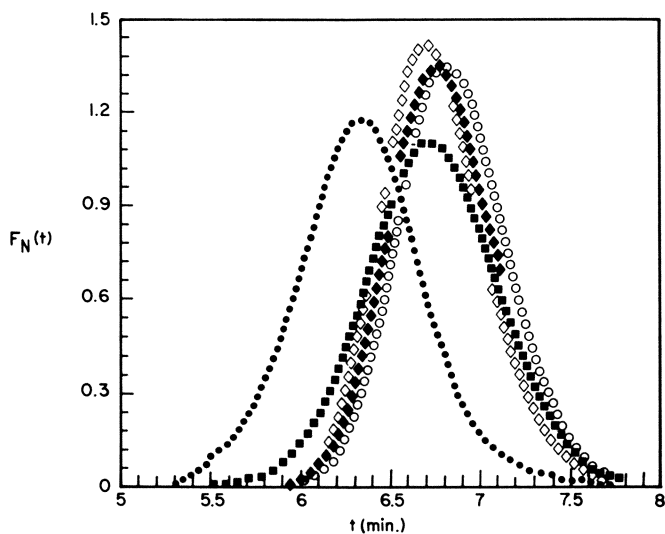


Figure 16. GPC #2 chromatograms obtained by sampling copolymer chromatograms on GPC #1 (letters correspond to samples in Table V—(●) A; (◇) B; (◆) C; (○) D; (■) E)

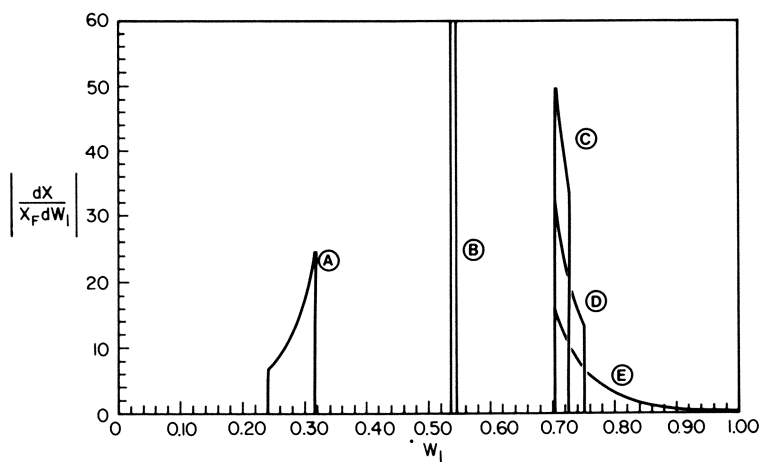


Figure 17. Theoretical normalized copolymer composition distributions ( $r_1 = 0.56$ ,  $r_2 = 0.40$ ; letters correspond to sample in Table V)

(a) Copolymer Composition Distribution Due to Relative Rates of Monomer Consumption. Figure 17 shows that the differential copolymer composition distributions from the classical kinetic model are in the same order as the chromatograms of Figure 16. The normalized differential form shown here can be derived from the cumulative distribution utilized by Hamielec (1):

$$G(W_1) = \frac{X}{X_F} \tag{5}$$

where  $G(W_1)$  = cumulative copolymer composition  
 $W_1$  = weight fraction of styrene in the copolymer  
 $X_F$  = final conversion  
 $X$  = present conversion

by differentiation:

$$\left| \frac{dG(W_1)}{dW_1} \right| = \left| \frac{1}{X_F} \frac{dX}{dW_1} \right| \tag{6}$$

The expression of  $\frac{dX}{dW_1}$  is obtainable from the literature (33).

The distributions are very narrow. This is in accordance with similar theoretical results by Stejskal and Kratochvil (34).

(b) Copolymer Composition Distribution Due to Instantaneous Statistical Fluctuations. Stockmayer (35) derived a form for the distribution of copolymer composition from chain to chain caused by statistical fluctuations over an instant of time. For a molecular weight of  $1.2 \times 10^5$  the standard deviation of the Gaussian distribution of compositions expected (36, 34) is  $1 \times 10^{-2}$ . Only for the near azeotropic composition and perhaps for the very high conversion samples where a large shift in Mn occurred would this contribution be significant. All the chromatograms of Figure 16 can be fit by a Gaussian shape (Table V).

(c) Sequence Distribution. Figure 18 shows weight sequence distribution for various copolymer samples. The order of increasing sequence length corresponds to the order of the chromatograms in Figure 16. These distributions are obtained by using Harwood's expression for the sequence distribution (37) and accumulating the result with respect to the contribution at each conversion.

That is, using the weight distribution function

$$A_{W,1} = \frac{n\alpha^{n-1}}{(1 + \alpha)^{n+1}} \tag{7}$$

where, for any incremental time:

$$A_{W,1} = \frac{\text{weight of monomer 1 sequences of length } n}{\text{total weight of all monomer 1 sequences}}$$

$$\alpha = r_1 f_1 / (1 - f_1)$$

$$f_1 = M_1 / (M_1 + M_2)$$

$M_1$  = moles/l of monomer 1 in the reaction mixture

This can be accumulated in a similar manner to that of instantaneous molecular weight distributions (11, 8):

$$\bar{A}_{W,1} = \frac{1}{X_{1,f}} \int_0^{X_{1,f}} A_{W,1} dX_1 \quad (8)$$

where  $X_1 = (c_{10} - c_1) / c_{10}$

$c_1$  = gms of styrene in unreacted monomer ( $c_0$  = initial value)

$$dX_1 = \frac{W_1 dX}{w_{10}}$$

$X_{1f}$  =  $X_1$  calculated at final  $C_1$

The number and weight average sequence lengths accumulated with conversion are calculated from:

$$\frac{1}{\bar{n}_{n,1}} = \frac{1}{X_{1,f}} \int_0^{X_{1,f}} \frac{1}{n_{n,1}} dX_1 \quad (9)$$

where (38):

$$n_{n,1} = \alpha + 1$$

and

$$\bar{n}_{w,1} = \frac{1}{X_{1,f}} \int_0^{X_{1,f}} n_{w,1} dX_1 \quad (10)$$

where (38):

$$n_{w,1} = 2\alpha + 1$$

TABLE V: AXIAL DISPERSION ANALYSIS

SAMPLE NO.	POLYMERIZATION TIME (min)	STYRENE IN MONOMER		INITIAL STYRENE IN MONOMER	GPC #2 CHROMATOGRAPH VARIANCE (min) <sup>2</sup>	GPC # INJECTED INTO	TOTAL AMOUNT OF POLYMER INJECTED (mg)	VOLUME INJECTED (cc)	GAUSSIAN FIT TO GPC #2 CHROMATOGRAM × 10 <sup>3</sup>
		CONVERSION	wt. fraction						
A	306.	0.6157	0.1872	0.2350	0.1179	1	1.64	1.5	1.05
B	120.	0.3121	0.5668	0.5573	0.0808	1	4.08	1.5	1.63
C	120.	0.3133	0.7743	0.7670	0.0916	1	1.76	1.5	2.57
D	240.	0.5269	0.7850	0.7670	0.0898	1	1.16	1.5	8.37
E	20.8 hrs.	1.0	1.0	0.7670	0.1356	1	0.750	1.5	3.43
F	NBS706	Polystyrene		—	0.1446	1	0.750	1.5	0.742
G	NBS706	Polystyrene		—	0.0974	1	0.750	1.5	4.72
H	Poly n-butyl Methacrylate	—		—	0.1093	1	0.750	1.5	2.15
I	70111	Polystyrene		—	0.0494	2	0.050	0.1	1.33
J	70111	Polystyrene		—	0.0379	1	0.300	1.5	14.81

$$(1) \sum_{i=1}^m \frac{(F_N(t) - F_G(t))^2}{m-1}$$

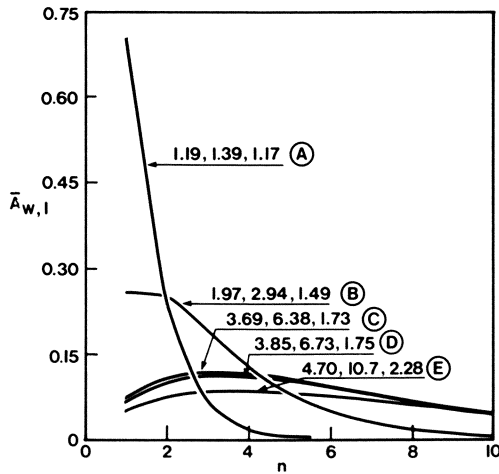


Figure 18. Theoretical weight sequence distributions (Equation 8) for samples of Table V ( $\bar{n}_{n,1}$ ,  $\bar{n}_{w,1}$ , and  $\bar{n}_{w,1}/\bar{n}_{n,1}$  are shown beside each curve)

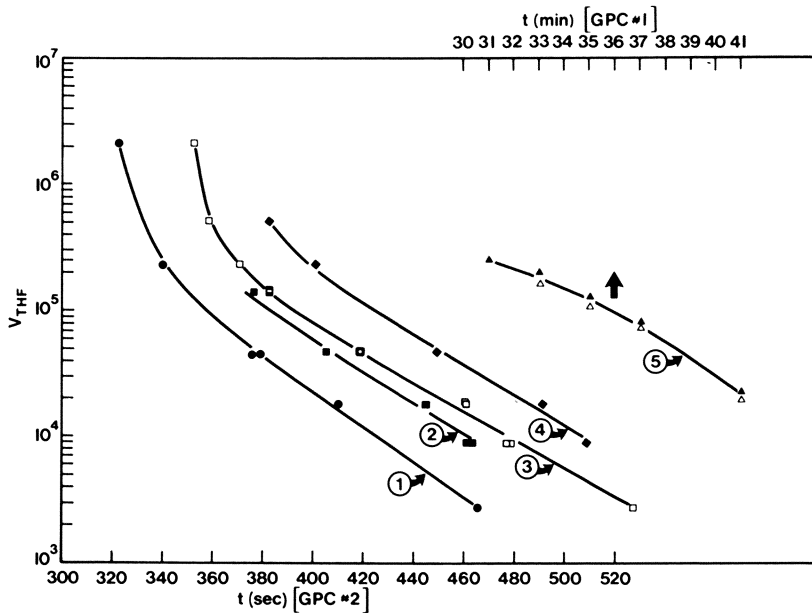


Figure 19. Universal calibration curves for GPC #1 and GPC #2 based on hydrodynamic volume in GPC #1 ( $V_{THF}$ ): (1) 100% THF (B3, Table I) obtained by sampling narrow standards injected into GPC #1 (A3, Table I); (2) 57% n-heptane in THF (B4, Table I) (obtained as in 1 above); (3) 57% n-heptane in THF (B4, Table I), obtained by direct injection into GPC #2; (4) 62% n-heptane in THF (B5, Table I) (obtained as in 3 above); (5) 100% THF (A3, Table I), obtained by sampling GPC #1 (NBS706, 0.375 and 0.750 mg into GPC #1 and using Curve 2)

(ii) Sources of Error.

a. Concentration Effects. Too high a concentration in GPC #1 can mean overloading and calibration curve shifts which would destroy hope of comparisons in GPC #2. Too low a concentration means undetectable concentrations for GPC #2.

Table V shows the concentrations of polymer (usually in THF/polymer/monomer mixtures), the GPC that they were directly injected into, and the Column Code involved (Ref. Table 1). No effect of different concentration was observed in the chromatograms from GPC #2 when concentrations of samples A to E inclusive were changed by 33%. GPC #1 chromatograms were too disturbed by sampling to be useful except as a rough guide to sampling position.

Figure 19 shows the Universal Calibration Curve obtained for the coupled GPCs in terms of the hydrodynamic volume in THF (Ref. Table II). The addition of the n-Heptane caused a dramatic shift downstream of the polystyrene standards.

The difference between curves obtained by sampling GPC #1 and by direct injection into GPC #2 (e.g. curves (2) and (3), Figure 19) is probably due to the more monodisperse nature of the former rather than to any concentration effect. (Concentrations into GPC #2 are approximately the same.)

b. Axial Dispersion. The output of GPC #2 is affected by axial dispersion in both GPC #1 and GPC #2.

Experimentally the resolution in GPC #1 was increased by the long column lengths and low flow rate but degraded somewhat by the high sample loadings. The high flow rate in GPC #2 was only necessary because in these exploratory studies many different runs had to be performed and necessitated short analysis times.

An important by-product of the development of this approach is that Orthogonal Chromatography provides a direct method of estimating the shape of the chromatogram for extremely narrow molecular weight distributions. This "shape function" is fundamental information for axial dispersion evaluation and is not otherwise easily obtained. Even commercially available "monodisperse" standards synthesized by anionic polymerization are too polydisperse.

Some authors have utilized manual collection of fractions and re-injection into the GPC (e.g.: 39, 40). In our case, sampling the chromatogram of a narrow standard at its peak will provide an extremely narrow fraction as input into GPC #2. The chromatogram from GPC #2 then provides a direct measure of the shape function for that GPC.

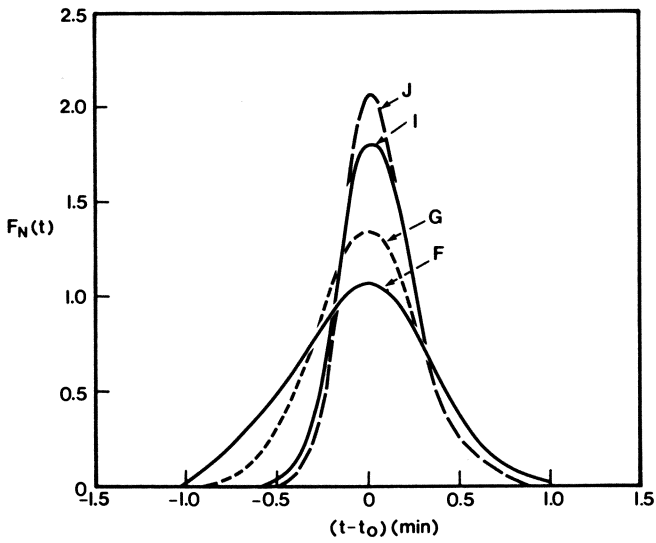
Figure 20 shows an example of its use. As expected, the GPC #2 chromatogram of a fraction of a monodisperse standard (obtained by sampling it with GPC #2 at its peak) is narrower than the whole standard which in turn is narrower than chromatograms of slices of broad polystyrene distributions. In Figure 20, two examples of the latter show the difference obtained by improving resolution in GPC #1.

Although there was some skewing towards low molecular weights particularly for the narrowest distribution, these curves were generally well fit by a Gaussian shape. Furthermore, the same was found for the copolymer fractions shown in Figure 16. Results are summarized in Table V.

No polydispersity due to compositional variation can be distinguished. Furthermore, when standard deviations were superimposed on the calibration curves (Figure 19) it was very evident that resolution in both GPCs had to be improved, particularly in GPC #1.

No attempt was made to optimize sampling of narrow fractions. A smaller injection volume or better resolution in GPC #1 would possibly provide a more optimistic picture of resolution in GPC #2.

Also, peak broadening appeared to increase with increased concentration of n-heptane. It is quite possible that mobile phase composition and/or polymer type affects axial dispersion.



Journal of Polymer Science

Figure 20. Evaluation of axial dispersion (letters correspond to samples in Table V) (27)

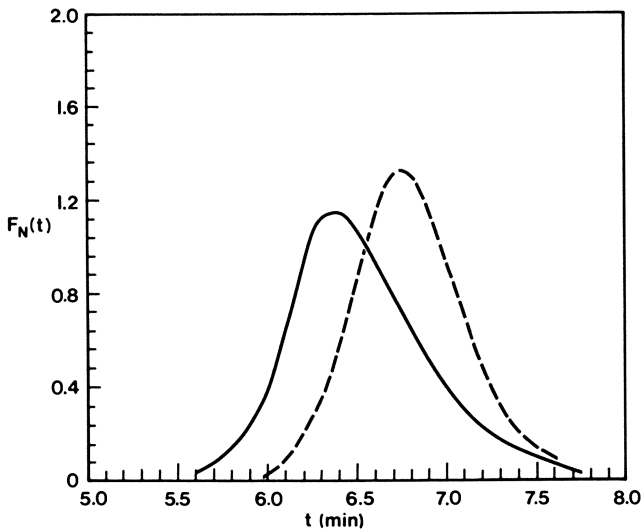


Figure 21. Separation of poly-n-butyl methacrylate ((—) 235 nm from NBS706 polystyrene; (---) 254 nm in 1:1 solution, 0.100 total % by weight)



The position of the peak (Figure 16) is of critical importance in distinguishing a composition based separation. The large axial dispersion in GPC #1 was attributed to the sample loadings being more than the 9 silica filled columns could handle. This had potentially serious consequences in terms of chromatogram sampling effects.

c. Chromatogram Sampling. When a slice of chromatogram is sampled, because of axial dispersion it will contain molecules from either side of the slice. Furthermore, the number of these misplaced molecules will generally be higher from the peak side of the sampling point than from the tail side. This effect will, therefore, depend upon the location of the slice, the axial dispersion in GPC #1 and to a lesser extent upon the size of the slice. The analysis by GPC #2 can then reflect an undesirable molecular size polydispersity independent of other properties.

In our case sampling was at 37 min. on column code A3. This is approximately equivalent to 11.2 min. on column code B2 and is shown on Figure 12. The order of the distributions' peaks in that figure around the sampling point are similar to that found in the GPC #2 chromatograms (Figure 16).

The effect could be elucidated by additional axial dispersion characterization of GPC #1. An alternate approach is to utilize only THF in both GPC #1 and #2 and to observe whether slices exit at the expected hydrodynamic volume.

Attempts to do this indicated that differences on the order of 30% of the peak separation shown in Figure 16 were probably due to such effects. At other sampling points, better and worse results were observed likely because the tail heights of distributions were being sampled.

Another sampling effect which deserves mention is that since the molecular weight distribution shifts towards higher molecular weights with conversion, a slice will not in general contain proportionate amounts of polymer from all conversions. This shifting can be accounted for in the theoretical predictions by incorporating it into accumulation of the instantaneous property distributions (e.g. Equation 8).

C. Practical Implementation. As a cross-fractionation method GPC has one very definite advantage over other methods—it can clearly show the number of variables affecting the results. Thus, despite the complexity of the problem, guidelines which minimize error and begin to provide useful results have been developed. They are summarized as follows:

1. Improved Resolution in GPC #1:

Curve G, Figure 20, (sample G in Table V) shows the results of adding columns to GPC #1 (resulting in Code A4, Table I). Now the variance for NBS706 has been reduced by 1/3 with a notable loss of the high molecular weight tail.

2. Use of an Internal Standard and Improved Resolution in GPC #2

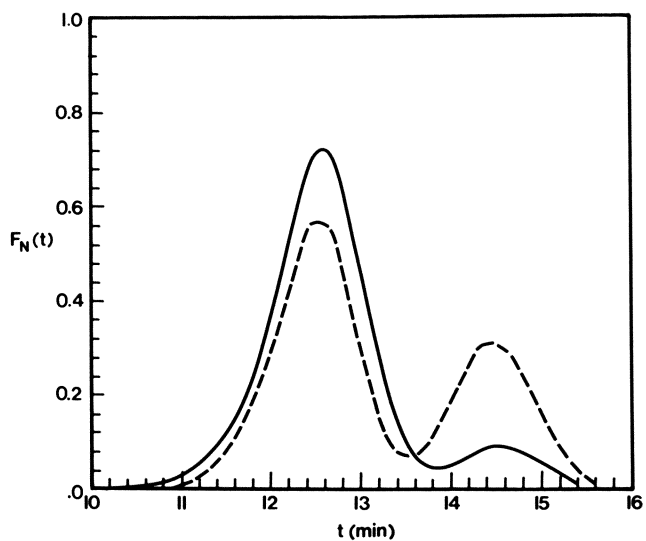
Figure 21 shows the result of sampling a 50:50 blend of NBS706 and poly n-butyl methacrylate using Column Codes A4 and B4 (Table I) injecting a total of 1.5 mg into GPC #1.

Figure 22 shows the result of sampling a 1.63:1 blend of sample A with NBS706 (Column Codes A4 and B6).

In each case both detectors provide strong evidence for the fractionation obtained. Composition is likely the dominant separation mechanism since both homopolymers and copolymers were separated.

3. Checking for Sampling Effects:

Running both GPCs with THF caused all of the curves shown in Figures 21 and 22 to collapse into a single curve. Since in each case the columns used in GPC #2 could readily resolve a molecular weight distribution in the region involved, this together with different responses on each detector is very good evidence of elimination of sampling effects.



Journal of Polymer Science

Figure 22. Separation of polystyrene n-butyl methacrylate (peak retention time: 12.5 min; A in Table V) from NBS706 polystyrene (14.5 min) ((—) 235 nm; (---) 254 nm in 1.63:1 solution, 0.131 total % by weight) (27)

D. Recommendations. Cross-Fractionation using Orthogonal Chromatography has high potential in the analysis of complex polymers and even polymer latices (with Hydrodynamic Chromatography). Multi-detector analysis, particularly utilizing spectrofluorometry, should be very useful in developing the technique.

#### IV Conclusions

GPC is much more than a source of molecular weight averages. Although averages can be a valuable output, particularly since they fit directly to the Method of Moments in kinetic analysis, they are often amongst the most difficult information to obtain accurately and reproducibly from a GPC. This is because they are weighted integrals which are strongly affected by axial dispersion and which emphasize the heights at the tails of the chromatogram.

An alternate approach is to utilize the chromatogram heights as representative of individual concentrations of molecular size. From the kinetic modeling viewpoint, this leads to treating the polymerization as a well-characterized, multi-component reaction system.

Phrasing kinetic models in terms of instantaneous property distributions which are summed to provide distributions at any conversion is then highly rewarding. The variation of individual concentrations with time from the GPC readily provides significant insight into the model requirements.

From the GPC interpretation viewpoint this alternate approach leads to two major operating modes:

1. appraisal of the whole GPC output for the most useful information obtainable and,
2. experimental use of the GPC in unconventional ways to obtain desired fractionation before detection.

In this paper the GPC interpretation underlying the kinetic model of methyl methacrylate polymerization previously published and by now shown to be useful is detailed and updated. It provides a prime example of the conventional experimental use of GPC in homopolymerization studies.

To study the bulk copolymerization of styrene n-butyl methacrylate both conventional and unconventional GPC analyses were used. The normally obtained chromatograms, (from dual U.V. detectors) primarily provided area ratios indicative of composition as a function of retention volume. However, even this information was only obtainable after average compositions had been otherwise determined. Furthermore, in general, since the GPC normally separates on the basis of hydrodynamic volume, the polydispersity of all polymer molecular properties at each retention time is of serious concern.

Two "unconventional modes" of GPC operation utilizing "Orthogonal Chromatography" were utilized to circumvent these problems:

1. Use of GPC to separate all polymer from all monomer and subsequent analysis of the monomer using HPLC:

The results obtained using a highly quantitative version of this approach are shown to be reproducible and in reasonable accord with those of other workers. Advantages of the method include monitoring of the polymer fractionation obtained.

2. Use of one GPC coupled to another with the conditions of the second chosen so as to effect a separation primarily on the basis of composition:

Property distribution predictions utilizing kinetic equations derived from the classical copolymerization model are shown for copolymer composition and styrene sequence length. These are compared to chromatograms obtained and sources of error are discussed. Development of a practical procedure for minimizing these errors is initiated and very recent results presented. With this work the distinction between the use of GPC and HPLC begins to dissolve as now we can begin to utilize GPC in a cross-fractionation mode for the HPLC of polymers while incorporating our knowledge of multi-detector analysis.

Axial dispersion characterization is a valuable by-product of coupling GPCs. By sampling chromatograms with the second GPC, extremely monodisperse fractions can be obtained and the concentration of misplaced molecules in any chromatogram slice revealed.

### Abstract

Polymerization kinetic model development often depends upon accurate GPC analysis. This paper shows attempts to use GPC to determine conversion, molecular weight distribution, copolymer composition distribution and sequence length distribution. The free radical homopolymerization of methyl methacrylate and copolymerization of styrene n-butyl methacrylate are used as examples. In each case previously published approaches are tried first with new methods developed when necessary. For homopolymers, calibration using hydrodynamic volume is satisfactory and the need for imperfect resolution correction is circumvented. For copolymers, conventional GPC analysis with dual detectors yields only average composition values. To emphasize desired fractionation as well as detection "Orthogonal Chromatography" was employed. For polymers this is a new method of analysis involving the orthogonal coupling of one GPC to another with the second run so as to obtain a "Cross Fractionation" of the copolymer. Results are compared to kinetic modelling expectations and sources of error are examined. The method enables GPC copolymer analysis to employ separation mechanisms normally reserved for the HPLC of small molecules. It should be generally useful for revealing property distributions of complex polymers and for direct determination of GPC resolution.

### Nomenclature

$A_i$	Area under chromatogram obtained at $\lambda = i$
$A_{W,1}$	Instantaneous weight sequence distribution for styrene
$\bar{A}_{W,1}$	Weight sequence distribution for styrene
$c_1$	gms of styrene in unreacted monomer ( $c_{10}$ = initial value)
$F_G(t)$	Gaussian fit to chromatogram
$F_i(t)$	Chromatogram of detector i
$F_N(t)$	Normalized chromatogram (Table IV)
$f_i$	Mole fraction of styrene in unreacted monomer
$G(W_1)$	Cumulative copolymer composition (Equation 5)
$g$	Weight of polymer
$h$	Resolution factor ( $= 1./2 \times$ variance of chromatogram of truly monodisperse sample))
$K_{i,j}$	detector response constant (Equation 1-4) for component i, detector $\lambda = j$
$m$	Number of heights
$M$	Molecular weight
$M_1$	Moles/ of styrene in unreacted monomer
$M_2$	Moles/ of n-butyl methacrylate in unreacted monomer
$M_n$	Number average molecular weight
$M_n(t)$	Absolute $M_n$
$M_n(\infty)$	GPC uncorrected $M_n$
$M_w$	Weight average molecular weight
$M_w(t)$	Absolute $M_w$
$M_w(\infty)$	GPC uncorrected $M_w$
$n$	Styrene sequence length
$n_{n,1}$	Instantaneous number average styrene sequence length
$\bar{n}_{n,1}$	Number average styrene sequence length

$n_{w,1}$	Instantaneous weight average styrene sequence length
$\bar{n}_{w,1}$	Weight average styrene sequence length
$r$	Polymer chain length
$r_1, r_2$	Reactivity ratios
$t$	Retention time
$t_s$	GPC #1 retention time at which chromatogram slice was obtained for GPC #2
$v$	Retention volume
$V$	Hydrodynamic volume of polymer (here considered equivalent to the "separation parameter" $KM^{a+1}$ , Table II for GPC calibration)
$V_{THF}$	V of polymer in THF in GPC #1
$W_r$	Weight fraction of molecules of length $r$ to $r + dr$ instantaneously produced
$W_i$	Weight fraction of component $i$ in copolymer instantaneously produced
$\bar{W}_i$	Average weight fraction of component $i$ in copolymer
$\bar{W}_i(V)$	Average weight fraction of component $i$ in copolymer contained in chromatogram time increment ("slice").
$w_i$	Weight fraction of component $i$ in unreacted monomer ( $w_{i0}$ = initial value)
$X$	Conversion (wt. fraction)
$X_1$	Conversion of component 1 (wt. fraction) (Equation 8)
$X_{1,f}$	Final conversion of component 1 (wt. fraction) (Equation 8)
$X_I, X_{II}$	Conversions at times I and II (Table IV)
$\alpha$	Variable defined after Equation 7
$\lambda$	U.V. wavelength (nm)

### Acknowledgement

We would like to thank Dr. L. Alexandru for kindly providing one of the computer programs for instantaneous polymer properties used in this study.

### Literature Cited

1. Hamielec, A.E., "Introduction to Polymerization Kinetics", "Polymer Reaction Engineering - Intensive Short Course on Polymer Production Technology", McMaster University, Hamilton, Ontario, Canada, June 1977.
2. Hamielec, A.E., "Computer Applications Modeling of Polymer Reactor Systems", Proceedings - Polymer Characterization Conference, Cleveland State University, Division of Continuing Education, Cleveland, Ohio, April 30 - May 1, 1974.
3. Reiss, G. and Callot, P., in Tung, L.H., Ed., "Fractionation of Synthetic Polymers", Marcel Dekker Inc., N.Y., N.Y. (1977).
4. Stojanov, C., Shirazi, Z., Audu, T., *Chromatographia*, 1978, 11, 274.
5. Friis, N., Hamielec, A. in Giddings, J.C., Grushka, E., Keller, R.A. and Cazes, J., Eds., *Advances in Chromatography*, Series 13, Marcel Dekker Inc., N.Y., N.Y. 1975.
6. Tung, L.H., Ed., "Fractionation of Synthetic Polymers", Marcel Dekker, Inc., N.Y., N.Y., 1977.
7. Rudin, A., Samanta, M.C., *J. Appl. Pol. Sci.*, in publication.
8. Balke, S.T., Hamielec, A.E., *J. Appl. Pol. Sci.*, 1973, 17, 905.
9. Friis, N., Hamielec, A.E., *J. Appl. Pol. Sci.*, 1974, 12, 251.
10. Gruber, E., Knell, W., *Makromol. Chem.*, 1978, 179, 733.
11. Balke, S.T., "The Free Radical Polymerization of Methyl Methacrylate to High Conversions", Ph.D. Thesis, McMaster University, August 1972.
12. Weiss, A.R., Cohn-Ginsberg, E., *J. Appl. Pol. Sci.*, A-2, 1970, 8, 148.
13. Ishige, T., Lee, S.I., Hamielec, A.E., *J. Appl. Pol. Sci.*, 1971, 15, 1607.

14. Kotaka, T., J. Appl. Pol. Sci., 1977, 21, 501.
15. Budtov, V.P., Podosenova, N.G., Polymer Science USSR, 1977, 19, 1881.
16. Braks, J.G., Huang, R.Y.M., J. Appl. Pol. Sci., 1978, 22, 3111.
17. Krishen, A., J. Chrom. Sci., 1977, 15, 434.
18. Berezkin, V.G., Alishogev, V.R., Nemirovskaya, J.G., "Gas Chromatography of Polymers", Elsevier, N.Y., N.Y., 1977.
19. Johnsen, E.L., Gloor, R., Majors, R.E., J. Chrom., 1978, 149, 571.
20. Johnson, M., Karmo, T.S., Smith, R.R., Eur. Pol. J., 1978, 14, 409.
21. Dionisio, J.M., O'Driscoll, K.F., J. Pol. Sci. B, 1979, 17, 701.
22. Podesva, J., Doskocilova, D., Makromol. Chem., 1977, 178, 2383.
23. Probst, J., Cantow, H.J., Kautschuk und Gummi, Kunststoffe, 1972, 25, 11.
24. Stutzel, B., Miyamoto, T., Cantow, H.J., Pol. J., 1976, 8, 247.
25. Ogawa, T., J. Appl. Pol. Sci., 1979, 23, 3515.
26. Garcia-Rubio, L.H., MacGregor, J.F., Hamielec, A.E., "Copolymer Analysis Using GPC with Multiple Detectors", presented at the "Symposium on Recent Developments in Size Exclusion Chromatography", 178th ACS National Meeting, Washington, D.C., September 9-14, 1979.
27. Balke, S.T., Patel, R.D., J. Pol. Sci., B, in publication.
28. Cantow, M.J.R., "Polymer Fractionation", Academic Press, N.Y., 1967.
29. Teramachi, S., Fukao, T., Pol. J., 1974, 6, 532.
30. Mori, S., Yamakawa, A., Anal. Chem., 1979, 51, 382.
31. Dawkins, J.V., Hemming, M., Makromol. Chem., 1975, 176, 1795.
32. Bakos, D., Bleha, T., Ozima, A., Brek, D., J. Appl. Pol. Sci., 1979, 23, 2233.
33. Myagchenkov, V.A., Frenkel, S.Y., Vysokomol. soyed., 1969, A11, 2348.
34. Stejskal, J., Kratochvil, P., J. Appl. Pol. Sci., 1978, 22, 2925.
35. Stockmayer, W.H., J. Chem. Phys., 1945, 13, 199.
36. Lamprecht, J., Stazielle, C., Dayantis, J., Benoit, H., Makromol. Chem. 1971, 148, 285.
37. Harwood, H.J., J. Pol. Sci. C, 1968, 25, 37.
38. Cantow, H.J., Ber. Bunseng., Physik. Chem., 1966, 70, 257, 275.
39. Taganov, N.G., Novikov, D.D., Korovina, G.V., Entelis, S.G., J. Chrom., 1972, 72, 1.
40. Ehrlich, B.S., Smith, W.V., in Ezrin, M., Ed., "Polymer Molecular Weight Methods", Adv. in Chem. Series, 125, American Chemical Society: Washington, D.C., 1973.

RECEIVED May 7, 1980.

# Molecular Weight and Peak Broadening Calibration in Size Exclusion Chromatography

## Use of Multiple Broad Molecular Weight Distribution Standards for Linear Polymers

A. E. HAMIELEC and S. N. E. OMORODION

Department of Chemical Engineering, McMaster University,  
Hamilton, Ontario, Canada L8S 4M1

Herein are reported improved methods of molecular weight calibration where simultaneously, peak broadening parameters ( $\sigma$ ) are obtained through the use of multiple polydisperse molecular weight standards. There are two basic methods covered. The first and most reliable method employs the universal molecular weight calibration curve obtained using narrow MWD polystyrene standards. The second method assumes that the molecular weight calibration curve is linear on a semilog plot and should be employed where universal calibration is not practical as with aqueous SEC. Several variants of these methods involving different molecular weight data for the standards are discussed. The proposed methods have been evaluated using aqueous SEC and polydextran standards and nonaqueous SEC with polyvinylchloride standards.

Previous methods of molecular weight calibration using broad MWD standards were of three basic types. Those which employ a broad MWD standard with known molecular weight distribution (1,2,3,4,5). Those which employ one or more broad MWD standards with known  $\bar{M}_N$ ,  $\bar{M}_W$  or  $[\eta]$  and assume a linear molecular weight calibration curve (6,7,8,9) and finally those which employ one broad MWD standard with known  $\bar{M}_N$ ,  $\bar{M}_W$  or  $[\eta]$  and use the universal molecular weight calibration curve obtained with narrow MWD polystyrene standards (10). Yau et al. (9) were the first to suggest that it is more general to search for the true molecular weight calibration curve rather than an effective molecular weight calibration curve. Their application of this principle unfortunately has two weaknesses. The first involves their assumption that the molecular weight calibration curve is linear. The second involves the use of peak broadening parameters measured with narrow MWD polystyrene standards for the polymer in question. This assumption may lead to significant error propagation in the calculation of the molecular weight calibration curve (11).

The present methods of determining the molecular weight cali-

bration curve overcome the deficiencies in the method proposed by Yau et al by simultaneously determining peak broadening parameters for the polymer in question. In addition, if the universal molecular weight calibration curve is available, the molecular weight calibration curve is not assumed to be linear. If the universal curve is nonlinear, the molecular weight calibration curve for the polymer in question will also be nonlinear.

In the following section the theoretical basis for the proposed methods will be established.

### Theory

Equations (1), (2) and (3) which give the number and weight-average molecular weights and intrinsic viscosity of a broad MWD standard in terms of a mass detector response ( $F_N(v)$ ), the true molecular weight calibration curve ( $M(v)$ ) and the peak broadening parameter (variance of a single-species chromatogram  $\sigma^2$ ) form the basis for the proposed methods of determining the molecular weight calibration curve  $M(v)$ .

$$\bar{M}_N \exp\left[-(D_2\sigma)^2/2\right] = \left[ \int_0^\infty F_N(v) M(v)^{-1} dv \right]^{-1} \quad (1)$$

$$\bar{M}_W \exp\left[(D_2\sigma)^2/2\right] = \int_0^\infty F_N(v) M(v) dv \quad (2)$$

$$[\eta] \exp\left[(aD_2\sigma)^2/2\right] = K \int_0^\infty F_N(v) M(v)^a dv \quad (3)$$

where  $K$  and  $a$  are Mark-Houwink constants for the polymer in question.

$\bar{M}_N$  and  $\bar{M}_W$  or  $[\eta]$  for the broad MWD standard are taken as known quantities.  $F_N(v)$  is the normalized chromatogram for the broad MWD standard obtained with a mass detector.  $D_2$  is the slope of the molecular weight calibration curve at the peak position of the chromatogram (the equation of the tangent is given by  $\bar{M}(v) = D_1 \exp(-D_2v)$ ).  $\sigma^2$  is the variance of the single-species chromatogram at the peak position. The corrections for imperfect resolution in equations (1) and (2) were first derived by Hamielec and Ray (12). The methods proposed by Yau et al employ equations (1) and (2) and assume that  $M(v) = D_1 \exp(-D_2v)$  and estimate  $\sigma^2$  using polystyrene values. They search for  $D_1$  and  $D_2$  constants in the assumed linear molecular weight calibration curve. We will now develop improved methods one step at a time.

### Methods Based on Universal Molecular Weight Calibration Curve

The nonlinear universal molecular weight calibration curve may be expressed as shown in equation (4).



$$[\eta](v) M(v) = \phi(v) \quad (4)$$

The molecular weight calibration curve for the polymer in question may be expressed as

$$M(v) = \alpha \phi(v)^\beta \quad (5)$$

where  $\beta = \left(\frac{1}{1+a}\right)$  and  $\alpha = K^{-\beta}$

Equations (1), (2) and (3) may now be rewritten as

$$\bar{M}_N \exp\left[-(D_2\sigma)^2/2\right] = \alpha \left( \int_0^\infty F_N(v) \phi(v)^{-\beta} dv \right)^{-1} \quad (1a)$$

$$\bar{M}_W \exp\left[(D_2\sigma)^2/2\right] = \alpha \left( \int_0^\infty F_N(v) \phi(v)^\beta dv \right) \quad (2a)$$

$$[\eta] \exp\left[(aD_2\sigma)^2/2\right] = \bar{\alpha} \left( \int_0^\infty F_N(v) \phi(v)^{\bar{\beta}} dv \right) \quad (3a)$$

where  $\bar{\beta} = \frac{a}{1+a}$  and  $\bar{\alpha} = K^{1-\bar{\beta}}$

#### Universal Molecular Weight Calibration Curve - One Broad MWD Standard.

There are three unknowns,  $K$ ,  $a$  and  $\sigma^2$ . One might question the availability of Mark-Houwink constants for the polymer in the open literature. Mark-Houwink constants in the literature differ widely for the same polymer and it is difficult to decide on the correct pair to employ. Another problem which can arise is that the universal molecular weight calibration curve may not apply exactly for the polymer in question. The use of the true Mark-Houwink constants would therefore introduce an error in the molecular weight calibration. Calibration with a broad MWD standard should eliminate this error. The Mark Houwink constants obtained in the calibration would in this instance be effective rather than true values.

In principle, one could solve equations (1a), (2a) and (3a) for  $K$ ,  $a$  and  $\sigma^2$ . Unfortunately,  $\bar{M}_W$  and  $[\eta]$  are often highly correlated and it is recommended that only one of these data be used per standard. A practical procedure is to estimate  $\sigma^2$  using narrow MWD polystyrene standards leaving two unknowns,  $K$  and  $a$ . To illustrate the method, suppose  $\bar{M}_N$  and  $\bar{M}_W$  data are available for the single broad MWD standard. Dividing equation (2a) by (1a) eliminates  $\alpha$  and one is left with a single-variable search for  $\beta$ . Once  $\beta$  is known a direct calculation using either equation (1a) or (2a) may be done. A similar single-variable search procedure may

be used when  $\bar{M}_N$  and  $[\eta]$  are known. We will now move on and remove the need to employ peak broadening parameters based on narrow MWD polystyrenes.

### Universal Molecular Weight Calibration Curve - Two or More Broad MWD Standards

Two Pieces of Molecular Weight Data Per Standard. This method uses the fact that when equations (1a) and (2a) or (1a) and (3a) with proper modification are multiplied the peak broadening parameter  $\sigma^2$  vanishes. The equations for two broad MWD standards where  $\bar{M}_N$  and  $\bar{M}_W$  are known follow:

$$\bar{M}_{N_i} \bar{M}_{W_i} = \alpha^2 \left( \int_0^\infty F_{N_i}(v) \phi(v)^\beta dv \right) \left( \int_0^\infty F_{N_i}(v) \phi(v)^{-\beta} dv \right)^{-1} \dots (6)$$

where subscript  $i$  represents the standard.

A single-variable search for  $\beta$  results when equation (6) for  $i=1$  is divided by the equation  $i=2, 3, \dots$  to eliminate  $\alpha$ . Once  $\beta$  is found a direct calculation using equation (6) gives  $\alpha$  and then once  $\alpha$  and  $\beta$  are known a direct calculation using equations (1a) or (2a) gives the peak broadening parameter  $\sigma_i^2$  for each of the broad MWD standards employed.

One Piece of Molecular Weight Data Per Standard. With this amount of molecular weight information per standard, one should estimate the peak broadening parameters ( $\sigma^2$ ) for each standard using narrow MWD polystyrene standards. With this method there are various possible combinations of molecular weight data,  $\bar{M}_N$ ,  $\bar{M}_W$  and  $[\eta]$ . The resulting equations for some of these combinations follow:

$$\bar{M}_{N_1} \text{ and } \bar{M}_{N_2}$$

$$\bar{M}_{N_1} \exp\left[-(D_2\sigma)_{1/2}^2\right] = \alpha \left( \int_0^\infty F_{N_1}(v) \phi(v)^{-\beta} dv \right)^{-1} \quad (7a)$$

$$\bar{M}_{N_2} \exp\left[-(D_2\sigma)_{2/2}^2\right] = \alpha \left( \int_0^\infty F_{N_2}(v) \phi(v)^{-\beta} dv \right)^{-1} \quad (7b)$$

$$\bar{M}_{N_1} \text{ and } \bar{M}_{W_2}$$

$$\bar{M}_{N_1} \exp\left[-(D_2\sigma)_{1/2}^2\right] = \alpha \left( \int_0^\infty F_{N_1}(v) \phi(v)^{-\beta} dv \right)^{-1} \quad (8a)$$

$$\bar{M}_{W_2} \exp\left(\frac{(D_2\sigma)_2^2}{2}\right) = \alpha \left( \int_0^\infty F_{N_2}(v) \phi(v)^\beta dv \right) \quad (8b)$$

$\bar{M}_{N_1}$  and  $[\eta]_2$

$$\bar{M}_{N_1} \exp\left(-\frac{(D_2\sigma)_1^2}{2}\right) = \alpha \left( \int_0^\infty F_{N_1}(v) \phi(v)^{-\beta} dv \right)^{-1} \quad (9a)$$

$$[\eta]_2 \exp\left(\frac{(aD_2\sigma)_2^2}{2}\right) = \bar{\alpha} \left( \int_0^\infty F_{N_2}(v) \phi(v)^{\bar{\beta}} dv \right) \quad (9b)$$

There are many additional combinations which may be employed. Any of these combinations of molecular weight data permit a single-variable search for 'a' followed by a direct calculation of K.

Methods which assume a linear molecular weight calibration curve will now be briefly considered.

#### Methods Based on a Linear Molecular Weight Calibration Curve

The assumed form of the linear molecular weight calibration curve is given in equation (10)

$$M(v) = D_1 \exp(-D_2v) \quad (10)$$

where  $D_1$  and  $D_2$  are positive constants. The approach used with the linear calibration is almost identical with that using universal calibration except that now the unknowns are  $D_1$  and  $D_2$  rather than  $K$  and  $a$ , the Mark-Houwink constants. This approach will be illustrated using two broad MWD standards with known  $\bar{M}_N$  and  $\bar{M}_W$ . The equations to be solved in this example follow:

$$\bar{M}_{N_i} \exp\left(-\frac{(D_2\sigma)_i^2}{2}\right) = D_1 \left( \int_0^\infty F_{N_i}(v) \exp(D_2v) dv \right)^{-1} \quad (10a)$$

$$\bar{M}_{W_i} \exp\left(\frac{(D_2\sigma)_i^2}{2}\right) = D_1 \left( \int_0^\infty F_{N_i}(v) \exp(-D_2v) dv \right) \quad (10b)$$

$$\bar{M}_{N_i} \bar{M}_{W_i} = D_1^2 \left( \int_0^\infty F_{N_i}(v) \exp(-D_2v) dv \right) \left( \int_0^\infty F_{N_i}(v) \exp(D_2v) dv \right)^{-1} \quad (10c)$$

A single-variable search for  $D_2$  is followed by a direct calculation of  $D_1$  using equation (10c) for at least two broad MWD standards. A direct calculation using equations (10a) or (10b) pro-

vides  $\sigma_i$  for each of the broad MWD standards.

Methods based on universal calibration will be illustrated using nonaqueous SEC and broad MWD PVC standards. The  $\bar{M}_N$  and  $\bar{M}_W$  of these standards is known. Methods based on the linear molecular weight calibration will be illustrated using aqueous SEC and broad MWD polydextran standards for which  $\bar{M}_N$  and  $\bar{M}_W$  are known.

### Experimental Calibration

#### Universal Calibration and broad MWD PVC Standards with $\bar{M}_N$ and $\bar{M}_W$ known

##### Case Study #1

##### SEC Operating Conditions

4 $\mu$ -Styragel columns - 10<sup>5</sup>Å, 10<sup>4</sup>Å, 10<sup>3</sup>Å, 500 Å

Mobile phase - THF containing 1% polypropylene glycol (PPG)

Flowrate - 1 ml/min.

Detector - differential refractometer

Temperature - ambient.

The molecular weight calibration curve for polystyrene was measured with a series of narrow MWD polystyrene standards using the peak positions of the chromatograms. The calibration curve obtained using non-linear polynomial regression is shown in Figure 1. Intrinsic viscosities for the narrow MWD polystyrene standards were measured in the mobile phase and the results are shown plotted in Figure 2. These data yielded the Mark-Houwink constants shown in the Figure. The often used Mark-Houwink constants for polystyrene in THF at ambient temperature ( $K = 1.60 \times 10^{-3}$  and  $a = 0.706$ ) agree quite well with the viscosity data as shown in Figure 2. It is not certain whether 1% PPG in THF has significantly altered the Mark-Houwink constants or whether the differences noted are largely due to the strong correlation of  $K$  and  $a$  found in fitting molecular weight and intrinsic viscosity data. The universal molecular weight calibration curve based on polystyrene is effectively the same for both pairs of Mark-Houwink constants. The molecular weight data for the two broad MWD PVC standards used in this investigation of universal calibration are given in Table I.

Table I. Broad MWD PVC Standards Employed with Universal Calibration Methods

Sample	$\bar{M}_N \times 10^{-3}$	$\bar{M}_W \times 10^{-3}$	$\bar{M}_W / \bar{M}_N$
PV2	25.5	68.0	2.67
PV3	41.0	118.0	2.88

Supplied by Pressure Chemical Co., Pittsburgh, PA.

The first calibration involved the use of two broad MWD PVC

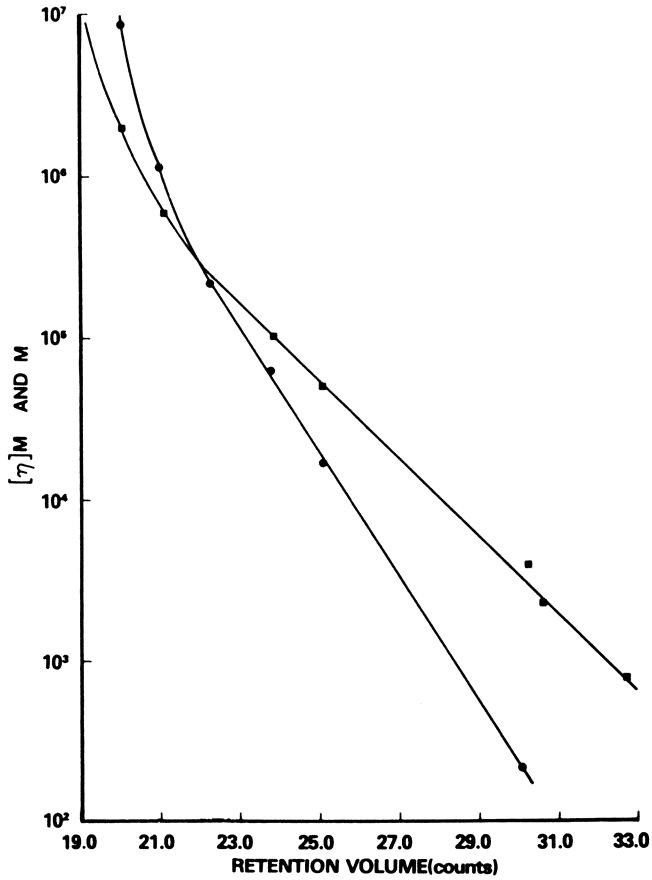


Figure 1. Molecular weight calibration curve for polystyrene and universal molecular weight calibration curve based on polystyrene ((●)  $[\eta]\bar{M}_w$ ; (■)  $\bar{M}_w$ )

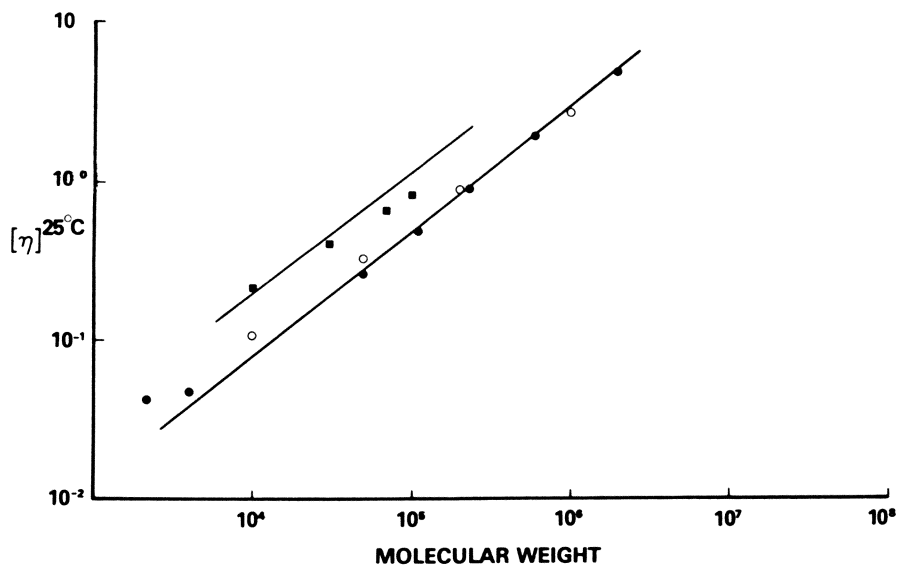


Figure 2. Intrinsic viscosity-molecular weight data for polystyrene and polyvinyl chloride measured by osmometry and by SEC using broad MWD standard calibration (polystyrene: (●)  $[\eta] = 7.06 \times 10^{-5} M^{0.77}$  in THF/1% PPG; (○)  $[\eta] = 1.60 \times 10^{-4} M^{0.706}$  in THF; polyvinyl chloride: (—)  $[\eta] = 1.63 \times 10^{-4} M^{0.766}$  in THF (13); (■)  $[\eta] = 0.93 \times 10^{-3} M^{0.589}$  in THF/1% PPG)

standards with known  $\bar{M}_N$  and  $\bar{M}_W$  to generate the peak broadening parameters ( $\sigma^2$ ) for both standards as well as the molecular weight calibration curve for PVC. This was followed with the use of one broad MWD PVC standard at a time to generate the molecular weight calibration curve for PVC using peak broadening parameters obtained in the first calibration. These results are tabulated in Table II and compared in Figure 2 with a typical Mark-Houwink equation for pure THF published in the literature. There appears to be a significant effect of the 1% PPG on the coil size of PVC molecules. The corrections for imperfect resolution for PV2 and PV3 are 16% and 21% respectively for the weight average molecular weights. The molecular weight calibration curves obtained for PVC are shown plotted in Figure 3. Table III shows an investigation of the effect of the peak broadening parameter ( $\sigma$ ) assumed when a single broad MWD PVC standard is used. The corrections for imperfect resolution for PV2 and PVC with a  $\sigma = 0.5$  are now reduced to about 4% for both standards. It is of interest to note that with a reduced correction for imperfect resolution the Mark-Houwink exponent obtained is closer to published literature values for PVC in THF (13). The use of the associated molecular weight calibration curve for PVC would reproduce the  $\bar{M}_N$  and  $\bar{M}_W$  of the PVC standards with errors of about 15%.

Table II. Results of Case Study #1 - Universal Calibration with One and Two Broad MWD PVC Standards with Known  $\bar{M}_N$  and  $\bar{M}_W$  ( $[\eta]_{PS} = 7.06 \times 10^{-5} M^{0.77}$ )

Method	$\sigma$ (counts)	$K \times 10^3$	a	(counts <sup>-1</sup> ) Calibration Curve Slope at Peak of Chromatogram
2-broad MWD Standards	0.861 (PV2) 0.981 (PV3)	0.930	0.589	0.625
1-broad MWD Standard				
PV2	0.861	1.881	0.522	0.653
PV3	0.981	1.9	0.522	0.653

Table III. Universal Calibration with Single Broad MWD PVC Standard with Known  $\bar{M}_N$  and  $\bar{M}_W$  - Effect of Peak Broadening Parameter( $\sigma$ ) ( $[\eta]_{PS} = 7.06 \times 10^{-5} M^{0.77}$ )

Sample	$\sigma$ (counts)	$K \times 10^3$	a	(counts <sup>-1</sup> ) Calibration Curve Slope at Peak of Chromatogram
PV2	0.5	0.231	0.721	0.578
	0.861	1.881	0.522	0.653
PV3	0.5	0.129	0.767	0.563
	0.981	1.947	0.522	0.653

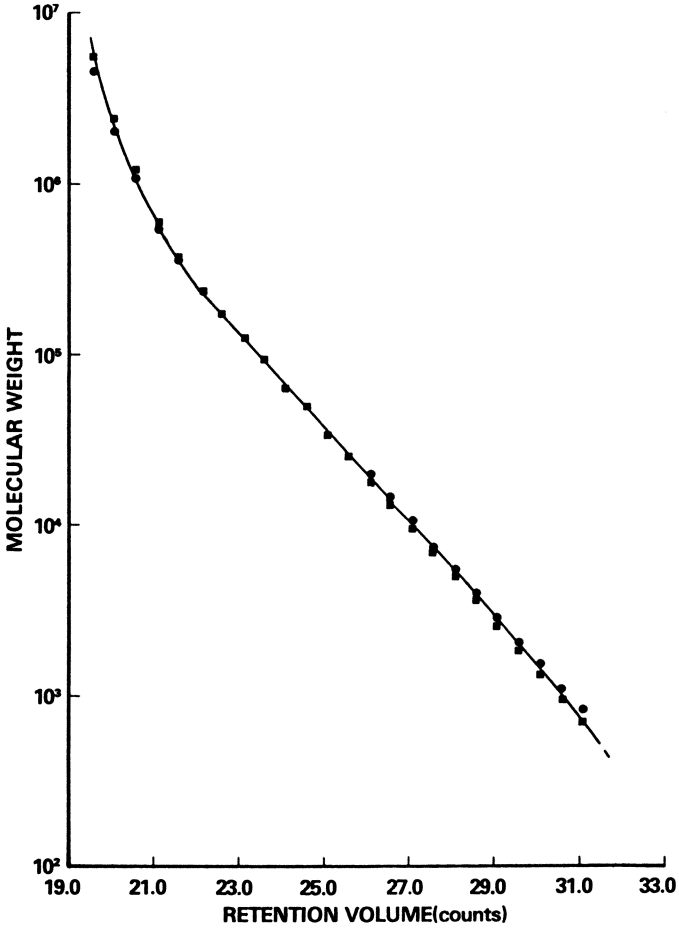


Figure 3. Molecular weight calibration curves for polyvinyl chloride obtained using universal calibration and one and two broad MWD standards (two broad standard method: (●)  $[\eta] = 7.06 \times 10^{-5} M^{0.77}$ ; single broad standard method: (■) PV3 ( $\sigma = 0.981$ ); (—) PV2 ( $\sigma = 0.861$ ))



We now move on to aqueous SEC and the use of the method of calibration based on a linear molecular weight calibration curve and two broad MWD polydextrans with known  $\bar{M}_N$  and  $\bar{M}_W$ .

Case Study #2

SEC Operating Conditions (See Ref.(14) for further details).

6 CPG10 columns - 729/700 Å, 700/500/370 Å, 370/327 Å,  
 (4' x 3/8") 240/120 Å, 120/88 Å, 88 Å.  
 Mobile phase - 0.05 M KF/0.02 wt.% NaN<sub>3</sub>/1.0% CH<sub>3</sub>OH/1 g  
 (pH = 2.66) Tergitol per 24 l H<sub>2</sub>O  
 Flowrate - 4.0 ml/min  
 Detector - differential refractometer  
 Temperature - ambient

Polydextran standards employed in this investigation are listed in Table IV.

Table IV. Broad MWD Polydextran Standards Employed with Linear Calibration Methods

Sample	$\bar{M}_N \times 10^{-3}$	$\bar{M}_W \times 10^{-3}$	$\bar{M}_W / \bar{M}_N$	$\bar{M}_{rms} \times 10^{-3}$
T500	173	509	2.94	297
T250	112.5	231	2.05	161.2
T150	86.0	154.0	1.79	115.1
T110	76.0	106.0	1.39	89.8
T70	42.5	70.0	1.65	54.5
T40	28.9	44.4	1.54	35.8
T20	15.00	22.3	1.49	18.29
T10	5.70	9.30	1.63	7.28

Supplied by Pharmacia Ltd.

The results of the calculations of  $D_1$  and  $D_2$  and the peak broadening parameter ( $\sigma^2$ ) are given in Table V. The agreement found for  $D_2$  the slope of the molecular weight calibration curve is remarkable considering the usual reproducibility of  $\bar{M}_N$  and  $\bar{M}_W$  for broad MWD polymers by SEC which is about  $\pm 5\%$  at 95% confidence level. The reproducibility seems to have had a much greater effect on  $D_1$  the intercept of the calibration curve. The corrections for imperfect resolution are negligible except for the highest molecular weight standard T500 where negative  $\sigma^2$  are somewhat disturbing. Overall one can conclude that these results for aqueous GPC and polydextran standards are very promising. Another interesting fact was observed when the molecular weight calibration curve using  $(D_2)_{avg} = 0.3$  and  $(D_1)_{avg} = 0.37 \times 10^9$  was compared with that using the  $\bar{M}_{rms}$  to obtain the calibration curve. This comparison is made in Figure 4. The excellent agreement suggests that the use of  $\bar{M}_{rms}$  values and chromatogram peak positions for broad MWD

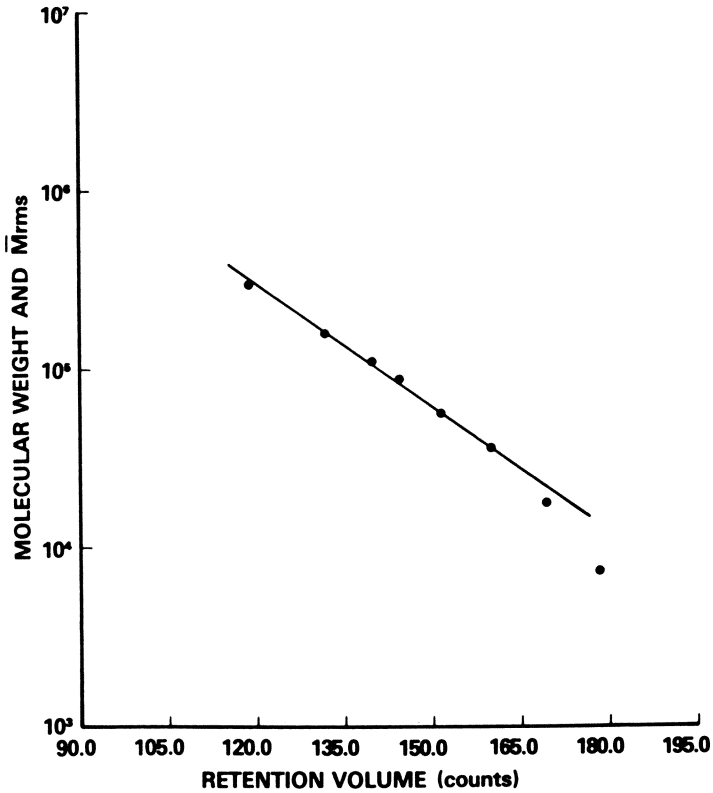


Figure 4. Molecular weight calibration curves for polydextran obtained using linear calibration and two broad MWD standards and by plotting  $M_{rms}(\sqrt{\bar{M}_N \cdot \bar{M}_W})$  vs. peak retention volume ((●)  $\bar{M}_{rms}$ ; (—)  $M(v) = 0.37 \times 10^9 \exp(-0.3 v)$ )

Table V. Results of Case Study #2 - Linear Calibration with Two Broad MWD Polydextran Standards with Known  $\bar{M}_N$  and  $\bar{M}_W$ .

Sample Pairs	$D_2(\text{Counts}^{-1})$	$D_1 \times 10^{-9}$	$\sigma^2(\text{counts}^2)$	Imperfect Resolution Correction Factor
T500 T150	0.296	0.339	3.12 0.32	0.87 0.99
T500 T110	0.304	0.406	-2.53 0.89	1.12 0.96
T500 T70	0.308	0.450	2.21 -0.37	0.90 1.02
T500 T40	0.300	0.376	-2.77 -0.06	1.13 1.00
T250 T110	0.292	0.295	0.64 -0.61	0.97 1.03
T250 T70	0.304	0.397	-0.04 0.22	1.00 0.99
T250 T40	0.295	0.317	-0.49 -0.12	1.04 1.08
T150 T40	0.304	0.416	0.01 0.17	1.00 0.99
T110 T40	0.297	0.334	-0.72 0.06	1.03 1.00
$(D_2)_{\text{avg}} = 0.300$		$(D_1)_{\text{avg}} = 0.370 \times 10^9$		

polymer standards is a useful approach for establishing a molecular weight calibration curve where narrow MWD standards are not available.

#### Concluding Remarks

Two improved methods of molecular weight calibration using broad MWD standards have been proposed and some evaluation has been done experimentally for aqueous and nonaqueous SEC. The experimental evaluations indicate that both methods appear very promising and justify further experimental investigation. It is recommended that these new calibration methods be evaluated for a wide range of polymers, packings and mobile phases.

Acknowledgements

The authors acknowledge the significant contribution of Dr. J. Johnston and Dr. T. MacRury of Union Carbide Corp., South Charleston, W. Va. to this publication. The SEC analyses of the broad MWD PVC standards were done in the Union Carbide Laboratories. The authors also acknowledge the assistance provided by Dr. N. Foster with the initial computer programming.

Literature Cited

1. Cantow, M.J.R.; Porter, R.S.; Johnson, J.F. J. Polymer Sci., 1967, A-1, 5, 1391.
2. Weiss, A.R.; Cohn-Ginsberg, E. J. Polymer Sci., 1970, A-2, 8, 148.
3. Wild, L.; Ranganath, R.; Ryle, T. J. Polymer Sci., 1971, A-2, 9, 2137.
4. Swartz, T.D.; Bly, D.D.; Edwards, A.S. J. Applied Polymer Sci. 1972, 16, 3353.
5. Abdel-Alim, A.H.; Hamielec, A.E. J. Applied Polymer Sci., 1974, 18, 297.
6. Balke, S.T.; Hamielec, A.E.; LeClair, B.P.; Pearce, S.L. Ind. Eng. Chem. Prod. Res. Develop., 1969, 8, 54.
7. Frank, F.C.; Ward, I.M.; Williams, T. J. Polymer Sci., 1968, A-2, 6, 1357.
8. Friis, N.; Hamielec, A.E. Advances in Chromatography, 13, (Giddings, J.C.; Grushka, E.; Keller, R.A.; Cazes, J. eds), Marcel Dekker p.41 1975.
9. Yau, W.W.; Stoklosa, H.J.; Bly, D.D. J. Applied Polymer Sci., 1977, 21, 1911.
10. Provder, T.; Woodbrey, J.C.; Clark, J.H. Separation Science, 1971, 6, 101.
11. Pollock, M.; MacGregor, J.F.; Hamielec, A.E. J. Liquid Chromatography, 1979, 2, 895.
12. Hamielec, A.E.; Ray, W.H. J. Applied Polymer Sci., 1969, 13, 1319.
13. Freeman, M.; Manning, P.B. J. Polymer Sci., 1964, A, 2, 2017.
14. Omorodion, S.N.E.; Hamielec, A.E.; Brash, J.L. "Optimization of Peak Separation and Broadening in Aqueous GPC", - to be published in ACS-Proceedings, Washington, September 1979.

RECEIVED May 7, 1980.

# Effect of Solute Shape or Conformation in Size Exclusion Chromatography

W. W. YAU and D. D. BLY

Central Research and Development Department, Experimental Station,  
E. I. Du Pont de Nemours & Company, Wilmington, DE 19898

## ABSTRACT

The dependence on molecular weight of the size of macromolecules or other large-particle solutes in solution varies as a function of the shape of the solute molecule or particle. Solute conformation or shape, therefore, affects the slope of the calibration curve and range of molecular weight separations available in size-exclusion chromatography (SEC). Various theories which have been derived for different solute conformations are unified in this work by expressing the size of the solute in terms of a reduced size parameter,  $R_g$ , the radius of gyration. It is predicted according to the unified theory, that a SEC column containing a single pore-size packing will have about two decades of MW separation range for random-coil polymers, three decades of MW range for solid-sphere solutes and only one decade of MW range for rod-like particles or molecules. This indicates that analysis of the slope of a SEC-MW calibration curve can be used to study the conformation of solute macromolecules

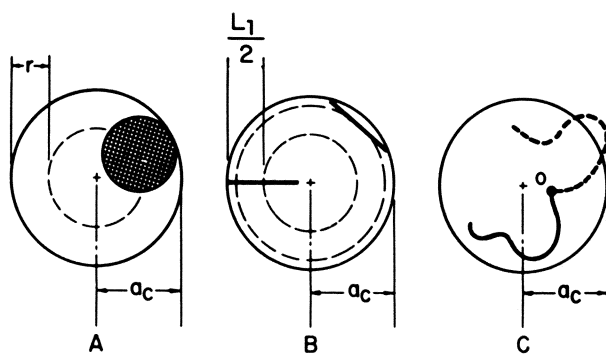
As the scope of size exclusion chromatography (SEC, or gel permeation chromatography, GPC) expands, for example, into particle measurements and biopolymer, gel filtration chromatographic (GFC) separations, increased needs for interpretation of solute shape are developing (e.g. hard-sphere for particles and colloids, rigid-rod for biopolymers, and random-coil for flexible polymers). The SEC retention characteristics for solutes with these different conformations have been studied separately in the theoretical treatments by Casassa, Giddings, Ackers and others (1-4). However, these are basically mechanistic theories, developed to provide fundamental understanding of SEC retention in terms of solute sizes; there remains a need to relate these theories to practical SEC calibration procedures which are based on solute molecular weight (MW).

In this communication are summarized some of the important practical insights which theory provides about SEC-MW calibration; predictions also have been derived to show the effect of solute conformation on the slope and molecular weight range of SEC calibration. For simplicity, the radius of gyration,  $R_g$ , was chosen as a common reduced solute size parameter to compare various theories concerned with different solute conformations. A more rigorous treatment would require the use of molecular projections as the common SEC size parameter (5). However, significant insights are still gained through the simplified approach. These provide a tie between theory and experimentally observed solute shape effects, and lead to a better understanding of SEC calibration practices.

### Background

Existing SEC retention theories have been independently developed for each of the molecular-shape models shown in Figure 1. The deep hollow cylindrical pore in the figure (A, B, and C) illustrates the SEC exclusion effect on three types of solute molecules, hard-sphere, rigid-rod, and random-coil, respectively. The individual theories and their bases of commonality are now reviewed briefly.

In the original works, theoretical models were developed to explain the SEC calibration curve



Journal of Physical Chemistry

*Figure 1. Exclusion effect in cylindrical cavities (1) ((A) hard sphere of radius  $r$ ; (B) thin rod of length  $L_1$  in two orientations in the plane of the cross section; (C) random-flight chain with one end at point  $O$  showing allowed conformation (—) and forbidden conformation (---))*

shape as a function of size and shape of the solute and column packing pore. The theoretical considerations in this paper are based particularly on the cylindrical pore shape model for simplicity in argument. Actual SEC packings generally have pore structures of a random or irregular shape, but it is expected that the results of this study as regards solute shape effects should be generally applicable using the cylindrical pore shape model.

In fundamental SEC studies retention is often described in terms of a distribution coefficient. The theoretical distribution coefficient  $K_E$  is defined as the ratio of solute concentration inside and outside of the packing pores under size exclusion conditions. The experimental distribution coefficient  $K_{SEC}$ , as defined in Equation 1, is a measurable quantity that can be used to check the theory.

$$K_{SEC} = (V_R - V_0) / (V_T - V_0) \quad (1)$$

where  $V_R$  is the retention volume for any particular solute and  $V_0$  and  $V_T$  are the respective interstitial volume and the total permeation volume of the packed SEC columns. (4)

The exclusion effect of hard-spheres is illustrated in Figure 1A., which shows a spherical solute of radius  $r$  inside an infinitely deep cylindrical cavity of radius  $a_c$ . Here the exclusion process can be described by straightforward geometrical considerations, namely, solute exclusion from the walls of the cavity. Furthermore, it can be shown that: (1)

$$K_E = \left(1 - \frac{r}{a_c}\right)^2 \quad (2)$$

The exclusion effect of a rigid-rod in the same cylindrical pore is shown in Figure 1B., where the length of the rod is  $L_1$ . Quantifying the exclusion process here is much more complicated than in the hard sphere case. Exclusion of the rod depends on the rod orientation in three dimensions and statistical methods must be used for the evaluation. For rigid-rods it has been shown that  $K_E$  is described by (2)



$$K_E = 1 - \frac{4}{3\pi\beta} [(1-\beta^2)E(\frac{\pi}{2}, \beta) - (1-\beta^2)F(\frac{\pi}{2}, \beta)] \quad (3)$$

where  $\beta = L_1/2a_c$ , with  $\beta \leq 1$ , and  $E$ ,  $F$  are elliptical integrals.

Figure 1C. illustrates two conformations of a flexible polymer chain with one end fixed inside the cavity. Even with one end fixed, the chain still can assume a large number of conformations. The presence of the cavity wall, however, does exclude some conformations, for example, the dashed one shown in the sketch. This restraint of conformational freedom causes a decrease in both the entropy and the solute concentration inside the cavity. For this case it has been shown that:<sup>(1)</sup>

$$K_E = 4 \sum_{m=1}^{\infty} \beta_m^{-2} \exp[-(\frac{\beta_m R_g}{a_c})^2] \quad (4)$$

where the numerical constant  $\beta_m$  is the  $m$ -th root of the Bessel function of the first kind of order zero, and  $R_g$  is the solute radius of gyration.

Each of the above existing SEC retention theories is uniquely related to only one particular solute-shape model. Because of the differences in the basic solute-size parameter,  $r$ ,  $L_1$ , and  $R_g$  in the individual cases, the theory of each solute-shape model stands alone. Since, under these conditions the different theories are not directly comparable, it is difficult to make integrated observations or to understand various practical implications in these theories. To gain more insights into SEC calibration, a common size parameter is needed to unify the SEC theories.

### Unification of Theory

Since the parameter  $R_g$  is known to be a basic SEC size parameter for random-coil type molecules (Equation 4), and since it is also a well-defined statistical average size parameter, applicable to solutes of any shape including the sphere and rodlike molecules,  $R_g$  has been chosen in this work to serve as a common, reduced, solute-size parameter for describing the theory of SEC separation. By definition:

$$R_g \equiv \sqrt{\sum_i^N \frac{x_i^2}{N}} \quad (5)$$

where  $N$  is the number of mass elements in a structure and  $X_i$  is the distance from the  $i$ -th mass element to the center of mass. For solid spheres and rigid rods, Equation (5) gives:

$$R_g \text{ (sphere)} = (3/5)^{1/2} r \quad (6)$$

$$R_g \text{ (rod)} = (1/12)^{1/2} L_1 \quad (7)$$

The composite plots of the theoretical  $K_E$  curves (Equations 2, 3 and 4) for the three solute shapes<sup>(1)</sup> in terms of the common reduced size parameter  $R_g$  (Equations 5, 6, and 7) are shown in Figure 2. This plot shows that on an  $R_g$  basis all solutes of different conformations should behave very similarly in an SEC experiment. (This result is consistent with the universal SEC calibration concept.<sup>(4)</sup>)

The molecular weight  $M$  of a solid-sphere is proportional to the volume of the sphere, i.e.,  $M \propto r^3$ ; therefore:

$$R_g \text{ (sphere)} = 0.78 r \propto M^{1/3} \quad (8)$$

For rods of length  $L_1$ ,  $M \propto L_1$  and:

$$R_g \text{ (rod)} = 0.29 L_1 \propto M \quad (9)$$

The MW dependence of  $R_g$  for random-coil polymers is related to the molecular expansion<sup>(6)</sup>

$$R_g \text{ (coil)} \propto M^\alpha, \text{ where } \alpha \approx 1/2 \quad (10)$$

The exponent  $\alpha$  is a function of solvent power: usually  $\alpha > 1/2$ , but for an idealized random-flight polymer,  $\alpha = 1/2$ .

The values of the exponent for  $M$  in Equations 8, 9, and 10 determine the rate at which the size of the respective macromolecular shapes change with the molecular weight. For example, a tenfold increase in molecular weight roughly corresponds to a  $10 \times L_1$ ,  $2 \times r$ , or  $3 \times R_g$  change in molecular size for the three different solute conformations under study. It is expected, therefore, that the linear portion of the SEC-MW calibration curve (see Figure 3) will be steepest for the sphere-like solutes (i.e. the least effective separation or resolution) and the calibration slope for spheres will be  $3/2$  of that for coiled molecules. The linear portion of the curve for the rodlike solutes is expected to have the shallowest slope (i.e. most resolution), only half that of coiled solutes. As expected and illustrated here in Figure 3, an SEC column containing a single-pore-size packing should have a MW separation range of about one decade for rodlike molecules and three decades for spheres, compared to the usual, approximately two-decade MW separation range for random-coil solutes.

#### Experimental Support for the Unified Theory

Published data in support of the above observations are shown in Figures 4 and 5. Figure 4 is the calibration curve for the SEC analysis of silica sol particles as a function of size (7) This curve illustrates the hard-sphere case where about one decade of particle diameter separation is observed; note this is equivalent to about 3 decades of MW. The calibration curve slopes for polybenzyl-L-Glutamate (PBLG) and polystyrene (PS) are compared in Figure 5. The lesser slope for the polybenzyl-L-Glutamate is consistent with the expected trend discussed above. (8) This difference in calibration curve slope is expected because of the molecular conformation difference between PBLG (rod) and PS (coil).

#### Conclusions

A simplified analysis of the effect of particle shape or molecular conformation on SEC calibration has led to the prediction that the more open structure of rigid rod shaped solutes gives a relatively flat SEC-MW calibration curve. As the solute conformation becomes more compact (random-coil to solid-sphere), the SEC-MW calibration curve becomes increasingly steep

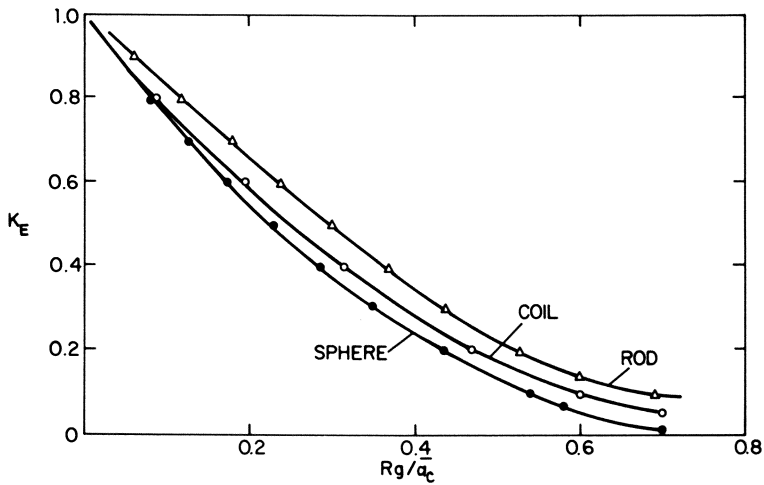


Figure 2. Theoretically predicted size exclusion effects of different solute types (cylindrical pores of single pore size). (○) random coil ( $R_g$ ); (●) hard sphere ( $R_g = r \sqrt{3/5}$ ); (△) rod ( $R_g = L_1 \sqrt{12}$ )

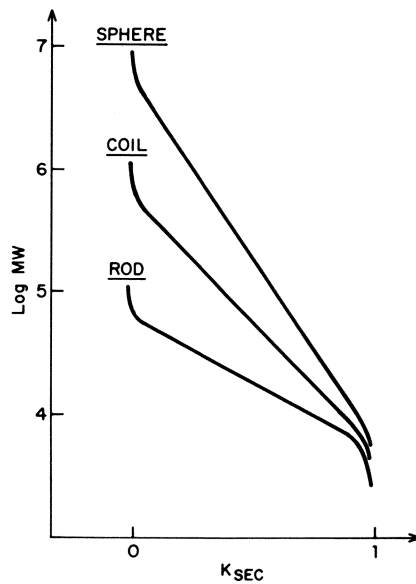
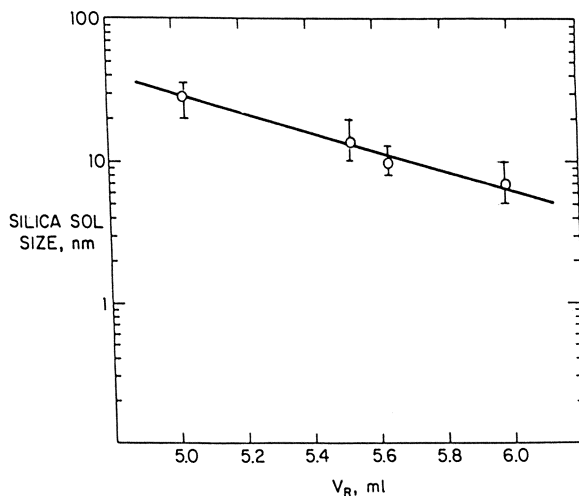
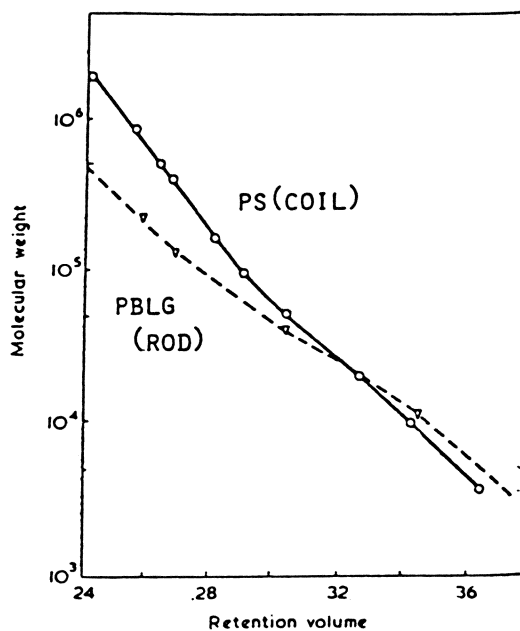


Figure 3. Theoretical SEC calibration curves for various shapes



Journal of Chromatography

**Figure 4.** SEC calibration curve for silica sol separation (hard sphere particles, single pore size column) (7). Column: PSM-1500 ( $8.9 \mu\text{m}$ ),  $30 \times 0.78 \text{ cm}$ ; mobile phase:  $0.1\text{M Na}_2\text{HPO}_4\text{-NaH}_2\text{PO}_4$ , pH 8.0



Polymer

**Figure 5.** SEC calibration curves: random-coil vs. rigid-rod (8) (SEC column set of several pore sizes, N,N-dimethylacetamide solvent at  $80^\circ\text{C}$ )

and covers a larger MW separation range. It should now be possible to use the slope of the SEC-MW calibration curves, generated from single pore size columns, to study the conformation of the solute molecules.

#### Acknowledgment

We thank J. J. Kirkland for his interest and helpful discussions on this work.

#### References

1. E. F. Cassassa, *J. Phys. Chem.*, 75, 3929 (1971).
2. J. C. Giddings, E. Kucera, C. P. Russell, and M. N. Myers, *J. Phys. Chem.*, 72, 4397 (1968).
3. G. K. Ackers, *Biochemistry*, 3, 723 (1964).
4. W. W. Yau and J. J. Kirkland, and D. D. Bly, "Modern Size-Exclusion Liquid Chromatography," Wiley, New York, 1979, Chapters 2 and 9.
5. E. F. Casassa, *Macromolecules*, 9, 182 (1976).
6. C. Tanford, "Physical Chemistry of Macromolecules," Wiley, New York, 1961, Chapters 3 and 5.
7. J. J. Kirkland, *J. Chromatography*, 185, 273 (1979).
8. J. V. Dawkins and M. Hemming, *Polymer*, 16, 554 (1975).

RECEIVED May 20, 1980.

# High-Performance Gel Permeation Chromatography Characterization of Oligomers Used in Coatings Systems

CHENG-YIH KUO and THEODORE PROVDER

Glidden Coatings and Resins, Division of SCM Corporation,  
16651 Sprague Road, Strongsville, OH 44136

Over the last five years the Coatings industry has had to develop new technologies to meet the challenges of governmental regulations in the areas of energy, ecology and consumerism. The greatest changes have occurred in the industrial or chemical coatings areas with the development of environmentally acceptable coatings systems such as High Solids, Powder, Water-borne and radiation curable coatings. These new coating technologies require the use of tailor-made low molecular weight polymers, oligomers and reactive additives which when further reacted produce higher molecular weight and crosslinked polymers concomitant with the minimization of the evolution of volatile products. In these types of coatings systems the control of the oligomer/polymer composition and molecular weight distribution (MWD) is critically important.

Conventional GPC does not provide the required resolution in the low molecular weight region for the control of MWD in these oligomer/polymer systems. With the advent of high efficiency columns, the resolution in the lower molecular weight region (molecular weights in the range of 200 to 10,000) has been greatly improved and the speed of analysis increased. These features make high performance GPC (HPGPC) an indispensable characterization tool for the analysis of oligomers/polymers in environmentally acceptable coatings systems. In this paper, we will describe the qualitative and quantitative HPGPC methodologies we have developed for the analysis of oligomers and polymers. Specific applications include a) quality control of supplier raw materials, b) guiding resin synthesis and processing c) modifying resin synthesis to improve end-use properties and d) correlating oligomer and polymer MWD with end-use properties.

## Experimental

The instrument used in this study was an in-house constructed HPGPC composed of a Waters Associates M-6000 solvent delivery system, Waters Associates U6K injector, Varian Instruments fixed

wavelength (254 nm) UV detector, Varian Instruments differential refractometer (DRI) and Waters Associates liquid volume counter.

The instrument was operated at room temperature with Burdick and Jackson distilled in glass THF as the eluting solvent. The sample column bank consisted of six  $\mu$ -Styragel<sup>®</sup> columns with the following porosity designations:  $10^4$ ,  $10^3$ , 500, 500, 100, 100A. The flow rate was adjusted to 0.6 ml/min. A 2.2- milliliter syphon was used to monitor retention volume.

The column plate count was determined from the expression

$$\text{Plate Count} = 16 (V_R/W_b)^2 \quad (1)$$

where  $V_R$  is the retention volume and  $W_b$  is the baseline width of the plate count standard. Using o-dichlorobenzene as the plate count standard yielded 24,000 plates for 180 cm. of column.

The resolution of the column set was determined from the expression derived by Bly [1]

$$R_s = \frac{2 (V_{R_2} - V_{R_1})}{W_{b_1} + W_{b_2}} \cdot \frac{1}{\log_{10} (M_1/M_2)} \quad (2)$$

where  $V_{R_2}$  and  $V_{R_1}$  are retention volumes,  $W_{b_1}$  and  $W_{b_2}$  are baseline widths and,  $M_1$  and  $M_2$  are peak molecular weights for polymer standards 1 and 2, respectively. For this set of columns, a polystyrene standards of molecular weights 37,000 and 2,000, obtained from Pressure Chemical Co., Pittsburgh, Pa., were used for standards 1 and 2, respectively. The value obtained for  $R_s$  was 2.2 at a flow rate of 0.6 ml/min. This value of  $R_s$  compares to a value of 1.14 at a 2 ml/min. flow rate reported in the literature [2]. At this flow rate the column set gave the optimum resolution per unit time. This relatively low flow rate also is required to preserve the column resolution over an extended period of time. This flow rate condition corresponds to the minimum in a Van Deemter plot of height equivalent theoretical plates vs. linear velocity and is in agreement with other published data on  $\mu$ -Styragel<sup>®</sup> columns [3,4].

The column set was calibrated with Pressure Chemical polystyrene standards over the molecular weight range of interest. The calibration curve for this column set is shown in Figure 1. The polystyrene molecular weight scale was used to provide quantitative estimates of MWD parameters such as number- and weight-average molecular weight ( $M_n$ ,  $M_w$ ) for relative comparison purposes in conjunction with the analysis of the MWD of oligomers and low molecular weight polymers used in coatings systems.

#### Data Acquisition and Analysis

The HPGPC has been interfaced to a Data General NOVA Model



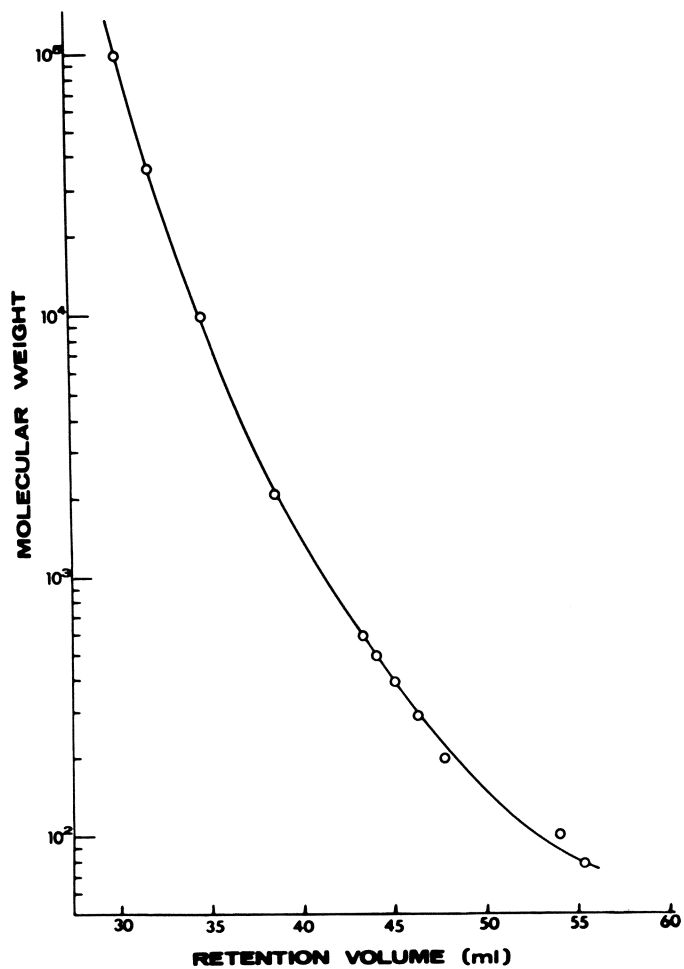


Figure 1. Polystyrene molecular weight calibration curve

1230 minicomputer for real-time data acquisition and analysis. The minicomputer system has been described previously [5]. The subsequent data reduction and analysis provides molecular weight averages ( $\overline{M}_n$ ,  $\overline{M}_w$ ,  $\overline{M}_z$ ,  $\overline{M}_{z+1}$ ) or the equivalent extended chain length averages as well as various polydispersity indices. In addition, statistical shape parameters such as variance, skewness and kurtosis for the number-, weight- and z-distributions are provided. A typical computer generated analysis report is shown in Figure 2. The data analysis program provides plots of baseline-adjusted height vs. retention volume as shown in Figure 3, as well as plots of the weight-differential and cumulative distributions of molecular weight with the locations of the respective molecular weight averages ( $\overline{M}_n$ ,  $\overline{M}_w$ ,  $\overline{M}_z$ ,  $\overline{M}_{z+1}$ ,  $\overline{M}_{z+2}$ ) marked on the differential curve as shown in Figure 4. The computation of MWD statistics and plots are based on the method given by Pickett, Cantow and Johnson [6].

For oligomeric samples with well defined peaks as shown in Figure 5, the relative percentage for each component can be obtained by integrating the area under each peak via a gas chromatography data reduction package also resident on the NOVA minicomputer [5].

### Results and Discussion

The resolution capability of the  $\mu$ -Styragel<sup>®</sup> column set is shown in Figure 6. A mixture of polystyrenes with molecular weights ranging from 97,000 to 600 were separated according to their molecular weights. The unique feature of microparticulate high efficiency columns, which include  $\mu$ -Styragel<sup>®</sup>, is the high resolution in the low molecular weight region [3,4,7,8,9,10]. For the 600 molecular weight polystyrene standard, conventional GPC columns would give only a broad peak. However, the  $\mu$ -Styragel<sup>®</sup> columns separated this sample into at least six well-defined peaks as shown in Figure 6 corresponding to monomer, dimer, trimer and other higher molecular weight oligomers. Even small molecules such as ortho-dichlorobenzene and benzene are readily separated. The high resolution in the low molecular weight regions is particularly suited for fingerprinting the oligomers used in chemical coatings systems. In Figure 6, both UV and DRI traces are shown. For clarity in comparisons, only UV traces will be shown for examples in subsequent discussion unless where specified otherwise.

Powder Coatings. One of the new coatings technologies which has developed as an innovative response to governmental regulation is powder coatings. These coatings systems are designed to be 100% solids. The development of coatings properties are a result of reacting the low molecular weight polymer with an oligomer crosslinking agent to produce crosslinked polymer. The

GPC:10      JOB 30289      1/14/80      OPR:AFK      REV 6.4  
 RERUN OF JOB 30211      OPERATOR SELECTED BASELINE  
 SAMPLE ID      5299  
 RUN NO.      1

## DETECTOR: ULTRAVIOLET

## MOLECULAR WEIGHT DISTRIBUTION

	NUMBER	WEIGHT	Z	Z+1	Z+2
MEAN	.723E 03	.124E 04	2206E 04	.318E 04	.465E 04
VARIANCE	.3/OE 06	.102E 07	.232E 07		
SKEWNESS	.292E 01	.238E 01	.212E 01		
KURTOSIS	.154E 02	.105E 02	.765E 01		

MEAN WT/MEAN NMBR	1.708
MEAN Z/MEAN WT	1.667
MEAN Z+1/MEAN Z	1.546
MEAN Z+2/MEAN Z+1	1.461
MEAN Z * MEAN Z+1/MEAN WT	.531E 04
RANGE	.144E 03 TO .132E 05

## RAW CHROMATOGRAM STATISTICS

MEAN	.217E 02	MAX PEAK COUNT#	21.56
VARIANCE	.689E 00	MAX PEAK HEIGHT	835.81
SKEWNESS	.143E 00	MOMENT 3 ABOUT MEAN	.938E-01
KURTOSIS	.239E 01	MOMENT 4 ABOUT MEAN	.263E 01
AREA	.180E 04		

## COLUMN AND BASELINE PARAMETERS

COLUMN SET	7	STARTING BASELINE COUNT	18.00
SOLVENT	THF	ENDING BASELINE COUNT	28.00
VOID VOLUME	8.00	BASELINE SLOPE	-.0160
TOTAL VOLUME	28.00	FIRST DATA POINT COUNT	19.00
CALIBRATION CURVE	21	LAST DATA POINT COUNT	24.80
CALIBRATION POLYMER	POLYSTYRENE 1/80		

#1 count unit = 1 syphon dump of 2.2 milliliters.

Figure 2. Typical computer-generated data analysis report

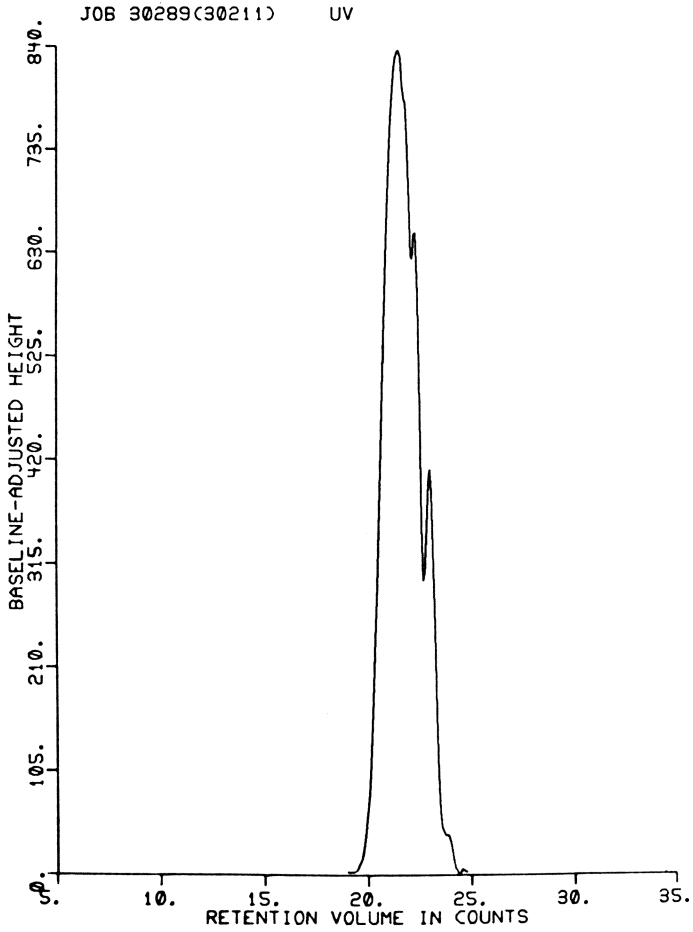


Figure 3. Typical computer-generated plot of baseline-adjusted height vs. retention volume

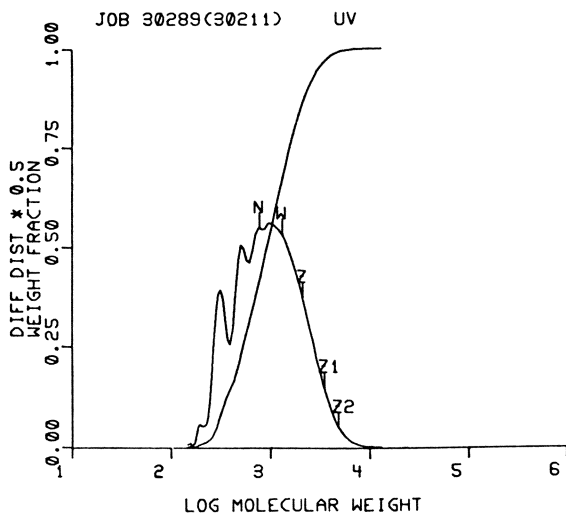


Figure 4. Typical computer-generated plot of weight differential and cumulative distributions of molecular weight

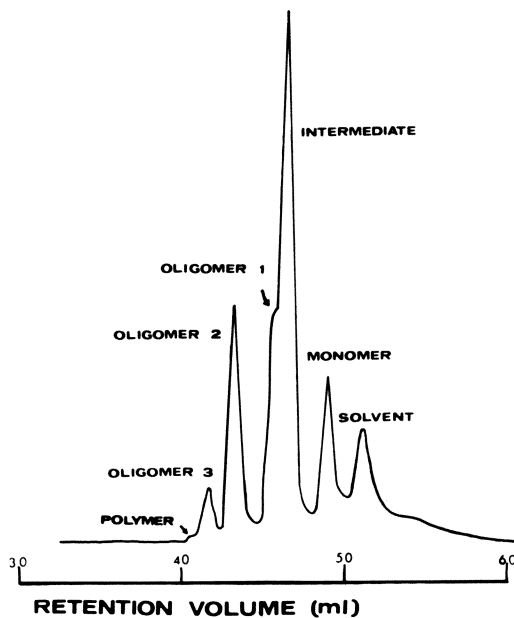


Figure 5. HPGPC chromatogram of a model compound of epoxy-ester

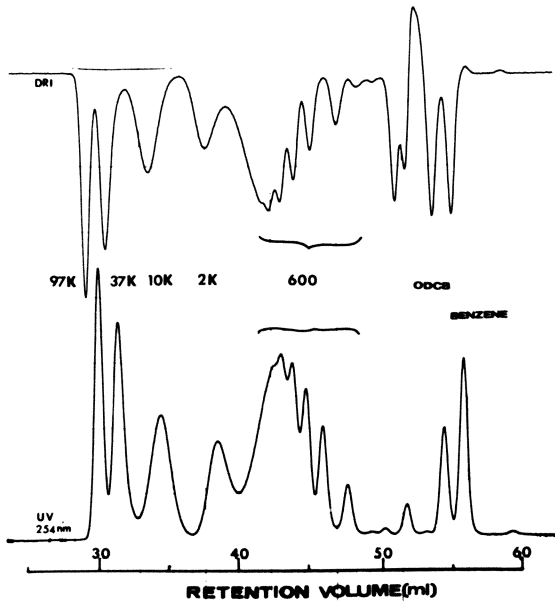


Figure 6. HPGPC traces (UV and DRI) of a polystyrene standard mixture (operating conditions: columns— $\mu$ Styragel  $10^4$ ,  $10^3$ , (2) 500, (2) 100 Å; solvent—THF; flow—0.6 mL/min)

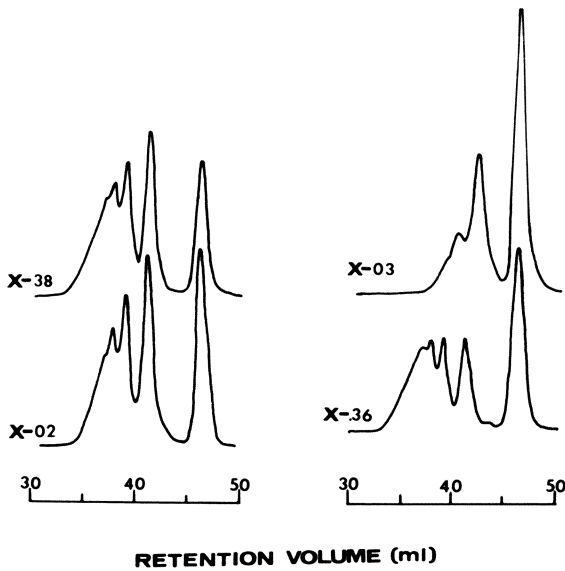


Figure 7. HPGPC chromatograms of four isocyanate cross-linkers

powder coating usually contains a small amount of an oligomeric flow agent to aid flow and leveling during the baking process. The MWD of the low molecular weight polymer, oligomeric crosslinking agent, and oligomeric flow agent must produce a coatings system such that a) the powder particles will not "block" (coalesce) upon shipment or storage, b) the resin system will melt and flow with appropriate leveling characteristics optimum for appearance properties prior to the crosslinking reaction within specific time constraints at a given temperature, and c) the crosslinking reaction must occur at the appropriate point in time after the resin has melted consistent with the development of both good appearance properties and good mechanical properties. Thus, the MWD of the polymer, crosslinking agent and flow modifier must be carefully designed and controlled to produce a powder coatings system which meets defined rheological, reactivity and mechanical property constraints.

Figure 7 illustrates the use of HPGPC to aid a resin chemist in developing an in-house isocyanate crosslinker for a powder coating system. Isocyanate crosslinker X-02 gave desired properties and is considered the standard. At the early stage of the development, resin X-03 was initially made. By changing the types of reactants, molar ratio of reactants and reaction conditions, resin X-36 was the next iteration in the resin synthesis process. Finally, X-36 was fine-tuned to produce X-38 which matched X-02 in both its chemical reaction properties and its MWD.

HPGPC also was used for quality control of incoming raw materials. Figure 8 shows the chromatograms of two different batches of blocked isocyanate crosslinkers. One was acceptable and the other was too reactive. As can be seen from the HPGPC traces, the level of the component eluted at retention volume 40 is much higher for CX-46 than for CX-48. This component was associated with free isocyanate functionality which in excess would make CX-46 too reactive. With this information, either the necessary adjustment for the presence of excessive free isocyanate functionality could be made or this particular batch from the supplier could be rejected.

Another example involved a batch of isocyanate crosslinker which was too tacky. Upon comparing the HPGPC trace of this sample with that of a control as shown in Figure 9, it is seen that the major difference between these two samples was the level of free caprolactam. The high content of free caprolactam in sample CX-006 depressed the glass transition temperature ( $T_g$ ) of the sample to such an extent that CX-006 became too tacky. This method of analysis has proved to be a reliable and useful technique for detecting low levels of free caprolactam in this type of oligomeric crosslinker.

Figure 10 shows the HPGPC traces of two different batches of in-house acrylic resins for powder coatings. It is seen that due to the presence of high levels of low molecular weight components

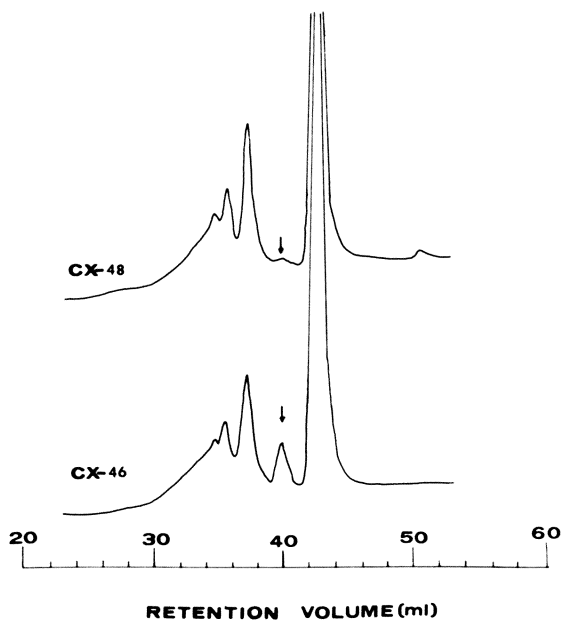


Figure 8. HPGPC chromatograms of two isocyanate cross-linkers from different batches

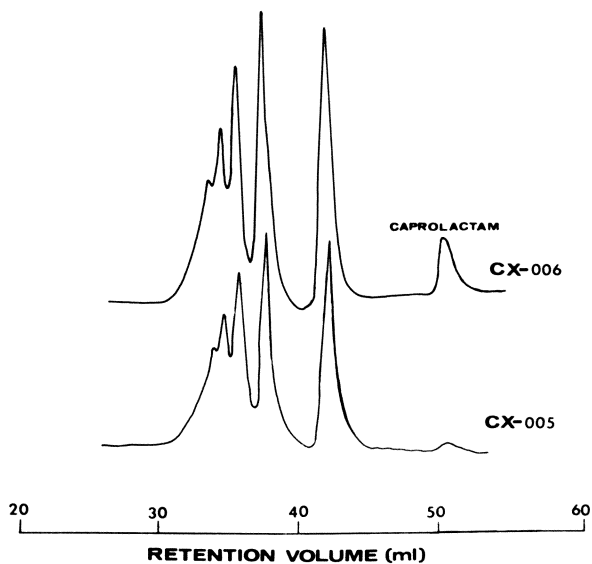


Figure 9. HPGPC chromatograms of two isocyanate cross-linkers from different batches



and residual monomer and solvent in sample TG-37, the  $T_g$  is 20°C lower than that of sample TG-57. Reducing the amount of low molecular weight components and residual monomer and solvent by vacuum stripping gave an increase in the  $T_g$  from 37°C to 48°C for sample TG-37. This brought the sample within the minimum acceptable  $T_g$  level consistent with non-"blocking" of the sample.

High Solids. Another technology which has evolved as a response to governmental regulations is high solids coatings. High solids coatings are those which are usually 62.5% non-volatile or greater on a volume basis. These coatings systems contain oligomers which are generally low in molecular weight, on the order of 500. As in powder coatings, these systems develop mechanical properties upon reaction with a crosslinking agent to produce a crosslinked polymer. The key design parameters in high solids coatings are low viscosity, low volatility and controlled reactivity [11,12]. Low coatings viscosity (100-500 cps) is required in order to be able to apply the coating with conventional spray application equipment. However, volatility of the resin system at the curing temperature must be minimal. These constraints necessitate the design of a carefully tailored molecular weight distribution to minimize the presence of volatile components consistent with molecular weights high enough to aid mechanical property development upon curing, but not too high to have a deleterious effect upon application properties and the ultimate appearance properties of the coating. The curing mechanism should be controllable under varying reaction conditions to produce crosslinked coatings at temperatures low enough to minimize volatile evolution and at the same time minimize energy usage during the cure process. In order to compensate for the decrease in molecular weight of a polymer designed for high solids coatings, there is an increasing dependence on the crosslinking agent for the development of mechanical properties. It becomes important to carefully match the crosslinking agent with the polymer both in terms of reactive functionality and MWD.

For high solids coatings HPGPC is very useful for screening various resins for the optimization of coatings viscosity and cured film properties. Among the five polyester resins shown in Figure 11, E-17 was finally chosen to be scaled-up due to the unique combination of good film properties (hardness and salt spray resistance) and lowest viscosity. The three resins on the right hand side of Figure 11 (E-44, E-38 & E-42) were not acceptable because their viscosities were too high as a result of high molecular weight components. While resin E-13 met the requirement of low viscosity for high solids, the film properties were not as good as those of E-17 due to the presence of a high level of unreacted monomer.

Figure 12 shows the HPGPC DRI traces of four high solids acrylic oligomers. The results of paint performance evaluation

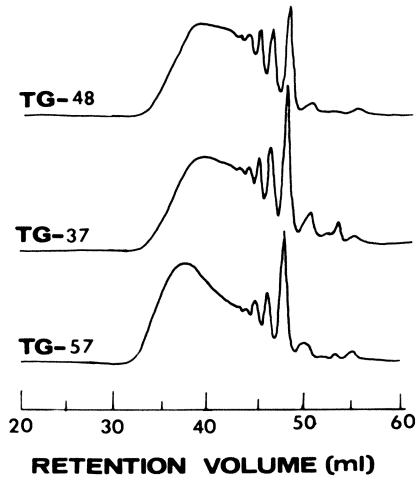


Figure 10. HPGPC chromatograms of acrylic resins

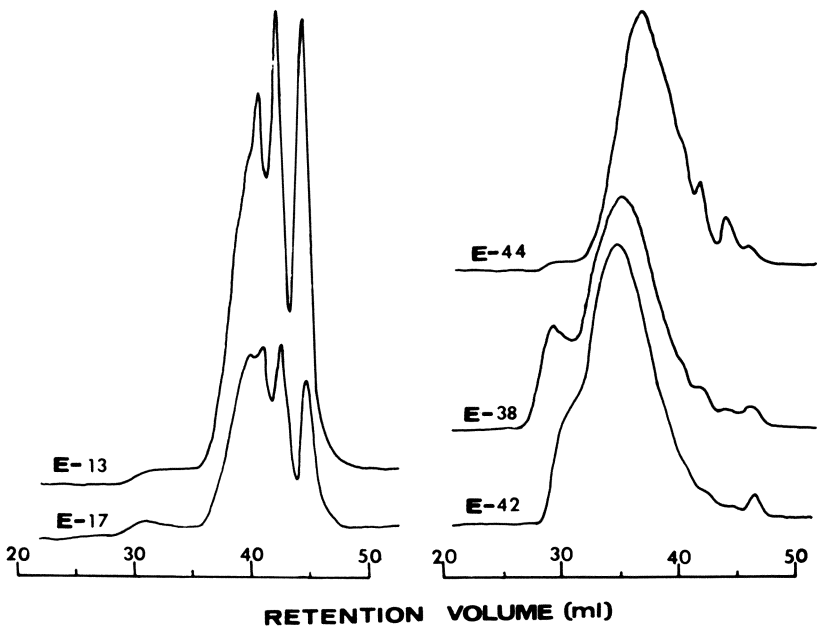


Figure 11. HPGPC chromatograms of high solids polyesters

on these acrylics showed that acrylic A-8 possessed similar paint viscosity, pencil hardness, impact, MEK resistance and adhesion properties to the commercial high solids acrylic R-42 due to the similar molecular weight range. Acrylics A-15 and A-16 possessed two to three units higher in hardness than acrylic A-8 due to the presence of large amounts of high molecular weight components. However, the coatings viscosity of coatings systems made with A-15 and A-16 was unacceptably too high.

HPGPC also was used to analyze the MWD of various amino crosslinkers, which are the most frequently used curing agent for industrial coatings. It is seen from Figure 13 that HPGPC resolved each crosslinker into several components despite the fact that the vendor's literature stated that M-03 and M-56 are monomeric. The effect of these amino crosslinkers in the properties of acrylic high solids coatings has been studied. Using the same set of acrylic resins, it has been shown that coatings prepared with the M-70 crosslinking agent had better 500 hours salt spray resistance but lower impact resistance than coatings prepared with the M-03 crosslinking agent. These properties are believed to be associated with the higher molecular weight of M-70.

Water-Borne Coatings. Water-borne coatings are replacing solvent-based coatings in such markets as metal decorating (beverage can liners), coil coatings and wood coatings as a response to meeting government regulations with respect to allowable amounts of volatile solvent emission during the baking process. These coatings usually are in the 5,000-30,000 molecular weight range and are prepared in water-miscible organic solvents up to 70 to 80% solids by volume. Chemically, these resins can be polyesters, alkyds, acrylics and epoxy esters. Generally, these resins can self-emulsify into water when their solution in organic solvents is introduced into water containing some amine [13].

In the production of epoxy ester water-borne coatings, it becomes important to monitor changes in the molecular structure of low molecular weight epoxy resins during storage. It is well-known that catalyzed liquid epoxy resins will undergo further reaction upon aging. HPGPC has been used to monitor retains of incoming shipments from the resin supplier and monitor periodic samples from storage tanks of production plants. Figure 14 shows that at the time of sampling the samples that came from the plant storage tank was essentially similar to the retained samples from the supplier. Also shown in the figure is an epoxy sample which has been aged for a year. It is seen that the low molecular weight components had undergone further reaction to form a much higher molecular weight compound. Observation of any changes in oligomer distribution such as this, at any time, will alert the respective production plant to take proper action.

UV Curable Coatings. Typically, UV curable coatings consist of very low molecular weight multi-functional oligomers diluted

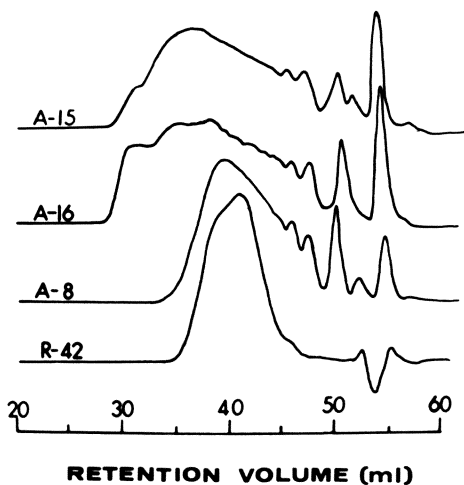


Figure 12. HPGPC chromatograms (DRI traces) of high solids acrylics

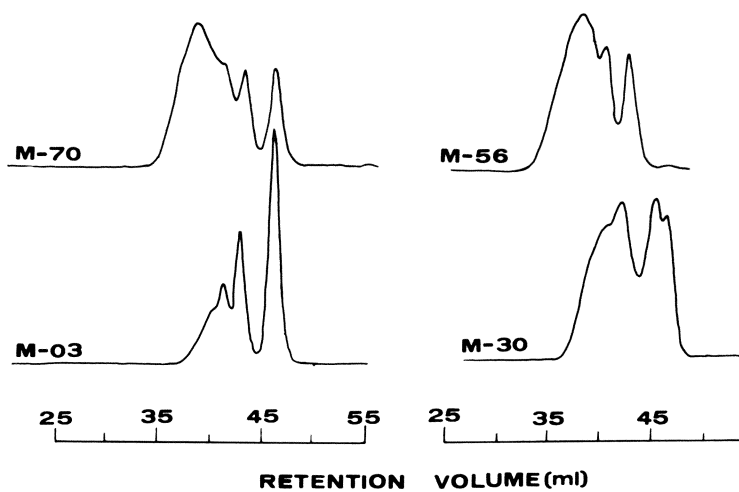


Figure 13. HPGPC chromatograms of melamine resins

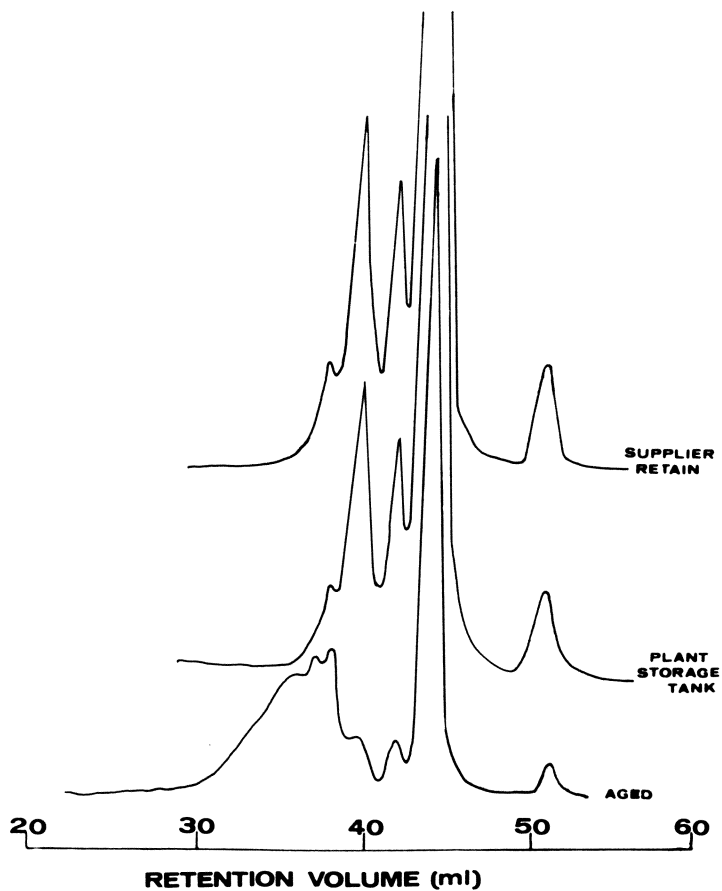


Figure 14. *HPGPC chromatograms of epoxy resins*

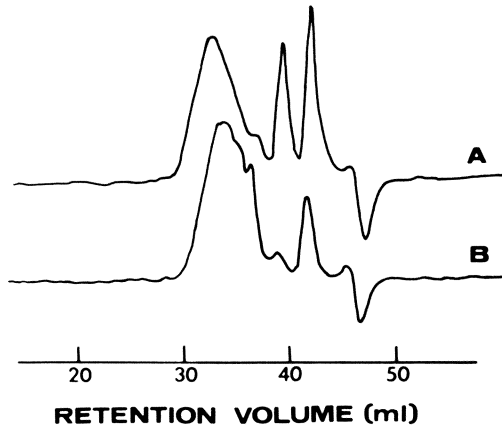


Figure 15. HPGPC chromatograms (DRI traces) of polyester urethane

with reactive monomers and contain a photosensitizer to promote the crosslinking reaction. The almost instantaneous rate of reaction permits very fast line speeds. This type of technology is ideally suited for flat stock such as floor tile and interior wood paneling. Often such coatings are applied by roll coating application methods. In order to have acceptable appearance properties after cure, the MWD of the oligomer system is one variable along with total coatings viscosity which must be controlled to have the appropriate rheological properties with respect to roll transfer, flow and leveling. The MWD of the oligomer must be maximized consistent with acceptable rheological properties in order to generate acceptable mechanical properties in the cured film.

HPGPC is very useful for guiding resin synthesis and process development. Figure 15 shows the HPGPC traces of two polyester-based urethane oligomers produced by varying the order of monomer addition to the reactor. The difference in the oligomer distribution is clearly seen in the 38-45 ml retention volume region. Due to the presence of the high level of very low molecular weight components, the resin produced from process A did not have acceptable mechanical properties compared to the resin produced from process B. The coatings system containing resin A produced a clear protective surface coating which when subjected to cure via UV radiation did not meet hardness specifications.

### Conclusions

The emergence of new coatings technologies such as high solids, powder, water-borne and radiation curable coatings as a response to governmental regulations has led to the development of resin systems where the measurement of the oligomer and low molecular polymer MWD is critically important in order to control the properties of these coatings systems. It has been shown that the HPGPC technique using high efficiency columns provides the necessary resolution in the low molecular weight regions of interest for these coatings systems.

This technique can be extended by use of other detectors. Chromatix [14] have shown that an on-line light scattering detector, under appropriate conditions can provide absolute molecular weight information in the low molecular weight region. In addition, it should be possible to unravel the subtle and important compositional dependence of the molecular weight distribution for these systems in the low molecular weight region by use of ultra-violet and infrared detectors [15].

Literature Cited

1. Bly, D. D.; J. Polym. Sci., Part C, 21, 13 (1968).
2. Yau, W. W., Kirkland, J. J., and Bly, D. D.; "Modern Size-Exclusion Liquid Chromatography", Wiley-Interscience, New York, 1979, p. 111.
3. Vivilecchia, R. V., Colter, R. L., Limpert, R. J., Thimof, N. Z., and Little, J. N.; J. Chromatogr., 99, 407 (1974).
4. Dark, W. A., Limpert, R. J., and Carter, J. D.; Polym. Eng. and Sci., 15 (12), 831 (1975).
5. Niemann, T. F., Provder, T., Metzger, V., and Kearney, R. J.; ACS Organic Coatings and Plastics Chemistry Preprints, 38, 133 (March, 1978).
6. Pickett, H. E., Cantow, M. J. R., and Johnson, J. F.; J. Appl Polym. Sci., 10, 917 (1966).
7. Kirkland, J. J., and Antle, P. E.; J. Chromatogr. Sci., 15, 137 (1977).
8. Krishen, A.; J. Chromatogr. Sci., 15, 434 (1977).
9. Krishen, A., and Tucker, R. G.; Anal. Chem., 49, 898 (1977).
10. Majors, R. E., and Johnson, E. L.; J. Chromatogr. Sci., 167, 17 (1978).
11. Antonelli, J. A.; Am. Paint J., 44 (March 31, 1975).
12. Koleske, J. V., Smith, O. W., and Kucsona, J. G.; Modern Paint and Coatings, 39 (Dec., 1977).
13. Myers, R. R., Gardon, J. L., Lauren, S.; Ed; Proceedings - Science of Organic Coatings Workshop, Kent State University, Kent, Ohio; "Gaps in the Current Physical Chemical Chemistry State-of-the-Art Related to New Coatings Systems", J. L. Gardon, 65 (June, 1978).
14. Chromatix KMX-6 Application Note, LS10, "Molecular Weight Distribution of Low Molecular Weight Polymers".
15. Provder, T., and Kuo, C.; ACS Organic Coatings and Plastics Chemistry Preprints, 36 (2), 7 (1976).

RECEIVED May 20, 1980.



# Size Exclusion Chromatography of Some Reversed Micellar Systems

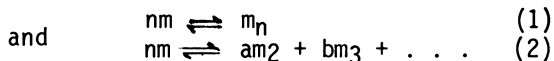
PAUL L. DUBIN

Memorex Corporation, San Tomas at Central Expressway, Santa Clara, CA 95052

## I. INTRODUCTION

With the development of new instrumental techniques, much new information on the size and shape of aqueous micelles has become available. The inception description of the micelle as a spherical agglomerate of 20-100 monomers, 12-30 Å in radius (1), with a liquid hydrocarbon interior, has been considerably refined in recent years by spectroscopic (e.g.: nmr, fluorescence decay, quasielastic light-scattering), hydrodynamic (e.g.: viscometry, centrifugation) and classical light-scattering and osmometry studies. From these investigations have developed plausible descriptions of the thermodynamic and kinetic states of micellar micro-environments, as well as an appreciation of the plurality of micelle size and shape.

The intermolecular structure of surfactant aggregates in apolar media is at present more obscure. Because the surfactant polar head groups must lie in the interior of these aggregates, they are described as "inverted micelles" or "reversed micelles." While these terms in themselves suggest a high degree of correspondence to the aqueous systems, substantial evidence indicates that the coalescence of surfactants in apolar solvents occurs through step-wise "mass-action-law" aggregation (2). In contrast to the situation for aqueous micelles, this form of equilibrium implies the absence of a sharp critical micelle concentration (CMC) below which only free monomers may be found. On the other hand, spectral and other physical properties of non-aqueous surfactant solutions sometimes show modest discontinuities in their concentration dependence, and some workers have interpreted these as "operational" CMC's (3). The central issue is the distinction between the two types of self-association:



\*Current address: Clairol Research, Stamford, CT.

0-8412-0586-8/80/47-138-225\$05.00/0

© 1980 American Chemical Society

where eq (1) may be used to describe cooperative (CMC-type) micelle formation, while eq (2) corresponds to indefinite self-association (4). In many early studies the "monomer  $\rightleftharpoons$  n-mer" association (4) of eq (1) was an implicit assumption behind the interpretation of conductance (5) or spectral (6) data. Recently, the indefinite self-association model has been found to provide the more realistic explanation of vapor phase osmometry (VPO) data (4) and nmr results (7).

At the present time, interest in reversed micelles is intense for several reasons. The rates of several types of reactions in apolar solvents are strongly enhanced by certain amphiphiles, and this "micellar catalysis" has been regarded as a model for enzyme activity (3). Aside from such "biomimetic" features, rate enhancement by these surfactants may be important for applications in synthetic chemistry. Lastly, the aqueous "pools" solubilized within reversed micelles may be spectrally probed to provide structural information on the otherwise elusive state of water in small clusters.

To interpret studies into the foregoing matters in detail, a clear understanding of the size and shape of reversed micelles is beneficial. Micelle aggregation numbers, i.e.:  $MW_{\text{micelle}}/MW_{\text{monomer}}$  have been obtained by a variety of methods, most notably vpo (8), but also classical light-scattering (9), inelastic light-scattering (10) and centrifugation (11). All of these molecular weight methods provide a single average value for the aggregation number, e.g., number-average from vpo or weight-average from light scattering, and thus yield information about micelle size distribution only indirectly. The same restriction has been encountered in the application of these techniques to the characterization of synthetic polymers. This limitation has in large part provided the impetus for the development of GPC, which can portray the whole distribution. Size exclusion chromatography has been sparsely applied to aqueous micellar systems. Gel filtration on Sephadex columns has been used to examine the state of association of alkyl and arylalkyl sodium sulfonate solutions (12,13) and to measure the size of alkylpolyethyleneoxide micelles (14). Porous glass was employed to study monomer-micelle equilibria in sodium dodecyl sulfate (15) and to fractionate casein micelles (16). However, no report has appeared describing the exclusion chromatography of surfactants in apolar solvents even though such solvents are typically the ones employed in modern high efficiency GPC systems.

The present work reports preliminary studies with a variety of amphiphilic solutes. The results, while somewhat fragmentary at this stage, suggest that GPC may be a rapid and versatile way to examine the size and stability of reversed micelles.

## II. EXPERIMENTAL

Di(2-ethylhexyl)sodium sulfosuccinate (diisooctyl sulfosuccinate, Aerosol OT, AOT) was obtained from Aldrich and purified by

recrystallization from ethanol. Hexadecyl-trimethylammonium bromide (CTAB), glycerolmonooleate (GMO) and di-N-octylamine hydrobromide (DNOAHBr) were obtained from the same source and used without further purification. Commercial Soya Lecithin\* was supplied by Chemurgy Division of Central Soya (Central 3FUB). This natural product was further purified by precipitation from THF into acetone, which removed the glycerides (soya oil). The precipitate, which contained the soya phosphatides, was further purified by precipitation from THF into ethanol to yield a supernatant consisting predominantly of chemical lecithin (phosphatidyl choline) henceforth referred to as the ethanol-soluble fraction.

GPC was carried out with a "main columns" system, or one of two "Oligomer GPC" systems. The former was a Waters ALC/GPC 204 equipped with  $10^5$ ,  $10^4$ ,  $10^3$  and 500 Å  $\mu$ Styragel columns with THF as an eluant. The latter was in one case a similar Waters instrument with a  $10^3$  Å  $\mu$ Styragel column or 500 Å + 100 Å  $\mu$ Styragel columns and benzene as eluant. The second Oligomer GPC was a high-speed, high-resolution system (25,000 theoretical plates) utilizing a Milton Roy mini-pump, a Rheodyne #7120 injector, and two Toyo Soda G2000H columns with THF as mobile phase. (The use of benzene as a mobile phase with the latter column set was avoided based on the manufacturer's recommendations for columns packed with THF.) A Waters R401 differential refractometer was the detector used in all experiments. The usual narrow distribution polystyrene standards were used for calibration and all reported MW values are relative to their elution ( $M^{PS}$ ).

### III. RESULTS

#### A. Chromatographic Behavior of Amphiphiles in Benzene

GPC chromatograms of AOT in benzene obtained with a 500 Å + 100 Å  $\mu$ Styragel column set, and over a range of injected sample weights, are shown in Figure 1. The apparent peak molecular weight increases with the amount of sample applied to the columns. At higher sample loads, the value of  $M_p^{PS}$  appears to approach a limit of 1200-1600. The apparent MWs observed at low concentrations (ca 500) may represent a lower limit corresponding to unassociated solute.

The influence of sample size on the apparent MW of AOT is shown in Figure 2 where sample mass in mg is plotted against  $M_p^{PS}$ . In the range 5-20 mg, the apparent MW increases in a nearly linear manner with the sample size. At higher solute concentrations,  $M_p^{PS}$  appears to attain a limiting value which, in spite of some scatter in the data, can be identified as 1400 + 200.

\* Soya lecithin is a natural product which contains about 34% glycerides (soya oil), 5% sugars, and 61% phosphatides. The phosphatides in turn are comprised of phosphatidyl choline, i.e., chemical lecithin (20%), phosphatidyl ethanolamine (20%), and phosphatidyl inositol (21%).

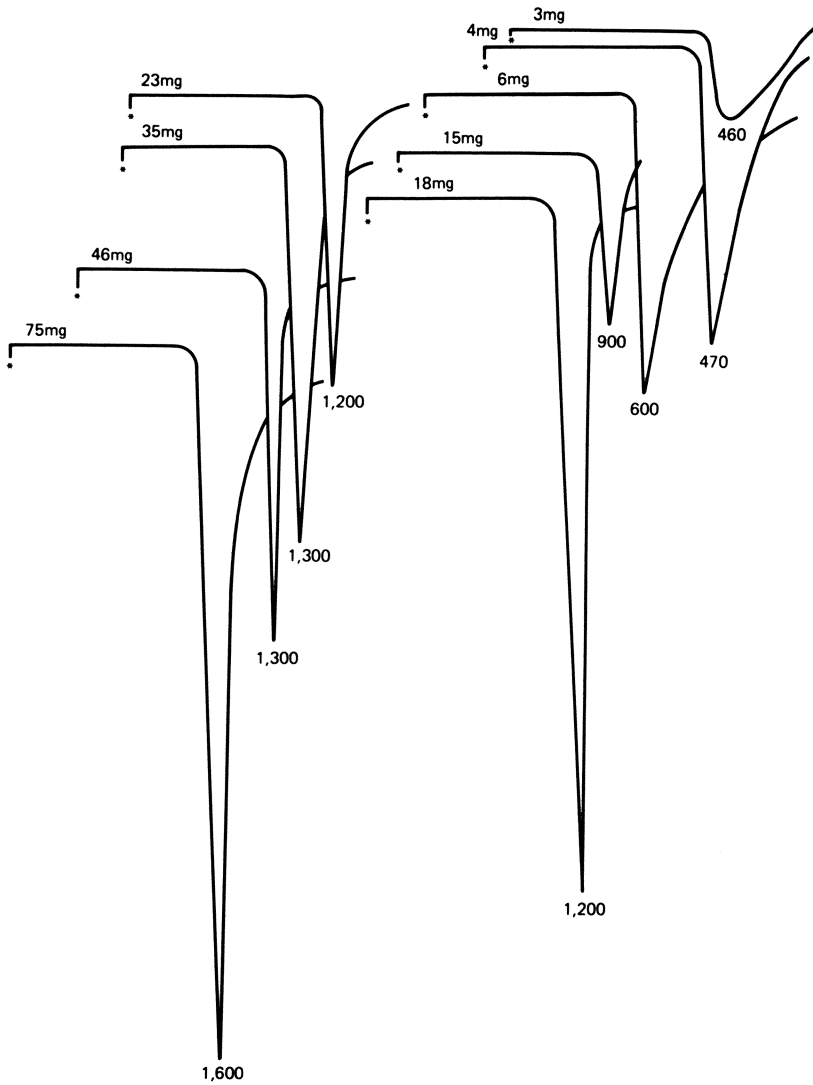


Figure 1. GPC chromatograms of Aerosol OT at varying sample loads (solvent: benzene; columns: 500 Å + 100 Å  $\mu$ Styragel; flow rate: 0.58 mL/min; injection volume: 750  $\mu$ L)

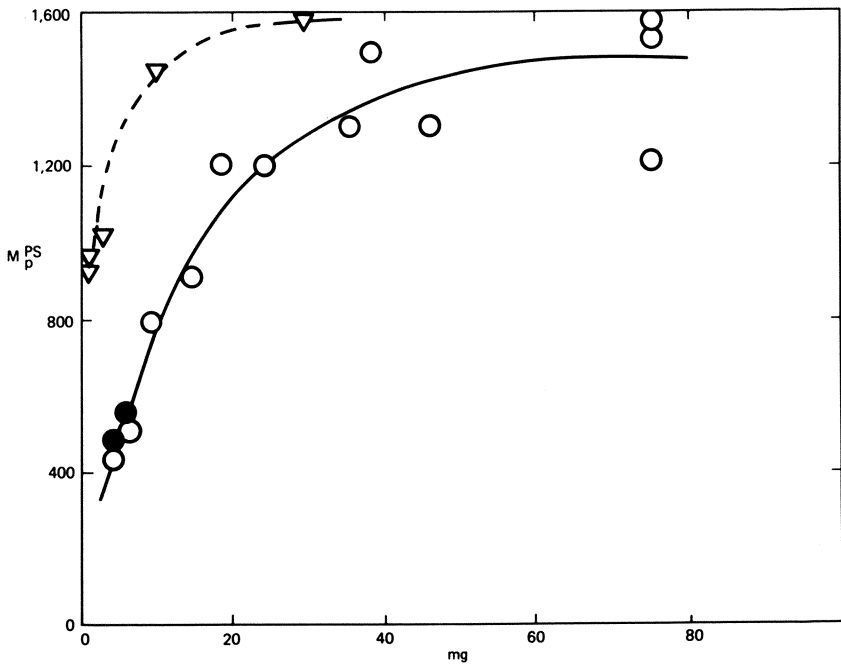


Figure 2. Dependence of apparent molecular weight on sample size, from data of Figure 1 ((●) injection volume 250  $\mu$ L; (---) data for AOT in THF)

Chromatograms obtained for the other compounds eluted in benzene are shown in Figure 3. Concentrations applied to the columns ranged from ca 2 mg/ml, near the limit of detection, up to the solubility limit. Over this range, no change could be observed for CTAB.

### B. Exclusion Chromatography in THF

Samples of AOT were eluted in THF on Toyo Soda Oligomer Columns at 118 ml/hr. A single rather narrow peak was observed for sample sizes from 0.1 to 31 mg. The dependence of  $M_p^{PS}$  on sample size is shown by the broken line in Figure 2.

The chromatogram of the commercial soya lecithin as shown in Figure 4 suggests a number of components and all subsequent work was done with the ethanol-soluble fraction, i.e., phosphatidyl choline, or the ethanol-insoluble fraction, comprised primarily of other phosphatides.

Chromatograms of the ethanol-soluble fraction were obtained in THF on Toyo Soda Oligomer columns over a range of sample masses, as shown in Figure 5. The exclusion limit of these columns is ca 50,000 and  $M_p^{PS}$  values above 10,000 are inaccurate because the calibration curve is very steep in this region. Consequently, chromatograms were also obtained on the "Main Column" GPC with the results shown in Figure 6.

The dependence of  $M_p^{PS}$  on sample size for the ethanol-soluble fraction is summarized by the solid lines in Figure 7. For both column sets, the apparent MW of the principal peak increases by nearly an order of magnitude as the mass of the injected sample is increased from one to four mg. In contrast, the ethanol-insoluble fraction exhibits a rather narrow chromatogram with  $M_p^{PS} = 20,000$ , essentially independent of the sample mass or the column system.

## IV. DISCUSSION

The decrease in retention time with increasing sample size, along with the high values of  $M_p^{PS}$ , is a clear indication of aggregation of these solutes in nonaqueous media. The two solutes studied in detail, AOT and soya phosphatides, both display limiting values of  $M_p^{PS}$  at high and low concentrations (see Figures 2 and 7) that may correspond to the most stable aggregate and the unassociated solute, respectively. The concentration dependence of  $M_p^{PS}$  in the intermediate region varies strongly. To some extent this may correspond to aggregates of intermediate size. On the other hand, the process of separation itself results in a continuous perturbation of the equilibrium and the position and breadth of the observed chromatogram may reflect in a complex way the process of disaggregation as the solute elutes through the column.

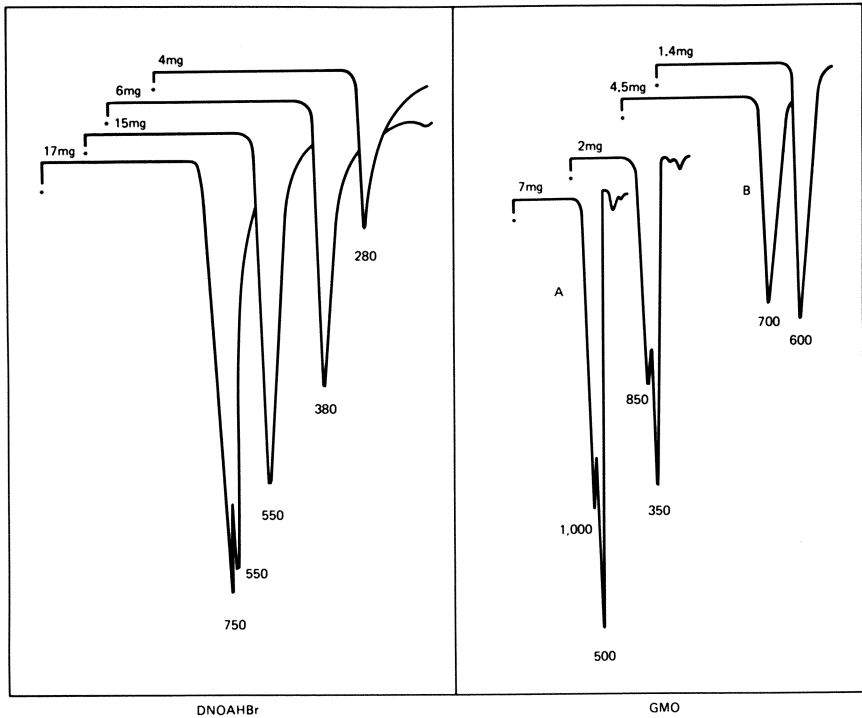


Figure 3. GPC chromatograms for DNOAHBr and GMO at varying sample loads (solvent: benzene; columns: 500 Å + 100 Å  $\mu$ Styragel (DNOAHBr) or 10<sup>3</sup> Å  $\mu$ Styragel (GMO); flow rate: 0.55 mL/min, except 1.13 mL/min for chromatograms in A; injection volume: 700  $\mu$ L)

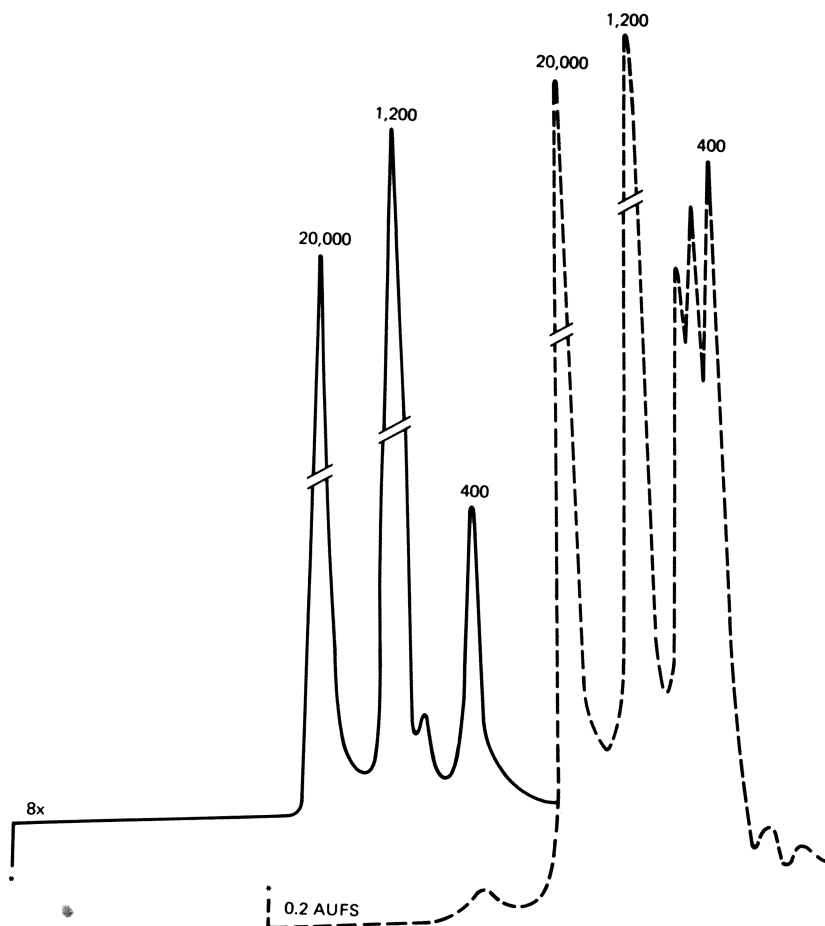


Figure 4. GPC chromatograms of commercial soya lecithin (solvent: THF; columns:  $2 \times$  G2000H Toyo Soda; flow rate: 1.96 mL/min; injection:  $50 \mu\text{L} \times 75 \text{ mg/mL}$ ; ---): 254 nm detection, 0.2 abs. units full-scale)



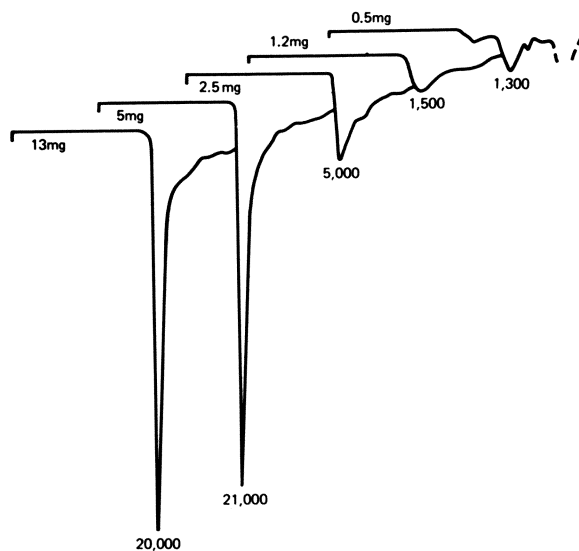


Figure 5. GPC chromatograms of phosphatidyl choline fraction of soya lecithin (conditions same as for Figure 4 except injection volume: 50–250  $\mu\text{L}$ )

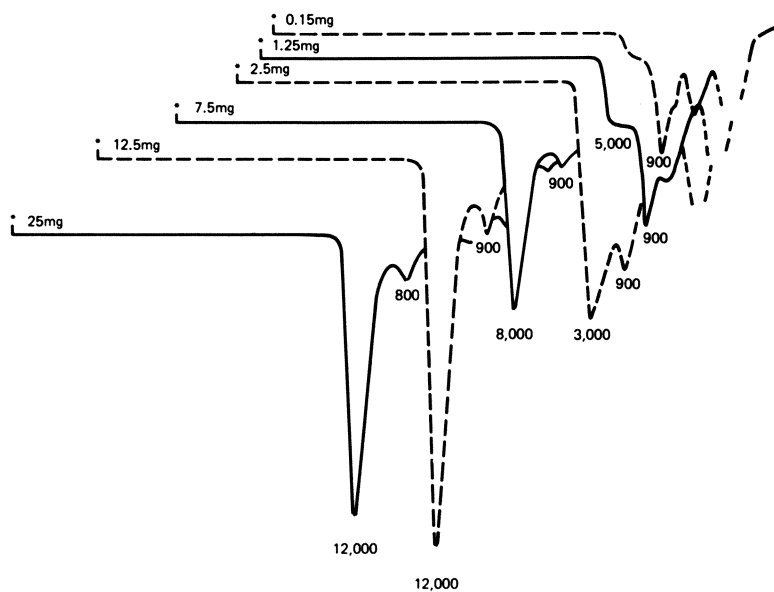


Figure 6. GPC chromatograms of phosphatidyl choline fraction (solvent: THF; columns:  $10^5 \text{ \AA} + 10^4 \text{ \AA} + 10^3 \text{ \AA} + 500 \text{ \AA}$   $\mu\text{Styragel}$ ; flow rate: 1.81 mL/min; injection volume: 25–250  $\mu\text{L}$ )

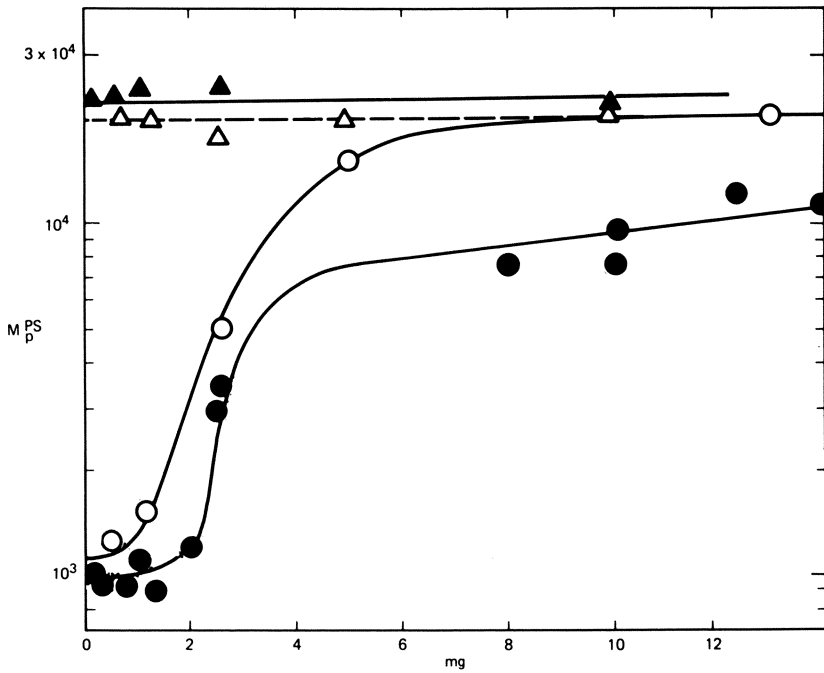


Figure 7. Effect of sample size on apparent molecular weight for soya lecithin phosphatide fractions (conditions same as for Figures 5 and 6; (O) ethanol-soluble fraction (phosphatidyl choline), "oligomer GPC"; (●) ethanol-soluble fraction (phosphatidyl choline), "main column"; ( $\Delta$ ) ethanol-insoluble fraction (other phosphatides), "oligomer GPC"; ( $\blacktriangle$ ) ethanol-insoluble fraction (other phosphatides), "main column")

### Micelle Size

In reviewing the literature on reversed micellar systems, Kertes (2) has tabulated mean aggregation numbers  $n$ , usually obtained by osmometry or light-scattering. In order to compare these values with the present findings, we can attempt to calculate  $n$  from the ratio of apparent size at high concentration to that at low sample size, assuming that the former value corresponds to the stable micellar aggregate. Several measures of molecular size have been proposed for the calibration of Oligomer GPC columns including molecular weight,  $M$  (17), the "universal calibration parameter"  $[\eta]M$  (18,19), the largest molecular dimension  $L$  (20), and the molar volume  $V_m$  (21,22). While all of these parameters are satisfactory for a homologous series of solutes, only the last two provide reasonable congruence for structurally different solutes in the range of  $10^2 < M < 10^4$ . From reported molar volumes for styrene oligomers and low MW homologs, 100-5000 MW (18,21,23), we can establish the following relationship:

$$V_m \text{ (cc/mole)} = 0.9 M^{\text{PS}} + 80 \quad (3)$$

The numerical values of the molar volume and  $M^{\text{PS}}$  are thus nearly equal over most of the MW range of interest. Hence, the ratio of  $M_p^{\text{PS}}$  at high and low solute concentrations should give the ratio of the molar volumes of micelle and monomer if the peak observed at high sample load corresponds to a stable micellar aggregate. The values of this  $M_p^{\text{PS}}$  ratio for soya lecithin (ethanol soluble) in THF and DNOAHBr in benzene are 20 and 2, respectively; these are in good agreement with literature values of the mean aggregation number  $n = 24$  and 2.5 (24,8e). (The value of  $n$  for lecithin is that reported for solution in butanol, the solvent closest in polarity to THF of those formerly studied.) For AOT and GMO, both in benzene, the values for the  $M_p^{\text{PS}}$  ratio, 4 and 1.6, are lower than literature values for  $n$  by factors of 5 and 10, respectively (2). Molar volumes calculated according to eq (3) for the free solutes are close to the expected values. Therefore, it appears likely that the low value found for  $M_p^{\text{PS}}(\text{agg})/M_p^{\text{PS}}(\text{mon})$  corresponds primarily to a negative error in  $M_p^{\text{PS}}(\text{agg})$  rather than to a high value for  $M_p^{\text{PS}}(\text{mon})$ . In the case of AOT and GMO, the observed peak might represent the front of a band of dissociating aggregates and so exhibit a retention time longer than that of a hypothetical stable micellar aggregate.

### Micelle Stability

Since aggregates elute more rapidly than free solute, the chromatographic front is not in equilibrium with the surrounding medium but continually undergoes further dissociation, as pointed out by Coll (15) and Tokiwa et al. (12). Working with aqueous alkylsulfate solutions, these authors found that this effect led

to broad chromatograms with sharp micellar fronts and long tails. In contrast, some of the chromatograms obtained here display a narrow aggregate peak and clear resolution between free solute and higher MW species. This is particularly so for lecithin (see Figures 4 and 6). The implication of this finding is that the dissociation of lecithin aggregates in THF is slow relative to the chromatographic separations. Thus, we can regard the apparent MW values as corresponding to species present in the sample prior to injection. It is interesting to note then that intermediate concentrations of the ethanol-soluble fraction lead to peaks with  $M_p^{PS}=3000-5000$  ( $M_p^{PS}(\text{agg})/M_p^{PS}(\text{mon})=3-5$ ) in light of the reported existence of "small" lecithin micelles with MW ca 3500 (25). Micelles formed from phosphatides other than chemical lecithin are apparently more stable yet, most notably at low concentrations: The ethanol-insoluble fraction exhibits only a high MW aggregate peak at applied sample concentrations as low as 0.1%.

We may contrast this behavior to that found for AOT. As shown in Figure 1, the chromatograms for AOT exhibit sharp fronts and somewhat diffuse tails, intermediate in shape between the symmetrical peaks typical of conventional solutes and the highly asymmetric chromatograms obtained for sodium dodecyl sulfate micelles in water (15). In addition, the concentration dependence of  $M_p^{PS}$  for AOT is gradual, not abrupt as for lecithin. These differences may be attributed to the lability of the AOT micelles which makes the observed retention time quite sensitive to the initial concentration (12) and leads to broadened chromatograms.

Similarly contrasting behavior was observed by Tanford and coworkers for n-dodecyl octaethyleneglycol monoether and its hexaethyleneglycol homolog eluted on Sephadex columns (14). The former detergent--like lecithin here--exhibits a narrow, symmetrical peak and no dependence of retention time on concentration; the latter compound yields chromatograms with a steep front and a long trailing edge, and displays a concentration-dependent peak position similar to that found here for AOT. However, these authors attributed the second type of behavior to slow equilibration among micelles of different sizes, in conflict with the reasoning adopted here.

## V. CONCLUSIONS

The size and stability of "reversed micellar" systems may be investigated using high-efficiency GPC. Different amphiphiles show contrasting behavior depending on micelle size and equilibration rate. The apparent size of the aggregates, based on retention volume, reflects both factors. To some extent, the dependence of retention time on sample mass is a measure of the lability of the aggregates. Chromatography using low concentrations of surfactant as a mobile phase is expected to provide more explicable results.

## REFERENCES

- (1) P. Mukerjee, *Adv. Colloid Interface Sci.*, 1, 241 (1967).
- (2) A. S. Kertes and H. Gutman, *Surface Colloid J.*, 8, 193 (1975).
- (3) J. H. Fendler, *Accounts Chem. Res.*, 9, 153 (1976).
- (4) F. Y. Lo, B. M. Escott, E. J. Fendler, E. T. Adams, Jr., R. D. Larsen and P. W. Smith, *J. Phys. Chem.*, 79, 2609 (1975).
- (5) A. K. Jain and M. J. Siddiqui, *J. Electroanal. Chem.*, 84, 195 (1977).
- (6) (a) A. Kitahara, *Bull. Chem. Soc. Japan*, 30, 586 (1957); (b) S. Ross and P. Olivier, *J. Phys. Chem.*, 63, 1671 (1959); (c) A. Ray, *J. Am. Chem. Soc.*, 91, 6511 (1969); (d) E. J. Fendler, J. H. Fendler, R. T. Medary and O. A. El Seoud, *J. Phys. Chem.*, 77, 1432 (1973); cited in ref. (2).
- (7) N. Muller, *J. Phys. Chem.*, 79, 287 (1975).
- (8) (a) A. F. Sirianni, J. M. G. Cowie and J. E. Puddington, *Can. J. Chem.*, 40, 957 (1962); (b) R. C. Little and C. R. Singleterry, *J. Phys. Chem.*, 68, 3453 (1964); (c) D. F. Evans and P. Gardam, *J. Phys. Chem.*, 72, 3281 (1968); (d) A. Kitahara, *J. Colloid Interface Sci.*, 35, 636 (1971); (e) J. David-Auslaender, H. Gutman, A. S. Kertes, and M. Zanger, *J. Phys. Chem.*, 74, 3568 (1974); (f) R. J. Braedley, D. H. Grant, V. C. Reinsborough and P. A. Ross, *J. Canad. Chem.*, 54, 3070 (1976); (g) K. Inoue, Y. Nose and H. Watanabe, *Bull. Chem. Soc. Japan*, 50, 2793 (1977); cited in ref. (2).
- (9) (a) P. Becker, *J. Phys. Chem.*, 64, 1221 (1960); (b) A. Kitahara, T. Kabayashi and T. Tachibana, *J. Phys. Chem.*, 66, 363 (1962); (c) E. Kissa, *J. Colloid Sci.*, 19, 279 (1964); cited in ref. (2).
- (10) C. Young, P. Missel, N. Mazer, G. Benedek and M. Carey, *J. Phys. Chem.* 82, 1375 (1978).
- (11) (a) J. B. Peri, *J. Am. Oil Chemists' Soc.*, 35, 110 (1958); (b) F. M. Fowkes, *J. Phys. Chem.*, 66, 1843 (1962); (c) J. B. Peri, *J. Colloid Interface Sci.*, 29, 6 (1969); cited in ref. (2).

- (12) (a) F. Tokiwa, K. Ohki and I. Kokubo, *Bull. Chem. Soc. Japan*, 41, 2285 (1968);(b) F. Tokiwa, K. Ohki and I. Kokubo, *ibid.*, 2845 (1968).
- (13) T. Sasaki, M. Yasuoka and H. Suzuki, *Bull. Chem. Soc. Japan*, 50, 2538 (1977).
- (14) C. Tanford, Y. Nozaki and M. F. Rohde, *J. Phys. Chem.*, 81, 1555 (1977).
- (15) H. Coll, in "Gel Permeation Chromatography," Ed. K. Altgelt, Dekker, New York, 1971, p. 329.
- (16) E. Almlöf, M. Larsson-Raznikiewicz, I. Lindqvist and J. Munyua, *Prep. Biochem.*, 7, 1 (1977).
- (17) A. Krishen and R. G. Tucker, *Anal. Chem.*, 49, 898 (1977).
- (18) J. Aurenge, Z. Gallot, A. J. DeVries and H. Benoit, *J. Polym. Sci.*, Polym. Symp. No. 52, 217 (1975).
- (19) M. R. Ambler, *J. Polymer Sci.*, *Polymer Letters*, 14, 683 (1976).
- (20) M. Duval, B. Block and S. Kohn, *J. Applied Polym. Sci.*, 16, 1585 (1972).
- (21) T. Yoshikawa, K. Kimura and S. Fujimura, *J. Applied Polym. Sci.*, 15, 2513 (1971).
- (22) J. Protivova and J. Pospisil, *J. Chromatogr.*, 88, 99 (1974).
- (23) R. A. Shanks, *Aust. J. Chem.*, 28, 189 (1975).
- (24) P. H. Elworthy and D. S. McIntosh, *J. Pharm. Pharmacol.*, 13, 663 (1961); cited in ref. (2).
- (25) P. H. Elworthy, *J. Chem. Soc.*, (1959), 813, 1951.

RECEIVED May 20, 1980.

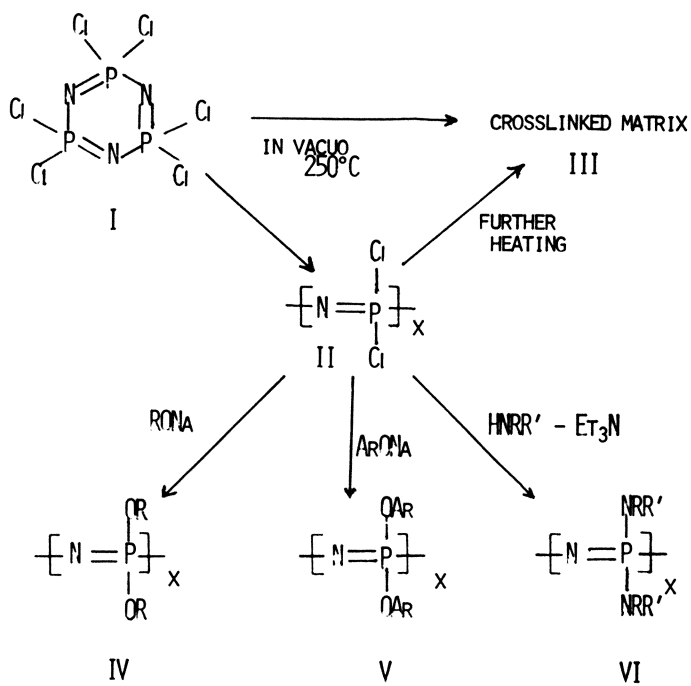
## Polymerization and Dilute Solution Characterization of Poly(dichlorophosphazene)

GARY L. HAGNAUER

Polymer Research Division, Army Materials and Mechanics Research Center,  
Watertown, MA 02172

The high temperature, melt polymerization of hexachlorocyclo-triphosphazene (I) to polydichlorophosphazene  $[\text{NPCl}_2]_x$  was first reported in 1897 (1). The polymer was usually obtained as a crosslinked matrix (III) and had many of the properties of a good elastomer ( $T_g = -66^\circ\text{C}$ ) except that it was hydrolytically unstable. Upon exposure to moist air, the P-Cl bonds hydrolyze and the polymer gradually degrades to phosphoric acid and ammonia. If the polymer is swollen in an organic solvent and water is added, the hydrolysis is quite rapid (2). More recently, soluble "open-chain" polydichlorophosphazene (II) has been prepared by using highly pure trimer and limiting the conversion in the bulk (ca.  $250^\circ\text{C}$ ) and solution (ca.  $200^\circ\text{C}$ ) polymerization reactions (3). In contrast to (III), (II) by virtue of its solubility can be rendered hydrolytically stable by replacing its chlorine atoms with various organic nucleophiles (IV-VI) (3,4). Hence, technologically promising poly(organo)phosphazenes are obtained if care is taken during polymerization to avoid gelation and to select proper conditions for complete chlorine substitution (4,5).

Although poly(organo)phosphazenes have been characterized using dilute solution techniques (4-10), attempts to characterize polydichlorophosphazene directly have been limited (11,12,13). The presence of gel and the fact that polydichlorophosphazene is moisture sensitive generally have precluded an accurate analysis of its molecular weight (MW) and molecular weight distribution (MWD). However it is now realized that, if precautions are taken during the purification and handling of the cyclic trimer (I) and if the polymerization yields are kept low, gel-free polydichlorophosphazene may be prepared routinely. A more difficult problem to handle has been the hydrolytic instability. Although polydichlorophosphazene is soluble in a variety of organic solvents, trace amounts of water cause hydrolysis with the formation of P-OH side groups. In apolar solvents like benzene and toluene, the presence of P-OH groups cause the polymer molecules to associate through





dipolar interactions; and depending upon the extent of hydrolysis, crosslinking may occur through the formation of P-O-P bonds. In polar solvents like acetone and dimethyl formamide, the polymer hydrolyzes rapidly, solutions turn turbid and a white precipitate is evident within a few hours to several days.

In this paper, techniques are described for preparing and handling dilute solutions of polydichlorophosphazene. Polymer samples are prepared by the melt polymerization of hexachlorocyclotriphosphazene in sealed, evacuated glass ampoules at 250°C. Precipitation techniques are used to separate the polymer from unreacted trimer and low molecular weight polymerization products. Under anhydrous conditions, the molecular weights and molecular weight distributions of the polymers are directly and accurately characterized. Viscometry, membrane osmometry, light scattering and liquid size exclusion chromatography (SEC) techniques are applied for dilute solution characterization. Additionally, SEC is used to analyze trimer purity and to characterize low and intermediate molecular weight polymerization reaction products. The accuracy of the polymer characterization is evaluated and the polymerization products of trimer obtained from different sources are characterized and compared.

### Experimental

**Materials.** Hexachlorocyclotriphosphazene (I), also designated as the phosphonitrilic chloride trimer, was obtained from two different sources - Ethyl Corp., Ferndale, MI and Inabata & Co., Minami-Ku Osaka, Japan. Under the conditions used for polymerization in this study, the trimer samples obtained from Ethyl Corp. were observed to form an insoluble matrix (III); whereas the Japanese trimer formed soluble polymer (I). Hence, two batches of trimer (PN-1 and PN-2) from Ethyl Corp. were purified by vacuum distillation, recrystallization from heptane and vacuum sublimation to remove inorganic impurities, hydrolysis products and higher molecular weight cyclics and oligomers. After purification, the samples were found to consist of pure trimer (mp 114°C) to the limits of detection using differential scanning calorimetry, gas chromatography and liquid size exclusion chromatography. The trimer from Inabata & Co. is a high quality, polymer grade material produced on a large scale under the trade name Phosnic 390. Phosnic 390 from two different lots, IJ-3 and IL-22, was obtained and used for polymerization without further purification. According to gas and liquid chromatographic analyses, the Phosnic 390 samples consist of 91% cyclic trimer and 9% cyclic tetramer (i.e., octachlorocyclotetraphosphazene).

The trimer samples were polymerized in sealed pyrex ampoules placed in an aluminum block oven at 250°C. Typically, the ampoules contained 50g of trimer sealed under vacuum (0.005 to 0.010 mm Hg) and the reactions were terminated by removing the ampoules from the oven. After cooling, the ampoules were opened and the contents removed.

The trimer samples and the polymerization reaction mixtures were stored under vacuum and handled in a dry box under a blanket of dry nitrogen. Dried solvents were used and precautions were taken to exclude moisture during isolation and handling of the polymers. In each case, the reaction mixture was dissolved in 80ml benzene and the polymer was precipitated with 400ml *n*-pentane. About 10-20% of the trimer and other low MW components are retained in the polymer fraction at this stage. To completely remove trimer, the polymer was dissolved and precipitated a second time. Solvent was removed, via a Rotavapor-R instrument, from the soluble, low molecular weight fractions and both the polymer and the low MW fractions were dried and stored under vacuum.

To remove water, the benzene was azeotroped and distilled over CaH<sub>2</sub>. The *n*-pentane was stored over LiAlH<sub>4</sub> and distilled over CaH<sub>2</sub>. Toluene was distilled over CaH<sub>2</sub>. Toluene from Burdick & Jackson, Muskegon, MI could also be used for dilute solution characterization without any adverse effects on polymer solubility. Tetrahydrofuran (THF) was dried over molecular sieves and doubly distilled over CaH<sub>2</sub>. The solvents were blanketed with nitrogen to maintain dryness.

Dilute Solution Characterization. The polydichlorophosphazene samples were characterized with toluene as the solvent at 25°C. The polymers were completely soluble in dilute solution and filtered with no difficulty through 0.8 $\mu$  and 5 $\mu$  membrane filters. The trimer samples and low MW fractions were dissolved and analyzed in THF solution. Solutions were prepared in an inert atmosphere and kept under a blanket of nitrogen except for short intervals during which transfer or injection operations were conducted as required for certain analyses.

Cannon-Ubbelohde dilution viscometers were employed for intrinsic viscosity  $[\eta]$  determinations and number-average molecular weights  $\bar{M}_n$ (OS) were obtained using a Mechrolab model 501 membrane osmometer. Light scattering measurements were made using a FICA 50 instrument operated with unpolarized light of wavelength  $\lambda_0 = 5461\text{\AA}$  and calibrated with benzene ( $R_B = 1.58 \times 10^{-5} \text{ cm}^{-1}$ ). The average value of the refractive index increment as determined using a Brice-Phoenix differential refractometer was  $(dn/dc) = 0.0635 \text{ ml/g}$ . A computer program incorporating a polynomial equation for the least-squares analysis of data and a plotting routine for the construction of Zimm plots was used to evaluate weight-average molecular weights  $\bar{M}_w$ (LS), second virial coefficients  $A_2$  and z-average radii of gyration  $\langle S^2 \rangle_z^{1/2}$ .

A Waters ALC/GPC-244 instrument with 6000A solvent delivery system, U6K injector, R400 refractive index (RI) detector and high performance columns was used for liquid size exclusion chromatography (SEC). A Spectra Physics SP4000 data system with SP4020 data interface and SP4050 printer/plotter was applied to format and integrate data. The following conditions were used for analyzing the polydichlorophosphazene samples:

Sample concentration - 2 $\mu$ g/ $\mu$ l  
Injection volume - 50 $\mu$ l  
Mobile phase - toluene  
Flow rate - 1 ml/min  
Columns -  $\mu$ Bondage1 2000 $\text{\AA}$ , E-linear, 125  $\text{\AA}$   
Detection - RI 16X, SP4050 Attenuation 10  
Chart speed - 4 cm/min  
Analysis time - 10 min  
Total plate count 10<sup>4</sup> plates

Discrete area segments were computed over four second time intervals during polymer elution and baseline corrections were made. The raw data were transferred to a Hewlett Packard HP9830 computer for evaluation and plotting. The following conditions were used to analyze the trimer samples and low MW fractions:

Sample concentration - 1 $\mu$ g/ $\mu$ l  
Injection volume - 50 $\mu$ l  
Mobile phase - THF  
Flow rate - 2ml/min  
Columns - (2) Shodex GPC A-800/S columns + (3) 100 $\text{\AA}$   $\mu$ Styragel columns  
Detection - RI 16X, SP4050 Attenuation 10  
Chart speed - 1cm/min  
Analysis time - 24 min  
Total plate count - 2(10<sup>4</sup>) plates

Polydichlorophosphazene and cyclic trimer and tetramer standards were used for calibration. Standard methods were applied for integrating peak areas.

Gas chromatographic and mass spectroscopic analyses were run using a Finnigan GC/MS instrument with an electron ionization detector at 70eV. Separations were achieved using 3% Dexsil 300 on 100/200 Supelcoport in a 5-ft x 1/4-in glass column programmed from 100° to 280°C at 20°C/min.

### Results and Discussion

Polymerization times and yields are given in Table I. The polymers and oligomer fractions are designated according to the batch or lot number of the trimer from which they were derived. The % polymer is based on the actual weights of trimer used for polymerization and polymer recovered from the second precipitation. The values in parenthesis include the weight of polymer (ca. 3-8%) retained in the soluble oligomer fractions as determined by SEC analysis. As shown in Figure 1, high MW polymer retained in the soluble oligomer fractions elutes at the exclusion limit (670s) as a sharp peak followed by another peak (705s) or a tail of high MW oligomers and a series of intermediate MW oligomers (880, 950, 990, 1040, 1070, 1100s). The cyclic tetramer elutes as a shoulder (1170s) on the trimer peak (1250s). The peaks at 1300 and 1390s are due to residual solvents from precipitation and drying. It is

Table I

## Polymerization Times and Yields

Sample	Time (hrs)	% Polymer	MW	% High MW Oligomers	% Intermediate MW Oligomers	% Total Conversion
PN-1	100	24.1 (30.8)		1.8	2.4	35.0
PN-2	89	27		-	-	-
IJ-3	45	23.4(26.0)		12.4	18.4	56.8
IL-22	21.5	23.6(31.4)		4.0	7.8	43.2

noted that the cyclic tetramer does not appear in the PN-1 and -2 reaction products.

Comparable polymer yields are obtained for the four samples; however, the Phosnic 390 samples IJ-3 and IL-22 have appreciably more high and intermediate MW oligomer products. Nearly half the trimer in the Phosnic 390 samples undergoes conversion compared to 35% for the purified trimer. Finally, it is noted that the Phosnic 390 samples achieve similar polymer yields in about one-fifth to one-half the time as the pure PN trimers. These observations suggest that the Phosnic 390 samples may contain component(s) that behave as catalysts or accelerators and that also tend to increase the high and intermediate MW oligomer yields.

Besides the trimer, the only component identified (by GC/MS and SEC) in the Phosnic 390 samples is the cyclic tetramer. However, it is difficult to understand how the tetramer might be accelerating trimer polymerization since the tetramer is reported to polymerize slower than the trimer and require a higher polymerization temperature (14,15). Metals, sulfur and oxygen-bearing compounds (alcohols, ethers, ketones and carboxylic acids), as well as the surfaces of glass reaction tubes, have been reported to enhance the polymerization rate (14,16-21). But it is noted that such rate enhancers also tend to promote crosslinking and the formation of an insoluble matrix (III). Since the polymerization products were soluble and since it is unlikely that the rate enhancers would intentionally have been added to Phosnic 390, their presence is questionable. More likely, the differences in polymerization are caused by the presence of trace impurities. For example, trace amounts of phosphorus pentachloride from the trimer synthesis and of water as a contaminant may be present in the Phosnic 390 samples. Allcock and coworkers found that very low concentrations of water (0.02 to 0.1 mol %) in the cyclic trimer markedly accelerates the polymerization reaction and have proposed a mechanism for catalysis based upon the formation of chlorophosphazene hydrolysis products (22). With trace amounts of water present during polymerization, they also found that the intrinsic viscosity of the polymer (II) decreased with increasing water concentration but apparently that no high or intermediate MW oligomers are formed. However, small amounts of  $\text{PCl}_5$  (0.02 mol%) added to the trimer does result in the formation of low MW polymerization products (22). Consequently, the differences in the yields and products obtained with the Phosnic 390 and PN samples as well as the Phosnic 390 IJ-3 and IL-22 samples themselves may be attributed to variations in the amounts of trace water and  $\text{PCl}_5$ .

In all cases the polymerization products were fully soluble in toluene and the toluene solutions were well-behaved. That is, the dilute polymer solutions filtered through  $0.8\mu$  membrane filters with no clogging; normal Huggins constants (23)  $k' \approx 0.5$  were obtained from the viscometric analyses; and regular Zimm plots were obtained from the light scattering analyses (Figure 2). To evaluate further

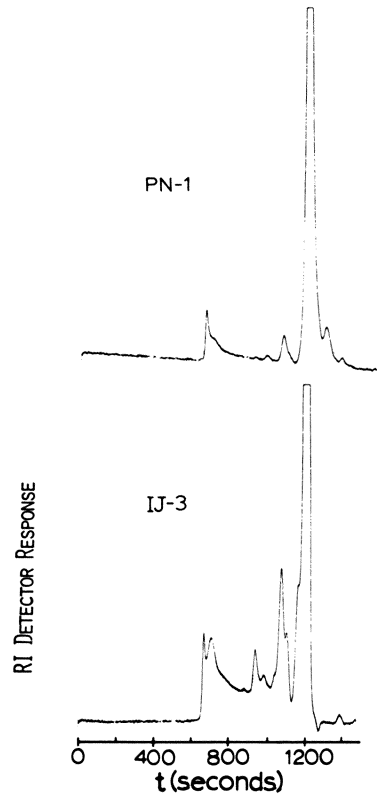


Figure 1. SEC analysis of soluble oligomer Fractions PN-1 and IJ-3

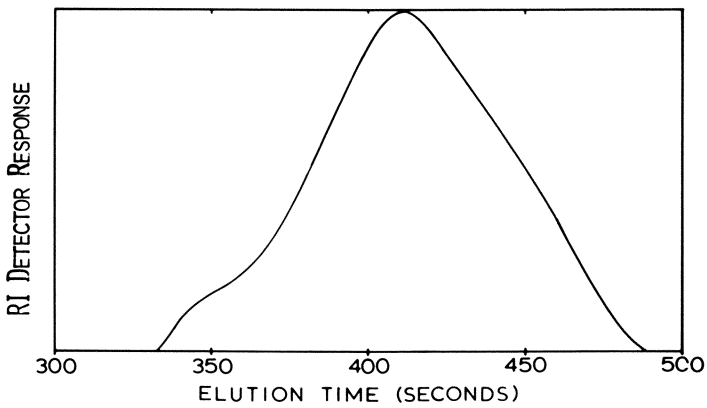


Figure 2. Zimm plot for poly(dichlorophosphazene) Sample IL-22

the validity of the polymer handling and characterization techniques, sample PN-1 was divided into three sections after polymerization. Each section was handled separately to determine the average polymer yield (Table I) and the polymers PN-1a, -1b and -1c were characterized at different times over a period of one month.

The dilute solution parameters are listed in Table II. All the samples have high molecular weights and broad molecular weight distributions. The parameters are consistent for samples PN-1a, -1b and -1c within the usual limits of experimental error expected for the dilute solution techniques. This means that the parameters for PN-2 are significantly different from those of the PN-1 polymers. Although both trimers were purified, trace differences in trimer purity or polymerization conditions evidently were responsible for the higher  $\bar{M}_n$  and  $\bar{M}_w$  values and the broader MWD of PN-2. Similarly, most parameter values for IJ-3 and IL-22 were different not only from those of the PN-1 and -2 polymers but also from those obtained for one another. The low values of the second virial coefficient  $A_2$  indicate that toluene is a thermodynamically poor solvent and perhaps a  $\theta$  solvent for polydichlorophosphazene; while the  $[\eta]$  and  $\langle S^2 \rangle_z^{1/2}$  values are comparable to values of the parameters obtained for other high MW polymers in  $\theta$  solvents (24). For a linear polymer, the values of  $[\eta]$  and  $\langle S^2 \rangle_z^{1/2}$  in a  $\theta$  solvent are the lowest values the parameters may assume without the solvent becoming a non-solvent. However, if the polymer is branched, the values of  $[\eta]$  and  $\langle S^2 \rangle_z^{1/2}$  will be less than those obtained for the linear polymer of identical MW. The  $[\eta]$  and  $\langle S^2 \rangle_z^{1/2}$  values obtained for polydichlorophosphazene are no lower than expected for the polymer in a  $\theta$  solvent. Therefore, if the polydichlorophosphazene samples are branched, they do not appear to be highly branched. Finally, it is noted that, regardless of differences in polydispersity, the polymers have similar  $\langle S^2 \rangle_z / \bar{M}_w$  values which suggests that they have a similar chain structure albeit linear or branched.

A typical SEC elution profile for polydichlorophosphazene is shown in Figure 3. All the samples eluted between 330 and 500 seconds with only slight differences in the shapes of their chromatograms, i.e., PN-1 and -2 had broader, more symmetrical chromatograms than IJ-3 and IL-22. No low MW peaks due to trimer or residual oligomers were evident. Upon analysis, the cyclic trimer had an elution time of 525 seconds. The polymers were compatible with the  $\mu$ Bondagel column packing such that, as long as dilute solutions were injected and anhydrous conditions were maintained, no increases in column back pressure or changes in elution times were observed.

Upon calibrating the columns with narrow MWD polystyrene standards, it was noted that the polydichlorophosphazenes eluted over a relatively straight region of the calibration plot. Therefore a two parameter equation,

$$\log M_i = c_0 + c_1 t_i \quad (1)$$

Table II  
 Polydichlorophosphazene Dilute Solution Parameters

Sample	$[\eta]$ (dl/g)	$M_n$ (OS) (g/mol) ( $10^{-5}$ )	$M_w$ (LS) (g/mol) ( $10^{-6}$ )	$M_w$ (LS)/ $M_n$ (OS)	$A_2$ (ml-mol/g) ( $10^{-5}$ )	$\langle S^2 \rangle_z$ (Å)	$\langle S^2 \rangle_z^{1/2}$ (Å <sup>2</sup> -mol/g)	$\langle S^2 \rangle_z / M_w$ (LS)
PN-1a	-	3.8	2.17	5.7	0.28	813		0.31
PN-1b	1.46	4.3	2.56	6.0	0.34	801		0.25
PN-1c	1.35	4.3	2.45	5.7	0.32	874		0.31
PN-2	-	5.2	3.77	7.3	5.38	1230		0.40
IJ-3	0.941	3.24	0.896	2.77	0	570		0.36
IL-22	1.68	4.15	1.81	4.36	4.17	774		0.33



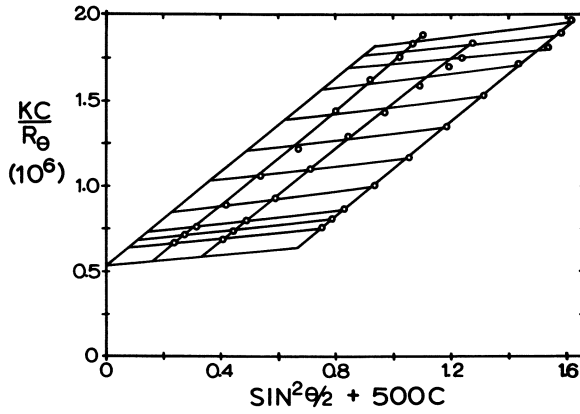


Figure 3. SEC analysis of poly(dichlorophosphazene) Sample IL-22

where  $c_0$  and  $c_1$  are constants, was calculated from the molecular weights  $M_i$  and elution times  $t_i$  of the standards eluting during the same interval as the polydichlorophosphazenes. Using Eq.1 and the polydichlorophosphazene segment areas  $A_j$ , number- and weight-average molecular weights were evaluated

$$\bar{M}_n = \frac{\sum_{j=1}^N A_j}{\sum_{j=1}^N (A_j/M_j)} \quad (2)$$

$$\bar{M}_w = \frac{\sum_{j=1}^N (A_j M_j)}{\sum_{j=1}^N (A_j)} \quad (3)$$

and were used to calculate the respective elution times

$$t_n = \frac{\log \bar{M}_n - c_0}{c_1} \quad (4)$$

$$t_w = \frac{\log \bar{M}_w - c_0}{c_1} \quad (5)$$

Next,  $t_n$  and  $t_w$  were substituted into Eq.1 with the respective polydichlorophosphazene absolute molecular weights  $\bar{M}_n$ (OS) and  $\bar{M}_w$ (LS) to form simultaneous equations which were then solved to obtain new constants

$$c_0 = \frac{t_n \cdot \log \bar{M}_w(\text{LS}) - t_w \cdot \log \bar{M}_n(\text{OS})}{t_n - t_w} \quad (6)$$

$$c_1 = \frac{\log \bar{M}_w(\text{LS}) - \log \bar{M}_n(\text{OS})}{t_w - t_n} \quad (7)$$

for the polydichlorophosphazene calibration curve. The calculations Eqs.2-7 were reiterated until the calculated values  $\bar{M}_n$  and  $\bar{M}_w$  agreed with the absolute parameters. The final constants were then used in Eq. 1 to obtain the cumulative

$$C(M_i) = \frac{\sum_{j=1}^i A_j}{\sum_{j=1}^N A_j} \quad (8)$$

and the differential molecular weight distributions (Figure 4).

$$F(\log M_i) = \frac{A_i}{4c_1 \sum_{j=1}^N A_j} \quad (9)$$

The "4" in the denominator of Eq. 9 is the integrated segment area interval in seconds.

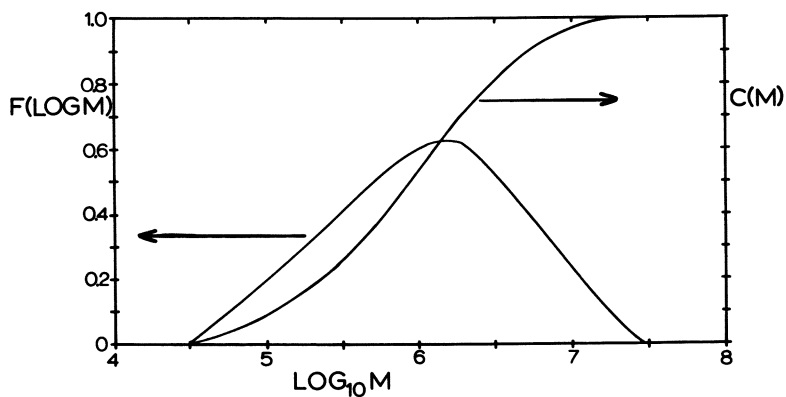


Figure 4. MWD for PN-1

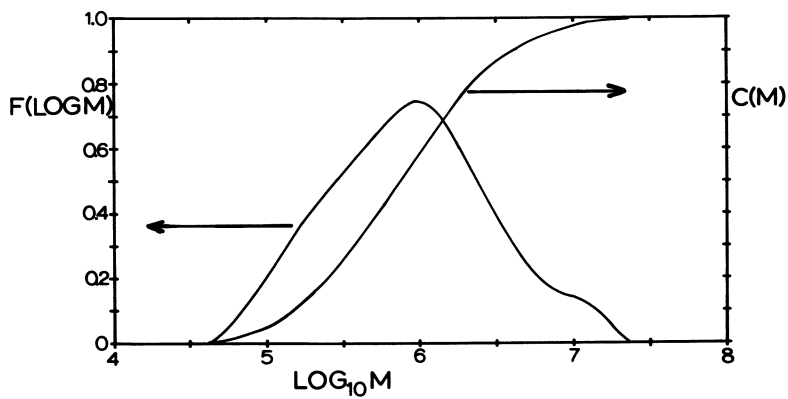


Figure 5. MWD for IL-22

Upon applying the calibration constants obtained from the data of one sample to evaluate the SEC data of the other samples, the calculated  $\bar{M}_n$  and  $\bar{M}_w$  values correspond fairly well (within 10-20%) with the absolute MW parameters of the samples. This agreement also suggests that the samples probably have similar chain structures. The distribution functions for samples PN-1 and IL-22 are plotted in Figures 4 and 5. The molecular weight distributions of both polymers are similar to distribution curves reported for derivatized poly(organo)phosphazenes (4-10).

### Conclusions and Comments

Techniques were developed for the dilute solution characterization of polydichlorophosphazene. The purity of the trimer has a significant effect on oligomer formation, polymerization time and polymer MW and MWD. The polymers prepared in this study have high molecular weights and broad molecular weight distributions and probably have similar, if not identical, chain structures. SEC analysis shows that some samples have a bimodal MWD. At this time it is not possible to tell whether the bimodality is an artifact of the polymerization mechanism or, perhaps, a consequence of partial hydrolysis of the polymer; i.e., the high MW shoulder in Figure 5 may be due to the formation of aggregates through intermolecular dipolar interactions of P-OH side groups or to polymer molecules crosslinked by P-O-P bonds.

Several assumptions were made in using the broad MWD standard approach for calibration. With some justification a two parameter equation was used for calibration; however the method did not correct or necessarily account for peak spreading and viscosity effects. Also, a uniform chain structure was assumed; whereas in reality the polymer may be a mixture of branched and linear chains. To accurately evaluate the MWD the polymer chain structure should be defined and hydrolysis effects must be totally eliminated. Work is currently underway in our laboratory to fractionate a low conversion polydichlorophosphazene to obtain linear polymer standards. The standards will be used in polymer solution and structure studies and for SEC calibration. Finally, the universal calibration theory will be tested and then applied to estimate the extent of branching in other polydichlorophosphazenes.

### Acknowledgement

The author gratefully acknowledges Dr. Robert E. Singler and Mr. Thomas N. Koulouris for their assistance in purifying the trimer samples and preparing the polymers for this study and Mr. A. J. Deome for running the GC/MS analyses.

Abstract

Polydichlorophosphazene samples are prepared by the high temperature, melt polymerization of hexachlorocyclotriphosphazene. Techniques are developed for the isolation and dilute solution characterization of the hydrolytically unstable polymer. Viscometry, membrane osmometry, light scattering and liquid size exclusion chromatography techniques are applied. The polymers are found to have high molecular weights, broad molecular weight distributions and apparently similar chain structures. The purity of hexachlorocyclotriphosphazene has a significant effect on oligomer formation, polymerization time and polymer molecular weight and molecular weight distribution.

Literature Cited

1. Stokes, H. N. Amer. Chem. J., 1897, 19, 1782.
2. Gimblett, F. G. R. Trans. Faraday Soc., 1960, 56, 528.
3. Allcock, H. R. "Phosphorus-Nitrogen Compounds", Academic Press: New York, 1972; Chapters 15 and 16.
4. Singler, R. E.; Schneider, N. S.; Hagnauer, G. L. Polymer Eng. & Sci., 1975, 15, 321.
5. Singler, R. E. and Hagnauer, G. L. "Organometallic Polymers", C. E. Carraher, J. E. Sheats, C. U. Pittman, Eds.; Academic Press: New York, 1978; p. 257.
6. Hagnauer, G. L. and Schneider, N. S. J. Polym. Sci., 1972, A-2, 10, 699.
7. Singler, R. E.; Hagnauer, G. L.; Schneider, N. S.; LaLiberte, B. R.; Sacher, R. E. and Matton, R. W. J. Polym. Sci., 1974, A-1, 12, 433.
8. Hagnauer, G. L. and LaLiberte, B. R. J. Polym. Sci., Polym. Phys. Ed., 1976, 14, 367.
9. Hagnauer, G. L. and LaLiberte, B. R. J. Appl. Polym. Sci., 1976, 20, 3073.
10. Hagnauer, G. L. and Singler, R. E. ACS Org. Coatings & Plastics Chem. Div. Preprints, 1979, 44, 88.
11. Patat, F. and Kollinsky, F. Makromol. Chem., 1951, 6, 292.
12. Patat, F. and Frombling, F. Monatsh. Chem., 1955, 86, 718.

13. Knoesel, R.; Parrod, J. and Benoit, H. C.R. Acad. Sci., 1960, 251, 2944.
14. Konecny, J. O. and Douglas, C. M. J. Polym. Sci., 1959, 36, 195.
15. Jacques, J. K.; Mole, M. L. and Paddock, N. L. J. Chem. Soc., (London), 1965, 2112.
16. Konecny, J. O.; Douglas, C. M. and Gray, M. Y. J. Polym. Sci., 1960, 42, 383.
17. Gimblett, F. G. R. Polymer, 1960, 1, 418.
18. Gimblett, F. G. R. Plast. Inst. Trans., 1960, 28, 65.
19. Chakrabartty, D. and Ghosh, B. N. J. Polym. Sci., 1962, 62, 5130.
20. MacCallum, J. R. and Werninck, A. J. Polym. Sci., 1967, A-1, 5, 3061.
21. MacCallum, J. R. and Tanner, J. J. Polym. Sci., 1969, B, 7, 743.
22. Allcock, H. R.; Gardner, J. E. and Smeltz, K. M. Macromolecules, 1975, 8, 36.
23. Huggins, M. L. J. Amer. Chem. Soc., 1942, 64, 2716.
24. Flory, P. J. "Principles of Polymer Chemistry", Cornell University Press: Ithaca, NY, 1953, Chapter 14.

RECEIVED June 2, 1980.

## Characterization of Poly(dichlorophosphazene) by Gel Permeation Chromatography

H. E. ADAMS, J. K. VALAITIS, C. W. HENDERSON, and E. J. STRAUS

The Firestone Tire & Rubber Company, Central Research Laboratories, Akron, OH 44317

It is well known that the trimeric phosphonitric chloride can be polymerized, at 200-300°C, to poly(dichlorophosphazene) (1), hereafter this polymer will be referred to as chloropolymer. Since this polymer contains hydrolytically-unstable chlorine groups, these groups are usually replaced with various alcohols, phenols, or amines to import the polymer stability. In our laboratories, the substitution is generally with alcohols or phenols. The reaction scheme is shown in Figure 1.

The substituted phosphazene polymers are both hydrolytically stable and show a wide range of physical properties. These properties may range from elastomers with good low temperature properties and good solvent resistance to plastics with fairly high structural integrity as well as polymers with fairly good high temperature stability (2,3,4,5,6).

A number of publications have discussed the characterization of the substituted polymers (4,5,7,8,9). However, because of the poor hydrolytic stability of the chloropolymer, characterization of it has been rather difficult and slow to develop, and the literature is rather scant in this regard (10,11). Conclusions about the structure and polymerization mechanism of the chloropolymer have sometimes been drawn from the analysis of the substituted polymers. These conclusions, of course, assume that there is very little, if any, change of the chloropolymer chain structure during the substitution reaction. It was felt that a direct analysis of the chloropolymer may lead to a more accurate understanding of both the polymer structure and the polymerization mechanism. From a quality control viewpoint, it was felt that if the quality of the chloropolymer predicts the quality of the substituted polymer, then considerable time

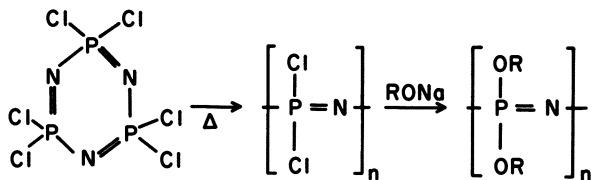


Figure 1. Scheme showing the polymerization of the trimeric phosphonitrilic chloride to poly(dichlorophosphazene) and its subsequent substitution with the sodium salts of alcohols or phenols

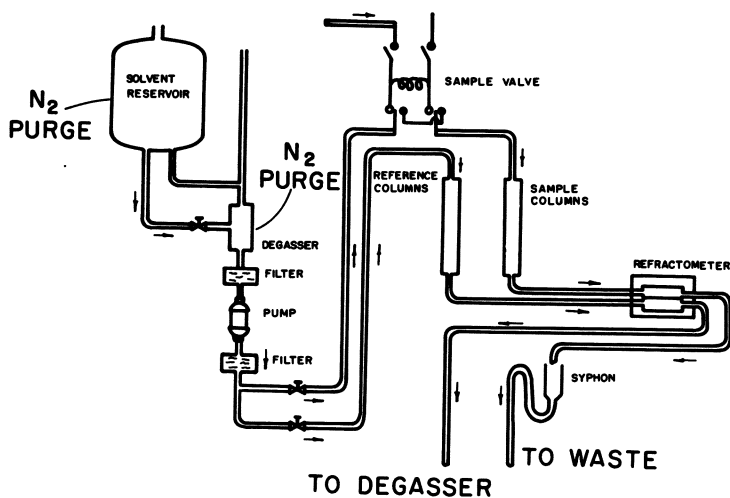


Figure 2. Partial schematic of the GPC used in this study



and expense could be saved by avoiding the substitution process if it is found that the chloropolymer does not measure up to the expected quality control standards.

It was felt, that the best tradeoff of information gained for time and effort expended in developing an analysis technique for the chloropolymer favored the gel permeation chromatography (GPC) technique. As a result, a GPC technique for this analysis was developed. Although it is felt that this technique needs further development, the initial results appear to be encouraging.

### Experimental

A schematic of the instrument employed, along with some of the modifications made, is illustrated in Figure 2. This is essentially a Waters Associates GPC Model 200 instrument. In addition to the usual nitrogen purge at the degasser, a nitrogen supply line is also connected to the bottom of the solvent reservoir. Nitrogen is allowed to slowly bubble through the solvent supply tank and, in this way, protects the solvent from the atmosphere. The small solvent supply tank heater was disconnected since too much solvent was lost by evaporation due to nitrogen bubbling through the tank. The solvent line is equipped with the usual 5-8  $\mu$  sintered metal filter before the solvent pump and the usual 0.01  $\mu$  asbestos filter after the solvent pump.

In this study, four Styragel columns were utilized; one column had a nominal porosity rating of  $10^4$ , two columns of  $10^5$ , and the fourth column of  $10^6$  Å. The refractometer was maintained at 37°C. A 5 ml syphon was used to monitor a solvent flow rate of 1 ml/min. The instrument was run at the highest sensitivity setting because the refractive index difference between our solvent and polymer was only moderate and because a number of samples analyzed had a broad molecular weight distribution (MWD).

The sample solutions were prepared to a concentration of 0.3% (wt/vol) in a dry box under nitrogen. Polymerization bottles with septum caps were used to hold the solutions until injection. The sample injection system was modified by removing the injection port heater and replacing the usual syringe-type injection fitting with a 1/16" tubing Swedgelock fitting. In this way, the sample can be injected directly via the sample filtering unit. Before injecting the sample, the filtering-injection system is

first flushed with nitrogen, then the solvent and finally the sample solution is introduced.

The filtering unit is shown in Figure 3. The sample solution is introduced into the filtering unit via a syringe through a septum located at the top of the steel screw cap of the filtering unit. The sample solution is forced through a  $0.5 \mu$  teflon filter and into the sample loop using nitrogen pressure. Both cellulose- and asbestos-type filters were utilized in the initial work, however, it was found that much of the polymer sample was adsorbed onto these type of filters. Approximately 10 ml of the sample solutions are allowed to overflow the 2 ml GPC sample loop in order to wash the loop with the specimen solution.

Certified ACS grade, Fisher Scientific toluene was utilized as the solvent in this work. The solvent is prepared for use by first mixing five gallons of toluene with 10 lbs of dessicant-type silica and allowing the mixture to stand for several hours. The solvent is then metered into a closed distillation system and flash distilled. A forefraction is removed via an azeotrope trap. The remaining solvent is stored in the closed distillation system's storage tank until it is needed. When the solvent is required, it is first passed through a silica gel column and then through a  $3 \text{ \AA}$  molecular sieve column, the dimensions of each column being 4 ft x 2 in. The solvent at this point generally contains about 20 ppm water. To further reduce the water level, 5 ml of trimethylchlorosilane is added to the toluene, in one-gallon amber glass containers, and allowed to stand overnight before use. In this way, the water content of the solvent is further reduced since trimethylchlorosilane is a well-known water scavenger (12). It may also react with other functional groups, such as OH groups, should such groups be present on this polymer. It is anticipated that these groups will react with the water scavenger and thus stabilize the polymer by preventing possible crosslinking reactions (Figure 4). Trimethylchlorosilane elutes at count 45 and is of opposite polarity from the chloropolymer. A drawback to using trimethylchlorosilane is that HCl is generated as a byproduct. Attempts were made to neutralize its potentially harmful effects on the instrumentation by introducing triethylamine as an acid acceptor. However, it was found that the resulting amine hydrochloride was insoluble in this solvent and thus this amine could not be used as an acid acceptor. It has since been found that tributylamine hydrochloride was soluble in our solvent and it is planned to use this amine as an acid acceptor in our future studies.

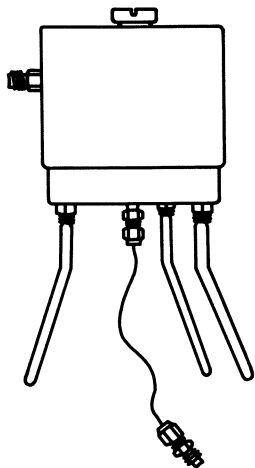


Figure 3. Filtering unit showing the attached Swedgelock fitting

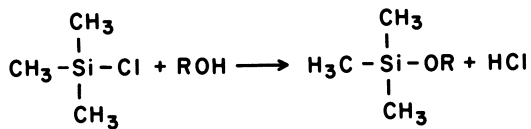


Figure 4. Scheme showing the reaction of trimethylchlorosilane with ROH, where R may be either H or a polymeric moiety

## Results and Discussion

The GPC instrument was calibrated with three relatively narrow MWD chloropolymers. It is recognized, however, that for an accurate  $\log \bar{M}_n$  vs. count calibration curve, monodisperse calibration standards are required. The number average molecular weights ( $\bar{M}_n$ 's) of the calibration samples were determined by osmometry, with toluene as the solvent. Extreme precautions were taken to minimize contact of the polymer and specimen solution with the atmosphere. This calibration is tentative and a more accurate calibration is planned which, in addition to  $\bar{M}_n$ 's, will utilize light scattering weight average molecular weights ( $\bar{M}_w$ 's). One of the broad molecular weight GPC calibration techniques (13-18) will then be employed for this analysis.

The  $\log \bar{M}_n$  vs. count calibration curve is shown on Figure 5. This is a fairly linear calibration curve, but it covers only a relatively narrow molecular weight range of 145,000 to 317,000 g/mole. Although we have sought to prepare higher MW samples for this purpose, we inadvertently obtained polymers with bimodal MWD's and did not use them for this calibration.

Even if all of the GPC analysis precautions described are adhered to there is no guarantee that a good analysis of the polymer will result if the polymer is exposed to the atmosphere during the polymer preparation stage. Figure 6 shows chromatographs of two samples that were exposed to the atmosphere during the polymer preparation stage. These polymers appear to elute very late and part of each sample elutes immediately before and after the impurity peak (counts 40-50). We have ascribed the latter phenomenon as being due to adsorption effects. We feel that the degree of adsorption of the sample may be related to the concentration of polar groups present on the polymer.

When precautions are taken to prepare and analyze the chloropolymer under stringently dry conditions, it is possible to study polymerization variables by this GPC technique. Chromatographs of three samples of the chloropolymer, prepared by three different polymerization techniques, are shown in Figure 7. The distinguishing feature of these chromatographs is that they show two components of widely different MW's; a relatively low MW component and a

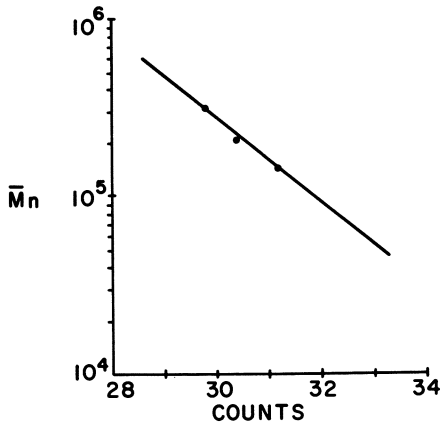


Figure 5. Calibration curve obtained with relatively narrow molecular weight samples of poly(dichlorophosphazene)

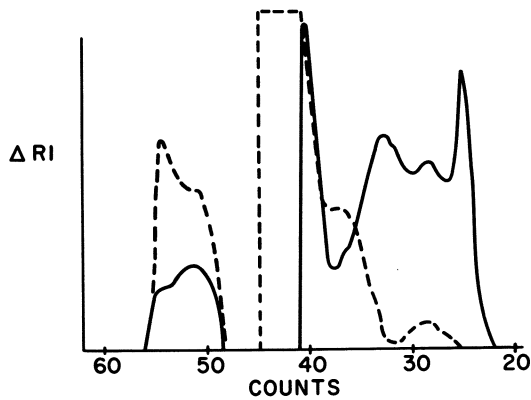


Figure 6. Chromatograms of two samples of poly(dichlorophosphazene) exposed to the atmosphere during polymerization

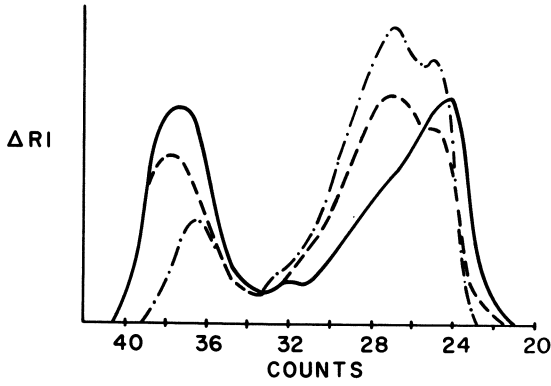


Figure 7. Chromatograms of three samples of poly(dichlorophosphazene) prepared by three different polymerization techniques

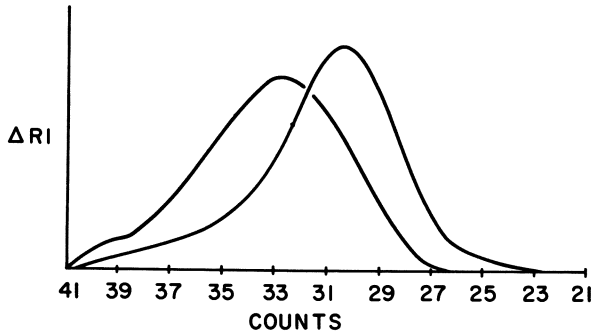


Figure 8. Chromatograms showing the effect of a coagulation process. Higher elution volume peak represents the original sample while the lower elution volume peak represents the coagulation recovered material.

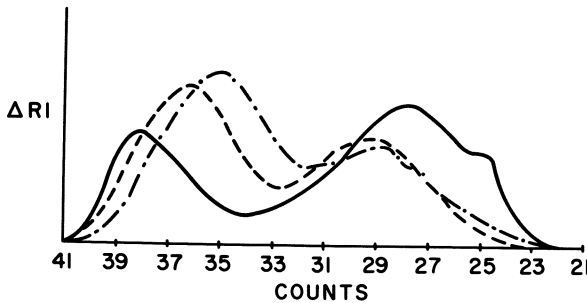


Figure 9. Chromatograms of three poly(dichlorophosphazene) samples that showed identical intrinsic viscosities in toluene

high MW component. The three different polymerization techniques also yield different ratios of high to low MW components. The presence of these two components may indicate that there are two separate processes taking place during the polymerization (either polymerization and degradation or polymerization and coupling for example). If one assumes a linear extrapolation of the calibration curve, then the low MW components range in MW from 4,000 to 8,000 g/mole while the high MW components range in MW from 300,000 to 8,000,000 g/mole. It is realized, however, that this assumption is subject to error, especially at the extreme ends of the MWD. It is interesting to note that the high MW components which show distinctly bimodal chromatographs show MW ratios of the higher MW peak to the sister lower MW peak of 3:1. This may indicate that a trifunctional coupling reaction is occurring with this polymer. Additional work is in progress to both ascertain this possibility and determine what the mechanism of this coupling reaction may be.

Since a number of the polymers that were analyzed showed rather broad MWD's, the low MW components were sometimes removed by a fractionation of the polymer with toluene/hexane as the solvent/non-solvent pair. Figure 8 shows the effect of such a fractionation process. The lower MW chromatograph is the original polymer while the higher MW chromatograph is the precipitated fraction which constitutes approximately 60% of the recovered precipitated material. Naturally, the recovered material has a higher peak MW since it is the precipitated higher MW component; but, as in a number of our attempted fractionations with this polymer, the higher MW fraction still retains much of the low MW material and has a broad MWD.

Solution viscosity measurements have sometimes been utilized as quality control tests for this polymer. Chromatographs of three samples that showed identical intrinsic viscosities (0.8 g/dl) in toluene are shown in Figure 9. These chromatographs indicate that the identical viscosities are the result of different combinations of high and low MW components. These three polymer samples probably have significantly different physical properties; and if viscosity measurements alone are utilized for quality control purposes, they may be quite misleading.

### Summary

It was shown that under stringently dry polymer

preparation and analysis conditions, it is possible to study the polymerization variables of the chloropolymer by the GPC technique. These stringently dry conditions were achieved by utilizing a number of safeguards which included distillation of the solvent before use, addition of trimethylchlorosilane to the solvent as a water scavenger, specimen preparation under a nitrogen atmosphere, and special sample injection and filtration procedures.

Utilization of this analysis technique revealed that the chloropolymer showed a rather broad MWD and often contained substantial amounts of low MW material. Different polymer preparation techniques resulted in polymers with substantially different MWD's. Often, polymers with nearly identical intrinsic viscosities did not show identical MW parameters and revealed varying MWD's. Comparison of some of the high MW bimodal chromatographs showed that the ratios of the MW's of the higher MW peak to the sister lower MW peak were 3:1. It was speculated that this bimodality may indicate that a trifunctional coupling reaction may be taking place with this polymer. It is felt that additional work is necessary to establish whether this phenomenon is general or unique to specific samples only. It was theorized that the presence of two components of widely different MW's may indicate that there are two separate processes occurring during the polymerization; such as polymerization occurring concurrently with coupling or degradation.

As stated in the introduction, the aim of this study was to develop a GPC technique for the analysis of the chloropolymer. It is felt that the techniques discussed should yield a valid analysis. Additional technique refinements should further improve this GPC analysis and will probably result in a better understanding of both the polymer structure and polymerization mechanism of the chloropolymer. These refinements are now being pursued.

When carefully prepared polymer samples were available in this study, attempts were made to interpret these GPC data. However, it is felt that these data are tentative and much work is necessary before any general conclusions can be drawn about the structure of this polymer.

### Acknowledgments

The authors wish to thank Dr. John Fieldhouse, of our laboratories, for preparation of polymer samples used in the calibration of the instrument and The Firestone Tire & Rubber Co. for support of this work.



Literature Cited

- (1) Stokes, H. N., Am. Chem. J., 19, 782 (1897).
- (2) Valaitis, J. K. and Kyker, G. S., J. Appl. Polym. Sci., 23, 765 (1979).
- (3) Kyker, G. S. and Valaitis, J. K., in "Stabilization and Degradation of Polymers," Advances in Chemistry Series 169, American Chemistry Society, Washington, D.C., 1978.
- (4) Singler, R. E., Schneider, N. S., and Hagnauer, G. L., Polym. Eng. and Sci., 15, 321 (1975).
- (5) Singler, R. E., Hagnauer, G. L., Schneider, N. S., La Liberte, B. R., Sacher, R. E., and Matton, R. W., J. Polym. Sci. A-1, 12, 433 (1974).
- (6) Mac Collum, J. R., and Tanner, J., J. Macromol. Sci.-Chem., A4 (2), 481 (1970).
- (7) Carlson, D. W., O'Rourke, E., Valaitis, J. K., and Altenau, A. G., J. Polym. Sci. 14, 1379 (1976).
- (8) Hagnauer, G. L., and Schneider, N. S., J. Polym. Sci. A-2, 10, 699 (1972).
- (9) Hagnauer, G. L., and La Liberte, B. R., J. Polym. Sci. A-2, 14, 367 (1976).
- (10) Patat, F., and Kollinsky, F., Makromol. Chem., 6, 292 (1951).
- (11) Knoesel, R., Parrod, J., and Benoit, H., Compt. rend., 251, 2944 (1960).
- (12) "Pierce Handbook and General Catalog 1979-80, Pierce Chemical Company, Rockford, Il.
- (13) Purdon, J. R., Jr. and Mate, R. D., J. Polym. Sci., A-2, 6, 243 (1968).
- (14) Almin, K. E., Polymer Preprints, 9, No. 1, 727 (1968).
- (15) Blake, S. T., Hamielec, A. F., and LeClair, B. P., Ind. Eng. Chem. Prod. Res. & Dev., 8, 54 (1969).

- (16) Abdel-Alim, A. H. and Hamielec, A. E., J. Appl. Polym. Sci., 18, 297 (1974).
- (17) Cardenas, J. N. and O'Driscoll, K. F., Polym. Letters, 13, 657 (1975).
- (18) Lay, B. R., J. Polym. Sci., 14, 2321 (1976).

RECEIVED May 7, 1980.

# Optimization of Peak Separation and Broadening in Aqueous Gel Permeation Chromatography

## Nonionic Polyacrylamides

S. N. E. OMORODION, A. E. HAMIELEC, and J. L. BRASH

Department of Chemical Engineering, McMaster University,  
Hamilton, Ontario, Canada, L8S 4L7

In the investigation reported herein, an attempt has been made to maximize peak separation and minimize peak broadening for aqueous GPC of polyacrylamides with CPG porous glass packings. To reduce or eliminate polymer solute/glass packing interactions the following parameters were optimized: a) pH, ionic strength and concentrations of additives such as nonionic surfactants, b) selection of pore sizes in a column combination.

It is found that most of the complicating effects in this system, tending to cause deviations from ideal, size-exclusion, behaviour can be attributed to ion exclusion.

Ideally GPC separates polymer molecules according to size in solution. Aqueous GPC has a number of complicating features, a common one of which is polymer adsorption on the packing. Also many water-soluble polymers exhibit polyelectrolyte properties in solution. Inorganic packings may have active sites which are positively or negatively charged. This can cause either irreversible adsorption or complete exclusion of polymer ions from the pores of the packing (ion exclusion). To reduce or eliminate complicating phenomena such as polymer adsorption, ion exclusion, ion inclusion and molecular aggregation, packing materials have been chemically surface-treated and different additives such as salts, acids, surfactants and alcohols have been included in the mobile phase (1) (2) (3) (4). Unfortunately, controversies and confusion still exist in the recent literature concerning definitions, mechanisms and methods of elimination of these undesirable phenomena (1) (2) (5) (6). This situation arises in large measure due to a lack of systematic investigation of these effects. It was the purpose of the present work, therefore, to make a thorough study of the complications in aqueous GPC arising from polymer-solvent and polymer-substrate interactions. In addition it was hoped to develop means of eliminating or minimizing these interactions for selected systems so that practically useful conditions (maximum

peak separation, minimum peak broadening) for GPC analysis could be defined. In this paper we report on the system polyacrylamide/controlled porous glass (CPG). Polyacrylamides are commercially available in a wide range of molecular weights although they are broadly distributed and not fully characterized with respect to MWD. Controlled porous glass is also readily available and can be obtained in a wide range of particle size and pore diameter suitable for an "optimization" study. These packings can be efficiently dry-packed and have been widely and successfully used in organic GPC (7).

### Experimental

The apparatus employed for this study was a Waters Associates Model ALC/GPC 300 with a differential refractometer as mass detector operated at room temperature. A 2 ml sample loop with polymer concentrations of 0.01-0.1 wt.% and a 5 ml siphon were employed with mobile phase flowrates in the range 1-8 ml/min. The columns were dry-packed with CPG-10 glass packing. All important details of column combination, mobile phase and flowrate will be specified when discussing the results of the study. Preliminary studies were done with distilled water as mobile phase. These were followed by studies using mobile phases containing salts, acids, surfactants and other additives. Two neutral surfactants were used as additives to minimize adsorption. These are (1) an alkylphenoxy polyethoxyethylene (Tergitol, from Union Carbide Corp.) and (2) a polyethyleneoxide (weight average MW 300,000 from Cellomer Assocs. Inc., Webster, N.Y.). Some polar organic solvents such as dimethylsulfoxide, dioxane, formamide and dimethylformamide were also used as additives in the mobile phase.

The polyacrylamides were obtained from Polysciences, Warrington, Pennsylvania. Weight average MW's for these polymers, supplied by the manufacturer, are given in Table I.

Table I. Characteristics of polyacrylamides.\*

Designation	Lot No.	$M_N \times 10^{-3}$	$M_W \times 10^{-3}$	$M_{rms} \times 10^{-3}$	$\bar{M}_W / \bar{M}_N$
PAM55	93-7	-	55.00	-	-
PAM100	93-3	-	100.00	-	-
PAM270	93-3	-	270.00	-	-
PAM500	93-5	-	500.00	-	-
PAM1000	95-6	-	1000.00	-	-
PAM2000	95-4	-	2000.00	-	-
PAM5000	94-3	-	5-6000.00	-	-

\* Data supplied by Polysciences

Intrinsic viscosity measurements were done with a large number of solvents varying in pH, ionic strength, etc., using Cannon-Ubbelohde semimicro dilution viscometers. This was done to provide information on the effect of mobile phase composition on the size of a polymer molecule in solution and thus to facilitate the interpretation of GPC behavior.

## Results and Discussion

### 1. Effect of pH, ionic strength and nonionic surfactants on polymer dimensions.

Intrinsic viscosity data for the nominally nonionic polyacrylamides are given in Figure 1. Duplicate measurements were made after an interval of 8 months and indicate good reproducibility and polymer stability. A variety of solvents, corresponding to those used in the GPC experiments, were employed. These range from distilled water to electrolyte solutions varying in pH from 2.5 to 7.0, in ionic strength from 0.013 to 0.503, and to which the nonionic detergents Tergitol and polyethylene oxide were added in varying amounts.

The intrinsic viscosities in distilled water do not show conventional behavior and clearly no simple Mark-Houwink relation is followed in this medium. The 500,000 and 55,000 MW polymers in particular show very high intrinsic viscosities (25 and 1 to 2 respectively). We have no satisfactory explanation for this behavior at the present time and can only speculate that these polymers may be hydrolyzed to varying degrees. At low ionic strength and high pH the negative charges associated with the carboxylate anions would exert a maximum effect on chain extension and thus would lead to high values of intrinsic viscosity.

In all the other solvents used, the intrinsic viscosities are smaller (possibly as a result of charge screening by electrolytes) and follow a single Mark-Houwink relation. This equation is found to be:

$$[\eta] = (0.212 \pm 0.039) \times 10^{-3} \bar{M}_w^{0.694 \pm 0.015}$$

This behavior shows that the dimensions of these polymers are independent of pH, ionic strength (in the ranges studied) and presence or absence of Tergitol or polyethyleneoxide. This result is of considerable help in interpretation of GPC behavior since in the absence of polymer-glass substrate interactions, the molecular weight calibration curves (log MW vs. elution volume) should be independent of pH, ionic strength or the two nonionic surfactants investigated.

### 2. Effect of ionic strength on GPC elution volumes.

For investigation of GPC behavior, a series of M.W. calibration curves (log MW vs. elution volume) was obtained for a number

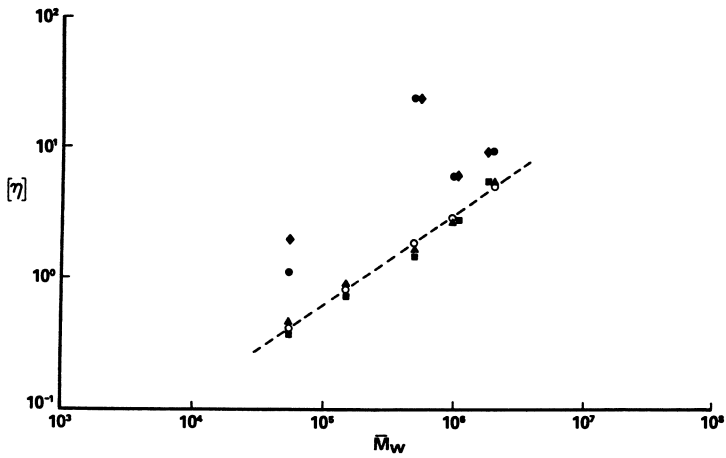


Figure 1. Intrinsic viscosities for nonionic polyacrylamides in water and aqueous solutions of various pH and ionic strength ((●, ◆) water; (▲, ○, ■) aqueous solutions (pH range 2.5–7.0 and ionic strength range 0.013–0.503) containing a nonionic surfactant (either Tergitol or polyethylene oxide;  $\bar{M}_w = 300,000$ ))

of mobile phase compositions. For optimal usefulness, these curves should ideally be linear with a relatively small slope indicating good molecular weight resolution.

Figure 2 shows molecular weight calibration curves for polyacrylamides in distilled water and in various NaCl solutions ranging from 0.001 to 0.5 M. Although the pH also varied between 5.0 and 6.18, this would be expected to have only a slight effect, if any, on the GPC process since carboxylic acid groups on polyacrylamide are almost fully ionized in this pH range. However, it is possible that charge density on the glass surface would vary somewhat over this pH range. In all these experiments a single column of length 4 ft, 3/8 in I.D. and pore size 2000 Å was used.

In distilled water, the polymers are completely excluded from the pores and elute at the column void volume. It is unlikely that this exclusion is based on size since the pore diameter is relatively large. Also, as already indicated, the intrinsic viscosities in water are only slightly greater than in salt solutions (with the exception of the 500,000 and 55,000 MW polymers). Again one is led to speculate that these polymers are partially hydrolyzed. The resulting polyanions would tend to be excluded by charge repulsion from the negatively charged pores of the glass substrate. Chain extension due to charging could also contribute to exclusion at the higher molecular weights.

With the addition of NaCl, pore permeation is seen to occur and this is again consistent with polyelectrolyte behavior. Thus addition of salt would be expected to screen the charge on the polymer and to attenuate the effect of the surface charge by compression of the associated electrical double layer. The anomalous behavior of the 500,000 and 55,000 MW samples is again evident, particularly at low ionic strength. These samples behave as molecular species that are abnormally large relative to the others in the series, again suggesting that they are more highly hydrolyzed and thus have a higher charge density.

As can be seen from Figure 2, pore permeation increases with ionic strength, but the curves are not linear and in particular show poor resolution at MW less than a million. Complete loss of resolution in this MW range is seen at 0.5 M NaCl reflecting, presumably total permeation. However the total permeated volume (as measured with NaCl) is significantly greater than the polymer elution volume at 0.5 M NaCl. Such a volume difference could be explained if a fraction of the pores is inaccessible to even the lowest M.W. polymer investigated.

On addition of polyethylene oxide of M.W. 300,000 at a concentration of 0.025 g liter<sup>-1</sup>, it is seen that a single calibration curve is obtained, independent of NaCl concentration. (It should be noted, however, that at very low NaCl concentration, less than about 0.005 M, the curve still appears at lower elution volumes). This curve is not linear but does exhibit fairly good resolution. It is likely that the effect of polyethylene oxide

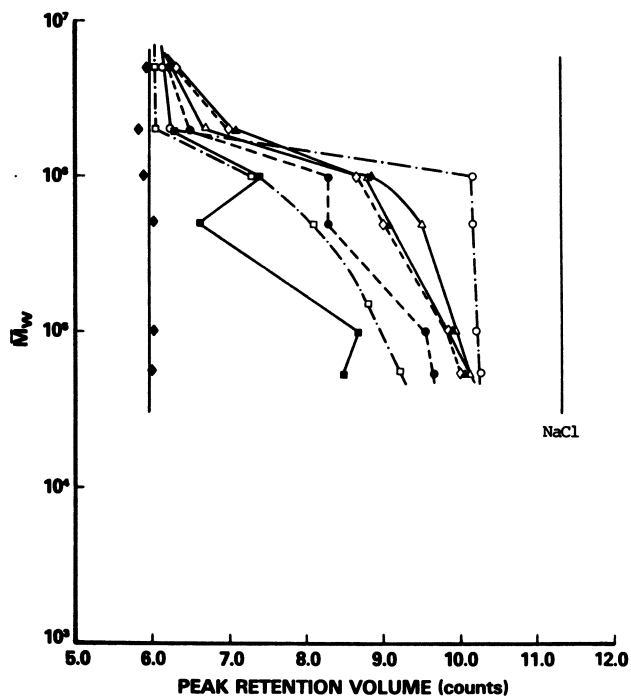


Figure 2. Molecular weight calibration curves for nonionic polyacrylamide for a single column (4 ft  $\times$   $\frac{3}{8}$  in. i.d.) containing 2000 Å CPG-10 (200/400 mesh) packing with aqueous salt solutions as mobile phase.

One mobile phase contains polyethylene oxide ( $\bar{M}_w = 300,000$ ) (For details see Table II). Mobil phase flow rate: 4.2 mL/min; ( $\blacklozenge$ ) water; ( $\square$ ) mobile phase containing polyethylene oxide ( $\bar{M}_w = 300,000$ ); ( $\blacksquare$ ) 0.001M NaCl; ( $\bullet$ ) 0.005M NaCl; ( $\diamond$ ) 0.025M NaCl; ( $\blacktriangle$ ) 0.050M NaCl; ( $\triangle$ ) 0.100M NaCl; ( $\circ$ ) 0.5M NaCl.



is to reduce further the effects of surface and polyanion charge by adsorbing on the glass. Such adsorption would also cause a reduction in the pore diameter relative to the polymer solute. The effective pore diameter would now be less than 2000 Å and complete permeation by polymer solute would no longer be possible. It should be mentioned that the salt peak retention volume was not significantly reduced suggesting that the effective pore volume was the same even in the presence of the adsorbed polyethylene oxide.

### 3. Effect of pH on GPC elution volumes.

The effect of pH is shown in Figure 3. These data again are for the same single 4 ft column with a pore diameter of 2000 Å and thus are comparable to those of Figure 2. The solutions were acidified with sulfuric acid to yield pH values between 2.25 and 1.6, in a range where carboxylic acid groups on the polymer chain may be expected to be undissociated. Variation in pH in the range indicated would thus be expected to cause changes in the charge density on the glass surface. As the pH decreases, the curves are seen to shift to higher elution volumes with some resolution evident in the higher molecular weight region particularly at higher pH. At very low pH, resolution is almost totally lacking and even the  $2 \times 10^6$  and  $5 \times 10^6$  MW samples show extensive pore permeation. As seen in Figure 2 there was very little permeation by these samples at high pH even in 0.5 M NaCl. As in Figure 2 there is a gap between the apparent total permeated volume and the total permeated volume as determined using NaCl.

The variations in elution volume with pH in this system can again be explained in terms of "ion exclusion". Thus the 2000 Å pores are almost totally permeable to polyacrylamide of molecular weight up to five million when charge effects are suppressed.

The effect of pH in the range studied is completely eliminated by addition of 300,000 MW polyethylene oxide with "collapse" of the data onto a single calibration curve. This competitive adsorption effect will be discussed more fully in section 4.

### 4. Effect of neutral surfactants on GPC elution volumes.

Figure 4 shows the effects of Tergitol and polyethylene oxide MW 300,000, on elution volumes using a column of 4 foot length and 2000 Å pore diameter. For Tergitol at various pH and ionic strength levels similar to those of Figures 2 and 3, the curves exhibit relatively good pore permeation and resolution and are similar, though not identical to each other. Thus Tergitol appears to modify but does not eliminate the effects of charge in this system. It may be postulated that this occurs through adsorption of the surfactant on the glass, thereby masking the surface charge and creating a new surface which is effectively uncharged and which, in addition, does not interact with polyacrylamide. This mechanism of charge suppression thus differs from

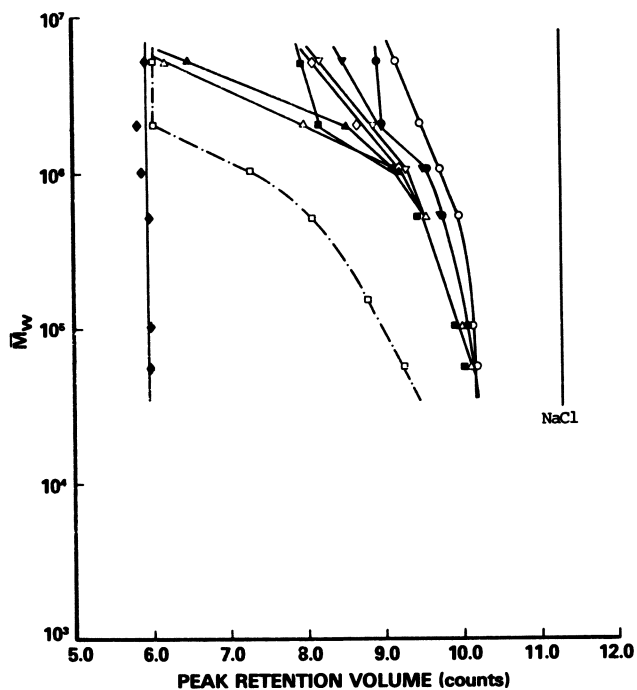


Figure 3. Molecular weight calibration curves for nonionic polyacrylamide for a single column (4 ft  $\times$   $\frac{3}{8}$  in. i.d.) containing 2000 Å CPG-10 (200/400 mesh) packing with aqueous solutions containing  $\text{Na}_2\text{SO}_4$  and  $\text{H}_2\text{SO}_4$ .

One mobile phase contains polyethylene oxide ( $\bar{M}_w = 300,000$ ) (For details see Table II). Mobile phase flow rate: 4.2 mL/min; ( $\blacklozenge$ ) water; ( $\square$ ) mobile phase containing polyethylene oxide ( $\bar{M}_w = 300,000$ ); ( $\triangle$ ) 0.0167M  $\text{Na}_2\text{SO}_4$ /0.005M  $\text{H}_2\text{SO}_4$  (pH = 2.28); ( $\blacktriangle$ ) 0.0167M  $\text{Na}_2\text{SO}_4$ /0.01M  $\text{H}_2\text{SO}_4$  (pH = 1.98); ( $\blacksquare$ ) 0.0033M  $\text{Na}_2\text{SO}_4$ /0.005M  $\text{H}_2\text{SO}_4$  (pH = 2.28); ( $\diamond$ ) 0.005M  $\text{H}_2\text{SO}_4$  (pH = 2.15); ( $\nabla$ ) 0.01M  $\text{H}_2\text{SO}_4$  (pH = 1.91); ( $\blacktriangledown$ ) 0.0312M  $\text{Na}_2\text{SO}_4$ /0.01M  $\text{H}_2\text{SO}_4$  (pH = 2.15); ( $\bullet$ ) 0.025M  $\text{H}_2\text{SO}_4$  (pH = 1.61); ( $\circ$ ) 0.0167M  $\text{Na}_2\text{SO}_4$ /0.025M  $\text{H}_2\text{SO}_4$  (pH = 1.62).

that involving pH and ionic strength in that whereas ion exclusion due to repulsion is prevented, attractive interactions are also inhibited. At low pH or high ionic strength, where charge effects are diminished, it is probable that physical adsorption of polyacrylamide occurs. That Tergitol does not completely suppress charge effects is shown by the slight differences in the calibration curves which show no clear trends but fluctuate randomly with pH and electrolyte concentration.

In the presence of polyethylene oxide MW 300,000 at a concentration of 0.025 g liter<sup>-1</sup>, variations in pH and ionic strength have no effect on elution volumes and a single calibration curve is obtained as shown in Figure 4 and Table II. This behavior presumably also results from modification of the glass surface by the polyethylene oxide surfactant, but in this case charge effects appear to be completely suppressed and the effective pore diameter and volume reduced. Such an interpretation is also in accord with the fact that the elution volumes are lower with polyethylene oxide than with Tergitol, since Tergitol is a much smaller molecule than the polyethylene oxide.

Table II. Peak Retention Volumes of Polyacrylamides with Polyethylene Oxide (300,000  $\bar{M}_w$ ) in Mobile Phase.

*Mobile-Phase	Peak Retention Volume (Counts)				
pH =	4.050	7.000	3.500	7.000	3.400
I =	0.025	0.025	0.025	0.250	0.100
<u>Sample</u>					
PAM 55	8.30	8.33	8.30	8.32	8.30
PAM 270	7.80	7.82	7.80	7.82	7.80
PAM 500	7.10	7.13	7.10	7.13	7.10
PAM 1000	6.35	6.40	6.35	6.40	6.35
PAM 2000	4.90	4.92	4.90	4.91	4.90
Std. A	4.80	4.80	4.80	4.80	4.80
ml/count	5.05	5.00	5.05	5.00	5.05

\*Mobile-phase contains 0.025 gm/l PEO (300,000  $\bar{M}_w$ )

Pore-Size: 2000 Å CPG-10 120/200 Mesh.

With a pore diameter of 2000 Å it is conceivable that the adsorbed polymer layer could significantly reduce the effective pore volume.

##### 5. Optimization of calibration curve.

The discussion thus far has dealt with composition of the mobile phase and its effects on deviations from ideal GPC behaviour, and we have presented data for a single column and single

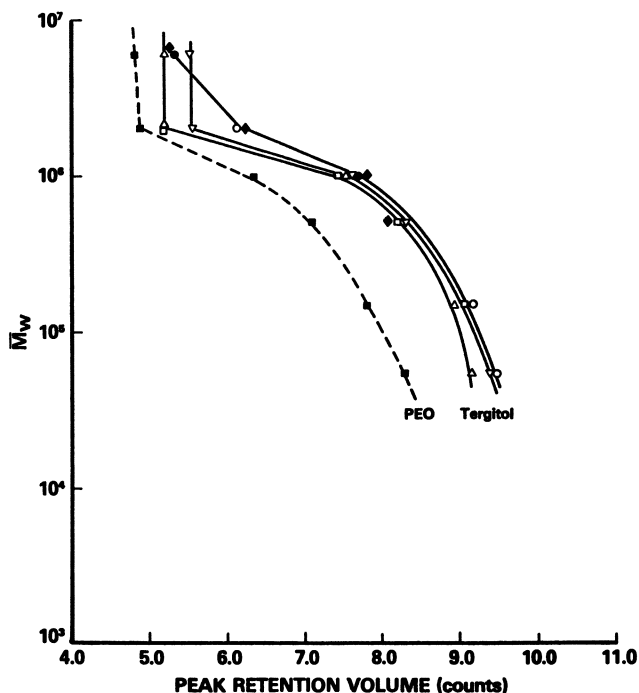


Figure 4. Molecular weight calibration curves for nonionic polyacrylamide for a single column (4 ft  $\times$   $\frac{3}{8}$  in. i.d.) containing 2000 Å CPG-10 (120/200 mesh) packing for a number of mobile phases containing either polyethylene oxide ( $\bar{M}_w = 300,000$ ) or Tergitol.

(■) See Table II for details of mobile phases; ( $\Delta$ ) 0.01M  $\text{KH}_2(\text{C}_2\text{O}_4)_2$  2H<sub>2</sub>O/0.02%  $\text{NaN}_3$ /1.0 gm/24 L T, pH = 2.50; (+) 0.0033M  $\text{Na}_2\text{SO}_4$ /0.02%  $\text{NaN}_3$ /1.0%  $\text{CH}_3\text{OH}$ /1.0 gm/24 L T, pH = 3.25; ( $\blacklozenge$ ) 0.0033M  $\text{Na}_2\text{SO}_4$ /0.02%  $\text{NaN}_3$ /1.0 gm/24 L T, pH = 2.75; (O) 0.05M KF/0.025 wt %  $\text{NaN}_3$ /1.0%  $\text{CH}_3\text{OH}$ /1.0 gm/16 L T; ( $\nabla$ ) 0.033M  $\text{Na}_2\text{SO}_4$ /1.0%  $\text{CH}_3\text{OH}$ /1.0 gm/24 L T, pH = 2.95.

pore size in order to simplify interpretation of these effects. Clearly if a useful calibration curve is to be obtained over a wide range of MW, it is necessary to use a multi-column system with a range of pore sizes corresponding to the molecular size range of interest. Data relevant to this question for CPG-10/polyacrylamide are shown in Figure 5 which present calibration curves on single columns of different pore sizes. These experiments were performed using an aqueous solution of 0.02 M  $\text{Na}_2\text{SO}_4$  containing 0.02 g  $\ell^{-1}$  Tergitol at pH 7. Under these conditions charge and adsorption effects should be minimal.

It is clear from Figure 5 that the smaller pore size columns, as expected, resolve the smaller molecules and exclude the larger ones while the larger pore size columns provide resolution for the larger molecules. Pore diameters of 3000 Å allow extensive permeation but little resolution of the intermediate molecular weight polyacrylamide samples when Tergitol was used in this study. With polyethylene oxide the reduction of pore diameter and volume with adsorption makes the 3000 Å most useful for the separation of the highest molecular weight polyacrylamides.

Figures 6, 7 and 9 show calibration curves using two multi-column combinations and illustrate the degree of "optimization" obtained in this system. The mobile phases for Figures 6 and 7 contained 0.025 g  $\ell^{-1}$  polyethylene oxide and ion exclusion and adsorption effects should therefore be largely eliminated. Figure 6 shows that reasonably good resolution can be obtained with a combination of five columns but does exhibit some loss of peak separation at the low and high MW ends. In Figure 7 the effect of adding a sixth column of small pore size is illustrated and it is seen that resolution at the low MW end is thereby somewhat improved. This calibration curve is effectively linear with a change of slope at 500,000 MW. It should provide a useful aqueous GPC system for MW and MWD determination of nonionic polyacrylamides.

The chromatograms obtained with the five column combination are shown in Figure 8, where Std.C a very high molecular weight, extensively hydrolysed polyacrylamide has been included to show the extensive separation possible at high molecular weights for this column combination and mobile phase. These chromatograms were used to estimate the molecular weights of the standards and then a comparison with the manufacturer's values was made in Table III. The single-species variance ( $\sigma^2$ ) gives a measure of peak broadening for the system, and the slope of the molecular weight calibration curve a measure of peak separation. The molecular weight correction factor P indicates that corrections for imperfect resolution for the three highest molecular weight standards is quite small being about 4%. The rather large corrections for the 55,000 and 500,000 standards is surprising. There is no obvious explanation for this result. One might speculate that these smaller molecules experience a certain amount of adsorption as they have a larger available pore volume and are thus exposed to a

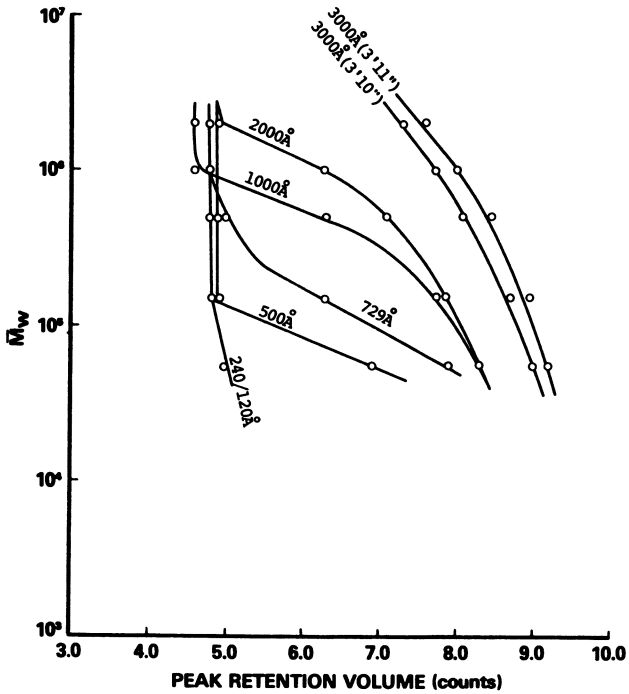


Figure 5. Molecular weight calibration curves for nonionic polyacrylamides for a number of single columns (4 ft  $\times$   $\frac{3}{8}$  in. i.d.) containing CPG-10 (200/400 mesh) packing.

Mobile phase: see Table II for details of mobile phases; all contain polyethylene oxide ( $\bar{M}_w = 300,000$ ); mobile phase flow rate: 4.2 mL/min.

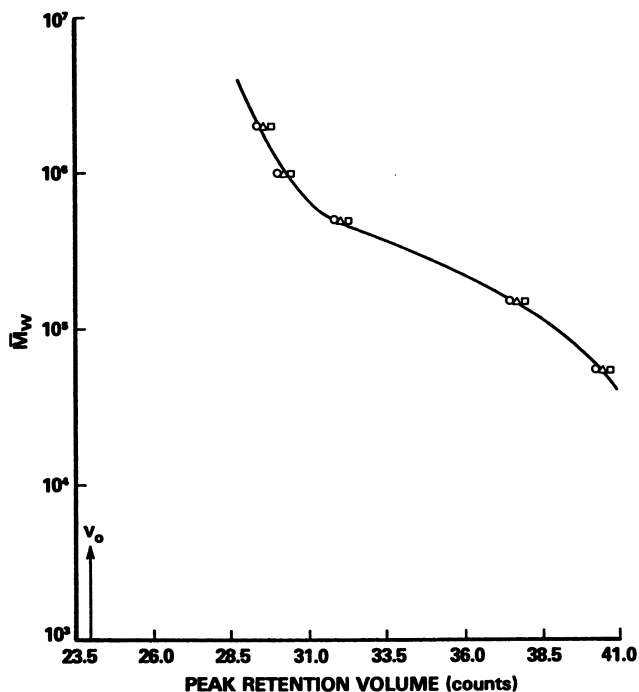


Figure 6. Molecular weight calibration curve for nonionic polyacrylamides for a 5-column combination (each 4 ft  $\times$   $\frac{3}{8}$  in. i.d.) with 3000 Å, 3000 Å, 2000 Å, 1000 Å, and 729 Å CPG-10 (200/400 mesh) packing.

Mobile phases: (○) pH = 7.0, I = 0.025; (△) pH = 7.0, I = 0.25; (□) pH = 3.5, I = 0.025. All solutions contain 0.025 gm/L polyethylene oxide, 1.50 gm/24 L Tergitol, and 2.5%  $\text{CH}_3\text{OH}$ ; mobile phase flow rate: 2.0 mL/min.

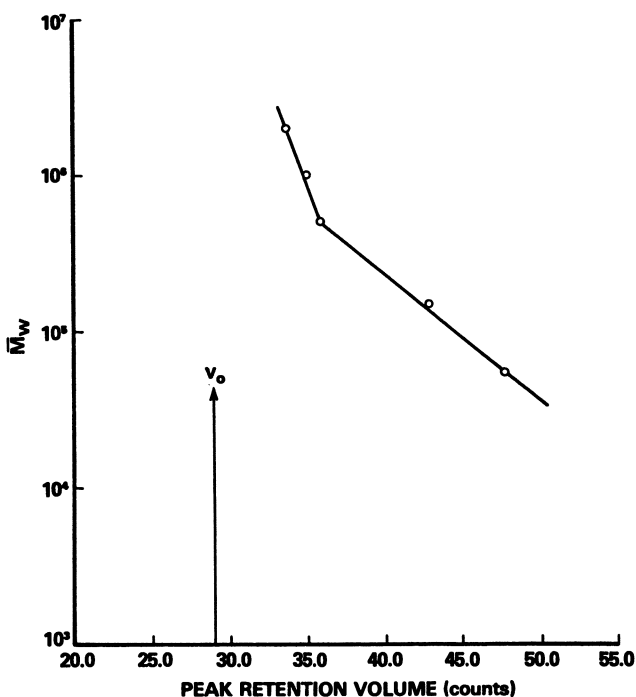


Figure 7. Molecular weight calibration curve for nonionic polyacrylamides for a 6-column combination (each 4 ft  $\times$   $\frac{3}{8}$  in. i.d.) with 3000 Å, 3000 Å, 2000 Å, 1000 Å, 729 Å, and 500 Å CPG-10 (200/400 mesh) packing.

Mobile phase: pH = 7.0, I = 0.25, 0.025 gm/L polyethylene oxide, 1.5 gm/24 L Tergitol, 2.5%  $\text{CH}_3\text{OH}$ ; mobile phase flow rate: 2.0 mL/min.

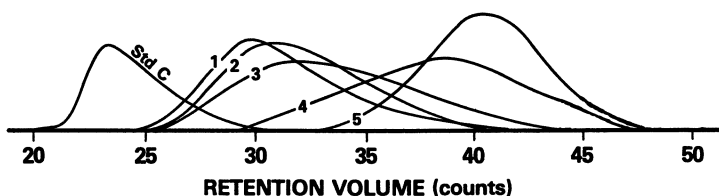


Figure 8. Chromatograms for nonionic polyacrylamide standards and Standard C for the column combination shown in Figure 6.

Mobile phase: pH = 7.0, I = 0.25, 0.025 gm/L polyethylene oxide, 1.5 gm/24 L Tergitol, 2.5%  $\text{CH}_3\text{OH}$ ; mobile phase flow rate: 2 mL/min. (1) PAM 2000; (2) PAM 1000; (3) PAM 500; (4) PAM 270; (5) PAM 55; all at 0.05 wt %; Standard C at 0.03 wt %.



Table III. Molecular Weight Calculations on Nonionic PAM Standards - Polyethylene Oxide in Mobile Phase.

Reported $\bar{M}_W \times 10^{-4}$	$\bar{M}_W$ (uc) * $\times 10^{-4}$	$\bar{M}_N$ (uc) * $\times 10^{-4}$	$\sigma^2$ (counts <sup>2</sup> )	P **
5.50	7.6	4.1	5.65	0.72
50.00	76.1	30.2	7.22	0.66
100.00	95.8	41.6	-	1.04
200.00	209.0	106.0	0.74	0.96
336.0 (Standard B)	356.0	162.0	0.80	0.96

\* Number and weight average molecular weights for Polysciences Standards and McMaster Standard B, calculated from raw chromatograms using the molecular weight calibration curve  $M(V) = 0.20 \times 10^{11} \exp(-0.341 V - 0.006 V^2)$  with V in counts (1 count = 5 ml).

\*\*  $P = \exp(-(D_2\sigma)^2 / 2)$  with  $D_2$  the slope of the molecular weight calibration curve at the peak position of the chromatogram of the Standard.

much larger surface area. The high molecular weight polyethylene oxide may be excluded from some of these same pores and thus be ineffective in preventing adsorption. The observation that the variance of the single-species chromatograms decreases with increase in molecular size is consistent with the observations of Tung and Runyon (9) who found a maximum in the variance at an intermediate molecular weight. Finally, Figures 9 and 10 and Table IV show a molecular weight calibration curve for a mobile phase containing Tergitol but no polyethylene oxide, the associated chromatograms and calculations of the weight average molecular weights for the polyacrylamide standards. Excellent peak separation over a wide molecular weight range is indicated. In fact, peak separation is better with Tergitol in the absence of polyethylene oxide at the high molecular weight end. However, the calculated weight average molecular weights for the 55,000 and 500,000 PAM standards are again considerably larger than reported by Polysciences. The previous explanation concerning possible adsorption of the lower molecular weight PAM standards would not be relevant in the absence of high molecular weight polyethylene oxide. We cannot offer a reasonable explanation for this observation.

#### 6. Relation of Present Results to Existing Literature

Two recent attempts to develop aqueous GPC for the characterization of nonionic polyacrylamide have been reported (10,11). The first (10) employed controlled porosity glass (CPG-10) with formamide containing KCl (0.005 M) as the mobile phase. The

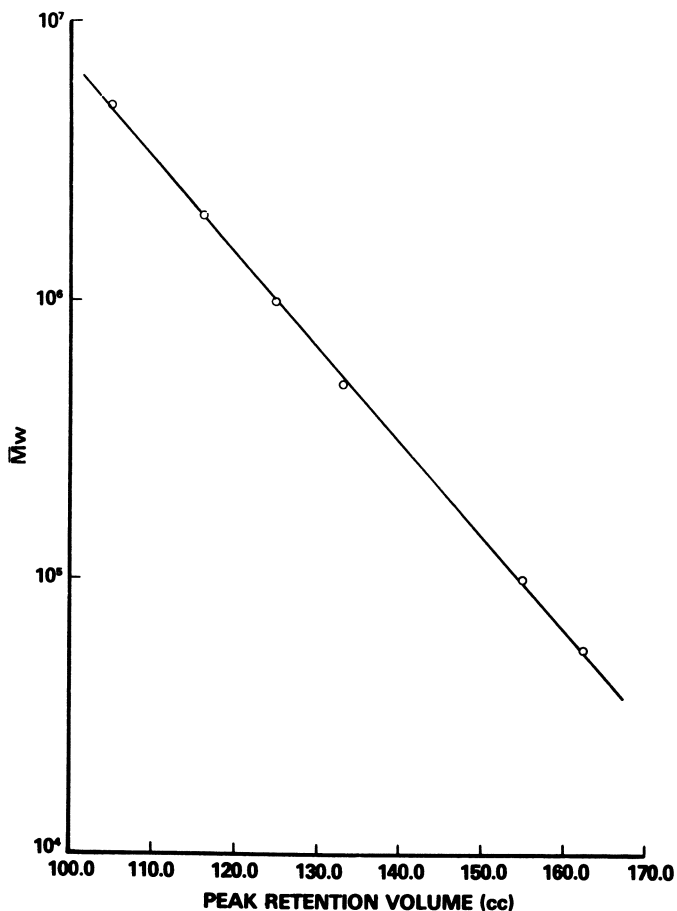


Figure 9. Molecular weight calibration curve for nonionic polyacrylamides for a 4-column combination (each 4 ft  $\times$   $\frac{3}{8}$  in. i.d.) with 3000 Å, 3000 Å, 1000 Å, and 370 Å GPC-10 (200/400 mesh) packing.

Mobile phase: 0.0167M  $\text{Na}_2\text{SO}_4$ /1.0%  $\text{CH}_3\text{OH}$ /0.05 wt %  $\text{NaN}_3$ /0.5 gm/24 L Tergitol; mobile phase flow rate: 4.2 mL/min.

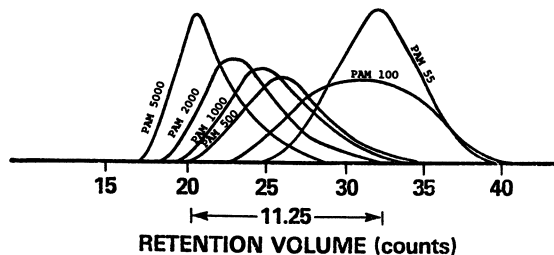


Figure 10. Chromatograms for nonionic polyacrylamide standards for the column combination (mobile phase and flow rate given in Figure 9)

Table IV. Molecular Weight Calculations on Nonionic PAM Standards - Tergitol in Mobile Phase (no Polyethylene Oxide)

Reported $\bar{M}_W \times 10^{-4}$	$\bar{M}_W$ (uc) * $\times 10^{-4}$	$\bar{M}_N$ (uc) * $\times 10^{-4}$	$\sigma^2$ (counts <sup>2</sup> )	P **
5.50	9.20	3.30	6.8	0.60
50.0	79.8	31.6	6.2	0.63
100.0	102.	39.2	0.21	0.98
200.0	207.	106.	0.47	0.97
500.0	387.	198.	-	1.29

\* Number and weight average molecular weights for Polysciences Standards calculated from raw chromatograms using the molecular weight calibration curve  $M(V) = 1.412 \times 10^{10} \exp(-.390 V)$  (1 count = 5 ml).

\*\*  $P = \exp(-(D_2\sigma)^2/2)$

Investigation was not comprehensive and the final separations achieved were not impressive. Four 4 ft. columns containing 3125Å, 486Å, 255Å and 75Å packing gave a 19.4 ml separation for molecular weights in the range of about 120,000 to  $5 \times 10^6$ . The use of 255Å and 75Å packing for high molecular weight polyacrylamides is not recommended based on our observations with single columns containing one pore size. No discussion is made of peak broadening. The second study (11) employed a newly commercialized organic gel packing TSK-GEL type PW (Toyo Soda Manufacturing Co., Japan). The packing particles were 15 microns in diameter. A 0.08 M tris-HCl buffer solution (pH = 7.94) was used as mobile phase. The peak separation obtained with a three column set (G 3000 PW + 2 G5000 PW) is comparable to the peak separation obtained in the present study for the molecular weight range, 120,000 to  $3.6 \times 10^6$ . Peak broadening appeared to be appreciable although no calculations of single-species variance were done.

### References

1. Neddermeyer, P.A., Rogers, L.B., *Anal. Chem.*, 1969, 41, 94.
2. Buytenhuys, F.A., Van Der Maeden, F.P.B., *J. of Chromatography*, 1978, 149, 489.
3. Abdel-Alim, A.H., Ph.D. Thesis, McMaster University (1973).
4. Cooper, A.R. and Matzinger, D.P., *J. Appl. Polym. Sci.*, 1979, 23, 419.
5. Rodriguez, H.T., *Anal. Lett.*, 1976, 9, 497.
6. Sygisaka, N., Petracek, F.J., *Fed. Proc., Fed. Amer. Soc. Exp. Biol.* 1977, 36, 89.
7. Spaterico, A.L., *J. of Appl. Polym. Sci.*, 1975, 19, 1601
8. Hendrickson, F.G., *J. Polym. Sci. A-2*, 1968, 6, 1903.
9. Tung, L.H. and Runyon, F.R., *J. Appl. Polym. Sci.*, 1969, 13, 2397.

10. Ibdam N., Furusawa, K., Yamaguchi, N., Komuro, S., J. of Appl. Poly. Sci., 1979, 23, 3631
11. Hashimoto, T., Sasaki, H., Aiura, M., Kato, Y., J. Poly. Sci., Poly. Physic. Edt., 1978, 16, 1789.

RECEIVED May 29, 1980.

## Biological Applications on Spherogel TSK-SW-Type Gel

### A New High-Performance Support for Aqueous Size Exclusion Chromatography

R. SOMACK, V. S. McKAY, and J. W. GILES

Altex Scientific, Inc., 1780 Fourth Street, Berkeley, CA 94710

Among the principal techniques used for the purification of proteins and other macromolecules of biological systems are size exclusion (gel filtration), ion-exchange, and biospecific affinity chromatography. Several very useful cellulosic, dextran, and polyacrylamide column materials have been available for some time for these types of chromatography. The essential properties of these stationary phase materials are their large porosities and hydrophilic surfaces which minimize undesirable interactions between solutes and the stationary phase. While these materials have been extremely useful in uncountable studies, they are not without disadvantages. Their drawbacks result from a lack of rigidity which causes their degree of swelling to change markedly in response to changes in pH or ionic strength. An even more serious consequence of their non-rigidity is a high susceptibility to compression when solvent flow rates exceed rather low limits. The restriction to quite slow flow rates when these compressible gels are used often extends the time required for a typical separation to many hours or even a few days (1).

Until recently, most efforts to develop rigid size exclusion or ion-exchange supports which do not adsorb or denature proteins and which would be compatible with a high performance liquid chromatography have met with little success. "Controlled porosity glass" supports have been developed (2, 3, 4), but the reactive exposed silanol groups irreversibly adsorb or denature many proteins (5). Attempts to eliminate these effects by coating the glass surface with various reagents have met with limited success (6, 7, 8, 9, 10). However, masking the reactive silica surface with carbohydrate like bonded phases appears to have eliminated some of these effects (11, 12). More recently, maximum coverage microparticulate bonded silica supports have been described which appear to exhibit the desired properties of low adsorption and high resolution (13, 14). In this study we have examined the suitability of Spherogel-TSK Type SW<sup>R</sup>, a new size exclusion support

of the latter type, for rapid, high resolution separations commonly encountered in biochemical research.

### Experimental Methods

High Performance Liquid Chromatography. All separations were performed using an Altex Scientific (1780 Fourth Street, Berkeley, CA 94710) Model 320 Advance Research Chromatograph, consisting of a model 100A dual piston analytical pump, a Model 153 UV detector, a Model 210 injection valve, and a Model 155 recorder. The columns (600 x 7.5mm) evaluated were the Spherogel TSK-SW-2000 and SW-3000 (Altex). Unless otherwise stated, all separations were carried out at 23° - 25°.

Proteins. Standard proteins for column calibration curves were obtained from Boehringer Mannheim. The methods outlined by Latham et al, (15) were followed to prepare and label crude rat liver nuclear extract with [<sup>125</sup>I]-triiodothyronine. Normal control serum was from Ortho Diagnostics and instant non-fat dry milk from Carnation. Alpha-chymotrypsin and alpha-casein were purchased from Sigma. Crude myosin subfragment 1 (S1) was purified by alpha-chymotryptic digestion of myosin using the method of Weeds and Taylor (16). A fraction containing all three myosin light chains was isolated as described by Holt and Lowry (17). All myosin derived proteins were dialyzed against mobile phase buffer consisting of 50 mM Na<sub>3</sub>PO<sub>4</sub> (pH 7.4), 0.2 M (NH<sub>4</sub>)<sub>2</sub>SO<sub>4</sub>, 1 mM EDTA, 0.2 mM dithiothreitol and 0.02% NaN<sub>3</sub>.

Assays. Protein concentrations were measured by the method of Bradford (18) and the various contractile protein ATPase activities by the method of Martin and Doty (19). Gel electrophoresis was carried out by the method of Ames (20) on 1.5 mm polyacrylamide slabs using the discontinuous SDS buffer system of Laemmli (21). Dried gels were scanned at 550 nm for densitometry measurements.

### Results and Discussion

Calibration Curves and Efficiency. Protein calibration curves for both the SW-2000 and SW-3000 columns are shown in Figure 1. Good linearity was evident over the range of molecular weights used with each column. However, cytochrome C which is a small, very basic protein eluted sooner than expected when chromatographed on the SW-2000 column. The fractionation of a mixture of four standard proteins ranging in molecular weight from 15,000 to 150,000 on the SW-2000 column is shown in the same figure. The recovery of absorbance units was essentially complete and no adsorption of the proteins tested was evident at the concentration of phosphate buffer used (0.2 M).

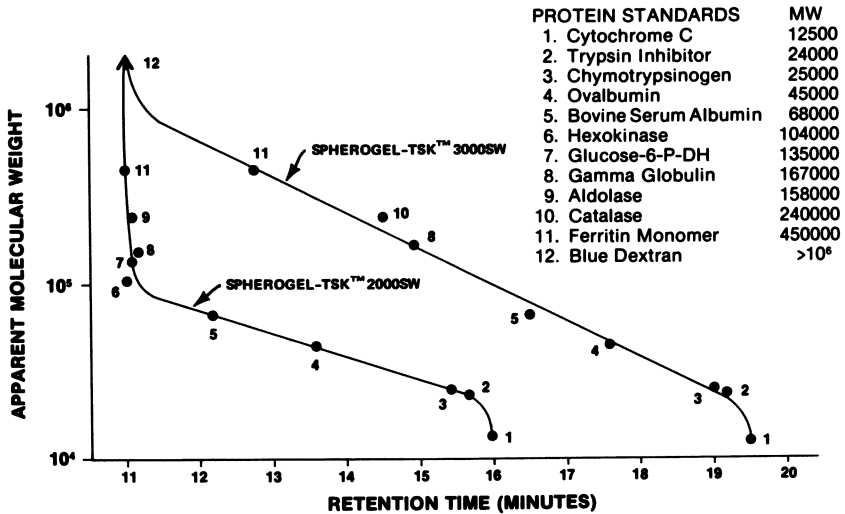
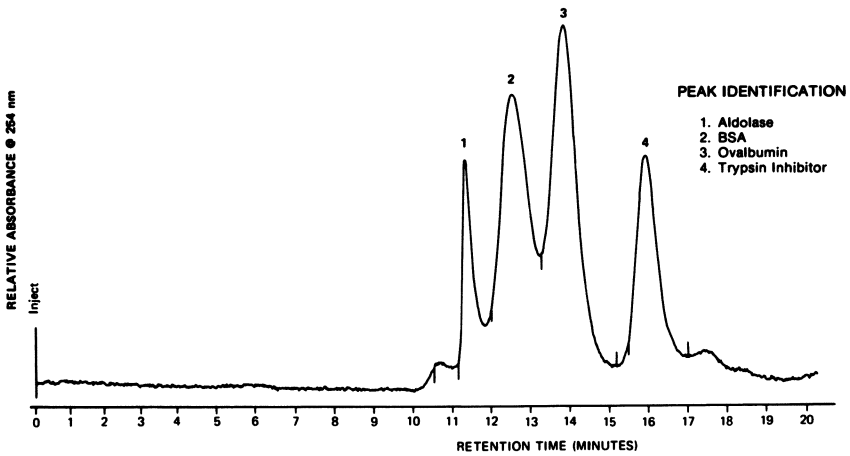


Figure 1. Protein calibration curves for the Spherogel TSK-SW 2000 and SW 3000 columns. Ten  $\mu\text{L}$  containing 10–100  $\mu\text{g}$  of each protein in 0.2M KPO<sub>4</sub> buffer (pH 6.8) was chromatographed in the same buffer at 1.0 mL/min. Detection was at 254 nm  $\times$  0.16 AUFS; pressure: 500 psi. A chromatogram of 4 proteins on the SW 2000 column is also shown.

Figure 2 shows the effect of flow rate on column efficiency using the SW-2000 column with cytochrome C. The column efficiency expressed as the number of theoretical plates ( $N$ ) was dependent on flow rate, a result typical of size exclusion chromatography.

Fractionation of Serum and Column Capacity. A Fractionation of human serum on the SW-3000 column is shown in Figure 3. A definitive identification of the proteins in each peak is not possible, however, the elution times of the peaks at 13-14 min. and 15 min. are close to the times which would be expected for gamma-globulins and albumins, two of the principal classes of serum proteins. These data also indicate the loading capacity of this column with serum. More than 14 mg. of undiluted serum was injected before evidence of overloading in the form of band broadening and peak distortion was observed.

Milk Proteins. Size exclusion chromatography is commonly used in biochemistry to observe interactive processes between proteins. We tested the capability of the SW-2000 gel to follow such phenomena in milk. Figure 4 shows the 254 nm absorbing profiles obtained after chromatographing identical volumes of three dilutions of non-fat dry milk in 0.2 M  $\text{PO}_4$  buffer, at pH 7. While the data are not amenable to quantitative analysis, dilution appears to have caused disaggregation of higher molecular weight material in the first peak with a concomitant accumulation of lower molecular weight material in the third peak. In order to establish that this effect was not due to the difference in total mass chromatographed, 10  $\mu\text{l}$  of undiluted whole milk was injected using a 10  $\mu\text{l}$  loop and the result compared to a run where 100  $\mu\text{l}$  of a 1:10 dilution was injected using a 100  $\mu\text{l}$  loop. Although the same sample mass was applied in both cases, the apparent disaggregation was still observed (data not shown). A similar effect was observed in whole milk. Upon rechromatographing material collected from the first peak, a shift of much of the material to a later eluting position occurred (Figure 5). A similar dilution effect can also be observed by chromatographing alpha-casein alone at different concentrations (Figure 6). Initially, the protein was chromatographed at approximately the same concentration at which it is present in whole milk. After diluting the protein 1:10, the profile clearly showed the disaggregation of material with a molecular weight of 80,000 daltons or greater. These observations are consistent with the known properties of alpha-casein, the major protein found in milk. Dry milk is 25% casein by weight, half of which is alpha-casein (22). The alpha-casein fraction makes up 50% of the total milk protein and all of the casein in milk participates in complex, reversible aggregation (23, 24). It seems reasonable to speculate that these dilution effects observed in whole milk are due to the disassociation of high molecular weight casein aggregates. High performance size



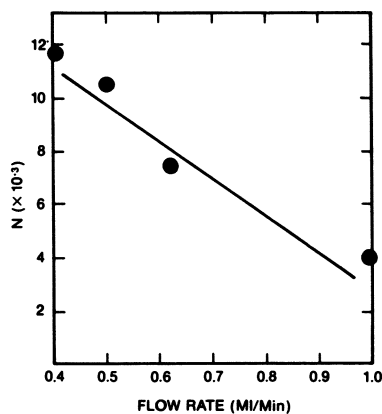


Figure 2. Effect of flow rate on the efficiency ( $N$ ) of the Spherogel TSK-SW 2000 column. The conditions were as indicated in Figure 1 using cytochrome C as test solute.

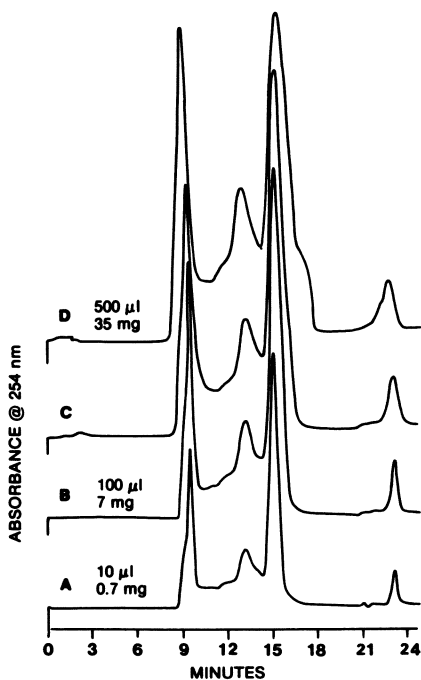
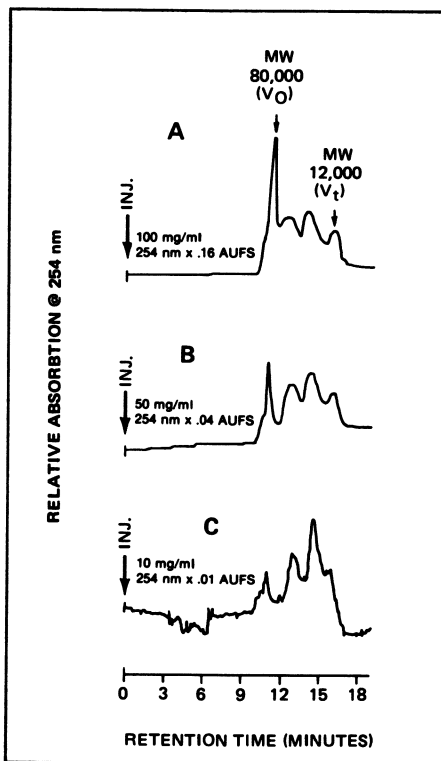


Figure 3. Fractionation of human serum proteins on Spherogel TSK-SW 3000. The conditions were as in Figure 1. The analyses were made using (A) a 50- $\mu$ L injection loop with an analytical flow cell; (B) a 100- $\mu$ L loop with a semipreparative flow cell; or (C, D) a 500- $\mu$ L loop with a preparative flow cell.



*Figure 4. Effect of sample concentration on the distribution of milk proteins on Spherogel TSK-SW 2000 column. Instant, nonfat, dry milk was dissolved in mobile phase at the indicated concentrations and 10- $\mu$ L aliquots injected under the conditions outlined in Figure 1.*

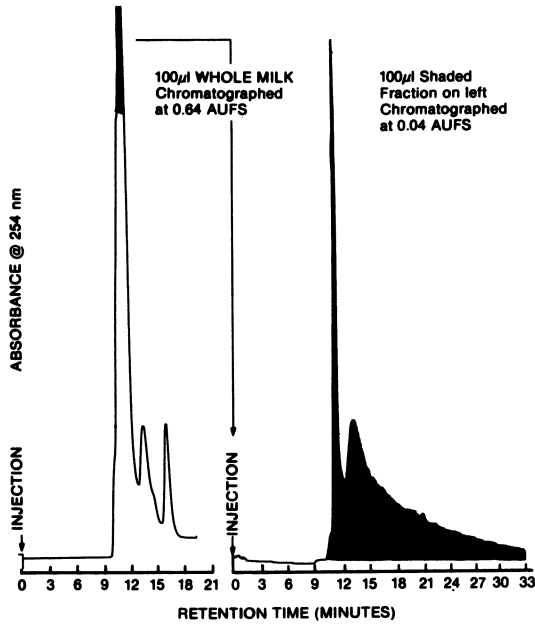


Figure 5. Redistribution of higher molecular weight milk proteins on the SW 2000 column. Whole milk (100  $\mu$ L) was fractionated under the conditions indicated in Figure 4. A 100- $\mu$ L aliquot of eluant collected from the shaded portion of the profile on the left was rechromatographed as shown on the right.

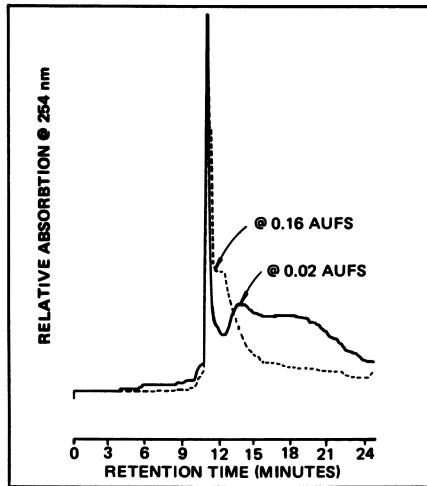


Figure 6. Fractionation of  $\alpha$ -casein on the SW 2000 column at 25 mg/mL (---) and 2.5 mg/mL (—). The conditions were shown in Figure 4.

exclusion chromatography promises to become a powerful technique for studying these types of phenomena in complex mixtures.

Purification of T<sub>3</sub>-binding Proteins. Another phenomenon in biology commonly studied by size exclusion chromatography is the interaction of proteins with small molecules. We tested the utility of the SW-3000 column in purifying the thyroid hormone nuclear binding protein from liver cell nuclei. These receptors have been previously purified by adding radioactive triiodothyronine (T<sub>3</sub>) to crude nuclear extracts, followed by conventional gel chromatography on soft carbohydrate gels (15). Nuclear extract containing approximately 100 µg of protein was incubated with [<sup>125</sup>I]-T<sub>3</sub> for two hours and chilled to 0°. An aliquot (100 µl) containing approximately 20 µg of nucleoprotein was applied at 0 - 4° C and a flow rate of 1 ml/min. The bulk of largely excluded nucleoprotein is clearly separated from the highly purified [<sup>125</sup>I]-T<sub>3</sub> - labelled receptor-complex (Figure 7). A large excess of unlabelled T<sub>3</sub> abolishes most of the specific binding. Essentially the same method was used by Latham, Ring and Baxter (15) using Sephadex G-100, however approximately five running hours were required. The high resolution, speed and reproducibility of this separation are currently being exploited to study interactions between purified hormone receptors and nuclear histones. Clearly, the potential of these columns for studying similar interactions is considerable.

Skeletal Muscle Contractile Proteins. The Spherogel columns were also tested for their suitability for purifying contractile proteins from skeletal muscle. A crude alpha-chymotryptic digest of myosin was fractionated on the SW-3000 column (Figure 8). This digest contains the two subfragments, S1 (LC<sub>1</sub>) and S1 (LC<sub>3</sub>) with reported molecular weights of 116,000 and 121,000 daltons, respectively (25, 26). The difference in size is due to the type of light chain (LC) associated with a common heavy chain (S1) of about 100,000 daltons. Polyacrylamide gel electrophoresis of eluate from the leading and trailing edges of the major peaks indicates a high degree of purification and confirmed that the first peak contains S1 (LC<sub>3</sub>) and the second, S1 (LC<sub>1</sub>). Heavy meromyosin (HMM) eluted in the excluded volume. The apparent molecular weights of the subfragments derived from this run are 140,000 daltons for S1 (LC<sub>3</sub>) and 158,000 daltons for S1 (LC<sub>1</sub>) which are higher than reported values estimated by gel electrophoresis (26). The protein recoveries in this run were nearly quantitative and the ATPase activities of HPLC-purified S1's (K<sup>+</sup>-EDTA-ATPase, Mg<sup>2+</sup>-ATPase and actin-activated ATPase) compared well with the published values for S1 purified by conventional size exclusion chromatography (26).

All three myosin light chains (LC<sub>1</sub>, LC<sub>2</sub> and LC<sub>3</sub>) were chromatographed on the SW-2000 column (Figure 9). The absorbance profile at 254 nm showed four major peaks, the last of which

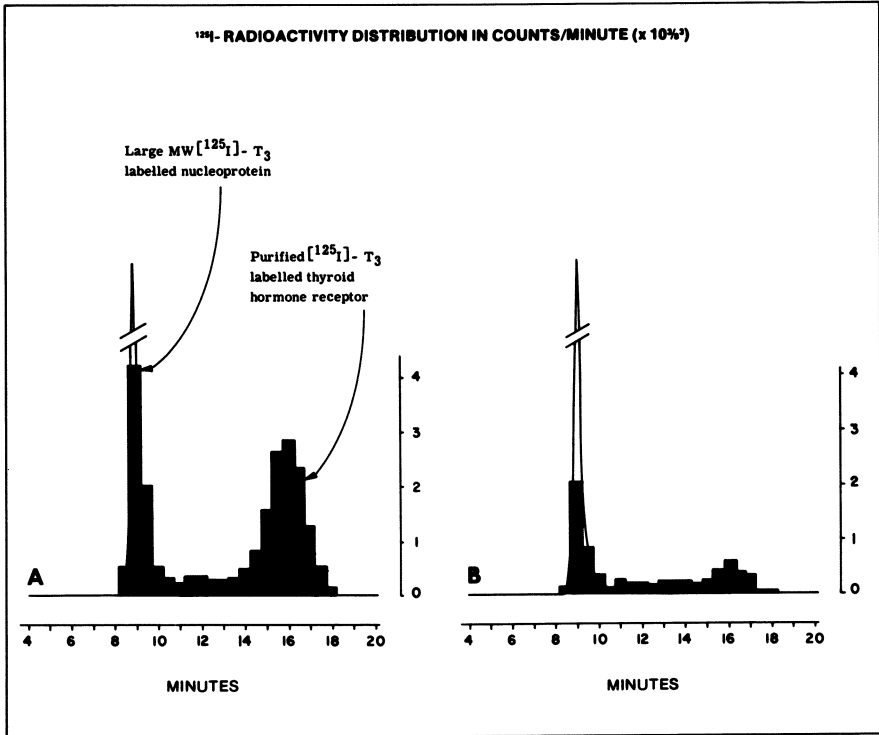


**Figure 7.** Purification of  $\text{T}_3$  nuclear receptors on the SW 3000 column. Crude liver nuclear extract was prepared and incubated with  $^{125}\text{I}$ - $\text{T}_3$ , as outlined in the Methods section. In A, 100  $\mu\text{L}$  of extract were injected and chromatographed at  $4^\circ$  using a mobile phase containing 50mM  $\text{NaPO}_4$  (pH 7), 0.2M  $\text{NH}_4\text{SO}_4$ , 1mM EDTA, 0.1mM dithiothreitol, and 5% glycerol; pressure: 700 psi. The profile shown in B was obtained after a 100-fold excess of unlabeled  $\text{T}_3$  was added to the  $^{125}\text{I}$ -labeled extract used in A.

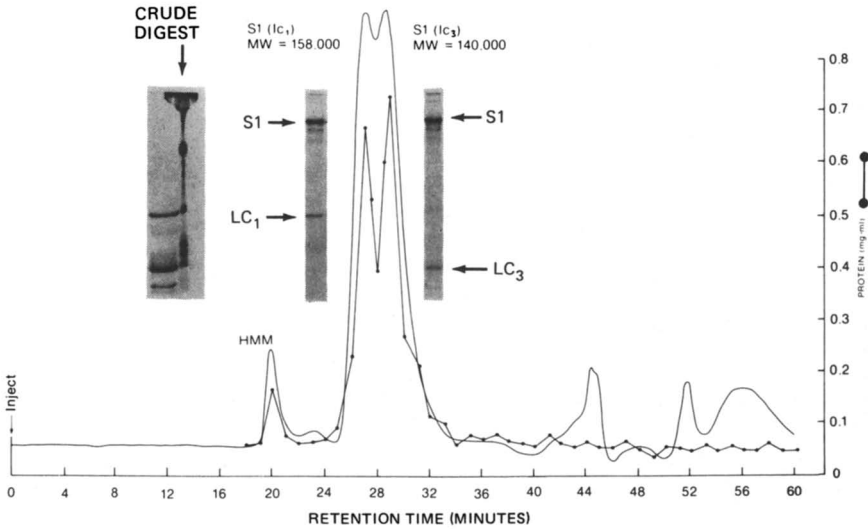


**Figure 8.** Fractionation of  $\alpha$ -chymotryptic digest of myosin on the SW-3000 column. A 500- $\mu$ L aliquot of crude digest containing 8.5 mg/mL of protein (see Methods section) was chromatographed as in Figure 7 at 24 $^{\circ}$  with a flow rate of 0.5 mL/min.

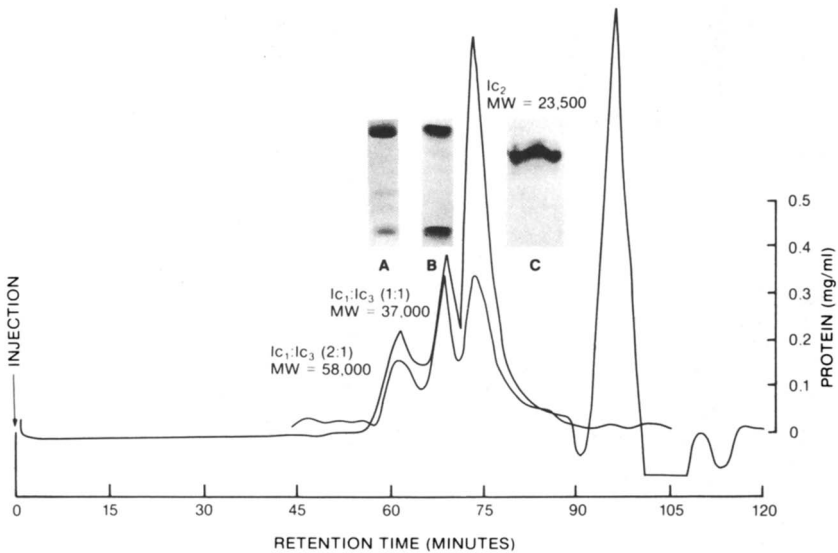


**Figure 9.** Fractionation of myosin light chains on the SW-2000 column. A 500- $\mu$ L aliquot of a mixture of light chains containing 10.0 mg/mL of protein (see Methods section) was chromatographed as in Figure 8 at a flow rate of 0.2 mL/min.

eluted after the total permeation volume. The protein profile, however, indicated that only the first three peaks contained protein. The apparent molecular weights of these peaks calculated from the retention times were 58,000, 36,000, and 23,500 daltons. Densitometry of electrophoretic gels run with aliquots from the column fractions confirmed that peak 1 consisted of a 2:1 mixture of LC<sub>1</sub> to LC<sub>3</sub>, peak 2, at 1:1 mixture of LC<sub>1</sub> to LC<sub>3</sub> and peak 3 was pure LC<sub>2</sub>. The molecular weights of the individual light chains estimated from these results are reasonable consistent with the accepted values of 20,000, 21,000 and 16,000 dalts for LC<sub>2</sub>, LC<sub>1</sub> and LC<sub>3</sub>, respectively. Similar LC<sub>1</sub> and LC<sub>3</sub> aggregates were reported using blue-sepharose chromatography (27).

These high performance size exclusion separations of alpha-chymotrypsin S1 and myosin light chains compare favorably with those achieved by ion exchange chromatography but require only a fraction of the time to accomplish. Furthermore, the very short retention times allow for separation of these labile proteins at room temperature, whereas operation at 0-40° C would otherwise be mandatory to avoid the loss of enzymatic activity.

### Abstract

The silica-based Spherogel TSK-SW 2000 and SW 3000 columns designed for aqueous size exclusion chromatography were evaluated for their ability to perform a variety of protein separations commonly encountered in biochemical research. These columns proved to be excellent for carrying out high speed, high resolution analytical and preparative separations of proteins. Little, if any, protein adsorption was noted with the proteins tested even when complex samples such as serum of milk proteins were chromatographed. Excellent recoveries of multiple enzymatic activities were achieved in the purification of contractile muscle subfragments with labile ATPase activity.

### Acknowledgement

The author gratefully acknowledges the cooperation of Dr. Roger Cooke, the Department of Biochemistry and Biophysics, U.C.S.F., for contractile protein-related materials and assays.

Literature Cited

- 1 Heftmann, E., "Chromatography," Reinhold Publishing Corp., New York, 1967, p. 405-428.
- 2 Haller, W., "Materials and Methods for Performing Steric Separations," U.S. Patent 3,549,524.
- 3 Bock, H. G., Skene, P., Fleischer, S., Cassidy, P., and Harshman, S., "Science", 1976, 191, 380.
- 4 Cooper, A. R., Bruzzone, A. R., Cain, J. H., and Barrall II, E. M., J. Appl. Polym. Sci., 1971, 15, 571.
- 5 Mizutani, T., and Mizutani, A., J. Chromatogr., 1979, 168, 143-150.
- 6 Hiatte, C. W., Shelokov, A., Rosenthal, E. J., and Galimore, J. M., J. Chromatogr., 1971, 56, 362.
- 7 Hawk, G. L., Cameron, J. A., and DuFault, L. B., Prep. Biochem., 1972, 2, 193.
- 8 Frenkel, M. J., and Blagrove, R. J., J. Chromatogr., 1975, 111, 397.
- 9 Mizutani, T., and Mizutani, A., J. Chromatogr., 1975, 111, 214.
- 10 Mizutani, T., and Mizutani, A., J. Chromatogr., 1976, 120, 206.
- 11 Regnier, F. E., and Noel, R., J. Chromatogr. Sci., 1976, 14, 316.
- 12 Persiani, C., Cukor, P., and French, K., J. Chromatogr. Sci., 1976, 14, 417.
- 13 Vivilecchia, R. V., Lightbody, B. G., Thimot, N. Z., and Quinn, H. M., J. Chromatogr. Sci., 1977, 15.
- 14 Fukano, K., Komiya, K., Sasaki, H., and Hashimoto, T., J. Chromatogr., 1978, 166, 47.
- 15 Latham, K. R., Ring, J. C., Baxter, J. D., J. Biol. Chem., 1976, 251, 7388.
- 16 Weeds, A. G., and Taylor, R. S., Nature (London), 1975, 257, 54.
- 17 Holt, J. C., and Lowey, S., Biochemistry, 1975, 14, 4600.
- 18 Bradford, M., Anal. Biochem., 1976, 72, 248.
- 19 Martin, J. B., and Doty, D. M., Anal. Chem., 1949, 21, 965.
- 20 Ames, G. F., J. Biol. Chem., 1974, 249, 634.
- 21 Laemmli, U. K., Nature (London), 1970, 227, 680.
- 22 Fennema, O. R., ed., "Principles of Food Science, Part I", Marcel Dekker, Inc., New York, 1976, p. 619.
- 23 Dalglish, D. G., "Recent Advances in the Physical Chemistry of Milk Proteins", International Dairy Congress, Paris, 1978, p. 745T.
- 24 Yaguchi, M., and Rose, D., J. Dairy Sci., 1971, 54, 1725.
- 25 Lowey, S., Slayter, H. S., Weeds, A. G., and Baker, H., J. Mol. Biol., 1969, 42, 1.
- 26 Cooke, R., Biochem. Biophys. Res. Comm., 1972, 49, 1028.
- 27 Toste, A. P., and Cooke, R., Anal. Biochem., 1979, 95, 317.

RECEIVED May 27, 1980.



# Use of Sephadex Gels with Aqueous Pyridine Solvent to Determine Purity Levels of Hydrophilic Polymeric Dyes Containing Hydrophobic Impurities

ANTHONY R. COOPER and DENA S. VAN DERVEER<sup>1</sup>

Process Development, Dynapol, 1454 Page Mill Road, Palo Alto, CA 94304

A new series of dyes (1), intended for screening as potential food additives, has been prepared by coupling reactive chromophores to a polymer backbone (2,3). This backbone provides the steric requirement for non-absorbability when ingested, and may also be tailored to produce a water-soluble dye from a water-insoluble chromophore. However, this introduces unique problems in both purification (4) and analysis of these polymeric dyes, because the hydrophobic character of the chromophore or its simple derivatives has the ability of binding strongly to the dye. The method described here has been developed for quantitative analysis of the hydrophobic impurities in the water-soluble polymeric dye product.

Sephadex<sup>®</sup>, a dextran gel cross-linked with epichlorohydrin, has been successfully used as a separation medium in a variety of biological and chemical applications. The gel may act as a molecular sieve to separate molecules on the basis of size, but can also separate molecules of similar size on the basis of polarity and available hydrogen  $\pi$ -bonding (5,6,7,8). For example, phenol was found to be significantly retarded in elution time due to interaction with the ether linkages in the tighter dextran gels G-10, G-15 and G-25 and especially LH-20 prepared by hydroxy alkylation of Sephadex G-25 (9). The choice of solvent pH and ionic strength also affects the separation of indole acids (10). Gelotte (5) found that acidic amino acids were excluded from Sephadex G-25, aromatic amino acids were adsorbed slightly, and basic amino acids were strongly absorbed when water was used as a solvent; however, these effects were negated in the presence of salt. Modification of the chromatographic properties of Sephadex has also been reported, using aqueous mixtures with pyridine (11,12) or alcohols (13,14,15). Marsden has discussed the theory of internal solvent composition of a gel in a mixed solvent (16). Thus, by careful selection of column packing and solvent composition, an optimal separation between a water-soluble polymer and hydrophobic impurities may be achieved.

<sup>1</sup>Current address: Geology Dept., U.C.S.B., Santa Barbara, CA.

## Experimental

The polymeric dye used for this study was made by coupling a bromo-anthrapyridone (Br·AMP), synthesized in-house, to an amino-ethylene-sodium ethylene sulfonate copolymer (2), synthesized in-house. The molecular weight relative to polystyrene sulfonate was  $\sim 50,000$ . The chromophore and polymer backbone structures are shown in Figure 1. Analogs of the bromo compound, containing a hydroxy (OH·AMP) or amino (NH<sub>2</sub>·AMP) group at the 4-position (both compounds synthesized in-house), are formed by hydrolysis or degradation in the coupling reactions. As impurities, these must be removed from the crude reaction mixture and detected to determine purity of the final product.

The Sephadex was soaked for 24 hours in the experimental solvent, and the fines decanted before being packed in the columns by pumping the swollen gel from a packing reservoir with the chromatographic eluent at  $\sim 2$  ml/min. Calibration standards of each of the Br·AMP, OH·AMP and NH<sub>2</sub>·AMP derivatives were obtained. Solutions of each were made up in the experimental buffer, at concentrations between 50 and 150 ppm, and chromatographed. The calibration curves are shown in Figure 2.

Spiking experiments were performed by first chromatographing solutions of each of the impurities at a given concentration. Then each impurity was added to separate solutions of 1 g/dl polymeric dye so that the impurity concentrations were identical to those of the first solutions. This spiked dye was also chromatographed, and the two traces compared.

## Results and Discussion

The anthrapyridone impurities encountered in our system are soluble in neat pyridine and in aqueous pyridine in the presence of base, whereas the polymer is water-soluble. The buffer pH value of 12 was chosen as a compromise between impurity solubility and the stability of the Sephadex column packing. The presence of pyridine and base in an aqueous buffer serves to solubilize the hydrophobic impurities, and allow the gel to separate the polymer from the impurities on the basis of molecular size. Pyridine concentrations above 15 v/v% caused tailing of the polymer peak into the region where the anthrapyridones elute. The anthrapyridone impurities all exhibited the same elution time. Below 15 v/v% pyridine, separation between the impurities was achieved, but elution times became too long. In the latter case, the absence of a high concentration of pyridine allows for greater interaction between the gel and the impurities. The final conditions chosen are shown in Table I. With the chromatographic conditions chosen, elution times for each of the species were: polymeric dye, 12.2 min.; OH·AMP, 23.2 min.; Br·AMP, 24.8 min.; and NH<sub>2</sub>·AMP, 27.6 min. When each of these species was chromatographed separately, different linear calibration curves which passed through the origin were

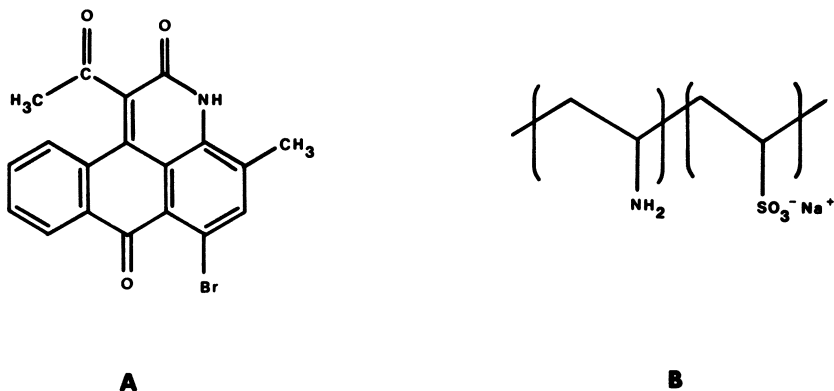


Figure 1. Chromophore (A) and polymeric backbone structures (B) used for synthesis of the polymeric dye

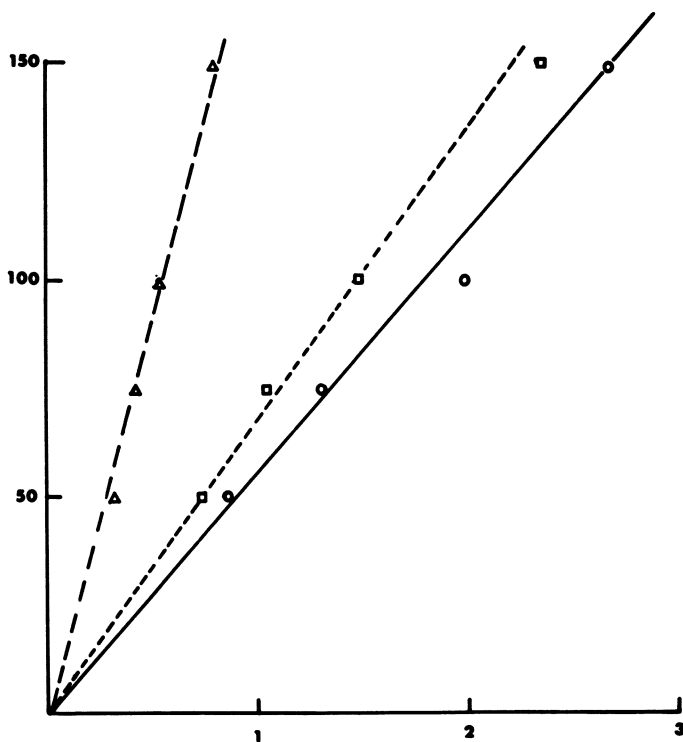


Figure 2. Calibration curves for OH · AMP (—○—); Br · AMP (—△—); and NH<sub>2</sub> · AMP (—□—) (for conditions, see Table I; ordinate: concentration of AMP derivative, ppm; abscissa: peak area, in.<sup>2</sup>)

Table I  
Final Chromatographic Conditions

Column Packing	Sephadex G-25 Superfine, soaked for 24 hours with in-use solvent before packing into the columns
Column Size	Three columns, 1 cm x 25 cm glass
Solvent	15 v/v% pyridine, 0.01M sodium phosphate, pH 12
Injection Concentration	Polymeric dye 1 g/dl
Injection Volume	0.2 ml
Lower Detection Limit for Impurities	10 ppm
Solvent Flow Rate	1 ml/min
Analysis Time	35 min
Detection	340 nm absorbance Varian Techtron Model 635 equipped with ISCO high-pressure flow cells

obtained for each one. This indicates that all of the solute injected was eluted from the column.

Sample chromatograms of the spiking experiments are shown in Figures 3 and 4. Figure 3 shows each of the impurities at 110 ppm, and superimposed are chromatograms of the polymeric dye spiked with each of the impurities at the same concentration. The chromatograms are essentially superimposable. A small discrepancy arises from the fact that the tail of the polymer peak overlaps the impurity peak. This makes the pure impurity peak appear lower than the dye-spiked impurity peak. This is also evident in Figure 4, where dye has been spiked with decreasing amounts of OH-AMP. In both cases, it is important to note that the impurities are not being irreversibly bound to the pure dye product. Quantitative amounts of spiked, injected impurities are being recovered.

An attempt was made to improve on the analysis by employing a single column of approximately the same volume. The details of this are shown in Figure 5 as Column A, and a comparison is made with the three-column style designated as B. The number of theoretical plates (TTP) and the number of theoretical plates per foot (TPPF) are higher for Column A. However, the separation is much poorer as a result of excessive tailing of the polymer when Column A was run at 1 ml/minute. Slowing the flow rate to 0.4 ml/minute for Column A did not improve the situation.

### Conclusions

A reliable chromatographic method has been developed for the quantitative analysis of hydrophobic impurities in water-soluble polymeric dyes. The method utilizes both the molecular sieve effect of normal gel permeation chromatography and solute-column packing interaction, modified by solvent composition. This method eliminates the need to extract the impurities from the polymeric dye with 100% extraction efficiency, as would be required for an ordinary liquid chromatographic analysis.

### ABSTRACT

Water-soluble polymeric dyes have been prepared from water-insoluble chromophores, viz., anthraquinone derivatives. Unreacted chromophore and its simple derivatives, which are all water-insoluble, remain in solution due to solubilization by the polymeric dye. A method has been developed to separate and quantitate the polymeric dye and these hydrophobic impurities using Sephadex column packing. The solvent developed has the property of debinding the impurities from the polymer, and further allows a separation of the impurities into discrete species. This latter separation is based on the functional groups on the impurity molecules, having a different interaction with the Sephadex surface in the presence of this solvent. The polymer elutes at the void volume

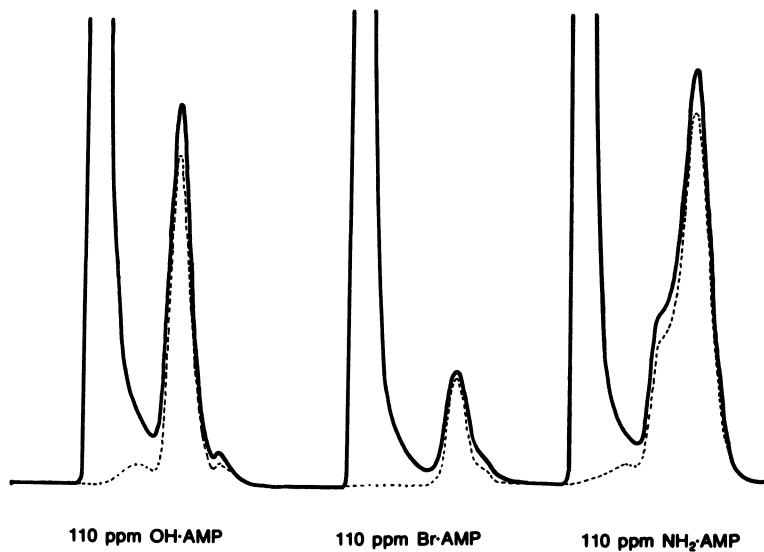


Figure 3. Chromatograms of  $\text{OH} \cdot \text{AMP}$ ,  $\text{Br} \cdot \text{AMP}$ , and  $\text{NH}_2 \cdot \text{AMP}$  at 110 ppm in the absence (---) and presence (—) of polymeric dye (1 g/dL) (ordinate: absorbance, 340 nm; abscissa: elution time, min)

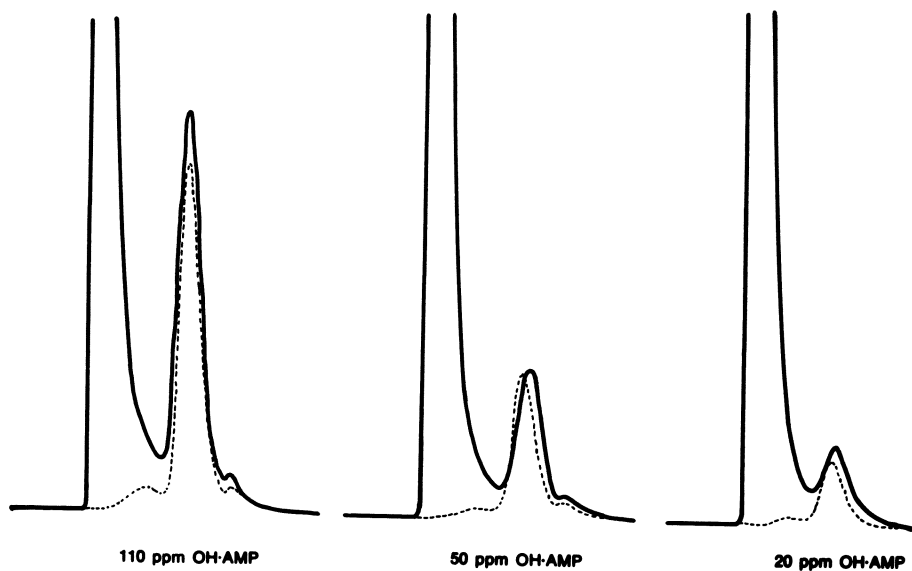
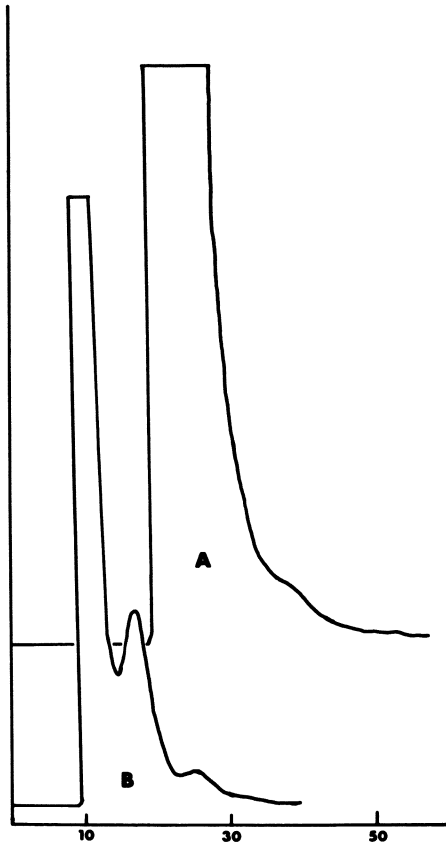


Figure 4. Recovery experiments for  $\text{OH} \cdot \text{AMP}$  at 110, 50, and 20 ppm in the absence (---) and presence (—) of polymeric dyes (1 g/dL) (ordinate: absorbance, 340 nm; abscissa: elution time, min)



**Figure 5.** Effect of column dimensions on the chromatographic separation (ordinate: absorbance, 340 nm; abscissa: elution time, min). Column A:  $1.5 \times 25$  cm; 44.2 mL; 397 theoretical plates/ft; 325 theoretical plates; 0.4 mL/min flow rate; Column B: three  $0.9 \times 25$  cm; 47.7 mL; 112 theoretical plates/ft; 275 theoretical plates; 1.05 mL/min flow rate.

and is easily quantitated. Quantitation of the various impurities was achieved by chromatographing pure standards. Spiking experiments were performed to demonstrate that complete separation of the impurities from the polymeric dye was achieved.

#### Literature Cited

1. Weinshenker, N., in "Polymeric Drugs," Donaruma, L. G.; Vogl, O., eds., Academic Press, New York (1978), p. 17.
2. Dawson, D. J.; Gless, R. D.; Wingard, R. E., Jr.; J. Am. Chem. Soc., 1976, 98, 5996.
3. Dawson, D. J.; Otteson, K. M.; Wang, P. C.; Wingard, R. E., Jr.; Macromolecules, 1978, 11, 320.
4. Cooper, A. R.; Booth, R. G.; Matzinger, D. P.; U.S. Patent No. 4,088,572.
5. Gelotte, B.; J. Chromatogr., 1960, 3, 330.
6. Janson, J.-C.; J. Chromatogr., 1967, 28, 12.
7. Porath, J.; Biochim. Biophys. Acta, 1960, 39, 193.
8. Eaker, D.; Porath, J.; Sep. Sci., 1967, 2, 507.
9. Determann, H.; Walter, I.; Nature, 1968, 219, 604.
10. Marklová, E.; Hais, I. M.; J. Chromatogr., 1977, 131, 205.
11. Katsoyannis, P. G.; Tometsko, A. M.; Zalut, C.; Fukuda, K.; J. Am. Chem. Soc., 1966, 88, 5625.
12. Blumenfeld, O. O.; Callop, P. M.; Howe, C.; Lee, L. T.; Biochim. Biophys. Acta, 1970, 211, 109.
13. Minamiura, N.; Matsumura, Y.; Yamamoto, T.; J. Biochem., 1972, 72, 841.
14. Somers, T. C.; Nature, 1966, 209, 368.
15. Lissitzky, S.; Bismuth, J.; Clin. Chim. Acta, 1963, 8, 269.
16. Marsden, N. V. B.; J. Chromatogr., 1975, 105, 1.

RECEIVED May 7, 1980.



# INDEX

## A

Absorbance of polystyrene particles ..	62
Acetate, polyvinyl .....	136
long-chain branching in .....	136
linear .....	137
Acetate polymerization, vinyl .....	137
Acetonitrile .....	77
Acrylic(s) .....	219
HPGPC chromatograms of high solids .....	220f
oligomers .....	217
resins, HPGPC chromatograms of ..	218f
Acrylonitrile .....	78, 82f, 83, 86, 90
concentration of polymerized .....	79
and methylacrylate, polymerization of .....	77
monomeric .....	79
and styrene .....	77
/styrene copolymers .....	86
Adhesion .....	219
Aerosol MA .....	5
Aerosol OT .....	48, 229f
Aggregation, mass-action law .....	225
Aggregation numbers, micelle .....	226
Alkyls .....	219
Alkylphenoxy polyethoxyethylene .....	268
Alkylpolyethyleneoxide micelles .....	226
AMA .....	4f, 5, 9
Amino-ethylene-sodium ethylene sulfonate copolymer .....	298
Amphiphiles .....	226
in benzene .....	227
AN/MA graft polymer, chromatogram of .....	80f
AN/S copolymers .....	86
chromatograms of .....	87f
polymer composition analyses for ..	88t
AN/S latex, chromatographic data on ..	89f
Analysis, particle size .....	1-25
Anthraquinone derivatives .....	301
AOT .....	227, 230
Apolar solvents .....	225
Aqueous pools .....	226
Average property determination for copolymers .....	159
Axial .....	
dispersion .....	175, 176f
characterization .....	180
velocity, eluant .....	3
velocity, particle .....	3

## B

Br · AMP (bromo-anthrapyridone) ..	298
Band-spreading correction .....	125
Beer-Lambert .....	16
Benzene .....	210, 235
Biological applications .....	285-296
Biomimetic features .....	226
Bonds, P—O—P .....	241
Branched polymers, characterization of .....	107-129
Branching in polyvinyl acetate, long-chain .....	136
Branching structure factor .....	142f
Broad MWD standards .....	183
polydextran .....	193t, 195t
PVC .....	188, 191
Broad-standard linear calibration .....	104
Broadening in gel permeation chromatography, optimization of peak separation and .....	267-284
Bromo-anthrapyridone (Br · AMP) ..	298
Bulk copolymerization of styrene ..	179
<i>n</i> -butyl methacrylate .....	163, 169
chromatogram, polystyrene .....	162f
styrene .....	164f

## C

Calibration .....	
curve(s) .....	
HDC universal .....	8f
for LEC system .....	12f
molecular weight .....	189f, 192f, 194f
linear .....	193
polystyrene .....	209f
universal .....	184-186
for PMMA .....	155f, 156f
SEC .....	38t
-MW .....	203
column .....	74
effect of ionic concentration on material recovery and universal .....	3
homopolymer .....	168f
linear .....	195t
broad-standard .....	104
SEC- $[\eta]$ .....	99
molecular weight .....	184
and peak broadening .....	183-196
universal .....	189f



*o*-Dichlorobenzene .....208, 210  
 Dichromate ion ..... 2  
 Dichromate, sodium ..... 56  
 Differential refractometry ..... 112  
 Dimethylformamide ..... 268  
 Dimethylsulfoxide ..... 268  
 Dioxane ..... 268  
 Dispersion, axial ..... 176*f*  
 Dispersion characterization, axial ..... 180  
 Distribution, resolution of particle size ..... 18  
 DNOAHBr ..... 235  
 chromatogram for ..... 231*f*  
*n*-Dodecyl octaethyleneglycol mono-  
 ether ..... 236  
 Dyes, hydrophilic polymeric .....297–304

## E

Elastomers, emulsion polymerized .... 77  
 Electron micrographs, scanning .....54*f*–55*f*  
 Electrophoresis, polyacrylamide gel .. 292  
 Electrophoretic gels, densitometry of 295  
 Emulsion polymerization ..... 150  
 Emulsion polymerized elastomers ..... 77  
 Epichlorohydrin ..... 297  
 Epoxy esters ..... 219  
 HPGPC chromatogram of ..... 213*f*  
 Epoxy resins, HPGPC chromato-  
 grams of ..... 221*f*  
 Esters, epoxy ..... 219  
 Exclusion effect in cylindrical cavities 199*f*  
 Exclusion effect of a rigid rod ..... 200  
 Extinction coefficient(s) .....56, 67, 74  
 measurement of ..... 52  
 for non-absorbing particles ..... 57  
 Extinction cross section ..... 17*f*

## F

Field-flow fractionation (FFF) ..... 2  
 Filtration effect ..... 5  
 Filtration, gel ..... 226  
 Floor tile ..... 223  
 Formamide ..... 268  
 Fractionation, field-flow (FFF) ..... 2  
 Fractionation of serum ..... 288  
 Fractosil .....7, 11, 12*f*  
 packings, partition coefficients for .. 13*f*

## G

Gel(s)  
 densitometry of electrophoretic .... 295  
 electrophoresis, polyacrylamide .... 292  
 filtration ..... 226  
 chromatography ..... 198

Gel(s) (*continued*)  
 permeation chromatography (GPC) 27,  
 91, 149, 150, 159, 167, 179, 198, 207,  
 210, 227, 236, 257, 260  
 and absolute Mn comparison .... 157*f*  
 and absolute Ms comparison .... 157*f*  
 analysis ..... 64*f*  
 characterization of poly(dichloro-  
 phosphazene) by ..... 255  
 chromatograms of phosphatidyl  
 choline fraction ..... 233*f*  
 soya lecithin ..... 233*f*  
 chromatograms of soya lecithin .. 232*f*  
 elution volumes, effect  
 of ionic strength on ..... 269  
 of neutral surfactants on ..... 273  
 of pH on ..... 273  
 high-conversion polymerization  
 kinetic modeling utilizing 149–182  
 HPLC ..... 169  
 Sephadex .....297–304  
 Gloss ..... 141  
 Glass packing, porous ..... 47  
 Glass transition temperature ..... 215  
 GMO ..... 235  
 chromatogram for ..... 231*f*  
 GPC (*see* Gel permeation chromatography)  
 Grafting ..... 78  
 Gyration, radius of ..... 197

## H

Hardness, pencil ..... 219  
 Haze ..... 141  
 HDC (*see* Hydrodynamic chroma-  
 tography)  
*n*-Heptane ..... 169  
 Hexachlorocyclotriphosphazene,  
 polymerization of ..... 231  
 High  
 -conversion polymerization kinetic  
 modeling utilizing GPC .....149–182  
 -performance  
 gel permeation chromatography  
 (HPGPC) .....207, 208, 215,  
 217, 219, 223  
 characterization of  
 oligomers .....207–224  
 chromatogram(s)  
 of epoxyester ..... 213*f*  
 of high solids acrylics ..... 220*f*  
 of high solids polyesters .... 218*f*  
 of isocyanate cross-  
 linkers .....214*f*, 216*f*  
 of polyester urethane ..... 222*f*  
 resins  
 of acrylic ..... 218*f*  
 of epoxy ..... 221*f*  
 of melamine ..... 220*f*

- High (*continued*)  
 -performance (*continued*)  
 liquid chromatography  
 (HPLC) .....163, 286  
 analysis ..... 162f  
 -pressure, low-density poly-  
 ethylenes .....145t, 146  
 resins (HP-LDPE) ..... 139  
 Homopolymer calibration ..... 168f  
 Homopolymerization ..... 179  
 of methyl methacrylate ..... 149  
 high-conversion ..... 150  
 HPGPC (*see* High-performance gel  
 permeation chromatography)  
 HPLC (*see* High-performance liquid  
 chromatography)  
 Human serum proteins ..... 289f  
 Hydrodynamic chromatography  
 (HDC) .....1, 13, 27, 47, 179  
 percent recoveries of latexes in ..... 6t  
 porous ..... 11  
 LEC and ..... 7  
 universal calibration curve ..... 8f  
 Hydrophilic polymeric dyes ..... 297-304
- I**
- Inelastic light scattering ..... 226  
 Interference effect ..... 62  
 Interpretation techniques, chromato-  
 graphic ..... 78  
 Intrinsic viscosity(ies) .....113, 190f  
 instantaneous branched ..... 134  
 instantaneous linear ..... 134  
 for nonionic polyacrylamides ..... 270f  
 ratios of ..... 109  
 Inverted micelles ..... 225  
 Ionic, effect(s) of  
 concentration on material recovery  
 and universal calibration ..... 3  
 strength on GPC elution volumes .. 269  
 strength on  $R_F$  .....4f, 12f  
 Isocyanate cross-linkers ..... 215  
 HPGPC chromatograms of ..... 214f, 216f
- K**
- Kinetics, copolymerization ..... 169  
 Kurtosis .....31, 40t, 41, 210
- L**
- Latex(es)  
 in HDC, percent recoveries of ..... 6t  
 monodisperse ..... 9  
 particles  
 diameter averages for .....69t, 70t, 71t  
 mixtures of ..... 71  
 polystyrene ..... 47
- Lattices, model ..... 27  
 LCB (*see* Long-chain branching)  
 LDPE (*see* Low-density polyethylene)  
 LEC (*see* Liquid exclusion chroma-  
 tography) ..... 236  
 Lecithin ..... 235  
 soya ..... 232f  
 GPC chromatograms of ..... 232f  
 phosphatidyl choline fraction  
 of ..... 233f  
 Light scattering ..... 241  
 classical ..... 226  
 detection .....107-129  
 inelastic ..... 226
- Linear  
 calibration ..... 195t  
 broad-standard ..... 104  
 SEC- $[\eta]$  ..... 99  
 molecular weight calibration curve 193  
 polymers .....183-196
- Liquid chromatography, high-  
 performance ..... 286
- Liquid exclusion chromatography  
 (LEC) .....1, 9, 10f  
 and porous HDC ..... 7  
 system, calibration curve for ..... 12f  
 Long-chain branching (LCB) .....131, 133,  
 139, 141  
 frequency .....143f, 144f  
 Low coatings viscosity ..... 217  
 Low-density polyethylene (LDPE) 131, 142f  
 application of MWBD method to .. 139
- M**
- Mark-Houwink  
 coefficients .....107, 109, 113,  
 127, 137, 139  
 constants .....103, 133, 184, 185, 187  
 relation ..... 269  
 Mass-action law aggregation ..... 225  
 Mass detector response ..... 184  
 Material recovery and universal  
 calibration, effects of ionic  
 concentration on ..... 3  
 Measurement, particle size ..... 48  
 MEK resistance ..... 219  
 Melamine resins, HPGPC chromato-  
 grams of ..... 220f  
 Membrane osmometry ..... 241  
 Methyl methacrylate ..... 163  
 homopolymerization of ..... 149  
 high-conversion ..... 150  
 polymerization ..... 179  
 Methacrylate .....79, 82f, 83  
 polymerization of acrylonitrile and 77  
 Micellar catalysis ..... 226  
 Micellar systems, reversed ..... 225-238

- Micelle(s)  
 aggregation numbers ..... 226  
 alkylpolyethyleneoxide ..... 226  
 inverted ..... 225  
 reversed ..... 225  
 size ..... 235  
 sodium dodecyl sulfate ..... 236  
 stability ..... 235
- Microparticulate high efficiency  
 columns ..... 210
- Mie scattering ..... 42*t*  
 Mie theory ..... 18, 29, 57*t*, 62, 66, 70, 73, 74  
 Milk proteins ..... 288, 290*f*, 291*f*
- Mixture rule, diameter averages  
 based on ..... 73*t*
- MMA ..... 150
- Model lattices ..... 27
- Molecular weight  
 and branching distribution method  
 (MWBD) ..... 131-148, 138*t*, 142*f*  
 to LDPE, application of ..... 139  
 calibration ..... 184  
 curve ..... 189*f*, 192*f*, 194*f*  
 linear ..... 193  
 universal ..... 184-186  
 and peak broadening ..... 183-196  
 universal ..... 189*f*  
 distribution (MWD) ..... 143*f*, 144*f*, 183,  
 219, 223, 257  
 broad ..... 257  
 polydextran standards ..... 193*t*, 195*t*  
 polystyrene (PS) ..... 111  
 PVC standards ..... 188, 191  
 curve ..... 91  
 low molecular polymer ..... 223  
 polystyrene standards,  
 narrow ..... 183, 185, 188  
 oligomers, low ..... 219  
 weight-average ..... 125
- MOLWT program ..... 112
- Monodisperse latex ..... 9
- Monodispersity ..... 74
- Monomeric acrylonitrile ..... 79
- Monomeric styrene ..... 78
- Multiple scattering ..... 29
- Muscle contractile proteins, skeletal .. 292
- MWBD (*see* Molecular weight and  
 branching distribution)
- MWD (*see* Molecular weight  
 distribution)
- N**
- NaCl, percent recoveries of poly-  
 styrene using SLS and ..... 6*t*
- NH<sub>2</sub> · AMP ..... 298
- Narrow MWD polystyrene ..... 111, 115*t*  
 standards ..... 183, 185, 188
- NBS  
 polystyrene SRM 706 ..... 114  
 SRM #1476 ..... 146*t*  
 SRM 706 polystyrene ..... 117*t*
- Nitrate, potassium ..... 48
- Nitrate, sodium ..... 48
- Nitrile resin polymerizations ..... 77
- Non-absorbing particles, extinction  
 coefficient for ..... 57
- Non-homopolymer character ..... 167
- Non-steric exclusion mechanisms ..... 169
- Non-porous packing, HDC ..... 2
- Normalized copolymer composition  
 distributions, theoretical ..... 170*f*
- O**
- OH · AMP ..... 298
- Oligomer(s) ..... 223  
 acrylic ..... 217  
 HPGPC characterization of ..... 207-224  
 polyester-based urethane ..... 223
- Operational CMC ..... 225
- Optical density ..... 16
- Orthogonal chromatography ..... 149, 175  
 cross fractionation by ..... 167, 168*f*, 179
- Osmometry ..... 190*f*  
 membrane ..... 241
- P**
- PBLG (polybenzyl-L-glutamate) ..... 203
- PCP (polychloroprene) ..... 111, 119*t*,  
 120, 122*f*, 123*f*
- PMMA (*see* Polymethyl methacrylate)
- P—O—P bonds ..... 241
- PPG (polypropylene glycol) ..... 188, 191
- PS (*see* Polystyrene)
- PSBD (polystyrene butadiene) ..... 5
- PVAc (*see* Polyvinyl acetate)
- PVAc-E4 ..... 138*t*
- PVC (*see* Polyvinyl chloride)
- Packing—HDC, non-porous ..... 2
- Packing procedure, column ..... 74
- PAM (*see* Polyacrylamide)
- Paneling, interior wood ..... 223
- Particle(s)  
 diameter(s) ..... 51*f*, 67  
 calculated ..... 42*t*  
 extinction coefficient for non-  
 absorbing ..... 57  
 recovery ..... 63  
 size  
 analysis ..... 1  
 distribution, resolution of ..... 18  
 measurement ..... 48, 65  
 standards ..... 52
- Partition coefficient(s)  
 for CPG packings ..... 13*t*

Partition coefficient(s) ( <i>continued</i> )	
for fractosil packings	13 <i>t</i>
separation factor and	33 <i>t</i> –35 <i>t</i>
PBC (potential barrier chromatography)	1
Peak	
areas for polymers and monomer	84 <i>f</i>
broadening calibration, molecular weight and	183–196
separation	47
and broadening in gel permeation chromatography, optimization of	267–284
Pencil hardness	219
Permeation chromatography, gel ( <i>see</i> Gel permeation chromatography (GPC))	
pH on GPC elution volume, effect of	273
Phosnic 390	245
Phosphatides	236
soya	230
Phosphatidyl choline fraction, GPC chromatograms of	233 <i>f</i>
of soya lecithin	233 <i>f</i>
Phosphonitrilic chloride	255
to poly(dichlorophosphazene), polymerization of the trimeric	256 <i>f</i>
Photosensitizer	223
Pinch effect, tubular	2
PN trimers	245
Poly <i>n</i> -butyl methacrylate, separation of	176 <i>f</i>
Polyacrylamide(s) (PAM)	268, 271, 283
gel electrophoresis	292
nonionic	272 <i>f</i> , 274 <i>f</i> , 276 <i>f</i> , 278 <i>f</i> , 279 <i>f</i> , 280 <i>f</i> , 282 <i>f</i>
intrinsic viscosities for	270 <i>f</i>
standards	281 <i>t</i>
with polyethylene oxide, retention volumes of	275 <i>t</i>
Polyacrylonitrile	81
Polybenzyl-L-glutamate (PBLG)	203
Polycarbonate	92
Polychloroprene (PCP)	111, 119 <i>t</i> , 120, 122 <i>f</i> , 123 <i>f</i>
Polydextran	194 <i>f</i>
standards, broad MWD	193 <i>t</i> , 195 <i>t</i>
Polydichlorophosphazene	231–254, 261 <i>f</i> , 262 <i>f</i>
dilute solution parameters	248 <i>t</i>
by GPC, characterization of	255
polymerization of the trimeric phosphonitrilic chloride to	256 <i>f</i>
Polyester(s)	219
-based urethane oligomers	223
HPGPC chromatograms of high solids	218 <i>f</i>
urethane, HPGPC chromatograms of	222 <i>f</i>
Polyethylene	92
oxide	268, 271, 281
retention volumes of polyacrylamides with	275 <i>t</i>
resins, high-pressure low-density (HP-LDPE)	136, 139, 145 <i>t</i> , 146
Polymer(s)	
characterization of branched	107–129
composition analysis for AN/S copolymers	88 <i>t</i>
intrinsic viscosity	107
linear	183–196
MWD, low molecular	223
peak area correlation	89 <i>f</i>
viscosity characterization	91
Polymerization(s)	
of acrylonitrile and methacrylate	77
emulsion	150
of hexachlorocyclotriphosphazene	231
methyl methacrylate	179
nitrile resin	77
of PMMA	159
radical-initiated	149
of the trimeric phosphonitrilic chloride to poly(dichlorophosphazene)	256 <i>f</i>
vinyl acetate	137
Polymerized acrylonitrile, concentration of	79
Polymerized comonomers	79
Polymethyl methacrylate (PMMA)	47, 92, 150, 151
calibration curve for	155 <i>f</i> , 156 <i>f</i>
chromatograms of	154 <i>f</i>
polymerization of	159
Polypropylene glycol (PPG)	188, 191
Polystyrene(s) (PS)	5, 81, 92, 104, 113, 189 <i>f</i> , 190 <i>f</i> , 203
broad MWD	111
butadiene (PSBD)	5
<i>n</i> -butyl methacrylate chromatogram	162 <i>f</i>
<i>n</i> -butyl methacrylate, separation of	178 <i>f</i>
latex particles	47
narrow MWD	111, 115 <i>t</i>
standards	183, 185, 188
NBS SRM 706	117 <i>t</i>
mixture of	210
molecular weight calibration curve	209 <i>f</i>
particles, absorbance of	62
using SLS and NaCl, percent recoveries of	6 <i>t</i>
SRM 706	120
NBS	114
standards	41
sulfonate	298
Polyvinyl acetate (PVAc)	111, 118 <i>t</i> , 120, 121 <i>f</i> , 122 <i>f</i> , 131, 138 <i>t</i> , 139
linear	137
long-chain branching in	136

- Polyvinyl chloride (PVC) 5, 190*f*, 191, 192*f*  
standards, broad MWD ..... 188, 191
- Pools, aqueous ..... 226
- Porous hydrodynamic chromatography ..... 2
- Potassium nitrate ..... 48
- Potential barrier chromatography  
(PCB) ..... 1
- Powder coatings ..... 210
- Protein(s) ..... 286  
calibration curves ..... 287*f*  
human serum ..... 289*f*  
milk ..... 288, 290*f*, 291*f*  
skeletal muscle contractile ..... 292
- Pyridine ..... 297–304
- R**
- Radical-initiated polymerizations ..... 149
- Radius of gyration ..... 197
- Random-coil ..... 205*f*
- Rayleigh ..... 73  
scattering ..... 66
- Recoveries of latexes in HDC, percent ..... 6*t*
- Recovery, particle ..... 63
- Refractometry, differential ..... 112
- Resin(s)  
HPGPC chromatograms  
of acrylic ..... 218*f*  
of epoxy ..... 221*f*  
of melamine ..... 220*f*  
polymerizations, nitrile ..... 77  
self-emulsifying ..... 219  
synthesis and processing ..... 207
- Resistance, MEK ..... 219
- Resolution of particle size distribution ..... 18
- Resolution, signal ..... 14
- Retention time ..... 159
- Retention volume ..... 29
- Reversed micellar systems ..... 225–238
- Reversed micelles ..... 225
- Rheological properties ..... 223
- Rigid rod(s) ..... 202, 205*f*  
exclusion of ..... 200
- Rod(s), rigid ..... 202  
exclusion effect of ..... 200
- ROH, reaction of trimethylchloro-  
silane with ..... 259*f*
- S**
- Scanning electron micrographs ..... 54*f*–55*f*
- Scattering  
coefficients ..... 29  
Mie ..... 42*t*  
multiple ..... 29  
Rayleigh ..... 66
- SEC (*see* Size exclusion chromatog-  
raphy)
- Self-emulsifying resins ..... 219
- Separation factor and partition  
coefficient ..... 33*t*–35*t*
- Sephadex gels ..... 297–304
- Serum, fractionation of ..... 288
- Serum proteins, human ..... 289*f*
- Serum proteins, human ..... 289*f*
- Shape, effect of solute ..... 197–206
- Shape function ..... 175
- Signal resolution ..... 14
- Silica sol separation ..... 205*f*
- Size exclusion chromatography  
(SEC) ..... 27, 31, 43  
calibration curves ..... 38*t*  
-[ $\eta$ ] calibration, linear ..... 99  
/LALLS ..... 108, 111, 115*t*, 118*t*, 119*t*  
-MW calibration curve ..... 203
- Size, micelle ..... 235
- Skeletal muscle contractile proteins ..... 292
- Skewness ..... 31, 40*t*, 41, 210
- SLS (*see* Sodium lauryl sulfate) ..... 5
- Sodium  
dichromate ..... 56  
dihexylsulfosuccinate (AMA) ..... 5, 9  
dodecyl sulfate micelles ..... 236  
lauryl sulfate (SLS) ..... 4*f*, 5, 7  
and NaCl, percent recoveries of  
polystyrene using ..... 6*t*  
nitrate ..... 48
- Solid spheres ..... 202
- Solute shape, effect of ..... 197–206
- Solvents, apolar ..... 225
- Soya lecithin ..... 235  
GPC chromatograms ..... 232*f*  
of phosphatidyl choline fraction  
of ..... 233*f*  
phosphatide fractions, effect of  
sample size on MW for ..... 234*f*
- Soya phosphatides ..... 230
- Spheres, solid ..... 202
- SRM 706 polystyrene NBS ..... 117*t*
- Stability, micelle ..... 235
- Standards  
broad MWD ..... 183  
polydextran ..... 193*t*, 195*t*  
PVC ..... 188, 191  
narrow MWD polystyrene ..... 183, 185, 188  
particle ..... 52  
polystyrene ..... 41
- Steric exclusion columns ..... 169
- Steric exclusion separation ..... 169
- Styrene ..... 78, 86, 163, 169  
acrylonitrile and ..... 77  
*n*-butyl methacrylate ..... 150, 164*f*  
high-conversion copolymeriza-  
tion of ..... 159  
composition in polymer, average ..... 166*f*  
-divinylbenzene copolymer beads .. 2  
monomeric ..... 78
- Sulfonate, polystyrene ..... 298

